Electrical properties of cadmium telluride and associated devices

Banda, I. M. Dharmadasa

Corrections.

I. Fig (3.4) — Schotky ⟶ Schottky.

II. Fig (5.17) — points A and B are missing.

III. Fig (7.17) — Intentensity ⟶ Intensity.

IV. Page 32. (last line) — $(N_a - N_d)$ ⟶ $(N_d - N_a)$.

V. Page 120. (line 5) — fabricated ⟶ fabricated.

ELECTRICAL PROPERTIES OF CADMIUM TELLURIDE

AND ASSOCIATED DEVICES

By

I. M. DHARMADASA BANDA, B.Sc.

A THESIS SUBMITTED FOR THE

DEGREE OF DOCTOR OF PHILOSOPHY

IN THE UNIVERSITY OF DURHAM

AUGUST 1980

ACKNOWLEDGEMENTS

I would like to express my gratitude to my supervisors, Professor G. G. Roberts and Dr. M. C. Petty, for their guidance and assistance during the course of this research. The financial support, granted by The Association of Commonwealth Universities and all the administration work by The British Council, are gratefully acknowledged. R.S.R.E., Malvern, and J.B.Mullin in particular, are thanked for supplying the material used in this work. Dr. G. J. Russell is thanked for taking the electron micrographs and valuable discussions. The expert knowledge and skills of the workshop staff, headed by Mr. F. Spence, have been invaluable. Members of the research group with whom the author has been associated are thanked for contributing their expertise. Mrs. S. Mellanby is thanked for her advice and her patience whilst typing this thesis.

Finally, I would like to thank my wife, Tamara, for her constant help and encouragement, and also my parents for their many sacrifices over the years.

PREFACE

The combination of wide bandgap, high average atomic number and reasonably high mobilities for both electrons and holes makes CdTe an attractive material for use in various electronic devices. Semi-insulating CdTe can be used as a material for gamma radiation detectors. This material offers the additional advantage that such devices can be operated at room temperature. The direct energy gap of CdTe can be varied easily by alloying with other compounds. When CdTe is mixed with HgTe, a continuous range of alloys with a direct energy gap, controllable by composition, from zero to 1.5 eV, can be obtained. These solid solutions of $Cd_x Hg_{(1-x)}Te$ have received much attention and are now used in detectors of infrared radiation. Alloying with ZnTe and particularly MgTe has also been successful and further alloying of CdTe-MgTe with Se produces mixed crystals with wider bandgaps. The luminescence obtained from these crystals is shifted far out into the visible region. These properties and the ability to prepare both n- and p-type crystals with resistivities over a wide range ($\sim 10^{-3}$-10^{12} Ωcm) make CdTe attractive in the electronics device industry. However, it is not widely used in semiconductor devices today, due to some unresolved technical problems. Chapter 1 of this thesis on "Introduction to CdTe" summarizes its history, method of preparation, some properties and possible applications.

Many properties of semi-insulating CdTe are not yet well understood. The first half of this thesis describes an investigation into the electrical properties of semi-insulating CdTe. Various experimental techniques such as d.c. conductivity, thermally stimulated currents, Hall effect and Schottky barrier measurements have been used to characterise the material. Chapters 2 and 4 describe the relevant theoretical background and experimental techniques respectively. The results obtained on

Cl-doped, Cr-doped and undoped semi-insulating single crystals are presented in Chapters 5 and 6. The Meyer-Neldel rule, observed on Cl-doped specimens, is also discussed and explained in terms of a new model (multi-valent theory) in Chapter 5.

CdTe possesses the optimum direct energy bandgap of 1.5 eV, and is a suitable material for terrestrial photovoltaic solar cells. Homo-junction and hetero-junction solar cell data on this material are available in the literature, but, data on MS and MIS photovoltaic structures are scarce. This might be due to unavailability of good quality CdTe single crystals and a suitable insulator for this material. Novel insulating films introduced by Langmuir and Blodgett based on organic compounds have been used to prepare MIS devices on low resistivity CdTe surfaces. The second half of this thesis concentrates on the electrical properties of MS and MIS photovoltaic structures. The results are presented in Chapter 7 while Chapter 3 reviews the theoretical background of these devices.

CONTENTS

CHAPTER 1

INTRODUCTION TO CADMIUM TELLURIDE

1.1 INTRODUCTION

Cadmium telluride has been known as a compound for about 100 years. In 1879 it was prepared along with many other tellurides in France by the chemist Margottat[1], who reacted Te with various metals at red heat. The heat of formation of the compound was subsequently reported by Fabre[2] in 1888, who showed that this process leads to well-crystallized material. The basic method of preparation of the compound has changed little to this day. Tibbals[3] in 1909 reported on another investigation of tellurides including CdTe. The Te he used was extracted from electrolytic slimes. Virtually all Tellurium is still obtained in this way today.

Even though this compound has been known since 1879, the only apparent use of CdTe reported up to the 1940's was as a pigment. In 1946, however, Frerichs and Warminsky[4] reported that the chalcogenides of Cd, in thin film form were highly photosensitive to a range of photon energies including β and γ radiation. They suggested that the effect could be used for the fabrication of γ-ray image converter tubes, or, if combined with suitably efficient amplifiers, in γ-quantum counters.

Photo cells of CdTe were made by 1948, and it was noted that preparation and heat treatment conditions as well as crystalline defects were of great influence in the performance of these devices. In the 1950's several detailed investigations of the behaviour of CdTe single crystals were made. In particular Kröger and de Nobel[5]; Bottaks, Konorov and Matveev[6] carried out detailed doping studies which established the basis for various uses of the compound. Finally in 1959 de Nobels[7] thesis appeared and it described the behaviour of the compound in great detail. It also

explained the behaviour of the dopants in terms of a coherent model.

As is well-known, CdTe is a semiconductor which has very advantageous properties as compared to the other semiconductor chalgogenides of Cadmium. Its comparatively high carrier mobility and the ability to control the conductivity from n- to p-type, and vice versa, may be used in semiconductor devices such as crystal diodes or transistors. It is also known that CdTe is photosensitive to many kinds of radiation, for example to infrared, visible, X- and γ-radiation, so that it may be used in photosensitive devices. These applications are described in a later section of this chapter.

1.2 PREPARATION OF CdTe

The CdTe compound is prepared directly from the elements[8]. The starting materials are usually 6N Cadmium shot and 6N Tellurium bars. The synthesis is carried out by careful heating of the two elements at $\simeq$ 1030°C, in an evacuated silica tube. The elements should be etched in a suitable solution to remove any surface oxide layer prior to the synthesis. Using this technique it is possible to synthesise up to 300 grams of CdTe. The final product is a polycrystalline solid boule.

Preparation of CdTe is hindered by the fact that, although the reaction between the elements starts at 550°C, temperatures well above 800°C are needed in order to get complete reaction. At such temperatures, however, CdTe tends to decompose markedly and no homogeneous phase will be obtained if this decomposition is not prevented. This can be achieved in two different ways. First, one can prepare CdTe from Cd and Te under a vapour pressure of one of its components. Then the equilibrium

$$CdTe\ (s) \rightleftharpoons Cd(g) + \frac{1}{2}\ Te_2\ (g).$$

is shifted to the left and decomposition does not occur. It is also possible to carry out the reaction by which CdTe is formed under a pressure of an inert gas.

(a) Single Crystal Growth

The need for good quality single crystals of CdTe is an established requirement for any device application. The most widely used methods of obtaining good quality crystals have been the modified Bridgman[9,10] and the THM (travelling heater method)[11,12] techniques. These are both solution growth methods in which growth of CdTe takes place by lowering the temperature of a cadmium-tellurium melt containing one component in excess.

The crystal growth can also be achieved by removing the excess component by evaporation. This method is called the Solvent Evaporation Technique (SET) and the experimental procedure is described in detail by Lunn and Bettridge[13]. In this method a mixture of cadmium telluride and cadmium shot are heated in an evacuated tube with a cadmium reservoir at the top end. When the solution is completely molten, the pressure of cadmium is reduced by cooling the Cd reservoir at a constant rate. This disturbs the equilibrium in the system ; cadmium evaporates from the solution and crystalline CdTe is formed. By maintaining the pressure at a suitable value, cadmium can be removed completely from the solution. Using this method good quality CdTe crystals up to 20 cm^3 (2cm diam. x 6cm long) have been obtained. All the crystals studied in this work were grown by solvent evaporation technique.

(b) Doping of CdTe

The pure material can be doped with a known amount of various foreign atoms. Possible impurity elements in CdTe are discussed in a later section 1.7 (a). One of the methods of doping involves using the zone-levelling procedure developed by Pfann[14]. In this method a known amount of a foreign element is placed at one end of a boat filled with pure CdTe and a molten zone is allowed to pass the CdTe bar in both directions. After about 10 passes the whole bar is homogeneously doped except for the section of the bar where the molten zone ends up. An alternative method of doping

CdTe consists of adding the dopant directly to the molten CdTe before crystallization. For example, a known amount of $CdCl_2$ is added to the melt in order to obtain chlorine doped CdTe[15].

1.3 STRUCTURAL PROPERTIES

Cadmium telluride is a member of the series of materials usually indicated as the II-VI compounds, which are built up from elements of the 2nd and 6th sub-group of the periodic table. Both Cd and Te are located in the fourth row of the table (Fig 1.1), with atomic numbers of 48 and 52, respectively. The average atomic number of 50 is the highest for any semiconducting compound in the II-VI series. Both HgSe and HgTe have higher average atomic numbers but are semi-metals. The important properties of CdTe are summarized in table (1.1).

Bulk CdTe has the cubic zincblende structure, each atom being tetrahedrally coordinated with four nearest neighbours of the other element. The type of bonding in CdTe is a mixture of ionic and covalent. The high polarizability of the tellurium ions leads to a deformation of the electron sphere which results in an increased electron density between the Cd and Te atoms. This accounts for the covalent contribution in the Cd-Te bond. The covalent contribution has been shown to be greater than 65%[7].

The lattice constant of CdTe is 6.481 Å and 4 molecules are contained in its unit cell. The model suggested by Hilsum and Rose-Innes[10] shows that there are two types of $\{111\}$ planes that alternate with each other, one consisting entirely of atoms of one element and the other consisting entirely of atoms of the other element, while the $\{110\}$ planes contain equal numbers of two kinds of atoms. Crystals can be cleaved quite readily on the latter planes.

Although the stable form of CdTe is the zincblende phase, which is always obtained for bulk samples at atmospheric pressure, thin films of CdTe can contain a proportion of the wurtzite phase. This proportion can

be varied with the method of preparation, and, under certain conditions, thin films with pure wurtzite structures have been obtained. Even in bulk CdTe, the zincblende structure is transformed into the rocksalt structure when a high pressure is applied. This transition occurs at a pressure of about 35 k bar. An abrupt drop in electrical resistance by about 6 orders of magnitude and a decrease in volume at this transition have been observed[16].

1.4 CRYSTALLINE DEFECTS

Perfect single crystals of CdTe have not yet been grown and the crystals obtained using the above methods contain defects such as grain boundaries, twins, dislocations and precipitates. The major visible defects are grain boundaries which separate individual single crystals. These are generally seen on the outside of the crystals and have been identified as both low angle grain boundaries and twin boundaries. The latter type are apparently always of the lamellar variety, that is they appear to originate and propagate in pairs. Dislocations can be revealed using a suitable etchant. Etch pit densities are moderately high for CdTe crystals prepared using SET. Typical densities for such material are of the order of (1-4) x 10^5 cm^{-2} [9].

Precipitates have also been observed in slices of CdTe crystals containing certain dopants. In particular the presence of precipitates in Cl and In doped CdTe has been established using a variety of techniques. IR transmission microscope[9] and electron-microscope[15] investigations reveal that precipitates exist in the bulk of the crystal. These precipitates occur mainly along grain boundaries, although they are by no means confined to them.

The origin of such precipitates may be understood by considering the enthalpy of formation (ΔH) of relevant compounds. These values for CdTe, In_2Te_3 and $CdCl_2$ are 1.05, 2.00 and 4.04 eV/molecule respectively[17]. The higher the enthalpy of formation of a compound, the higher should be

the probability of formation of large clusters dissolved in the crystal lattice. Since the ΔH of $CdCl_2$ is considerably higher than that of CdTe, the process of clusterization is probable even at high temperatures. In the case of In_2Te_3, the clusterization at high temperatures should be weak. However, at low temperatures ($\sim$ 500°C) the clusterization effects are important also in the In-doped crystals due to low reactivity of Cd and Te.

1.5 THERMAL AND MECHANICAL PROPERTIES

The linear thermal expansion coefficient of CdTe, α , is 4.9×10^{-6} K^{-1} at room temperature and increases with increasing temperature[18,19]. Below room temperature α decreases, becoming negative at about 62 K. Negative expansion coefficients are also exhibited by other zincblende structure compounds at low temperatures, but CdTe represents an extreme case.

The thermal conductivity at 300 K for CdTe, 0.075 W cm^{-1} K^{-1}, is the lowest for any of the tetrahedrally coordinated II-VI compounds except HgSe and HgTe. The other important thermal and mechanical properties of CdTe at 300 K are summarized in table (1.1).

1.6 OPTICAL PROPERTIES

In this section the interaction of γ-rays and optical photons with CdTe are described briefly. There are several ways in which gamma rays interact with matter ; the most important are the photo-electric effect, compton scattering and pair production. One or more of these will play a part in every event.

In the photo-electric effect all the energy of an incident photon is converted into the kinetic energy of an electron ; the photon loses its energy in creating electron-hole pairs. The photo-electric effect may be preceded by other events. With compton scattering, part of the gamma ray energy is converted into the kinetic energy of an electron, the amount being

dependent on the (scattering) angle between the original and the scattered gamma-ray. After the gamma-ray has been scattered, its remaining energy may be absorbed in a single photo-electric event, or multiple scattering may occur. If the energy of the gamma-ray is above 1022 MeV, an electron-positron pair may be created.

The interaction of optical photons with a semiconductor, unlike those of high-energy ionizing radiation, are determined by the details of the semiconductor's electronic and mechanical properties. Fig (1.2) shows the energy band structure of cadmium telluride[8,20]. As in other II-VI semiconductors with the zincblende or wurtzite structure, the lowest conduction band edge and highest valence band edge are both at Γ, so that the energy gap is direct. The bandgap is 1.606 eV at liquid helium temperature, and the second lowest conduction band edge is located at the L-point, 1.35 eV above the lowest. The energy gap of CdTe is the lowest for any of the II-VI compounds except HgSe and HgTe, which are semi-metals with zero or possibly negative energy gaps.

For optical photon energies greater than the semiconductor energy gap, E_g, there are very strong absorptions due to excitation of electrons from the valence band to the conduction band and, for sufficiently high energies, due to photo-emission from the valence band to vacuum. For photon energies less than E_g but greater than about twice the longitudinal optical phonon energy the absorption is relatively weak. This absorption arises primarily from interactions with free carriers, electronic levels within the bandgap, localized vibrational modes due to impurities, or defects such as precipitates. Finally, for sufficiently low photon energies the absorption again increases due to photon-phonon interactions.

The absorption edge data obtained by Marple[21] at several temperatures for single-crystal samples show that mechanical damage significantly increases the lower absorption coefficients. These data also show that

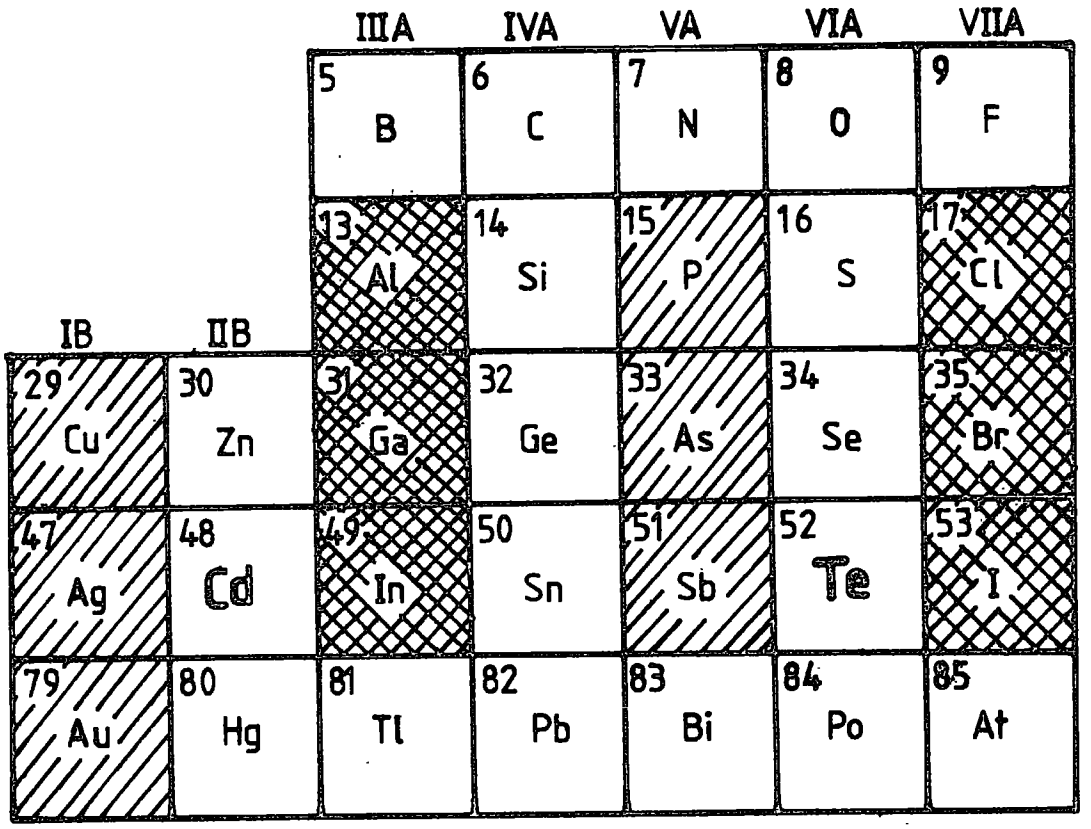

FIG.1·1 PORTION OF THE PERIODIC TABLE INCLUDING THE ELEMENTS OF GROUPS IIB AND VIA.

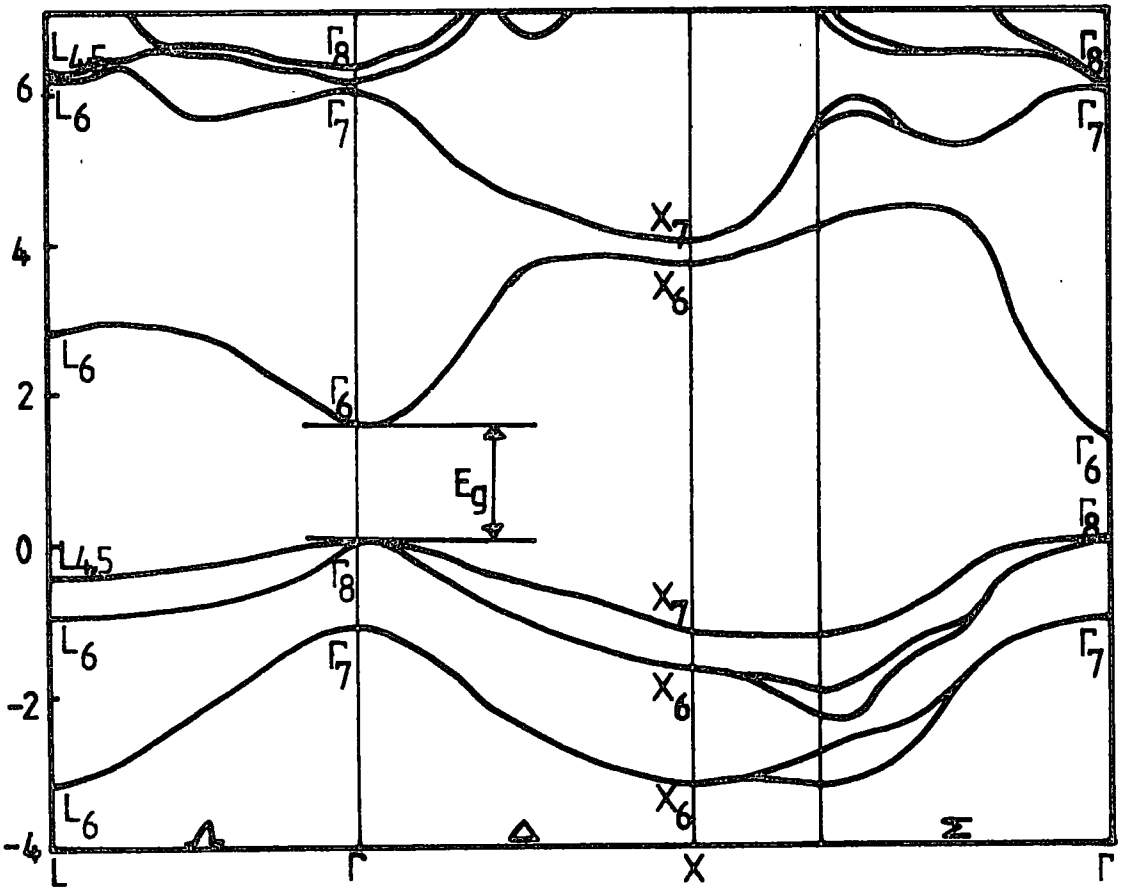

FIG.1·2 CALCULATED ENERGY BAND STRUCTURE OF CdTe.

the bandgap for CdTe shifts to lower values with increasing temperature. This behaviour is very similar to the temperature dependence exhibited by most semiconductors. The reflectance data of Thomas[22] and of Marple[23] show that as the temperature is increased from liquid helium temperature, E_g decreases very slowly up to about 20 K, then begins to decrease more rapidly. Between the temperatures 80 K and 150 K, E_g decreases linearly at the rate of $\simeq -3.5 \times 10^{-4}$ eV/K. Extrapolation to 300 K gives $E_g = 1.52$ eV, in rather good agreement with the values obtained by other experimental techniques. This energy gap is very close to the optimum value required for the conversion of solar radiation to electric power by means of semiconductor photo-voltaic solar cells.

1.7 ELECTRICAL PROPERTIES

Electrical properties of semiconductors are limited by their electronic band structure and the lattice vibration modes. These determine the intrinsic carrier concentration (n_i) of the material and the values of electron and hole mobilities respectively. However, the electrical properties are influenced to a much greater extent by impurities, native defects, and the interactions between them.

The intrinsic carrier concentration of a semiconductor is determined by its energy bandgap, E_g, and the effective masses for electrons and holes. With the experimentally observed values of the above parameters, the intrinsic carrier concentration in CdTe is calculated to be about 1.0×10^6 cm^{-3} [20] at 300 K. It is clear that this concentration is low to account for conduction at room temperature in any CdTe samples. The lowest room temperature carrier concentration is 8.3×10^7 cm^{-3}, as reported by Alekseenko et al[24] for a p-type sample.

(a) Possible Impurities in CdTe

The above discussion shows that the current carriers responsible for conduction in CdTe at room temperature and below must be generated by the ionization of impurities, native defects, or complexes between them.

Impurity atoms in the columns adjacent to Cd in the periodic table can substitute for Cd atoms in the lattice and those adjacent to Te can substitute for Te. Then these foreign atoms act as donors or acceptors depending on whether they have more or less electrons than the atom they replace. Since elements in adjacent columns differ by one valence electron, all the impurities considered here should be singly ionized acceptors or donors.

The group IB elements (Fig 1.2) Cu, Ag and Au are acceptors, presumably substituting for Cd. De Nobel[7] has reported the electrical properties of CdTe doped with these elements and they all show a p-type conduction with activation energies in the range 0.33 $\pm$ 0.05 eV. The group V elements P, As and Sb are also acceptors presumably substituting for Te, with ionization energies in the range from 0.036 to 0.060 eV. These crystals have hole mobilities of 24 to 39 $cm^2/V.sec$, and hole concentrations of 5.0×10^6 to 6.0×10^{17} cm^{-3} at room temperature[25]. The group IA elements Na and Li, are also acceptors in CdTe, that possibly can substitute for Cd.

The two types of donor impurities that have been identified in CdTe are both shown in fig (1.1). The group III elements (Al, Ga and In), and the group VII halogens (Cl, Br and I), presumably substitute for Cd and Te respectively.

The ability to control the conductivity type using various impurities can be difficult in II-VI semiconductors due to the formation of electrically active native point defects. These can be associated with deviations from the stoichiometric composition or due to presence of one element in excess. The defects associated with excess metal are generally donors and those associated with excess non-metal are generally acceptors. In those compounds that exhibit only n-type conductivity, any impurities that would normally be acceptors are rendered ineffective by the presence of native donors.

The purest samples of CdTe so far reported have been obtained by Triboulet and Marfaing[26] from single crystals grown by the vertical zone melting of ingots synthesized by the Bridgman method. Most of these samples have room temperature carrier concentration between 1 and 5×10^{13} cm^{-3} and resistivities of 100-400 Ωcm. It has been estimated that the total concentration of electrically active centres in these crystals is about 10^{14} cm^{-3}.

(b) Compensation in CdTe

Although CdTe can exhibit both p-type and n-type conductivity, like the other II-VI compounds its electrical properties are strongly affected by native defects. When donor impurities are added to a semiconductor with acceptor-like native defects, the donor electrons fill up the vacant shallow acceptor levels. Therefore it is the difference between shallow donor and acceptor concentrations, that is important in electronic conduction. When $N_a \simeq N_d$ the crystal is said to be compensated. An attempt to bring about exact compensation by careful doping would,in most cases, be difficult. However, in a large gap semiconductor, under favourable circumstances, there exists a force tending to equalize the concentrations of donor and acceptor states. When the concentration of a deep donor level becomes high enough to exceed (N_a-N_d) the Fermi level will rise abruptly from the vicinity of the shallow acceptor level to the vicinity of the deep donor level, where it remains pinned to yield semi-insulating material over a wide range of deep donor concentration. This mechanism is termed auto-compensation and has been extensively employed to obtain CdTe samples with carrier concentrations low enough to give the high electrical resistivity needed for γ-ray detectors.

(c) Localized Electronic Levels in CdTe

Numerous localized electronic levels lying within the energy gap of CdTe, many of which undoubtedly involve native defects, have been detected by applying various characterization techniques to high-resistivity

Table 1.1

	Property (unit)	Reported values	Refs.
1.	Lattice constant ($\mathring{A}$)	6.481	8,9,20.
2.	Molecules per unit cell	4	8,20.
3.	Density ($g.cm^{-3}$)	5.86	8,20.
4.	Melting point (C^{o})	1092	7,8,20.
5.	Linear expansion coefficient at 300 K (K^{-1})	4.9×10^{-6}	18,19.
6.	Thermal conductivity at 300 K ($W.cm^{-1}\ deg^{-1}$)	0.058	20.
7.	Heat capacity C_p ($Cal.g\text{-}atom^{-1}\ K^{-1}$)	5.9	20.
8.	Refractive index	2.64-2.75	39
9.	Dielectric constant (low frequency)	10.0-11.0	39,40,7
10.	Energy gap at 2 K (eV)	1.606	22,23
11.	Optical bandgap at room temperature (eV)	1.529	22,23,41
12.	Experimental $\frac{dE_g}{dT}$ (eV/K)	-3.0×10^{-4}	42
13.	Theoretical $\frac{dE_g}{dT}$ (eV/K)	-4.2×10^{-4}	43
14.	Electron affinity (eV)	4.28	1,8.
15.	The energy required to produce an e-h pair by ionizing radiation (eV)	4.46	44
16.	Conductivity type	n or p	8,20.
17.	Intrinsic carrier concentration at 300 K(cm^{-3})	1.0×10^{6}	20.
18.	Electron mobility ($cm^2/V.sec$)	700-1200	17,29,45,46
19.	Hole mobility ($cm^2/V.sec$)	8.2-200	13,17,29,33, 45,46.
20.	Effective mass of electrons	0.14	7
21.	Effective mass of holes	0.37	7

CdTe. The energies of some of the prominent levels that have been reported to exist within the energy gap are shown in fig (1.3). Most of these values correspond to the activation energy observed by various workers in conductivity versus temperature measurements on high-resistivity samples[27,28,29]. Thermally stimulated currents[28,30,31,32], Hall effect measurements[33,34,35,36], time-of-flight method[17,30,37] and photo-capacitance methods[38] have also been used to characterize this material. The possible origin of the traps are also shown in fig (1.3).

(d) Electron and Hole Mobilities in CdTe

To investigate the mobilities of electrons and holes in CdTe, Hall effect and the time-of-flight techniques have been used. The electron mobility measured for the purest sample at 300 K is 1100 $cm^2/V.sec$, the highest reported for CdTe by Triboulet and Marfaing[26]. Their Hall effect measurements on different samples taken from different locations in the crystal boule show that the impurity content increases systematically from head to tail.

The reported values of hole mobility in CdTe vary over a wide range. The minimum value is $\simeq$ 8.2 $cm^2/V.sec$[33,46], and the maximum is $\simeq$ 200 $cm^2/V.sec$[46] at room temperature. The exact value of hole mobility depends on the method of preparation and the type of impurities present. The performance of γ-ray detectors depends critically on the products of mobility and trapping time for electrons and holes. Alekseeno et al[24] have reported the values 2.6 x 10^{-3} and 4 x 10^{-4} $cm^2\ V^{-1}$ for electrons and holes in CdTe.

1.8 APPLICATIONS

(a) Nuclear Detectors

The principal shortcoming of the materials so far used as semiconducting detectors of radiation, Ge(Li) and Si(Li), is their temperature instability. In order to prevent possible precipitation of Li and because

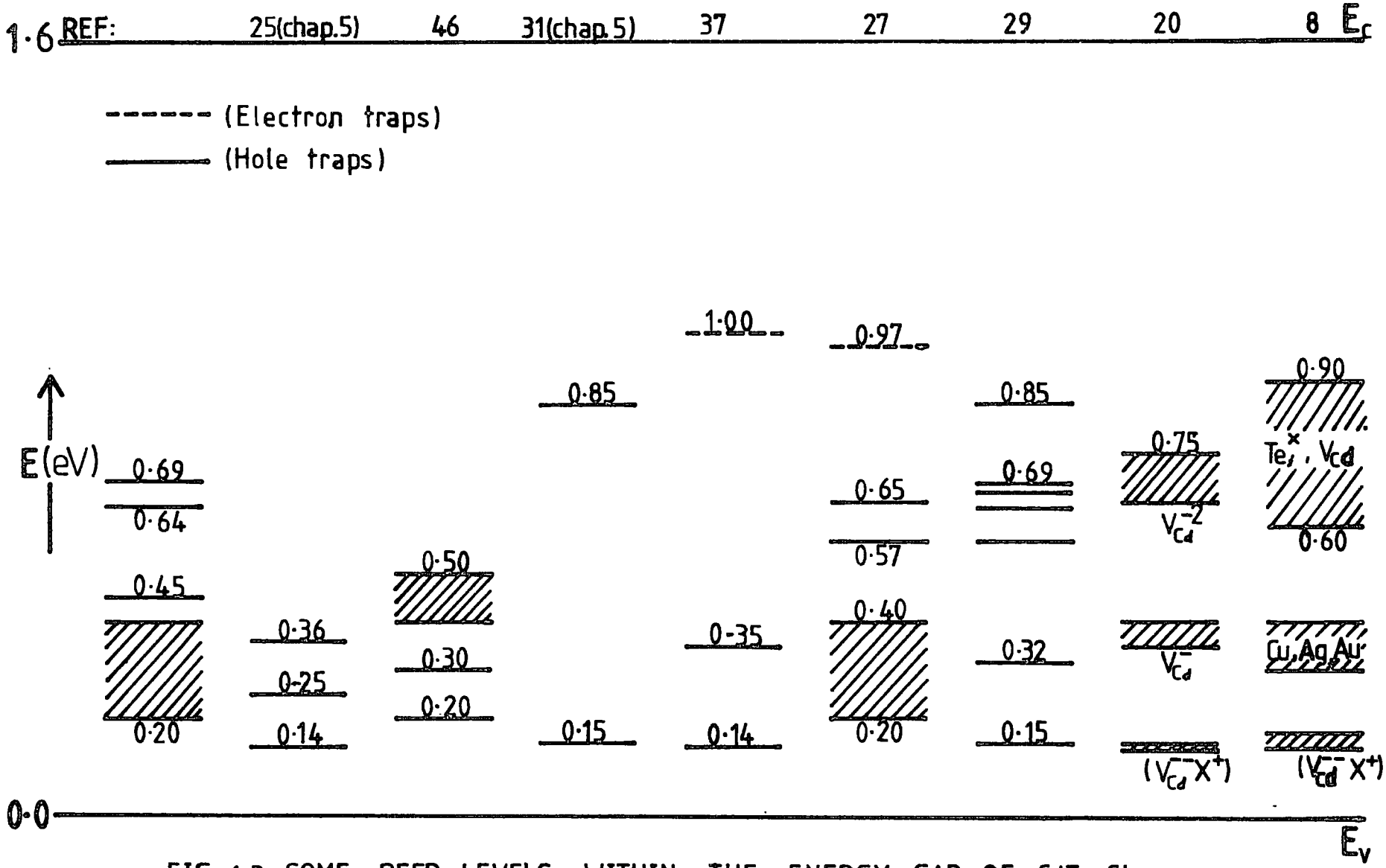

FIG. 1·3 SOME DEEP LEVELS WITHIN THE ENERGY GAP OF CdTe:Cl.

of the small electronic bandgap (0.67 eV), Ge(Li) detectors must be operated below the room temperature. Si(Li) detectors possess improved temperature characteristics but they exhibit low value of the photoelectric cross-section, which is proportional to the fifth power of atomic number.

Approximately ten years ago (≃ 1970), semiconductor detectors based on CdTe crystals started to show a remarkable improvement in performance. CdTe has a high average atomic number of 50, a large bandgap of 1.50 eV and relatively high electrons and hole mobilities at room temperature, i.e.≃ 1000 and ≃ 100 cm^2/V.sec, respectively. Since the average atomic number of CdTe(50) is higher than Ge(32) and Si(14), the effective photon interaction is higher in CdTe. For example, the photoelectric absorption coefficient in CdTe is more than 100 times larger than in Si and the Compton absorption coefficient in CdTe is about 4 times larger than in Si. The intrinsic carrier concentration in CdTe at room temperature is about 10^6 cm^{-3}. For these reasons CdTe is an attractive material for nuclear radiation detectors, especially when small size, room temperature and above (up to ≃ 100°C) operation are desired.

(b) Solar Cells

CdTe has important advantages as a material for photovoltaic solar cells, namely its appropriate value of direct energy gap and the ability to produce thin films using most of the cheap techniques. In addition, CdTe has a high optical absorption coefficient ; less than 2μ of CdTe would be capable of absorbing all the usable energy from the solar spectrum.

These favourable properties alone are not enough to infer that CdTe is a good material for photovoltaic conversion. The value of diffusion length for minority carriers should also be considered. The collection of photocarriers is limited by recombination losses, which depends on the diffusion length $L = \sqrt{D\tau}$ (τ = minority carrier lifetime,

$D = \frac{\mu}{kT}$ where μ is the minority carrier mobility). To avoid huge recombination losses, the diffusion length should be of the order of the absorption length $1/\alpha$ (α = mean absorption coefficient for $h\nu > E_g$). Heavy doping of the photoelectric material decreases L, while it also decreases the series resistance losses of the cell. Therefore, there exists an optimum doping of the material.

Another requirement for a solar cell is the ability to build an efficient collector junction. The collecting structure could be a p-n junction, a heterojunction, a metal-semiconductor barrier or a MIS structure. All these structures are possible on CdTe surfaces. A maximum efficiency of 10.5% has been reported[47,48] for a p-n junction solar cell. A variety of heterojunctions with CdTe have been studied and 7.5% is the maximum observed efficiency reported by Cusano[49,50]. Although various papers deal with metal-CdTe structures, only a few of them have been tested as solar cells. Schottky barrier solar cells reported in literature[51,52] show quite erratic behaviour and the conversion efficiency under AMO illumination has never exceeded 1.5%. Very little work has been made on collection structures with thin film CdTe. The anomalous photovoltaic effect has been observed[53,54] in CdTe thin films but the photocurrents produced were extremely low due to the high film resistance.

The above mentioned low conversion efficiencies may be understood by looking at the minority carrier lifetime in CdTe. Some data obtained for different CdTe samples are shown in table (1.2)[55].

Table 1.2

(Minority-carrier lifetime data for some CdTe Samples)

Purity and Dopant	τ(s)	L(μm)
$n = 6.3 \times 10^{17}$ cm^{-3}. (I) $p = 1.7 \times 10^{17}$ cm^{-3}. (P) $n = 5.5 \times 10^{17}$ cm^{-3}. (In)	$\tau_p = 6.8 \times 10^{-9}$ $\tau_n = 10^{-10}$ $\tau_p = 5.4 \times 10^{-8}$	$L_p = 0.82$ $L_n = 0.01$ $L_p = 3.30$

The available data are not consistent probably because of the complexity of the point imperfections in CdTe. Diffusion lengths larger than the absorption length may be obtained in compensated CdTe, but these are not suitable for solar cells because of their too high resistivity. On the other hand, for doped CdTe, the measured diffusion lengths are too small. Bell et al have calculated that the theoretical efficiency for a p-n junction with 10^{16} cm^{-3} doping is 27% for very long lifetimes, but is reduced to 20% for $\tau = 10^{-7}$ S, to 10% for $\tau = 10^{-8}$ S and 3% for $\tau = 10^{-9}$ S. It appears that recombination losses will not be negligible for the doping range 10^{16} - 10^{17} cm^{-3}. Therefore, to obtain a lifetime of 10^{-6} sec, for both holes and electrons, and hence high conversion efficiencies, the concentration of deep recombination centres should be sufficiently low. The only economic method to achieve long lifetime in CdTe is to find a natural compensation process which minimizes the number of native defects that cause the short minority carrier lifetime in low resistivity materials.

(c) Infrared Elements

CdTe is well known as a good infrared transmissive material. With the advent of single crystal CdTe, many of the optical properties have been much improved and single crystal windows are now commercially available. When CdTe is mixed with HgTe, a continuous range of alloys with a direct energy gap, controllable by composition, from zero to 1.50 eV can be obtained. These mixed crystals (Cd_x $Hg_{(1-x)}$Te) can be used as detectors in the far infrared region.

More recently CdTe has been discussed as a material for very high power CO_2 laser windows and it indeed has potential in this area. The only disadvantage of this material is its low value of thermal conductivity and mechanical strength. However, it is clear that the extremely flat transmission from the band edge to $\sim$ 30μ is not easily matched by any other material of equal resistance to chemical attack. Thus, there should always

be a good application potential for CdTe and its mixed crystals in this area.

(d) Electro-optic Modulators

One important application of CdTe will most certainly be as an electro-optic modulator in both the near and the far infrared. In order to be useful for any modulation, the CdTe must be of high optical quality with few impurities and very little strain. Single crystals must be available with reasonable dimensions (the order of centimeters) and good homogeneity. A very high resistivity is also necessary to eliminate Ohmic losses and free carrier absorption. All of these important parameters have already been achieved in CdTe crystals grown in various laboratories, and CdTe modulators, just like IR windows are commercially available today.

(e) Luminescence

CdTe has a significant history as a material for electroluminescence diodes. In general all these investigations showed two important emissions; (1) approximately band-to-band emission into a shallow acceptor and (2) emission into an $\simeq$ 0.15 eV acceptor level. Both of these, therefore, lie in the infrared region. To shift the luminescence into the visible, alloying with ZnTe and particularly MgTe has been successful. By further alloying of CdTe-MgTe with Se the luminescence can be shifted far out into the green at 540 nm[8].

In all these solid solutions the general mechanism of the recombination appeared to be the same as in pure CdTe, namely an emission at two wavelengths, one close to the bandgap energy and another one of the order 10% less than bandgap energy.

In all these cases a drastic reduction in luminescent efficiency occurs between liquid nitrogen and room temperature. This behaviour is attributed to "killer" centres near the middle of the gap. It appears that CdTe and its alloys could have significant application as electro-

luminescent materials if these "killer" centres could be removed.

(f) Miscellaneous Applications

A variety of miscellaneous uses has been reported for CdTe. Some of the more interesting appliations are as photoconductors, Gunn diodes, microwave devices, substrates for various applications and for use in integrated optics. In some cases basic material limitations prevent practical use. In other cases either the material is not sufficiently developed or alternative materials offer advantages.

1.9 ASSOCIATED PROBLEM AREAS

As we have seen above, CdTe has significant application potential in several areas of solid state electronics. It is easily sublimed and, therefore, thin film device processing should lead to definite fabrication advantages. Even though most of the conditions for widespread uses are fulfilled with this material, CdTe is not widely used in semiconductor electronics today. This is due to three main problem areas concerned with (a) minority-carrier (killer) centres, (b) thin films and (c) electrical contacts.

(a) Minority Carrier Centres

Even though the behaviour of both types of majority carriers in CdTe have studied in detail, no comparable effort has been made to understand the behaviour of minority carriers in CdTe. This is somewhat surprising, since most of the applications potential of CdTe is in areas where minority carrier behaviour is of the greater importance.

The experimentally observed minority lifetime of CdTe is very short, but theoretically lifetimes > 10 μs should be achievable in CdTe even when doped to relatively low resistivities (10^{18} carriers/cm^3). Hole lifetimes of ≃ 1 μs have been observed for some samples even though there are a variety of compensating donor and acceptor centres present in concentrations of ∿ 10^{16} cm^{-3}. However, the concentration of midgap centres

in such materials is quite low. The "killer" centres near the middle of the bandgap are responsible for the low quantum efficiency of electro-luminescence (EL) diodes and the low open-circuit-voltages of solar cells. Since these are two significant applications for which CdTe holds high promise, it is very important to identify the chemical nature of the responsible centres. It is clear that centre gap killer centres in low resistivity n-type and p-type material must be more closely investigated, and their control would significantly enhance the practical utility of CdTe. In fact it appears that removal of such centres would greatly increase the lifetimes in both n- and p-type CdTe and thus would presumably allow preparation of far more efficient solar cells and room temperature EL diodes.

(b) Thin Film Problems

Although CdTe is quite easily prepared by sublimation, the thin film problem presents itself by the fact that only high resistivity films are frequently obtained and control of film properties is quite difficult. Reasonable control over the majority carrier properties is possible only for n-type material and only for a limited number of deposition methods. Good p-type material with low resistivity cannot be prepared and CdTe homojunctions are therefore not possible by thin film techniques. The majority carrier lifetimes in both n-type and p-type films are exceedingly short and no detailed investigation of minority carrier behaviour in thin films as a function of preparation conditions has been carried out.

(c) Electrical Contacts

For devices which require very low series resistances, such as solar cells, good electrical contacts are essential. Theoretically a good Ohmic contact may be achieved by establishing a proper work-function matching on the surface, and lowering the surface barrier by heavily doping the region underlying the contact. In both cases one has to start by

knowing the nature of the semiconductor surface which determines its electron emission behaviour. The uncleavable polar surfaces such as <111> (consisting only of Cd or Te atoms respectively) may have significantly different properties.

If surface states play an important role, then the work-function matching will not have any significant effect on the contacts. The true surface states, obtained under high vacuum conditions, will also be immediately modified by absorption when exposed to real atmosphere. Undoubtedly, this effect is significant for CdTe[52]. Most of the Schottky diodes prepared under high vacuum conditions increase their barrier height appreciably when exposed to air and even more when exposed to Ozone.

Since etching and heat treatments are also often employed before or during contact formation, further complications have to be considered. Among these are the loss of Cd from the surface and a consequent inversion of an n-type surface into p-type. However, when oxygen is present during heating, preferential oxidation of the Cd to CdO can occur on the surface. In this way, n-p-p structures on p-type material and n-p-n structures on n-type are formed. Hence the curious fact that one can sometimes obtain rectifications with all metals on both types of material can be explained. Finally, etching and subsequent rinsing can cause hydrolysis of Te ions and thus results in the deposition of Te on the surface, again falsifying results based on clean surface behaviour.

Another way of making contacts to CdTe is by electrochemical reactions. One reason for the popularity of such electroless contacts is obviously the fact that the electrochemical reaction proceeds significantly below the surface thus avoiding many of the cited surface complications. Another reason may well be that an actual lowering of the barrier occurs, because it has been demonstrated recently that the electrochemical exchange

does not generate pure metal on the surface but results in a mixture of Te and a metal-telluride. Clearly, it would be desirable to make a detailed investigation of the metallurgy of these contacts. In some classes of devices such as solar cells and γ-ray detectors, the contact problem appears to be one factor which causes a great deal of trouble.

CHAPTER 2

ELECTRICAL CONDUCTION IN SEMI-CONDUCTORS

2.1 D.C.CONDUCTIVITY

Electrical transport experiments provide information concerning many of the basic properties of a material, for example the type and number of mobile charge carriers that contribute to the conductivity. The effective scattering processes and some idea of the purity of the material may also be obtained. The influence of temperature on the conductivity is usually expressed via an activation energy. Analysis of both Ohmic and space charge limited activation energies can provide the positions and concentrations of deep impurity levels within the forbidden energy gap. The theory introduced by Roberts and Schmidlin for this purpose is summarized in section (2.1.1). An introduction to the Meyer-Neldel rule is also given at the end of this section. Hall effect and thermally stimulated current measurements have also been used to confirm some of the activation energy results. The relevant theories of these two techniques are reviewed in sections 2 and 3.

Reliable electrical contacts must be made to semiconductors if reproducible results are to be obtained. The different kinds of electrical contacts and their associated energy band diagrams are now described.

(a) Metal-Semiconductor contacts

Metal-semiconductor contacts play a very important role in determining the properties of most electronic devices[1]. These properties can be complex due to the presence of surface states and contamination. It is, however, of interest to investigate so called "ideal" contacts. A contact may be defined as ideal if the surfaces are free from contamination and the effects of surface states are ignored.

Fig (2.1) shows the situation for both n-type and p-type semi-

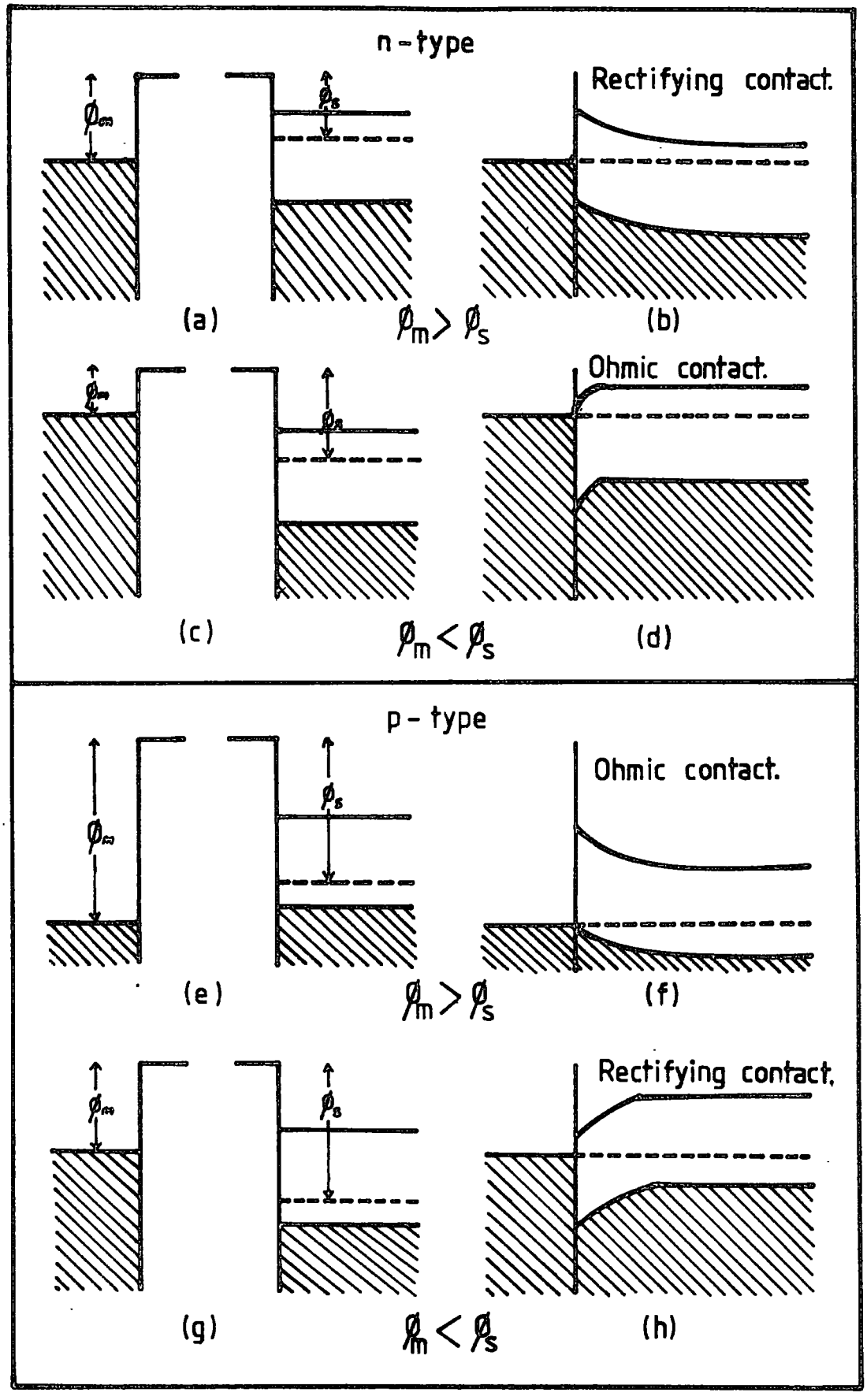

Fig. 2·1 Energy band diagrams for metal/semiconductor contacts Figures a, b, c, d show the situation for an n-type s/c; figures e, f, g, h describe contact to a p-type s/c. ϕ_m, ϕ_s are work functions of metal and semiconductor respectively.

conductors with metals having different work functions (the work function is the escape energy of an electron with energy corresponding to the Fermi level of the material). Only the contacts on n-type semiconductors are described here since it is evident that an alternative energy level scheme can be explained for a p-type semiconductor in a similar fashion.

As shown in fig (2.1a), consider a metal and an n-type semiconductor with work functions ϕ_m and ϕ_s respectively. If $\phi_m > \phi_s$ the Fermi level of the semiconductor lies above that of the metal before contact is made. When these two surfaces make an intimate contact with each other, electrons will flow from the semiconductor into the metal. Electronic equilibrium is established when the Fermi levels on both sides are lined up. The Fermi level of the semiconductor has been lowered by an amount equal to $\phi_{ms} = (\phi_m - \phi_s)$. This is called the contact potential. As a result a boundary layer is formed which has a high electrical resistance due to majority carrier depletion. This type of contact is therefore termed a rectifying contact and is described in detail in chapter 3.

If $\phi_m < \phi_s$, the Fermi level of the semiconductor lies below that of the metal before contact is made. In this situation electrons will flow from metal into the semiconductor and the band bending is shown in fig (2.1d). These electrodes provide a plentiful supply of majority carriers which can take part in the conduction process and are called "Ohmic contacts".

When contact is made to a p-type semiconductor, the very opposite effects to those described above take place. That is an "Ohmic" or injecting contact is produced when $\phi_m > \phi_s$ and a rectifying contact when $\phi_m < \phi_s$.

(b) Electronic transport in semiconductors

The electrical conductivity of a semiconductor depends on the number of mobile charge carriers it contains (electrons, holes or both), their distribution of thermal velocities, and the change from an equilibrium distribution caused by an applied electric field. The primary linear

relation for the conduction process is that between the drift velocity of an electron or hole and the applied electric field. As long as the drift velocities due to the external field are small compared to the mean thermal velocity, this relation takes the form

$$V = \mu E \tag{2.1}$$

In this equation, V is the drift velocity of the carriers, E is the electric field, and μ is a parameter called the drift mobility of the electrons or holes. The current density J is given by

$$J = \sigma E = n e \mu E. \tag{2.2}$$

and the conductivity σ by

$$\sigma = n e\mu = (N_c e\mu).e^{-\Delta E/kT}$$

where N_c is the effective density of states in the conduction band. This can be written as,

$$\sigma = \sigma_o . e^{-\Delta E/kT} \tag{2.3}$$

where ΔE is the activation energy, k the Boltzmann constant and T is the absolute temperature. If the $\log_{10} \sigma$ is plotted against the reciprocal of the absolute temperature, a straight line is obtained from whose slope the activation energy, ΔE, can be obtained. The intercept of this line on conductivity axis yields the value of the pre-exponential factor σ_o.

The temperature dependence of the electrical conductivity involves the contributions of both the carrier concentration and the carrier mobility. In the majority of materials, the temperature dependence of the mobility, as deduced from Hall effect measurements and transit time techniques, varies typically as T^n with $-3 \lesssim n \lesssim 3/2$ [2]. The effective density of states in

the transport bands vary as $T^{3/2}$. Consequently in the particular case of lattice scattering controlling the mobility ($\mu \alpha T^{-3/2}$), a relatively weak temperature dependent contribution is therefore to be expected from the product of mobility and state density. Should the mobility be controlled by impurity scattering ($\mu \alpha T^{3/2}$) then the logarithm of $J/_T 3$ versus reciprocal temperature might be expected to yield a straight line.

(c) Current injection in solids

By applying a sufficiently large electric field to a solid with suitable electrodes, the injection of charge carriers can be observed[3]. For this observation the electrodes must be Ohmic and the thermally generated carriers should be negligible. Another requirement is that the material must be relatively free from trapping effects. When the injection takes place a cloud of space charge carriers will form in the vicinity of the contacts. Mutual repulsion between the individual carriers limits the total injected charge in the crystal and the resulting current is said to be space charge limited (SCL). This is the solid-state analogue of the thermionic vacuum diode conduction. The fundamental differences between the two cases, however, arises due to the interaction between space charge and the crystal lattice, and the presence of trapping sites. If hole injection as well as electron injection (double injection) takes place in a solid, this then brings in the added complication of recombination. Consequently, the SCLC in a solid medium are lower than the corresponding ones in a vacuum by several orders of magnitude.

Mott and Gurney[4] were the first to obtain an approximate expression relating the current, voltage, and thickness for SCL currents in a trap free insulator. More refined treatments are now available and the one carrier SCLC is related to the voltage and thickness by

$$J = \frac{9}{8} \theta_n \varepsilon \mu_o \frac{V^2}{L^3} \qquad (2.4)$$

where μ_o is the microscopic mobility, ε is the permittivity and Θ_n is the fraction of injected carriers which are free. The above equation is a special case of the general scaling law for bulk space charge currents in a homogeneous medium which is

$$J \alpha L \left\{ \frac{V}{L^2} \right\}^n \tag{2.5}$$

where n is a constant which need not necessarily be an integer. For example in the trap free insulator case, n = 2, while for double injection, n = 3, and for recombinative space charge injection, n = $\frac{1}{2}$ (5,6).

In the case of double injection the current is proportional to V^3 and is given by(5)

$$J = 8\varepsilon\tau \mu_n \mu_p \frac{V^3}{L^5} \tag{2.6}$$

where μ_n and μ_p represent the mobilities of electrons and holes respectively.

The introduction of deep trapping centres in the crystal can result in very complicated current-voltage relations. The first approximate treatment of this problem was by Lampert(7) who considered a model containing a set of defect states at a single discrete energy level. Fig (2.2) illustrates the current-voltage curve that he predicted.

At low voltages, the injection of excess carriers is negligible and Ohm's law is observed. The current is carried by the thermally generated carriers and there is no significant departure of the Fermi-level from its steady state value. When the injected free electron concentration becomes comparable to the concentration of thermally generated carriers, the transition takes place from Ohmic to SCL at the voltage V_x. At this voltage both the Ohmic and SCL currents are equal. By equating

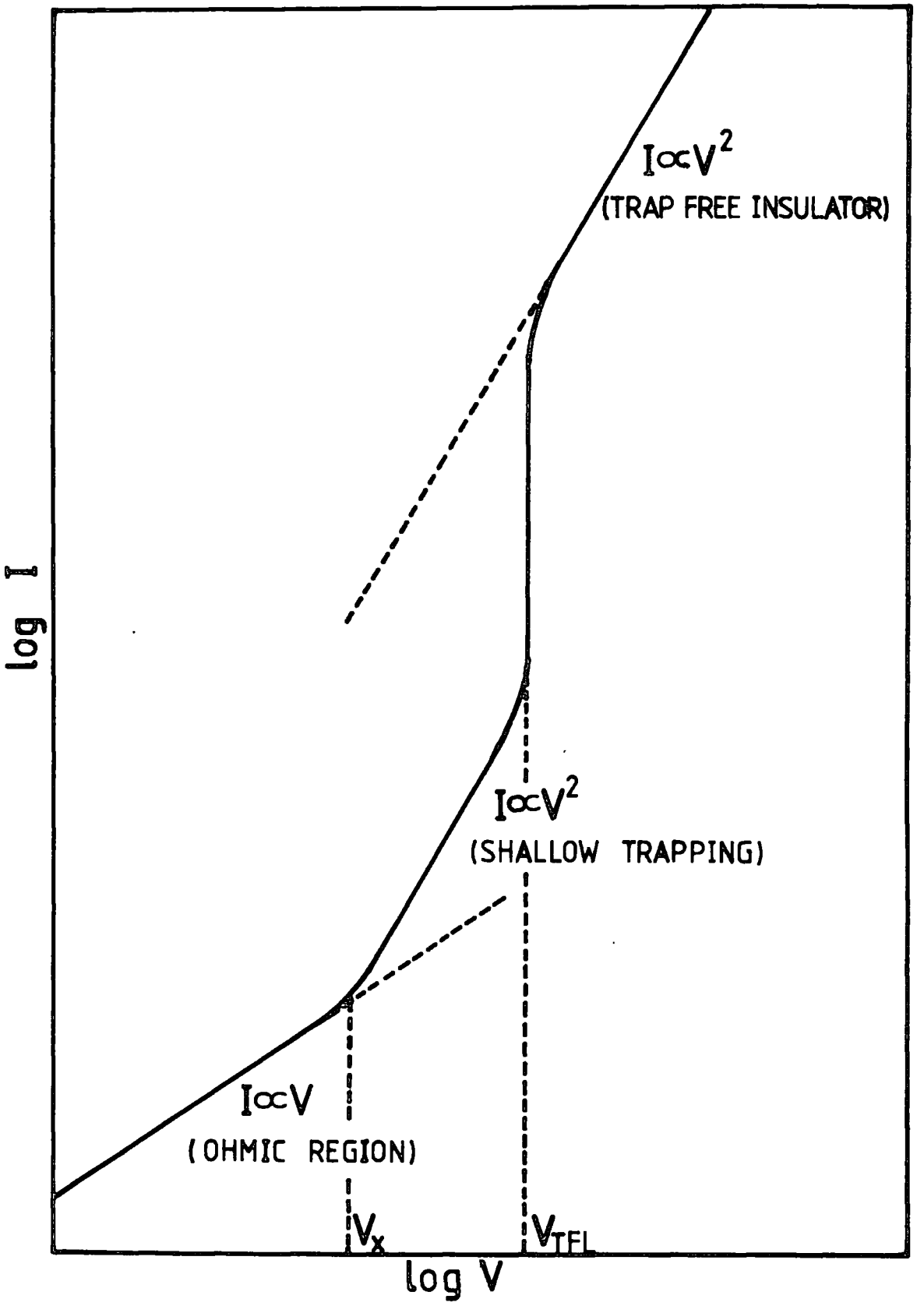

FIG. 2·2 SCHEMATIC CURRENT-VOLTAGE CHARACTERISTIC FOR ONE-CARRIER SCL CURRENT INJECTION CONTROLLED BY A SINGLE SET OF TRAPPING CENTRES.

the expressions (2.2) and (2.4) the crossover voltage can be obtained.

$$V_x = \frac{8(enL^2)}{9\varepsilon\Theta_n} \tag{2.7}$$

The level of injection of charge carriers increases with applied voltage and this corresponds to a motion of the Fermi level. When this motion is sufficient to fill a deep trapping level, all the injected space charge will enter the transport band and contribute to the conduction. This causes a steep rise in the current-voltage characteristics, at a threshold voltage V_{TFL}. This trap-filled-voltage can be related to the trap density, N_m by[3]

$$V_{TFL} = \frac{N_m eL^2}{\varepsilon} \tag{2.8}$$

For voltages greater than V_{TFL} the equation (2.4) applies with $\Theta_n = 1$.

2.1.1. The Simple Activation Energy

Activation energies for electronic conduction as described in the introduction to this chapter mainly depend on the bandgap of the material, the impurities involved and the temperature range of interest. The possible cases are discussed briefly in the following sections.

(a) Intrinsic semiconductors

The intrinsic excitation becomes dominant at high temperatures (where the energy gap is a small multiple of kT) in any reasonably pure intermediate bandgap semiconductors. The wide bandgap semiconductors or semi-insulators require an ultra-purification to observe this conduction below their decomposition or melting points.

In the case of intrinsic conduction, electrons are thermally excited from the valence band to the conduction band and the Fermi level,

E_F, is given by

$$E_F = Eg/_2 + kT/2 \cdot \ell n \left\{ \frac{N_v}{N_c} \right\} \qquad (2.9)$$

Normally, $\frac{kT}{2} \cdot \ell n \frac{N_v}{N_c}$ is small compared to $Eg/_2$ so that the intrinsic Fermi level lies close to the middle of the energy gap. The intrinsic carrier concentration calculated using the above expression is

$$n = P = (N_v N_c)^{\frac{1}{2}} \cdot \exp \left\{ -Eg/_{2kT} \right\} \qquad (2.10)$$

The activation energy, therefore, is equal to $Eg/_2$.

(b) Semiconductors controlled by partly compensated impurities

In the majority of the semiconductors, both donors and acceptors influence the conductivity. Energy considerations dictate that electrons, from shallow donor levels, fill up any vacant acceptor levels. Therefore, it is the difference between donor and acceptor concentrations that is important. When $N_a \simeq N_d$ the crystal is said to be compensated. In a material with partly compensated impurities the free carrier concentration is given by[8]

$$n = N_c \left\{ \frac{N_d - N_a}{N_a} \right\} \cdot \exp \left\{ (E_d - E_c)/kT \right\} \qquad (2.11)$$

The activation energy for conduction is $(E_d - E_c)$ for this type of material.

(c) Semiconductors controlled by a single uncompensated impurity species

For a material with an uncompensated donor species, the number of free electrons in the conduction band (assuming the non-degenerate situation) is given by[8,9,10]

$$n = \frac{N_c}{2} \cdot \exp \left\{ (E_d - E_c)/kT \right\} \cdot \left\{ -1 \pm \left[1 + \frac{4N_d}{N_c} \cdot \exp \left\{ (E_c - E_d)/kT \right\} \right]^{\frac{1}{2}} \right\} \qquad (2.12)$$

1. For low donor concentrations or high temperature values

$$\left\{\frac{4N_d}{N_c}\right\} \cdot \exp\left\{(E_c-E_d)/kT\right\} << 1$$

and therefore $n = N_d$. Under these conditions, all the donor atoms are ionized, their electrons being in the conduction band.

2. In the second limit

$$\left\{4N_d N_c\right\} \cdot \exp\left\{(E_c-E_d)/kT\right\} >> 1$$

and

$$n = (N_c N_d)^{\frac{1}{2}} \cdot \exp\left\{(E_d-E_c)/2kT\right\} \qquad (2.13)$$

Ideally, an activation energy plot for this type of material should fall into three distinct regions. At low temperatures the Fermi level is about midway between the conduction band and the donor level, and the electron concentration increases exponentially with an activation energy of $(E_d-E_c)/2$. In the exhaustion region where all the donors are ionized the electron concentration is approximately constant. The electron concentration where the curve is horizontal equals the donor concentration, N_d. Following the exhaustion range, for higher temperatures, intrinsic behaviour determined by equation (2.10) is observed.

(d) Activation energy in a compensated semiconductor

The thermal activation energy for electrical conduction in semiconductors and insulators is traditionally interpreted in one of these three possible ways, i.e. half the bandgap (material presumed intrinsic), some trap depth (material presumed extrinsic), or half the trap depth (material highly doped). Even for these simple situations, it is clear that extreme care must be exercised in interpreting activation energy

curves. These interpretations, corrected appropriately to account for degeneracy, are frequently correct for relatively narrow bandgap (E_g < 1.00 eV) semiconductors. However, a fourth possibility exists that is particularly relevant to wide-bandgap semiconductors. Roberts and Schmidlin[8,9] have solved this statistics problem and confirmed the theory by application to some new measurements on materials like HgS, GaP, CdS and ZnS:Cd. The following section summarizes the original statistical theory introduced by these authors.

In narrow bandgap materials, the transport bands (conduction and valence) control the electrical conduction, whereas in wider bandgap materials some localized levels within the gap tends to be dominant instead. The importance of these dominant levels is that their concentrations and locations in energy together with the concentration of electrons contributed by excess donors, completely determine the location of the Fermi energy. Consider the model described in the schematic band diagram in fig.(2.3a), showing the arbitrary reference level E_o and localized levels i and j.

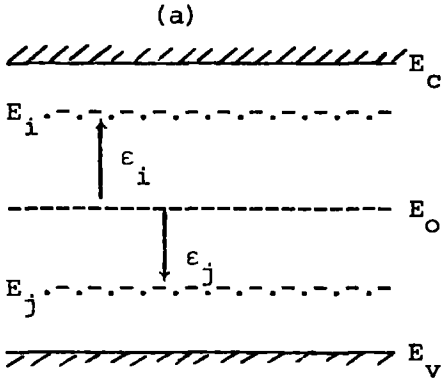

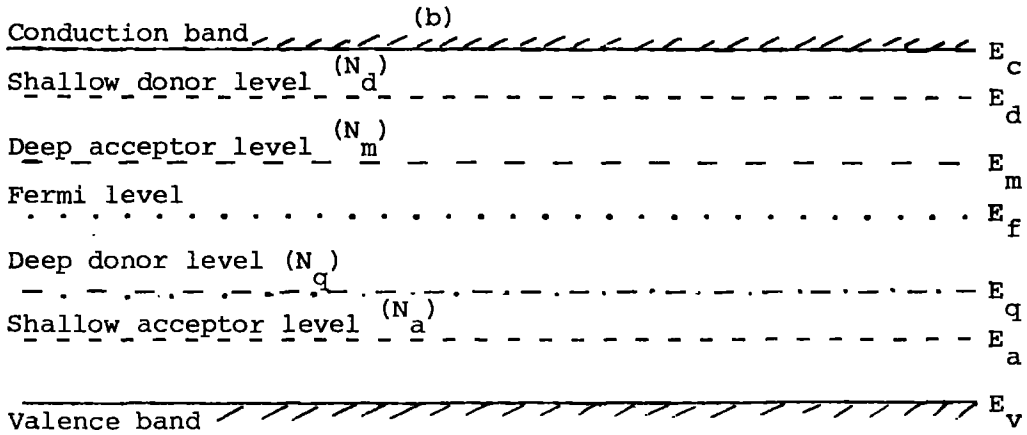

Fig (2.3)

The position of the Fermi level E_f is determined by the constraint

$$N = \sum_i n_i = \sum_i N_i \left\{ 1 + \exp (E_i - E_f)/kT \right\}^{-1}$$

where $$N = N_v + N_d + \sum_{j=1}^{k} N_j - N_a$$

is the total number of electrons in the system. N_j is the number of localized states at one of k possible levels below the Fermi level and n_i is the number of electrons occupying the ith level. Other symbols have their usual meanings. When the Fermi level happens to fall away (by few kT) from a relatively concentrated local level, Maxwell Boltzmann statistics are a good approximation for the distribution of the carriers and the above equation becomes

$$(N_d - N_a) = XQ_e - Q_p/X \qquad (2.14)$$

where

$$X \equiv \exp(E_f - E_o)/kT.$$

$$Q_e \equiv N_e . \exp(-\varepsilon_c/kT) + \sum_i N_i . \exp(-\varepsilon_i/kT).$$

$$Q_p \equiv N_v . \exp(-\varepsilon_v/kT) + \sum_j N_j . \exp(-\varepsilon_j/kT).$$

The terms contained in Q_e and Q_p are simply the partition functions for the electrons and holes. The largest terms in each partition function define the dominant levels which are designated by the subscripts m (for electrons) and q (for holes). In general E_m may be E_c or some E_i while E_q may be E_v or some E_j. These levels are shown in fig (2.3b). For n-type materials ($N_d > N_a$), the meaningful solution to eqn. (2.14) is

$$X = (N_d - N_a)/2Q_e + \left[\left\{ (N_d - N_a)/2Q_e \right\}^2 + Q_p/Q_e \right]^{\frac{1}{2}} \qquad (2.15)$$

For p-type material ($N_a > N_d$), the negative square root should be chosen which gives the equivalent solution for holes.

In general, the results represented by equation (2.15) lead to activation energies for electronic conduction which vary continuously with temperature. To obtain a constant activation energy (that is, a straight line segment on a plot of logJ versus $\frac{1}{T}$) two conditions must be satisfield.

First, single terms in Q_e and Q_p, due to the dominant levels E_m and E_q, must dominate the statistics ;

that is $Q_e \simeq N_m.\exp(-\varepsilon_m/kT)$ and $Q_p \simeq N_q.\exp(-\varepsilon_q/kT)$

Second, (N_d-N_a) must either be much greater than $2(Q_eQ_p)^{\frac{1}{2}}$ or much less than $2(Q_eQ_p)^{\frac{1}{2}}$.

When $(N_d-N_a) >> 2(Q_eQ_p)^{\frac{1}{2}}$, equation (2.15) yields

$$E_f = E_m + kT.\ \ell n \left\{ (N_d-N_a)\ /N_m \right\} \qquad (2.16)$$

and

$$n = X\,N_c.\exp\,(-\varepsilon_c/kT) = \frac{(N_d-N_a)N_c}{N_m}.\exp\left\{(E_m-E_c)/kT\right\} \qquad (2.17)$$

when $(N_d-N_a) << 2(Q_eQ_p)^{\frac{1}{2}}$, equation (2.15) yields

$$E_f = \frac{1}{2}\ (E_m + E_q) + \frac{1}{2}\,kT.\ \log_e\,(N_q/N_m) \qquad (2.18)$$

and

$$n = N_c\left\{\frac{N_q}{N_m}\right\}^{\frac{1}{2}}.\exp\left[\left\{(E_m-E_c) + \frac{1}{2}\ (E_q-E_m)\right\}\ /kT\right] \qquad (2.19)$$

To compute the activation energies for conduction we need to calculate the population of carriers in the transport bands. In general, the relative population of states for each carrier is given by the ratio of terms in their respective partition functions. Thus the fraction of

total carriers which are in the transport bands are

$$\theta_n = \frac{N_c.\exp(-\varepsilon_c/kT)}{\varrho_e} \quad \text{and} \quad \theta_p = \frac{N_v.\exp(-\varepsilon_v/kT)}{\varrho_p}$$

for the electrons and holes respectively. But when one level dominates the statistics for each carrier, the θ factors simplify to

$$\theta_n = \frac{N_c}{N_m} . \exp(E_m-E_c)/kT \quad \text{and} \quad \theta_p = \frac{N_v}{N_q} . \exp(E_v-E_q)/kT \qquad (2.20)$$

The Ohmic and SCL currents were discussed in the earlier part of this chapter and are given by

$$J_n = ne\mu \frac{V}{L} \quad \text{and} \quad J_{sc} = \frac{9}{8} \theta_n \varepsilon\mu_o \frac{V^2}{L^3} .$$

In general both these currents are thermally activated and their corresponding activation energies are contained in n and θ_n.

Thermal activation energies according to equation (2.17) and equation (2.19) are given by (E_m-E_c) and $(E_m-E_c) + \frac{1}{2}(E_q-E_m)$. The activation energy for SCL conduction is equal to (E_m-E_c), and identical with the first case. In the second situation, however, the two activation energies (Ohmic and SCL) are different and the activation energy for Ohmic conduction is greater than this by half the separation between the dominant levels for the electrons and holes. These two cases are known as extrinsic and non-extrinsic, and the direct comparison between the two situations enabled Roberts and Schmidlin[9] to present the following theorem.

"The existence of different (or identical) activation energies for Ohmic and SCL conduction is both a necessary and a sufficient condition for Ohmic conduction to be non-extrinsic (or extrinsic)".

As a result of self-compensation in wide bandgap semiconductors, the excess donor concentration, (N_a-N_d), can be smaller than the concentra-

tion of electrons excited from the dominant hole level (E_q) to the dominant electron level (E_m). In such a situation the Fermi energy is located between the two dominant levels in such a way as to equalise the concentrations of electrons and holes in the E_m and E_q levels. This is known as the non-extrinsic situation.

In fact, when the electronic conduction is controlled by transport bands (E_c and E_v) instead of dominant levels (E_m and E_q) in the forbidden gap, equation (2.19) reduces to the familiar intrinsic equation given by (2.10).

Now it is clear that a change in the activation energy with temperature for Ohmic conduction can occur whenever a new term in the electron-and hole-partition functions becomes dominant, or the Fermi energy crosses a sufficiently dense level to change the relationship between the contributed and non-extrinsic carrier concentrations. A transition can also occur when the "majority" carrier shifts from electrons to holes or vice-versa. Roberts and Schmidlin have discussed,in detail, the causes and the rules for interpreting the temperature-induced changes in activation energies in their article[9].

It is apparent, therefore, that the dominant level approximation is a generally useful method for interpreting Ohmic activation energies, particularly in wide band gap materials. This theory has been used to analyse the D.C. conductivity measurements on semi-insulating CdTe presented in this thesis. It was found that the graphical method[9] of solving the statistics problem introduced by the same authors is very useful for the analysis. The following section describes this method in detail.

2.1.2. Graphical Analysis

This technique is useful, for finding the position of the Fermi energy, to identify dominant state densities and to visualize the temperature induced changes in the activation energy.

The energy levels in equation (2.14) are measured relative to an arbitrary reference level E_o. If E_o is chosen to be the Fermi level, then the number of electrons in a state with density, N_i, is

$$n_i = N_i . \exp(-\varepsilon_i / kT)$$

Therefore,

$$\log_{10} n_i = \log_{10} N_i - 0.434 . \frac{\varepsilon_i}{kT} \qquad (2.21)$$

Fig (2.4) shows a schematic diagram of $\log_{10} N_i$ as a function of energy. The extremities of the energy axis are the conduction and valence band edges. N_d and N_a are assumed to be shallow donors and acceptors, while the other levels are assumed to be deep traps. A "V" is constructed in fig (2.4) with sides having a slope of $\pm$ 0.434/kT and with an apex that lies somewhere on the energy axis. When the apex of the "V" is at the Fermi energy then it follows from equation (2.21) that the vertical extensions of the state densities above the left-hand side of the "V" are equal to the electron population on those states. Similarly the vertical extensions of the state densities above the right-hand side of the "V" are equal to the hole population of those states. Then the two states which have the longest extension on the two sides of the "V" are important and these two dominant levels control the electronic conduction.

When a "V" (having an appropriate slope for the temperature) slides along the energy axis two conditions can be obtained.

1. The total number of electrons equals the total number of holes, which is the non-extrinsic condition. That is, the extensions of the two dominant levels above the "V" matches together and this is shown in fig 2.4a.

2. The total number of electrons equals $(N_d - N_a)$, which is the extrinsic conduction. That is, the extension of the dominant electron level above the "V" matches the $\log_{10}$(excess donor concentration). This is

Fig. 2·4

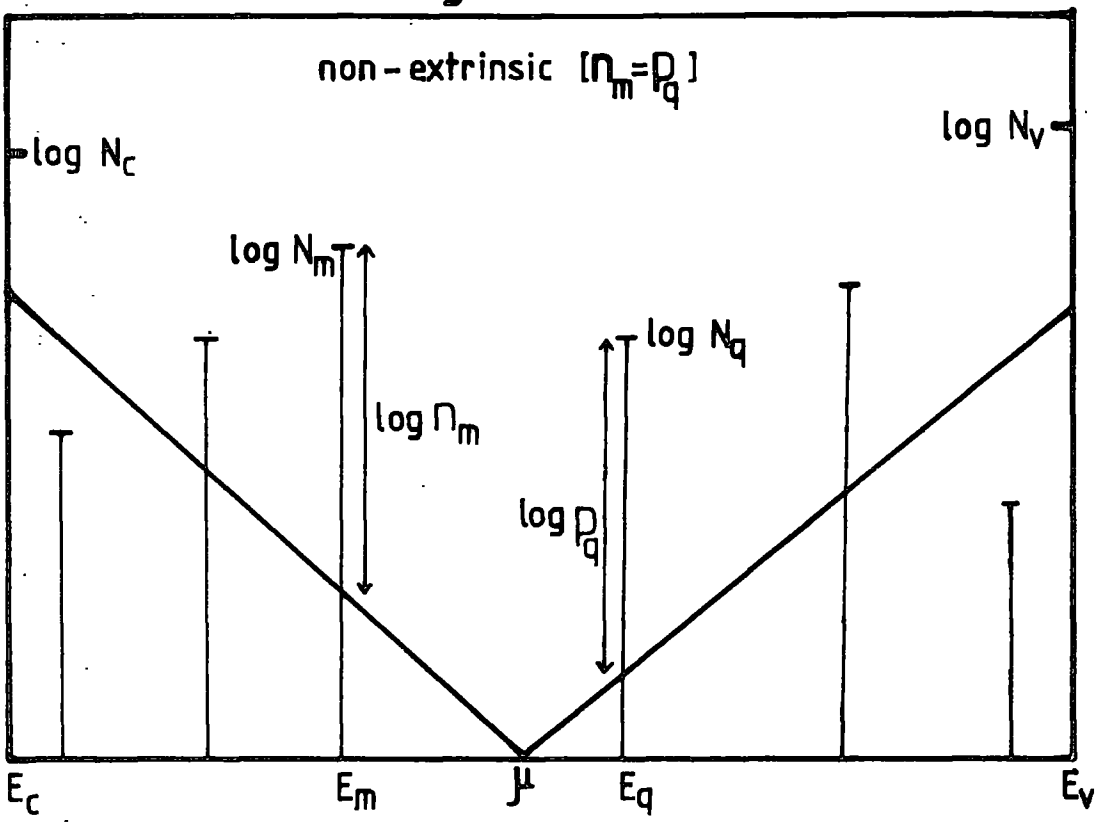

(a). Graphical analysis of the population of states in an non-extrinsic semiconductor.

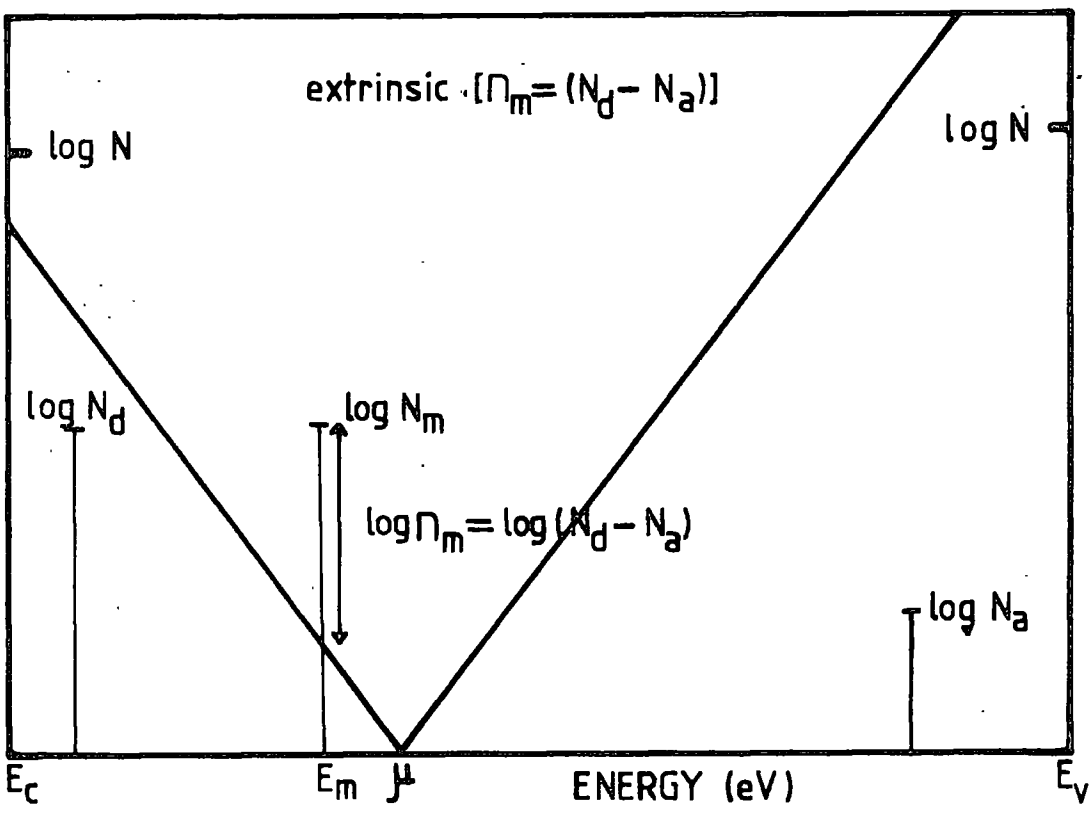

(b). Graphical analysis of the population of states in an extrinsic semiconductor.

illustrated in fig 2.4b.

Once the activation energies for Ohmic and SCL conduction are known, the solution obtained from this method is unique.

2.1.3 The Meyer-Neldel Rule

The electrical conductivity of many materials is found to obey the Arrhenius relation given by equation (2.3)

$$\sigma = \sigma_o \cdot \exp(-\Delta E/kT)$$

Arrhenius plots which are obtained when $\ell n\ \sigma$ is plotted as a function of reciprocal temperature are usually found to consist of straight line regions for most semiconducting and semi-insulating materials. Activation energies (ΔE) and the pre-exponential factors (σ_o) may be calculated from the slope and the intercept of these straight line segments. Many solids[11,12,13], especially organic semiconductors[14,15] exhibit different activation energies for electrical conduction depending on their method of preparation. For these solids the experimental data are usually presented as a series of straight-line activation-energy plots which extrapolate to a common focal point at a temperature T_c.

This behaviour was first observed by Meyer in 1933. Subsequently Meyer and Neldel (1937)[16] showed that there was a linear relationship between the slopes (ΔE) and intercepts (σ_o) of the conductivity Arrhenius plots for various solids. This may be written

$$\log \sigma_o = \alpha \cdot \Delta E + \beta \qquad (2.22)$$

where α and β are constants. This equation is often referred to as the Meyer-Neldel or compensation law.

Rosenberg et al (1968)[17] showed that equation (2.3) was incomplete in the case of activation energy curves intercepting at a focal point $T = T_c$ and not infinity. To explain their results these authors

suggested a three constant equation of the form

$$\sigma = \sigma_o' \cdot \exp(\Delta E/kT_c) \cdot \exp(-\Delta E/kT) \qquad (2.23)$$

The additional constant T_c, was referred to as the characteristic temperature. Comparing equations (2.3), (2.22) and (2.23) shows that

$$\alpha = (kT_c)^{-1} \quad \text{and} \quad \beta = \log_e \sigma_o' . \qquad (2.24)$$

Rosenberg et al (1968)[17] have tabulated results for a number of organic substances and show T_c to vary from 270 K to infinity. They suggest that this parameter is a molecular property of the material and is independent of the crystal structure and the nature of the electrodes.

Although there have been several attempts to explain the Meyer-Neldel rule for specific experimental data (Nespurek et al (1976), Dewsbery (1976)), to date there is no general theory for this empirical relationship. Roberts (1971)[18] has discussed the Meyer-Neldel rule in terms of non-extrinsic conduction. This author considered a solid which is subjected to a disturbance so that the statistical distribution of carriers in the energy gap is changed, and derived expressions relating the characteristic temperature to the state densities and energy levels before and after the disturbance. The analysis assumes that the carrier mobilities are unaffected by this disturbance. As an example suppose a level E_{m1} of density N_{m1} (in an p-type solid) is replaced as the dominant hole level by a state with density N_{m2} and energy E_{m2}. At the same time although the dominant electron level remains at the same energy, its density is altered to N_{q2}. The conductivity versus reciprocal temperature curves (in the non-extrinsic region) before and after the disturbance will then intersect at $T = \infty$ provided

$$\frac{N_{m2}}{N_{m1}} = \frac{N_{q2}}{N_{q1}} \qquad (2.25)$$

Following the approach of Roberts'(1971) paper, the following condition is obtained for a finite focal point to be observed in the case of non-extrinsic conduction.

$$\frac{N_{m2}.N_{q1}}{N_{m1}.N_{q2}} = \exp\left\{\frac{E_{m2}-E_{m1}}{kT_c}\right\} \qquad (2.26)$$

Using equation (2.17), a similar expression can be obtained for the case of extrinsic conduction.

A distribution of states[19] in the forbidden gap can also account for a finite characteristic temperature and constraints required can be obtained with the basic parameters of the system. However, in a real solid complications can occur due to several reasons and therefore the effects could be more complex. This is discussed further in section 5.2(g) in terms of multivalent centres to explain the observation of Meyer-Neldel effect in semi-insulating CdTe:Cl.

2.2 HALL EFFECT

Measurements of electrical conductivity yield information about the product of carrier density and mobility. The Hall effect, measured simultaneously with conductivity, makes it possible to determine the sign of the charge carriers, their density, and their mobility as separate quantities. The temperature dependence of conductivity and carrier density also provides extra information about the impurity levels within the forbidden gap of a semiconductor. The effect was discovered by E.H.Hall in 1879 during an investigation of the nature of the force acting on a conductor carrying a current in a magnetic field. This has developed into one of the most powerful tools for studying the electronic properties of semiconductors[20].

One-Carrier Conduction

When charge carriers in a semiconductor are subjected to a magnetic field, B, as well as an electric field, E, then the total force on a hole

of velocity V is given by

$$F = e\left[E + (V \times B)\right] \tag{2.27}$$

The effect of the magnetic field is constantly to change the direction of the motion of the hole (fig 2.5b), since the Lorentz force is in the direction of (V x B). Therefore, in the steady state, the total electric field, E, has components parallel to and perpendicular to the current density, J. Under these combined influences, the steady-state solution of the Boltzmann equation is[2]

$$\sigma E = \left[J - (R_H). J \times B \right] \tag{2.28}$$

where σ is the conductivity of the semiconductor and the parameter R_H is called the Hall coefficient. This quantity (which determines the magnitude of the response perpendicular to both current and magnetic field) is given by

$$R_H = \frac{r}{pe} = \frac{\langle\tau^2\rangle}{\langle\tau\rangle^2} \cdot \frac{1}{pe} \tag{2.29}$$

The dimensionless quantity r is called the Hall factor. It depends on the combination of scattering process and on how the free time between collisions (τ) varies with electron energy.

For semiconductors with spherical constant energy surfaces, $\tau = a.E^{-S}$, where a and S are constants. $S = \frac{1}{2}$ for phonon scattering and $S = \frac{3}{2}$ for ionized impurity scattering. Using the general form of τ,[21]

$$\langle\tau^2\rangle = a^2(kT)^{-2S} . \Gamma(\tfrac{5}{2} - 2S) \; / \; \Gamma(\tfrac{5}{2}) \quad \text{and}$$

$$\langle\tau\rangle^2 = \left[a\,(kT)^{-S} . \Gamma(\tfrac{5}{2} - S) \; / \; \Gamma(\tfrac{5}{2}) \right]^2$$

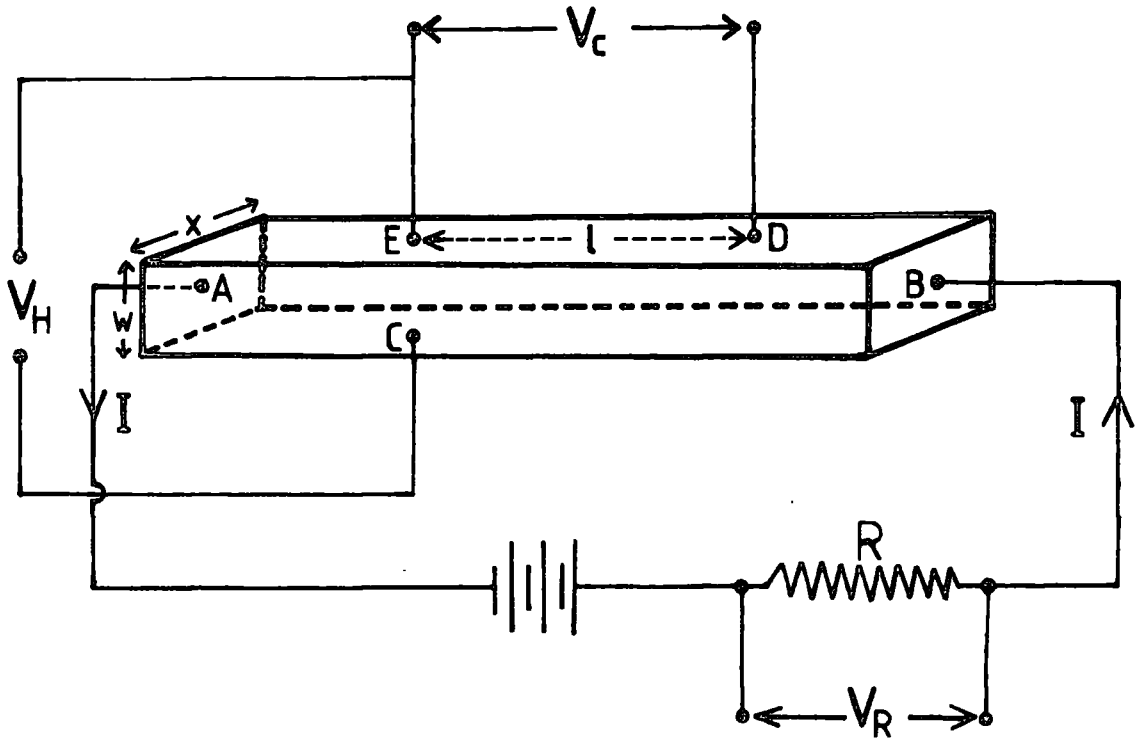

FIG. 2·5a BASIC SETUP FOR HALL EFFECT EXPERIMENT.

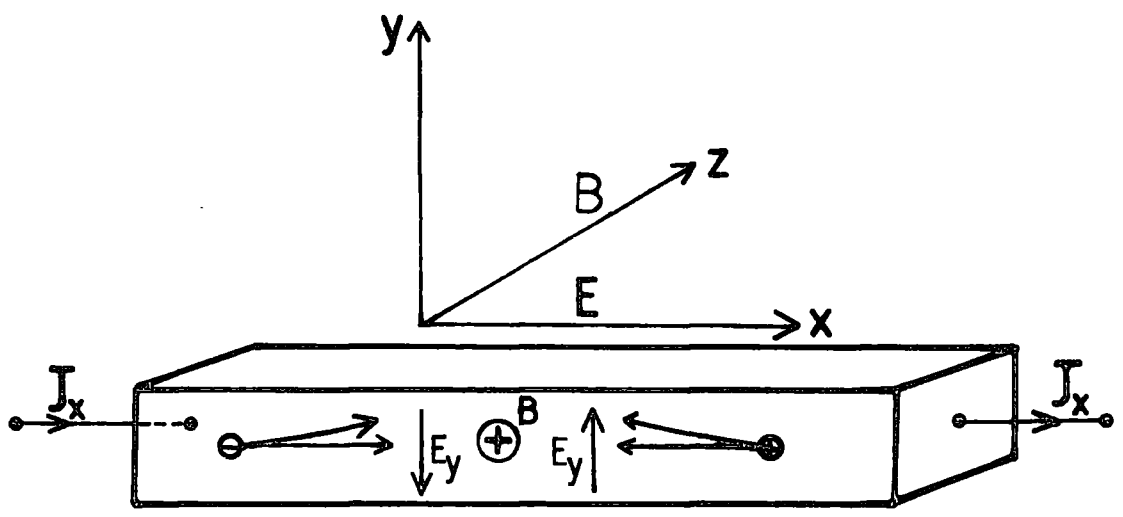

FIG. 2·5b THE EFFECT OF LORENTZ FORCE ON ELECTRONS AND HOLES.

In the above expressions $\Gamma(n)$ is the gamma functions defined as

$$\Gamma(n) = \int_0^\infty x^{n-1} \cdot e^{-x} \cdot dx, \quad (\Gamma(\tfrac{1}{2}) = \sqrt{\pi})$$

The value of r can now be evaluated for different scattering mechanisms.

$$r = \frac{3\pi}{8} = 1.18 \text{ for phonon scattering and}$$

$$r = \frac{315\pi}{512} = 1.93 \text{ for ionized impurity scattering.}$$

The Hall mobility μ_H is defined as the product of Hall coefficient and conductivity,

$$\mu_H = |\sigma R_H| \tag{2.30}$$

This quantity should be distinguished from the drift mobility, $\mu = \mu_H/r)$, which does not contain the factor r.

The Hall coefficient (R_H) and the conductivity (σ) can be calculated in terms of experimentally measured values (fig.2.5a), by using the following relations,

$$R_H = \frac{V_y \cdot d}{B_z \cdot I_x} \tag{2.31}$$

$$\sigma = \frac{\ell \cdot I_x}{V_x \cdot bd} \tag{2.32}$$

These results have been used to analyse the Hall effect measurements presented in chapter 6.

2.3 THERMALLY STIMULATED CURRENTS

This method of analysing trap densities and positions was introduced by Urbach (1930)[22], but did not come into extensive use until the work of Randall and Wilkins (1945)[23] was published. When a crystal is excited at a low temperature so as to fill trapping centres and is then heated in the dark, the resultant conductivity is temporarily enhanced. This procedure gives rise to a series of peaks in the current versus temperature curve which is known as the thermally stimulated current (TSC) spectrum. Simultaneously light can be emitted which is known as thermally stimulated luminescence (TSL) or thermoluminescence. These two types of experiments are often used to investigate the trapping parameters of a semiconductor. Kivits and Hagebeuk[24] (1977) have reviewed all the available techniques by which TSC and TSL curves can be analysed to yield information concerning the associated traps. About 31 different methods have been published to date, some for TSC and others for TSL. In practice, however, many of the methods are applied to both types of curve without proving that this is permissible. In the literature, the results of some of these methods are compared experimentally. It has been found that different methods do not produce the same trap depth for a given TSC or TSL peak.

In the following sections the recombination kinetics associated with the thermal release of electrons from traps is considered (a similar treatment applies to hole traps). Then the various techniques which have been used in the analysis of TSC results are described. The experimental results obtained for Cl-doped CdTe are presented and compared with those reported in Chapter 5.

2.3.1 Basic Theory for TSC

The simple model which one generally uses to describe the TSC process is shown in fig (2.6). Electrons are thermally excited from trap

N_t to the conduction band (transition 1) where they contribute to the conduction. From this band they can either be retrapped (transition 2) or can recombine with a hole trapped at a recombination centre a (transition 3). The latter transition may be accompanied by the emission of light.

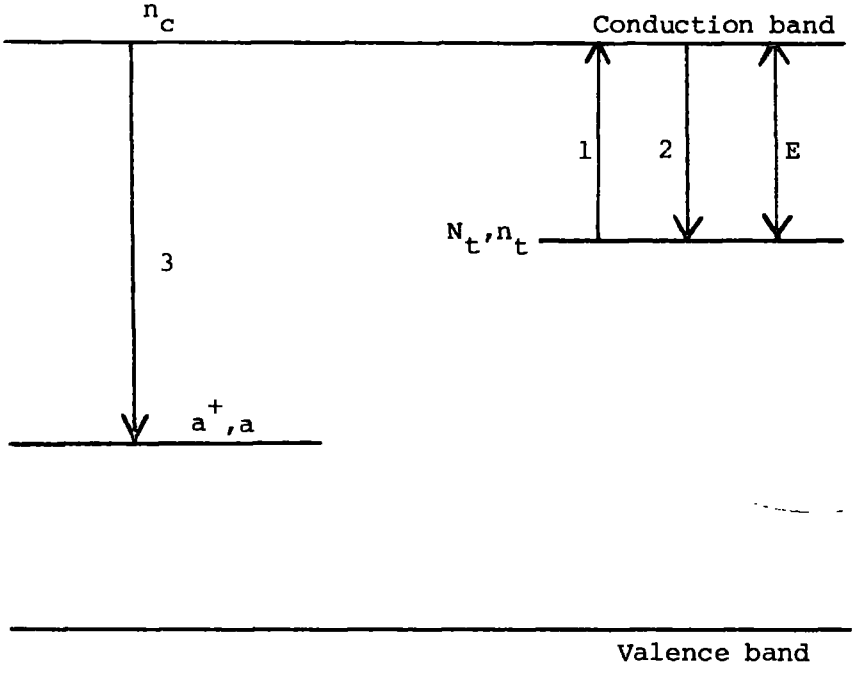

Fig (2.6)

The probability, p, of an electron escaping from a trap at a temperature T is given by

$$P = \nu \cdot \exp(-E/kT) \qquad (2.33)$$

where, k is the Boltzmann constant, and ν is the attempt to escape frequency of the electron. Also

$$\nu = N_c V S_t \qquad (2.34)$$

where N_c is the effective density of states in the conduction band, V is the thermal velocity of the electrons (proportional to $\sqrt{T}$) and S_t is the cross-section for capture of electrons by traps.

The rate of change of the trapped electron density, n_t, and the

free electron density in the conduction band, n_c, are given by the equations

$$\frac{dn_t}{dt} = -n_t \nu . \exp(-E/kT) + \gamma . n_c (N_t - n_t) \qquad (2.35)$$

and

$$\frac{dn_c}{dt} = -\frac{dn_t}{dt} - \alpha . n_c a^+ \qquad (2.36)$$

In which γ and α are trapping and recombination rate constants ($cm^3 s^{-1}$). These coefficients are given by

$$\alpha = S_r V \quad \text{and} \quad \gamma = S_t V \qquad (2.37)$$

where S_r is the cross-sections for capture of electrons by recombination centres. Assuming that the recombination lifetime $\tau_r = 1/\alpha a^+$ is short and therefore that $\frac{dn_c}{dt} << \frac{n_c}{\tau_n}$, eqn. (2.36) becomes

$$n_c = \tau_r \cdot \frac{dn_t}{dt} \qquad (2.38)$$

Equations (2.35) and (2.38) govern the process of emptying trap of density N_t, as a function of time. The heating rate β and the temperature are given by

$$\beta = \frac{dT}{dt} \quad \text{and} \quad T = T_o + \beta t \qquad (2.39)$$

Three limiting cases of the recombination kinetics are usually considered.

(a) Monomolecular kinetics

Under these conditions there is no appreciable retrapping of freed electrons (i.e. $S_t << S_r$). The equation (2.35) simplifies to

$$\frac{dn_t}{dt} = -n_t \nu . \exp(-E/kT) \qquad (2.40)$$

If the temperature at the start of the heating is T_o and the density of filled traps at this temperature is n_{to}, then from equations (2.38) and (2.40)

$$\sigma = n_c e \mu_n = n_{to} \tau_n e \mu_n \nu . \exp\left[-(E/kT) - \int_{T_o}^{T} \frac{\nu}{\beta} \exp(-E/kT) . dT\right] \tag{2.41}$$

where σ is the thermally stimulated conductivity at a temperature T.

(b) Bimolecular kinetics

Garlick and Gibson (1948) considered the case where a free electron has equal probability of recombining or of being retrapped (i.e. $S_t = S_r$). The resultant conductivity then becomes[25]

$$\sigma = \frac{n_{to}^2 \tau_n e \mu_n \nu . \exp(-E/kT)}{N_t \left[1 + \frac{n_{to} \nu}{N_t \beta} \int_{T_o}^{T} \exp(-E/kT) dT\right]^2} \tag{2.42}$$

An important feature of bimolecular recombination is that the temperature T_m of the maximum conductivity, depends on the extent of trap filling, whereas T_m is independent of the ratio n_{to}/N_t in the monomolecular case.

(c) Fast retrapping

Under these conditions a freed electron has a high probability of being retrapped. i.e. $S_t >> S_r$. Fast retrapping has been considered by several authors, and Haering and Adams (1960) have shown that the TSC is described by[22]

$$\sigma = \frac{N_c n_{to} e \mu_n}{N_t} . \exp\left[-(E/kT) - \frac{1}{N_t \beta \tau_n} \int_{T_o}^{T} N_c . \exp(-E/kT) dT\right] \tag{2.43}$$

2.3.2 Methods of Analysing TSC

In this section the methods utilized to evaluate TSC results are summarized. Only five methods were used in this analysis and the first method was selected due to its historical value and simplicity.

1. Randall and Wilkins method

This is the earliest published method for trap depth determination although Franz Urbach must be considered as the founder of thermoluminescence theory. In this method it is assumed that p=1 for $T = T_m$ and the trap depth is given by

$$E = 25\ kT_m \tag{2.44}$$

2. Garlick and Gibson method

The technique devised by Garlick and Gibson (1948) for the analysis of TSC curves is independent of the recombination kinetics operative during trap emptying. In the initial stages of the release of electrons from traps the integrals in (2.41), (2.42) and (2.43) are negligibly small and consequently

$$\sigma = \text{constant} \times \exp(-E/kT) \tag{2.45}$$

The constant is different for each of the three limiting cases. If N_c and μ_n are independent of temperature, then a plot of the logarithm of the current as a function of 1/T for the initial part of the rising side of a TSC peak should give a straight-line of slope -E/k. Some authors have concluded that this method becomes more accurate for larger S and lower E values. This also becomes more accurate if the analysis is done on the currents less than 15% of maximum value[24].

3. Hoogenstraaten method

The thermally stimulated conductivity as a function of temperature is given by equation (2.41) for the case of negligible retrapping. The

temperature, T_m, corresponding to the maximum value of σ for a given trap depth E, can be calculated by setting $d(\ell n\sigma)/dT = 0$. If we neglect the temperature dependence of τ, N_c, S and ν, then[26]

$$E = kT_m . \ell n \left\{ \frac{N_c S \nu k T_m^2}{\beta E} \right\} \tag{2.46}$$

This can be rewritten with the substitution $\nu = N_c SV$ as

$$\ell n \left\{ \frac{T_m^2}{\beta} \right\} = \frac{E}{kT_m} - \ell n \left\{ \frac{\nu k}{E} \right\} \tag{2.47}$$

Hence a plot of $\ell n \left\{ \frac{T_m^2}{\beta} \right\}$ versus $\left\{ \frac{1}{T_m} \right\}$ should yield a straight line with a slope E/k. This method for trap depth determination was originally derived by Bube for TSC.

4. The Quasi Fermi Level (Bube's) Method

This method is only valid when the traps empty under conditions of fast retrapping. Bube(1955) assumed that the Fermi level coincides with the trapping level when the conductivity is a maximum. According to Bube, therefore, it is only necessary to evaluate the position of the Fermi level at the maximum to obtain the trap depth, i.e.[23]

$$E = kT_m . \ell n(N_c/n_c^*) \tag{2.48}$$

where n_c^* is the density of freed electrons at the maximum temperature, T_m. Eliminating n_c^* in terms of the maximum conductivity, σ_m, the position of the Fermi level is given by

$$E = kT_m . \ell n \left\{ \frac{N_c e \mu}{\sigma_m} \right\} \tag{2.49}$$

At low heating rates where the condition of thermal equilibrium should be more nearly followed, this method should produce more reliable values of trap depths.

5. Chen 4 Method

Some methods making use of geometrical approximations are also available for analysis of TSC and TSL curves. The general shape of a TSC curve is shown in the figure with definition of some characteristics quantities. These quantities have been used for the derivation of several expressions for the trap depth. In this particular method the following expression is obtained.

$$E = 1.52.\ kT_m^2/\lambda - 3.16\ kT_m \qquad (2.50)$$

Since all quantities in this equation are measurable, E can be evaluated.

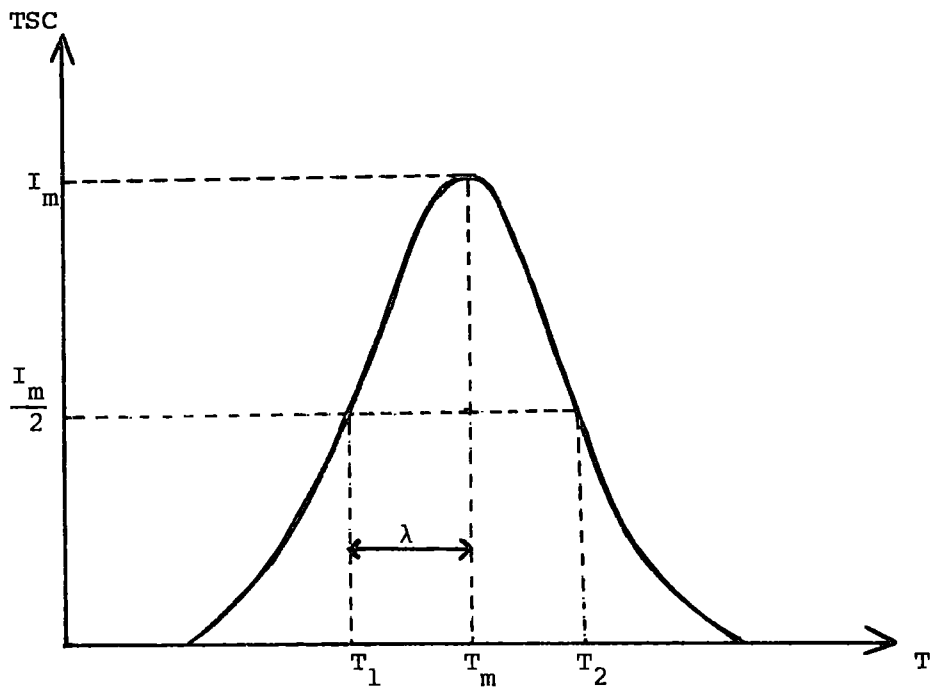

CHAPTER 3

THEORY: ELECTRICAL CONDUCTION ACROSS INTERFACES

The results presented in Chapter seven deal mainly with the electrical properties of Schottky barriers and associated solar cells. This chapter summarizes the theoretical background necessary to analyse and understand the experimentally observed data for such devices. The simple theories and the method of analysis of Schottky barrier data are summarized in the first part of the chapter. The basic properties of MIS devices are also discussed. Finally a brief review of Schottky barrier and MIS solar cells is given.

3.1 SCHOTTKY BARRIERS

3.1.1 Schottky Effect

In a metal-vacuum system the minimum energy necessary for an electron to escape in to vacuum from the Fermi level is defined as the work function, $q\phi_m$ (in electron volts). This value varies from 2.0 to 6.0 eV for metals and is very sensitive to surface contamination.

When an electron is at a distance x from the metal, a positive charge will be induced on the metal surface. The force of attraction between the electron and the induced positive charge is equivalent to the force which would exist between the electron and an equal positive charge located at (-x). The attractive force, F, called the image force, is given by Coulombs' law

$$F = \frac{-q^2}{4\pi(2x)^2\varepsilon_o} \tag{3.1}$$

where ε_o is the permittivity of free space. The potential energy of an electron at a distance x from the metal surface is

$$E(x) = \int_{\infty}^{x} F.dx = \frac{q^2}{16\pi\,\varepsilon_o x} \tag{3.2}$$

When an external field E is applied, the total potential energy, PE, in eV is given by

$$PE(x) = \frac{q^2}{16\pi\,\varepsilon_o x} + qEx \tag{3.3}$$

In the presence of such a field the thermionic work function has an effective value which is smaller than $q\phi_m$ by an amount $\Delta\phi$. The situation is shown in the fig.3.1(b) (the potential energy is measured downwards from the x-axis). The location of the potential maximum is given by the condition $d\left[P.E(x)\right]/dx = 0$. That is

$$x_m = \sqrt{\frac{q}{16\pi\ \varepsilon_o E}}\ \text{cm}, \tag{3.4}$$

$$\Delta\phi = \sqrt{\frac{qE}{4\pi\ \varepsilon_o}} = 2Ex_m \text{ volts} \tag{3.5}$$

The lowering of the metal work function by an amount $\Delta\phi$ as a result of the image force and the electric field is called the Schottky effect.

(a) Metal-Semiconductor System

The above ideas can also be applied to metal-semiconductor systems. In this case the field should be replaced by the maximum field at the interface, and the free space permittivity ε_o should be replaced by an appropriate low frequency permittivity ε_s characterizing the semiconductor medium. Because of the larger values of ε_s in these systems, $\Delta\phi$ and x_m are smaller than those for a corresponding metal-vacuum system. For example, if $\varepsilon_s = 16\ \varepsilon_o$, $\Delta\phi = 0.03$ V for $E = 10^5$ V/cm. Although this barrier lowering is small, it can have a considerable effect on current transport processes in metal-semiconductor systems.

(b) Energy Band Relations

To understand how a barrier may be formed when a metal comes into contact with a semiconductor, we first consider equilibrium relations in the absence of surface states. Fig 3.1(a) shows the energy band diagrams of a system consisting of a metal and an n-type semiconductor before and after contact is made. When the metal comes into contact with the semiconductor, charge will flow from the semiconductor to the metal in order that the Fermi levels on both sides line up. To establish this thermodynamic equilibrium, the Fermi level in the semiconductor is lowered by an amount $q\phi_m - q(\chi + V_n)$, where $q\chi$ is the electron affinity measured from the

Fig 3·1.

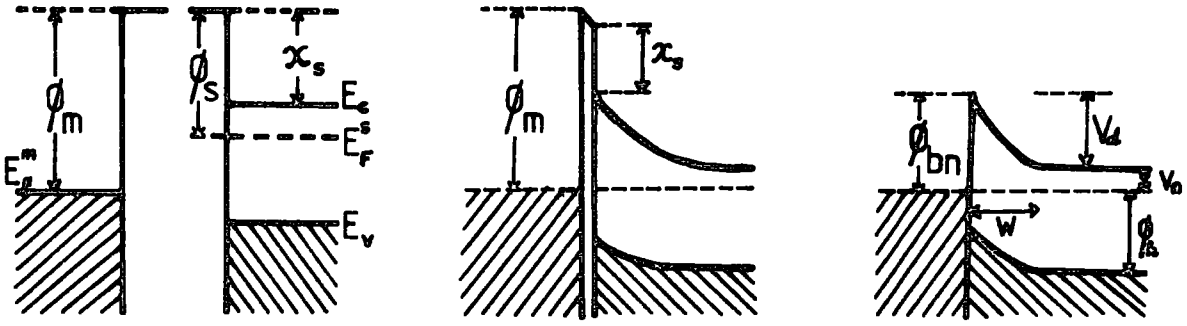

(a). Energy band diagrams of metal-semiconductor contacts.

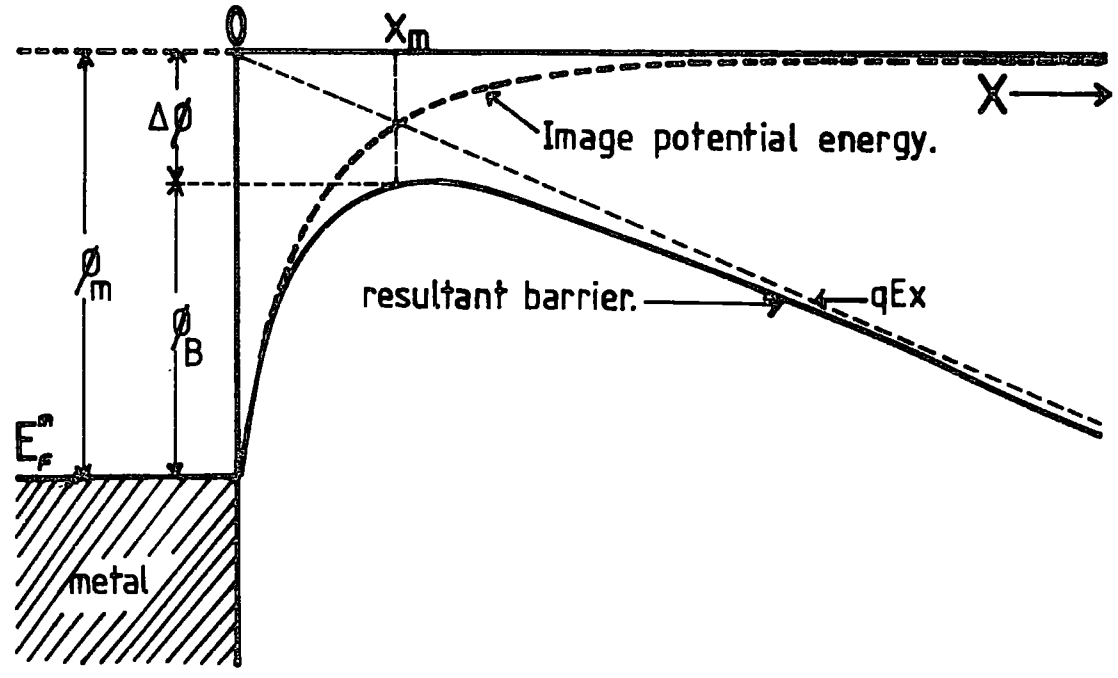

(b). The image-force lowering due to the combined effects of the electric field and the image force.

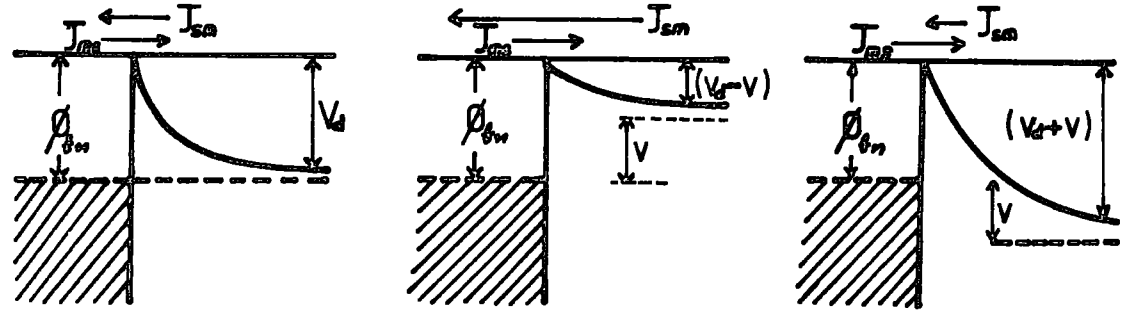

(c). Schottky barrier under (a). zero (b). forward and (c) reverse bias.

bottom of the conduction band to the vacuum level and V_n is the depth of Fermi level from the edge of the conduction band. As a result of the electron flow from the semiconductor to the metal, a negative charge is built up at the metal surface. This is neutralised by an equal and opposite charge in the semiconductor. Because the donor concentration is many orders of magnitude less than the concentration of electrons in the metal, the ionized uncompensated donors occupy a depletion layer of appreciable thickness, W, and the bands in the semiconductor are bent upwards. The resultant barrier height (neglecting the Schottky lowering) is given by

$$q\phi_{bn} = q(\phi_m - \chi) \tag{3.6}$$

For an ideal contact between a metal and a p-type semiconductor, the barrier height, $q\phi_{bp}$, is given by

$$q\phi_{bp} = E_g - q(\phi_m - \chi) \tag{3.7}$$

For a given semiconductor and for any metals, the sum of the barrier heights on n-type and p-type substrates is thus expected to be equal to the bandgap, or

$$q(\phi_{bn} + \phi_{bp}) = E_g \tag{3.8}$$

At the surface of a semiconductor there are usually dangling valence bonds from the valence electron sites which are not paired with electrons as they are in the bulk. The discontinuity in the electron binding gives extra states for the electrons over and above those in the bulk ; these are called surface states. If the density of the surface states is sufficiently large to accommodate any additional surface charges resulting from a contact with a metal without appreciably altering the occupation level E_F, then the space charge in the semiconductor will remain

unaffected. As a result the barrier height is determined by the property of the semiconductor surface and is independent of the metal work function.

(c) Height and Thickness of the Barrier

To obtain the relation between the height and the thickness of the barrier, we solve Poisson's equation with the following boundary conditions.

$$\rho = qN_d \quad \text{for} \quad x < W.$$

$$\rho = 0 \quad \text{for} \quad x > W. \text{ and}$$

$$\frac{dV}{dx} = 0 \quad \text{at} \quad x = W.$$

where ρ is the space charge density and N_d is the ionized donor concentration. x is measured from the surface of metal into the bulk of the semiconductor. The Poisson's equation in one dimension can be written

$$\frac{d^2V}{dx^2} = -\frac{\rho}{\varepsilon_s} \tag{3.9}$$

A simple integration of the above equation gives

$$\frac{dV}{dx} = \frac{qN_d}{\varepsilon_s}(W-x) \tag{3.10}$$

A further integration with the condition $V = -\phi_{bn}$ at $x = 0$ gives

$$V(x) = \frac{qN_d}{\varepsilon_s}\left(Wx - \frac{1}{2}x^2\right) - \phi_{bn} \tag{3.11}$$

In the bulk of the semiconductor at $x = W$, $V = -V_n$, and hence

$$(\phi_{bn} - V_n) = V_d = \frac{qN_dW^2}{2\varepsilon_s} \tag{3.12}$$

This relates the height of the barrier to its thickness. The image effects and the electronic space charges in the depletion layer have been neglected in the above analysis. Higher permittivity values and low donor concentrations give rise to thick barriers and electronic space charge has to be taken into account in these cases.

(d) Effect of an external applied voltage on the barrier

If an external voltage is applied to a two electrode system, a current flows and the total voltage is shared between the two contact resistances and the bulk resistance of the semiconductor. In many important cases one of the electrodes is an Ohmic contact and the potential drop across the bulk resistance is negligible. Hence the external voltage is mainly dropped across the depletion layer of the Schottky barrier. The different situations which can occur are shown in fig 3.1(c).

If a bias voltage is applied to the contact so that the semiconductor (n-type) is negative, the bands in the semiconductor are raised in energy relative to those in the metal and the electric field in the barrier region decreases. As a result the height of the barrier as seen from the semiconductor side decreases and a relatively large electron current will flow from the semiconductor to the metal. This is the "easy" or "forward" direction of current flow. If the bias voltage is reversed so that the semiconductor is positive, the energy bands in the semiconductor are lowered relative to those in the metal and the barrier height is increased. Now the electron flow from semiconductor to the metal is relatively small. This is known as the "hard" or "reverse" direction of current flow.

The shape and thickness of the barrier in the presence of an applied voltage can be found, using equation (3.11). For the reverse bias case, $V(W) = (V-V_n)$ at $x = W$, so that

$$\phi_{bn} + V - V_n = (V + V_d) = \frac{q N_d W^2}{2 \varepsilon_s} \qquad (3.13)$$

The thickness of the barrier changes with the applied voltage, and hence changes the capacitance. If we neglect the contribution of the free carriers to the electric field, the capacitance of the barrier is only due to the space charge , $Q_{sc} = q N_d AW$, and therefore,

$$C = \frac{d Q_{sc}}{dV} = q N_d A. \frac{dW}{dV} \tag{3.14}$$

Substituting for $\frac{dW}{dV}$ from equation (3.13) gives the differential capacitance of the Schottky barrier with contact area A.

$$C = \frac{\varepsilon_s A}{W} \tag{3.15}$$

By eliminating W, using equation (3.13) gives

$$\frac{1}{C^2} = \left(\frac{2}{A^2 \varepsilon_s q N_d}\right) . (V_d + V) \tag{3.16}$$

The capacitance is therefore not constant but decreases as the reverse bias increased. If N_d is constant throughout the depletion region, a plot of $1/C^2$ against reverse voltage should be a straight line with an intercept of $-V_d$ on the voltage axis. This forms the basis of a method of measuring barrier heights. The slope of the line yields the important quantity, N_d, the uniform doping concentration. If N_d is not constant, this plot is not linear, but the slope at any point is still given by $2/A^2 \varepsilon_s q N_d$, where N_d is now the donor density at the edge of the depletion region. In this case this provides a very convenient method of measuring the doping profile.

3.1.2 Current Transport Mechanisms in Schottky Barriers

The current transport in metal-semiconductor barriers is mainly due to majority carriers and this section discusses the various possible transport mechanisms. A barrier on an n-type semiconductor is considered

throughout the discussion. The various ways in which electrons can be transported across the junction under forward bias are shown schematically in fig (3.2). The inverse processes occur under reverse bias. The mechanisms are (a) emission of electrons from the semiconductor into the metal over the top of the barrier, (b) quantum-mechanical tunnelling through the barrier, (c) recombination in the space-charge region, and (d) recombination in the neutral region (hole injection).

The process (a) leads to nearly ideal Schottky barrier diodes, but in practice processes (b), (c) and (d) cause departures from this ideal behaviour.

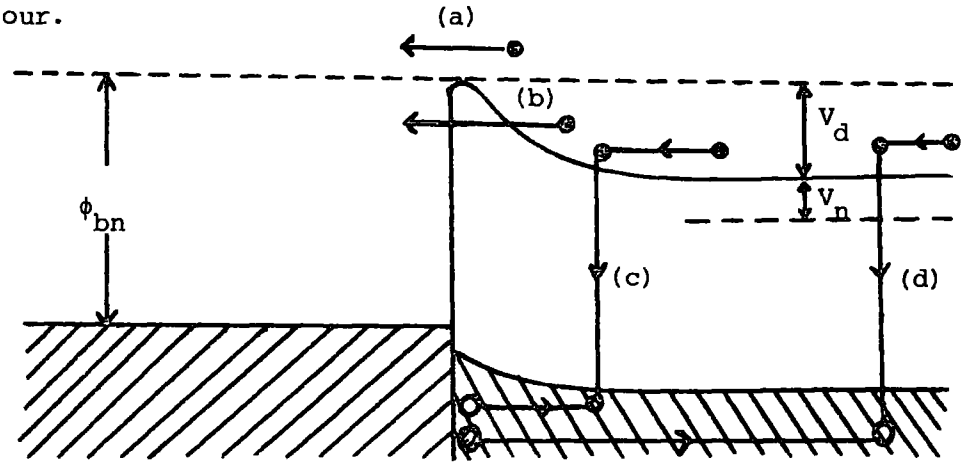

Fig (3.2)

(a) Emission over the barrier

In the process of emission over the barrier, electrons must first be transported from the bulk of the semiconductor to the interface. In crossing the depletion region of the semiconductor, their motion is governed by (1) the mechanisms of diffusion and drift in the electric field of the barrier, and (2) the height of the potential barrier at the interface.

These two processes are effectively in series, and the current is determined predominantly by whichever causes the larger impediment to the flow of electrons. According to the diffusion theory by Schottky[1], the main obstacle to current flow is provided by the diffusion and drift in the depletion layer. In the thermionic emission theory by Bethe, the

current flow is completely controlled by the height of the barrier. In practice, the true behaviour will lie somewhere between the two extremes of the diffusion theory and the thermionic emission theory. A more general theory is given by Crowell and Sze by combining the above two approaches into a single thermionic-emission/diffusion theory. The main features of these theories are now summarized.

The diffusion theory:

This theory is derived using the following assumptions : (1) the barrier height is much larger than kT ; (2) the effect of electron collisions within the depletion region is predominant ; (3) the carrier concentrations at x = 0, and x = W are unaffected by the current flow ; (4) the impurity concentration of the semiconductor is nondegenerate ; (5) a further approximation which is made is that the charge carrier mobility remains constant. The image force effects are also neglected in this approach.

With these assumptions and using the depletion approximation with a constant donor density, the expression for the current density obtained from this theory is[1,2]

$$J = J_{sd}\left[\exp\left(\frac{qV}{kT}\right) - 1\right] \tag{3.17}$$

where J_{sd}, the saturation current density, is given by

$$J_{sd} = \frac{q^2 D_n N_c}{kT}\left[\frac{2q\,(V_n - V)\,N_d}{\varepsilon_s}\right]^{\frac{1}{2}} \cdot \exp\left(\frac{-q\,\phi_{bn}}{kT}\right) \tag{3.18}$$

D_n is the diffusion constant of electrons.

Thermionic emission theory:

Some of the approximations used in this theory are similar to those used in the diffusion theory. The basic difference, however, is that electron collisions within the barrier are neglected. Because of the above assumption, the shape of the barrier profile is immaterial and

the current flow depends solely on the barrier height.

The current-voltage characteristics according to the thermionic-emission theory are given by[1,2]

$$J = J_{st}\left[\exp\left(\frac{qV}{kT}\right) - 1\right] \tag{3.19}$$

with

$$J_{st} = A^{*}T^{2}.\ \exp\left(-\frac{q\phi_{bn}}{kT}\right) \tag{3.20}$$

and

$$A^{*} = \frac{4\pi\, m^{*}\, k^{2}}{h^{3}} \tag{3.21}$$

A^{*} is the Richardson constant for thermionic emission. For free electrons A^{*} = 120.0 Amp/cm^{2}/K^{2} and for electrons in CdTe A^{*} = 12.0 Amp/cm^{2}/K^{2} with an electron effective mass of 0.1 m_{o}.

Thermionic emission - diffusion theory

The two theories summarized above consider two extreme cases, but the real situation comprises a combination of the two mechanisms. Several authors (Schultz, 1954, Gossick, 1963, Crowell and Sze, 1966) have combined these two theories but the most fully developed theory is that of Crowell and Sze. They introduced the concept of a "recombination velocity" V_{r} at the top of the barrier ; V_{r} is defined by equating the net electron current into the metal to $V_{r}(n-n_{o})$, where n_{o} is the equilibrium electron density at the top of the barrier at zero bias. With these ideas they obtained the following expressions for the current-voltage characteristics[2]

$$J = J_{s}\left[\exp\,(qV/kT) - 1\right] \tag{3.22}$$

$$J_{s} = A^{**}\,T^{2}.\ \exp\left(-\frac{q\phi_{bn}}{kT}\right) \tag{3.23}$$

where

$$A^{**} = \frac{f_{p}\,f_{Q}\,A^{*}}{(1 + f_{p}f_{Q}.\ V_{r}/V_{D})} \tag{3.24}$$

A** is the effective Richardson constant, V_D the effective velocity due to drift and diffusion of electrons, and f_p, f_Q are the probability of electron emission over the barrier and the quantum mechanical transmissions coefficient through the barrier respectively.

The applicability of these different theories depends on the relative values of V_r and V_D in the barrier region. If $V_D >> V_r$ the above equation reduces to equation (3.19) and the thermionic emission theory applies. If $V_D << V_r$, equation (3.22) reduces to equation (3.17) ; the current is controlled by drift and diffusion in the depletion region and the diffusion theory applies.

(b) Tunnelling through the barrier

Under certain circumstances it may be possible for electrons with energies below the top of the barrier to penetrate the barrier by quantum-mechanical tunnelling. This may be understood by reference to the following energy diagram.

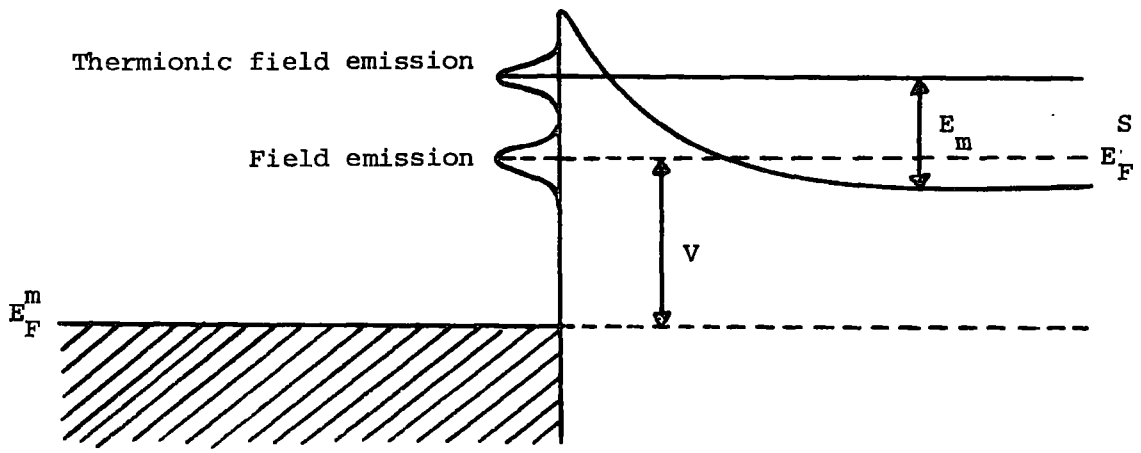

Fig 3.3

In the case of a very heavily doped (degenerate) semiconductor at low temperature, the current in the forward direction arises from the tunnelling of electrons with energies close to the Fermi energy in the semiconductor. This is known as "field" emission. If the temperature is raised, electrons are excited to higher energies and the tunnelling probability

increases very rapidly because the electrons "see" a thinner barrier. On the other hand, the number of excited electrons decreases very rapidly with increasing energy, and there is a maximum contribution to the current from electrons which have an energy E_m above the bottom of the conduction band. This is known as "Thermionic-field-emission". If the temperature is raised still further, all of the electrons gain enough energy to go over the top of the barrier and pure thermionic emission occurs.

According to the thermionic-field-emission theory introduced by Padovani and Stratton[3], the forward current-voltage relationship is given by

$$J = J_s . \exp (V/V_o) \tag{3.25}$$

where

$$V_o = V_{oo} . \coth (qV_{oo}/kT) \tag{3.26}$$

and

$$V_{oo} = \frac{\hbar}{2} \left[N/m^* \varepsilon\varepsilon_o \right]^{\frac{1}{2}} \tag{3.27}$$

At low temperatures, $V_o \simeq V_{oo}$ so that the slope of the graph of ℓn J against V is independent of temperature. This is the case of field emission. At high temperatures, V_o is slightly greater than $\frac{kT}{q}$, and the slope of the graph of ℓn J against V can be written as $\frac{q}{n\ kT}$, where $n = \frac{q\ V_o}{kT}$. There is therefore a smooth transition from thermionic field emission to pure thermionic emission.

(c),(d) Recombination in the depletion and neutral regions

The other two mechanisms of current-transport across the barrier are due to recombinations in both depletion and neutral regions. The recombination in the depletion region normally takes place via localized centres and the most effective centres are those with energies lying near to the centre of the gap. The current density due to such a recombination centre is given approximately by[2]

$$J_r = J_{ro} \left\{ \exp \left(qV/2kT \right) - 1 \right\} \tag{3.28}$$

where
$$J_{ro} = \frac{q\, n_i\, W}{2\, \tau_r} \qquad (3.29)$$

Here n_i is the intrinsic electron concentration proportional to $\exp(-qE_g/2kT)$, W is the thickness of the depletion region, and τ_r is the lifetime within the depletion region. If the recombination current contributes to the total current across the barrier, this may therefore cause deviations from ideal Schottky barrier behaviour.

If the height of a Schottky barrier on n-type material is greater than half the bandgap as is often the case, the region of the semiconductor adjacent to the metal becomes p-type and contains a high density of holes. One might expect some of these holes to diffuse into the neutral region of the semiconductor under forward bias, thus giving rise to the injection of holes and recombination in the neutral region. These currents, therefore, introduce added complications to current-voltage characteristics and analysis becomes more difficult.

3.1.3 Deviation from the Ideal Behaviour

Reverse characteristics:

According to the thermionic-emission theory, the reverse current density of an ideal Schottky diode should saturate at the value

$$J_{st} = A^{**}\, T^2 . \exp\left(-\, q\phi_b/kT\right)$$

In practice the reverse current increases with applied voltage and this departure from ideal behaviour can be explained using one of the following considerations.

1. The field dependence of the barrier height.

2. The effect of tunnelling.

3. Generation of carriers in the depletion region.

If the barrier height, ϕ_b, is dependent on the electric-field strength in the barrier, the reverse characteristics will not show

saturation. There are two major reasons for such a field-dependent barrier height. Firstly the value of ϕ_b decreases due to the image force and the magnitude of barrier lowering can be calculated as described in section (3.1.1). Barrier lowering due to image force effects is proportional to $E^{\frac{1}{2}}$. The other main cause is the presence of an interfacial layer. Almost all Schottky diodes have a thin oxide layer ($\simeq$ 10 Å) between the metal and the semiconductor. Because of the potential drop in the layer, the zero-bias barrier height is lower than it would be in an ideal diode. These two factors combine, resulting in a barrier height that decreases with increasing reverse voltage. If $\Delta\phi_b$ is the total lowering of the barrier, then the reverse current does not saturate but increases proportionally to exp ($q\ \Delta\phi_b/kT$). The effect of this field dependent barrier height on the forward current is discussed in the next section.

Tunnelling through the barrier becomes more significant at lower doping levels in the reverse direction than in the forward direction because the bias voltages involved are much greater. The application of a moderately large reverse bias can also cause the potential barrier to become thin enough for significant tunnelling of electrons from the metal to the semiconductor to take place. The effect of tunnelling can again be described as either field emission or thermionic-field-emission.

In the case of high barriers on low-lifetime semiconductor, there may be an appreciable reverse current due to the generation of electron-hole pairs in the depletion region. This is the inverse of recombination in the space-charge region, and gives rise to a current-density component proportional to the thickness of the barrier[2]. This generation current is more pronounced at low temperatures than at high temperatures because it has a lower activation energy than the thermionic-emission component.

Forward characteristics

The current-voltage relationship predicted by the thermionic-

emission theory is of the form of the ideal rectifier characteristic (eqn. 3.19).

$$J = A^* T^2 . \exp\left(-\frac{q\phi_b}{kT}\right) . \left\{ \exp\left(\frac{qV}{kT}\right) - 1 \right\}$$

provided the barrier height is independent of bias. However, even in a perfect contact with no interfacial layer, the barrier height is modified as a result of the image-force by an amount $\Delta\phi_{bi}$ which depends on the bias voltage. The effective barrier height can therefore be written as $\phi_e = \phi_b - \Delta\phi_{bi}$. In the presence of an interfacial layer, ϕ_b depends on the bias voltage so that ϕ_e may be bias dependent for two reasons. Let us suppose that $\frac{\partial\phi_e}{\partial V} = \beta$ happens to be constant so that we may write

$$\phi_e = \phi_{bo} - \left(\Delta\phi_{bi}\right)_o + \beta V \qquad (3.30)$$

where ϕ_{bo} and $\left(\Delta\phi_{bi}\right)_o$ refer to zero bias. The coefficient β is positive because ϕ_e always increases with increasing forward-bias. The modified current density now becomes

$$J = A^*T^2 . \exp\left[-q \left\{ \phi_{bo} - \left(\Delta\phi_{bi}\right)_o + \beta V \right\} /kT \right] \left\{ \exp\,(qV/kT) - 1 \right\}$$

$$= J_o \,.\exp\left(-\frac{\beta qV}{kT}\right) . \left\{ \exp\,(qV/kT) - 1 \right\} \qquad (3.31)$$

where

$$J_o = A^*T^2 . \exp\left[-q \left\{ \phi_{bo} - \left(\Delta\phi_{bi}\right)_o \right\} /kT \right] . \qquad (3.32)$$

The equation (3.31) can be written in the form,

$$J = J_o \exp\,(qV/nkT) \left\{ 1 - \exp\,(-qV/kT) \right\} \qquad (3.33)$$

where $\frac{1}{n} = 1 - \beta$

n is often called the "ideality factor". If $\beta = \frac{\partial \phi_e}{\partial V}$ is constant, n is also a constant and for values of V greater than $\frac{3kT}{q}$, equation (3.32) can be written as

$$J = J_o \cdot \exp\left(\frac{qV}{nkT}\right) \tag{3.34}$$

Hence the ideality factor n can be obtained from the experimental J/V characteristic through the relationship

$$\frac{1}{n} = \frac{kT}{q} \cdot \frac{d(\ell n\ J)}{dV} \quad . \tag{3.35}$$

When the coefficient β is not a constant the plot of $\ell n(J)$ against V is not linear.

If the departure of n from unity arises from image-force lowering or from interfacial layer effects, n should be independent of temperature. But the majority of Schottky diodes exhibit n values which depend on temperature. Padovani and Sumner[4] first reported that some of their I-V data of Au-GaAs Schottky barriers fitted the following equation :

$$J = AT^2 \cdot \exp\left\{-\phi_{bo}/k\ (T + T_o)\right\} \cdot \left[\exp\left\{qV/k(T + T_o)\right\} - 1\right] \tag{3.36}$$

where T_o is known as the "excess temperature" and is independent of temperature and voltage over a wide range of temperatures. At a given temperature, n can be related to T_o as

$$n = 1 + \frac{T_o}{T} \tag{3.37}$$

however, if T_o is a constant, then n will no longer be a constant as the temperature is varied. Padovani[5] (1971) has reported that for a large number of Au-GaAs, Schottky diodes T_o varied from 10 K up to 100 K. Other Au-GaAs diodes have been reported (Goldberg, Posse and Tsarenhav,1975)[6]

which exhibit almost ideal J/V characteristics with $T_o \simeq 0$. The effect is evidently not an intrinsic property of ideal Schottky barriers but an artifact introduced by the fabrication process.

Various attempts have been made to explain such a temperature dependence in terms of tunnelling (Crowell and Rideout, 1969)[7], particular distributions of interface states (Saxena, 1969[8], Levine,1971[9], Rhoderick, 1975[10]) and a non-uniformly doped surface layer (Padovani, 1971[5], Crowell,1977[11]). It is quite possible that more than one of these mechanisms may operate simultaneously.

3.1.4 Method of Analysis of Schottky Barrier Data

To analyse the experimental data, the Schottky equation, equation (3.15), can be written in the form,

$$J = J_o \left(e^{V/V_o} - 1 \right) \tag{3.38}$$

For the voltage range of interest where $V \geq 3\ V_o$, the above equation may be written as

$$J = J_o \cdot e^{V/V_o} \tag{3.39}$$

When $\ell n(J)$ is plotted against V, a straight line is obtained whose slope gives V_o and its intercept at zero volt gives J_o. When V_o is plotted against $\frac{kT}{q}$, the following five cases may be observed as shown in fig(3.4)[8].

(1) If the diode obeys ideal Schottky theory, equation (3.15), the V_o data will lie on the straight line labelled 1, which has unity slope,i.e.

$$V_o = \frac{kT}{q} . \tag{3.40}$$

(2) If the diode obeys equation (3.23), then the V_o data will lie on the straight line labelled 2, whose slope is >1, i.e.

$$V_o = n . \frac{kT}{q} . \tag{3.41}$$

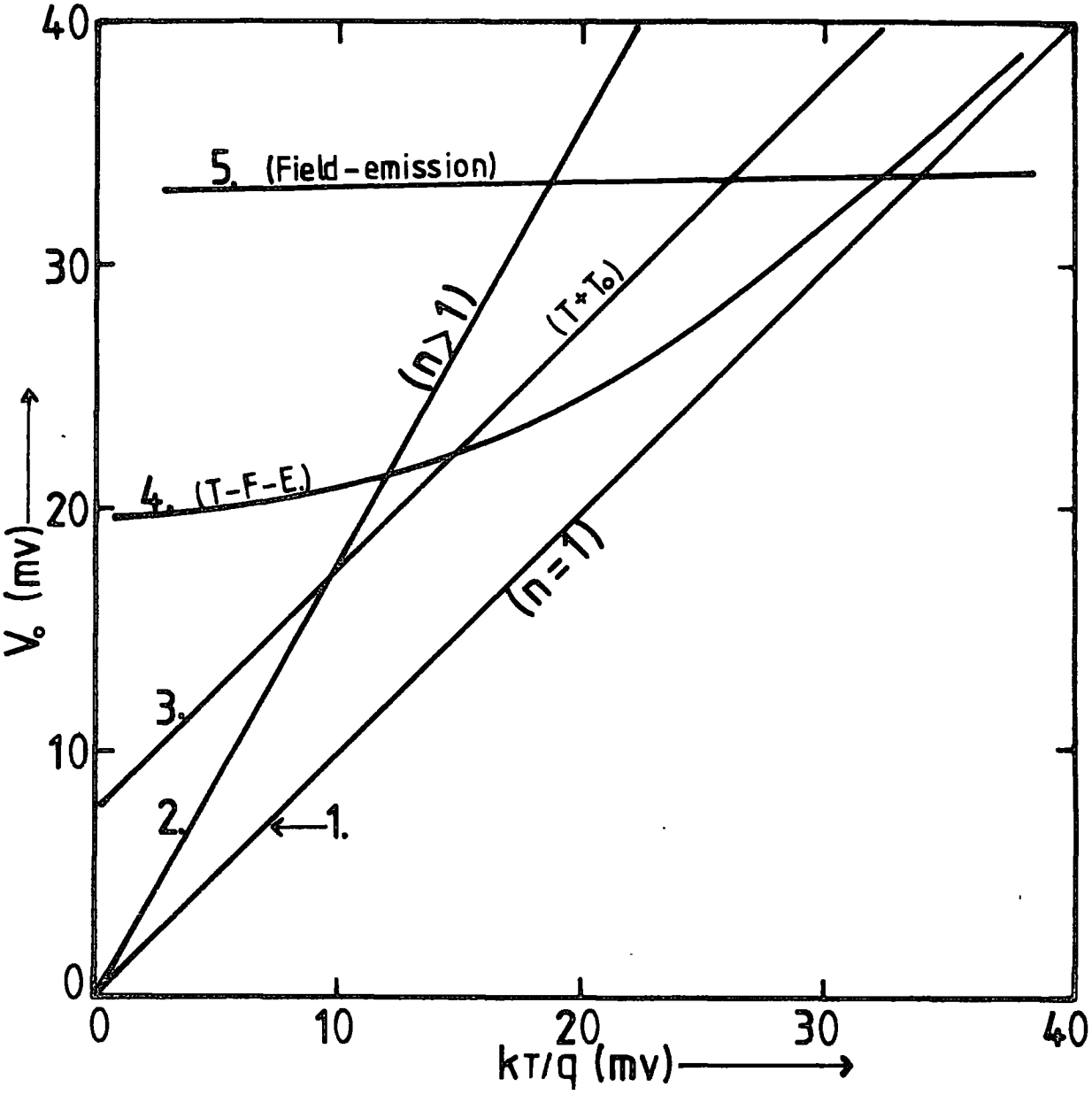

Fig. 3·4 Plot of V_0 versus kT/q. Various lines refer to agreement with (line labelled as 1) or deviations from (lines labelled 2-5) the Schotky theory.

where the constant n does not depend on temperature.

(3) If the diode obeys equation (3.24), then the V_o data will lie on the straight line labelled 3, which is parallel to the unity slope line labelled as 1. In this case

$$V_o = k (T + T_o) /q . \qquad (3.42)$$

where T_o is a constant >0 and it is independent of temperature.

(4) If the diode obeys thermionic-field emission (T-F-E) theory of Padovani and Stratton[3], the J/V relationship is given by equation (3.19). In this case

$$V_o = V_{oo} . \coth (q V_{oo}/kT)$$

If equation (3.24) is used to fit the J-V characteristics of a diode in which T-F emission is present, then in this case T_o is not constant with respect to temperature. It increases at lower temperatures. The V_o data will lie on the curve labelled 4.

(5) If field-emission dominates, then the V_o data will lie on a straight line labelled as 5. In this case V_o is independent of temperature and $V_o = V_{oo}$.

3.1.5 Measurement of Schottky Barrier Height

(a) Current-voltage measurement:

As shown in section (3.1.2), most of the Schottky diodes possess J/V characteristics given by the thermionic-emission theory, provided the forward bias is not too large. In practice, diodes never satisfy the ideal equation exactly, but always the modified equation (3.34)

$$J = J_o . \exp (qV/nkT)$$

for values of V greater than 3kT/q. The saturation current J_o is given by (equation 3.20).

$$J_o = A^* T^2 . \exp(-q\phi_e/kT)$$

where $\phi_e = \phi_b - \Delta\phi_{bi}$ is the effective barrier height. Therefore, a plot of $\ell n J$ against V in the forward direction should give a straight line and the parameter n can be evaluated from the gradient. The extrapolated value of current density to zero voltage gives the saturation current J_o. In order to determine the value of ϕ_e, one of the following methods can be adopted.

1. If A* is known, the value of the effective barrier height can be obtained from the relation

$$\phi_e = \frac{kT}{q} \cdot \ell n \left(\frac{A^* T^2}{J_o} \right) \tag{3.43}$$

Since the value of ϕ_e is not very sensitive to the choice of A*, it is not necessary to know A* very accurately. At room temperature, a 100% increase in A* will cause an increase of only about 0.02 volt in ϕ_e.

2. If A* is not known, the temperature dependence of J_o can be used to find the effective barrier height. By measuring either forward or reverse characteristics as a function of temperature, a set of J_o values can be obtained at various temperatures. Then a plot of $\ell n(J_o/T^2)$ against $1/T$ should yield a straight line of slope $-q\phi_{eo}/k$ and an intercept on the vertical axis equal to ℓn A*. This plot is usually known as the "activation energy plot" and ϕ_{eo} is the barrier height at 0 K. The barrier height is generally a decreasing function of temperature and can be written approximately as

$$\phi_e = \phi_{eo} - \alpha T \tag{3.44}$$

where α is the temperature coefficient of the barrier height. This method is reliable only if the forward plot of ℓn J against V is a good straight line with a low value of n. For large values of n (n> 1.1), or non-linear plots of ℓn J against V, the diode is far from ideal and the barrier height

is not clearly defined. This non-ideality situation may arise due to one or more reasons discussed in the previous section.

(b) Capacitance-voltage measurement

The barrier height can also be determined by the capacitance measurements. The differential capacitance C under reverse bias is given by equation (3.16), for a non-degenerate semiconductor. If the donor concentration N_d is constant and V_d is independent of applied voltage (i.e. if there is no appreciable interfacial layer), a plot of $1/C^2$ against reverse voltage should yield a straight line. The intercept on the voltage axis gives the diffusion voltage V_d, and barrier height is then given by

$$\phi_b = V_d + V_n \tag{3.45}$$

where V_n is the depth of the Fermi level below the conduction band. If we take into account the contribution of free carriers in the barrier region a small correction term kT/q appears in the above expression. Furthermore, because the differential capacitance is determined by the width of the depletion region which depends only on V_d and N_d, the barrier height given by the above equation does not include the image-force lowering, $\Delta\phi_{bi}$. The more accurate barrier height therefore is given by

$$\phi_b = V_d + V_n + \frac{kT}{q} - \Delta\phi_{bi} \tag{3.46}$$

(c) Photoelectric measurements

When monochromatic radiation with quantum energy exceeding $(\phi_b - \Delta\phi_{bi})$ is incident on the metal surface of a Schottky barrier, electrons excited from the Fermi level of the metal have sufficient energy to cross into the semiconductor. As a result a photovoltaic e.m.f. is developed causing a current to flow in an external circuit. The photocurrent per absorbed photon, R, as a function of the photon energy, $h\nu$, is given by the Fowler

theory (1931) [1]

$$\frac{R}{T^2} = B\left[\frac{\pi^2}{6} + \frac{x^2}{2} - \left(e^{-x} - \frac{e^{-2x}}{4} + \frac{e^{-3x}}{9} - \ldots\right)\right] \qquad (3.47)$$

for $x \geq 0$.

where B is a constant and $x = h(\nu-\nu_o)/kT$. The threshold energy $h\nu_o$ is equal to the effective barrier height $(\phi_b - \Delta\phi_{bi})$. For $x > 3$, the above equation reduces to

$$R = (\text{constant}).(h\nu - h\nu_o)^2$$

or

$$\sqrt{R} = K \,.\, (h\nu - h\nu_o) \qquad (3.48)$$

So a plot of $\sqrt{R}$ against $h\nu$ should give a straight line and the intercept on energy axis is equal to the effective barrier height.

3.2 MIS STRUCTURES

The metal-insulator-semiconductor (MIS) structure is of academic importance for the understanding of transport mechanisms and the study of semiconductor surfaces. This has also been able to account for the non-ideal behaviour of Schottky barriers. These devices with thick insulating films (d ≃1000 Å) can be used as electroluminescence diodes and high efficiency optical detectors. Potentially the most important applications of MIS devices are in photovoltaic energy conversion. For this application the insulating film should have a tunnellable thickness (d< 50 Å) and the following section is mainly concerned with tunnelling MIS structures.

Tunnelling in MIS structures with ultra-thin insulating layers was first studied by Gray (1965) [12] in an attempt to probe the interface states at a semiconductor surface. More detailed studies of Waxman et al (1967) [13] and by Dahlke and Sze (1967) [14] on well defined thermally grown

silicon dioxide layers together with the theoretical studies of Freeman and Dahlke (1970)[15] have elucidated the various tunnelling currents present in these structures. Subsequent studies by Card and Rhoderick (1971)[16], Clarke and Shewchun (1971)[17], and Kar and Dahlke (1972)[18], which take into account the dependence of the statistics of minority carriers and electrons in interface states on the thickness, d ,of the insulating layer, have solved most of the features of electrical characteristics. The following sections summarizes the basic characteristics of MIS structures and both MS and MIS solar cells.

Basic Characteristics

The MIS structure is shown schematically in fig.3.5(a) and the electron energy-band diagram is illustrated in fig 3.5(b), for the particular case of an n-type substrate ; d is the thickness of the insulator, and V the applied voltage on the barrier metal. In the ideal situation the insulator represents a complete barrier to the motion of charge between the metal and semiconductor (the resistivity of an ideal insulator is infinite). The only charges which can exist in the structure under any biasing conditions are those in the semiconductor and those with the equal but opposite sign on the metal surface. When an ideal MIS diode is biased with positive or negative voltages, there are basically three cases which may exist at the semiconductor surface. Accumulation depletion or inversion can occur depending on the bias voltage. In real semiconductor-insulator interfaces, there are usually surface charges and the resultant interface energy states (E_t), are shown in figures 3.5(b) and (c). These localized electronic states are caused by the bond defect structure or by impurities. ϕ_{BO} is the potential barrier between the metal and the insulator, and ϕ_{bo} the corresponding Schottky barrier when there is no applied voltage.

When the insulating layer is made very thin (less than $\simeq$ 50 Å) appreciable currents can be made to flow between the metal and semiconductor

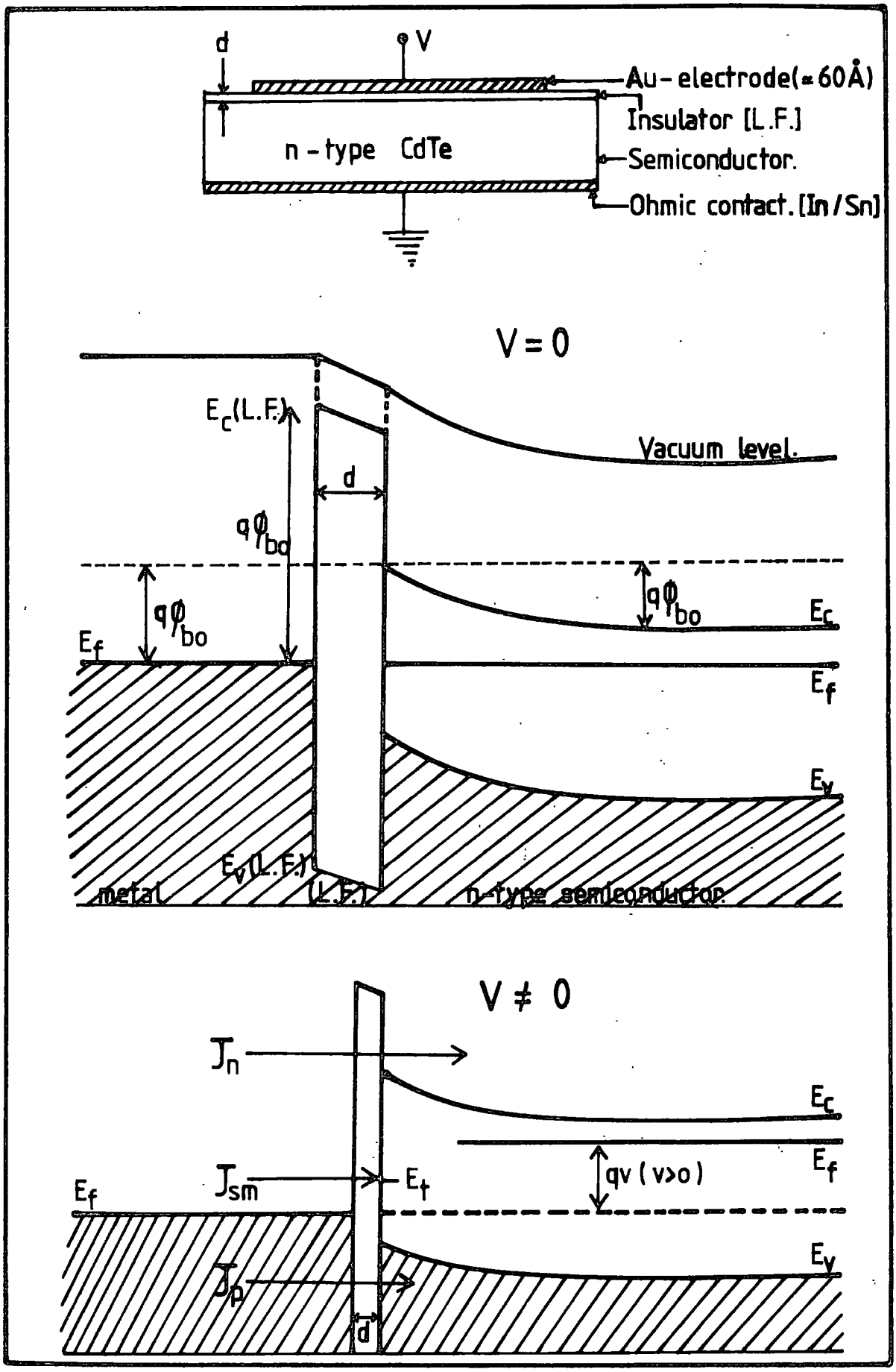

Fig. 3·5 Energy band diagrams for an m.i.s. structure under zero and forward bias conditions.

by quantum-mechanical tunnelling, even for modest electric fields. The tunnel currents which flow between the metal and the semiconductor under an applied bias voltage are shown in fig 3.5(c). J_n is associated with tunnelling transitions between the metal and the conduction band of the semiconductor, J_p is due to transitions involving the valence band, and J_{sm} is due to transitions to and from the interface states. When the transitions to the majority carrier band dominate the tunnelling current (J_n), the device is called the majority-carrier MIS diode. In minority-carrier MIS diodes, the transitions to the minority carrier band is dominant (J_p).

In the presence of an insulating layer the majority carriers overcoming the potential barrier would have to tunnel through the distance d. The transmission coefficient of the barrier is thus modified with a resulting decrease in the current density. Card and Rhoderick (1971)[16] have shown that an appropriate expression to cover this situation is a simple extension of equation (3.34), namely

$$J_n = AT^2.\exp\left(-\chi^{\frac{1}{2}}.d\right).\exp\left(-q\phi_b/kT\right)\left[\exp\left(qV/nkT\right) - 1\right] \quad (3.49)$$

where χ(eV) is the mean barrier height presented by the interfacial film whose thickness d is measured in Å. $A = 4\pi mqk^2/h^3$ is the Richardson constant. They also have shown that if the majority of the voltage continues to be dropped across the depletion region in the semiconductor, then the ideality factor is given by

$$n = 1 + \frac{\left(d/\epsilon_i\right)\left(\epsilon_s/W + q\,D_{sb}\right)}{1 + \left(d/\epsilon_i\right)q\,D_{sa}} \quad (3.50)$$

where ϵ_i and ϵ_s are the permittivities of the insulating layer and the semiconductor, W is the width of the depletion region in the semiconductor, and D_{sa} and D_{sb} are respectively the densities of interface states

(in cm^{-2} eV^{-1}) in equilibrium with the metal and with the majority carriers in the semiconductor. The n value increases as the insulating layer thickness is increased due to the term $qD_{sb}d/\varepsilon_i$ in the above equation. The saturation current decreases due to the increase in the tunnelling exponent $\chi^{\frac{1}{2}}.d$ in equation (3.49).

3.3 SOLAR CELLS

A solar cell is a photovoltaic device designed to convert sunlight into electrical power and to deliver this power into a suitable load in an efficient manner. Materials having energy gaps of ≈1.50 eV are suitable for this energy conversion, and solar cells have been made using many semiconductors such as Si, GaAs and CdS. Even though CdTe possess the optimum value of bandgap (1.50 eV) at room temperature, rather little work has been devoted to the study of Schottky barrier and MIS solar cells on this material. In this work, both MS and MIS photovoltaic structures have been studied in detail. The following sections summarize the relevant theories of these solar cells with the definitions of their important parameters.

(a) MS Solar Cells

A schematic diagram of a Schottky barrier solar cell is shown in fig 3.6(a). This consists of a depletion layer formed on the front surface and a large back Ohmic contact. The surface barrier can also be a p-n junction or a heterojunction. The equivalent circuit of the solar cell under illumination is shown in fig 3.6(b), where I_L is the strength of constant current source due to the incident light.

The J-V characteristics of a Schottky barrier device in the dark is discussed in section (3.1.2) in detail. In homo- and hetero-junctions, the space-charge region extends into both semiconductor parts, where as in Schottky solar cells it can only exist in the semiconductor base. It is very important that as many photons as possible can penetrate the top

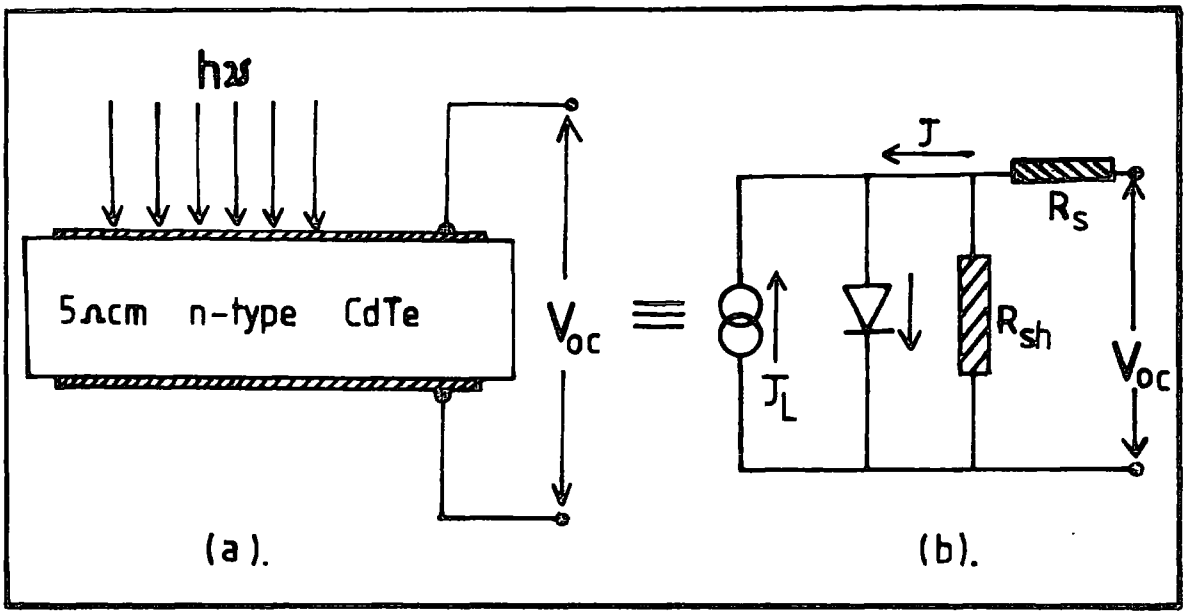

Fig. 3·6 [a]. Basic structure of a Schottky barrier solar cell.
[b]. The equivalent circuit of a solar cell.

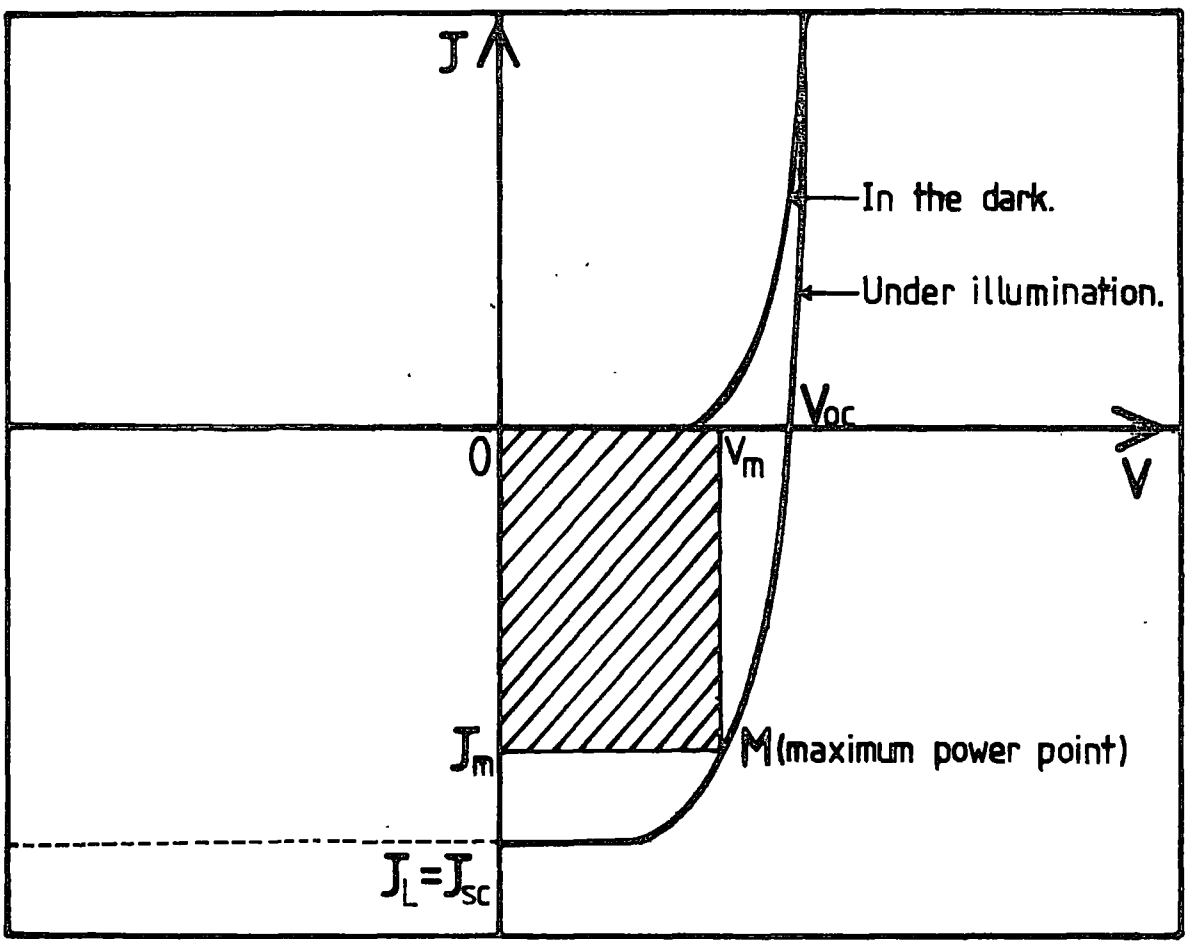

Fig. 3·7 Current - Voltage characteristics of a solar cell in the dark and under illumination.

layer to generate excess electron-hole pairs in the barrier region. The characteristics of such a diode when illuminated can be written in the form[1,19,20]

$$J = J_s \left(e^{eV/nkT} - 1 \right) - J_L \qquad (3.51)$$

where J_L is the current density produced under illumination.

Fig (3.7) shows the representation of the dark and the illuminated I-V characteristics. It is seen that the curve passes through the fourth quadrant and, therefore, that power can be extracted from the device. This curve can be used to define some important solar cell parameters.

From equation (3.51) we obtain for the open-circuit voltage (when J=0)

$$V_{oc} = n \left[\phi_b + \frac{kT}{q} \cdot \ell n \frac{J_L}{A^* T^2} \right] \qquad (3.52)$$

The short-circuit current of the device is defined by V = 0 in equation (3.51).

$$J_{sc} = - J_L \qquad (3.53)$$

By properly choosing a load, it is possible to extract close to 80% of the product $I_{sc} \times V_{oc}$, as indicated by the maximum power rectangle in fig (3.7). If point $M \equiv (V_m, J_m)$ represents the maximum power point, then the fill factor, F.F, is defined as the ratio

$$F.F. = \frac{J_m \cdot V_m}{J_{sc} \cdot V_{oc}} \qquad (3.54)$$

and the conversion efficiency η as

$$\eta = \frac{J_m . V_m}{I_{ph}} = \frac{J_{sc} . V_{oc} . FF}{I_{ph}} \qquad (3.55)$$

where I_{ph} is the incident light intensity on the solar cell. The illumination is very often given in AMX (air mass X), where X is the secant of the sun's angle relative to the zenith, measured at sea level. AMO is the solar spectrum in outer space and AM1 is the spectrum at the earth's surface for optimum conditions at sea level (the sun at zenith). The currently accepted standard value of AMO is 135.3 mW/cm^2 (19).

For practical solar cells, η represents the most interesting parameter and the value at room temperature is approximately a factor of 2 smaller than the predicted value ; for GaAs 15% instead of 28%. This is mainly due to unavoidable losses in the devices. Efficiency losses arise due to the following reasons.

(a) Photons with energies lower than E_g cannot contribute to the photo-current. Absorbed photons with energies higher than E_g generate, in general, one electron-hole pair with energy E_g and the excess energy is released to the lattice as heat. It is evident from equation (3.52) that the efficiency decreases with increasing temperature. This shows that the conversion efficiency η depends very strongly on the spectral energy distribution of the irradiated spectrum.

(b) Photo-voltages are normally less than the bandgap of the semiconductor, and therefore efficiency decreases due to voltage losses.

(c) Losses due to the fill factor ; A low fill factor usually means the presence of series or shunt resistance which leads to avoidable internal losses of the cell. In an ideal case $R_s = 0$ and $R_{sh} = \infty$.

(d) Reflection at the surface, even if an anti-reflection coating is applied. This is more prominent in Schottky barrier solar cells due to the shiny metal surface.

(e) The collection efficiency can be considerably smaller, due to recombination at the surface, in and near the space-charge region.

The spectral response of a solar cell is defined as the SCC or OCV as a function of the wavelength of the incident light. It has been shown theoretically[1] that in order to increase the short-wavelength response, the barrier should be made closer to the surface since $1/\alpha$ (α = absorption coefficient) is small for short wavelength ; while in order to increase the long-wavelength response the barrier must be made comparatively deep below the surface. If the surface recombination velocity is high, the lifetime near the surface is reduced, thus reducing the response to short wavelengths of incident light.

(b) MIS Solar Cells

Schottky barrier solar cells for terrestrial use are attractive owing to advantages such as low cost, low temperature fabrication, exceptional shortwave-length response and adaptability to semiconductor thin films. However, because of reduced band bending at the barrier, the Schottky barrier solar cells have a lower open-circuit-voltage compared with p-n junction cells. They cannot produce high photocurrents due to the large reflection loss by metal films. Moreover, the sheet resistance of thin metal films becomes very important for use under high illumination.

It has recently been discovered that the presence of an interfacial layer can appreciably improve the photovoltaic properties of S/B solar cells, by increasing the open-circuit voltage. This MIS structure is currently receiving much attention in solar cell studies. The fabrication of MIS diodes is relatively cheap and simple, when compared to p-n junction diodes, and thus the possibility of obtaining p-n-like performance from such a structure is very attractive.

This improvement of solar cell parameters was first demonstrated for GaAs by Stirn and Yeh (1975)[21] and for Si by Shewchun et al (1974)[22]

for minority-carrier MIS structures, and by Charlson an Lien (1975)[23], Lillington and Townsend (1976)[24] for majority-carrier MIS structures. An abundance of experimental and theoretical work has confirmed these findings. It is consistently observed that the open-circuit-voltage of the MIS cell is improved over that of the ideal Schottky barrier, and in the best cases approaches that of a p-n junction. This may be understood in terms of the suppression of the dark current by the insulating layer.

The problem is to understand the experimental observation that the photocurrent is the same as that of a Schottky barrier for d< 40 Å. Unlike the dark current this is not suppressed by the insulating layer. For majority-carrier solar cells, the dark current is dominated by tunnelling transitions between the metal and the majority-carrier band. If the current-voltage relation in the dark is given by equation (3.49), the open-circuit-voltage of an MIS solar cell is

$$V_{oc} = n\left[\phi_b + \frac{kT}{q}.\chi^{\frac{1}{2}}.d + \frac{kT}{q}.\ln\left(\frac{J_L}{A^*T^2}\right)\right] \qquad (3.56)$$

The V_{oc} has been increased from that of a Schottky barrier due to the increases in n and $\chi^{\frac{1}{2}}.d$ in the above equation. For low values of d ($d \leqslant 40$ Å), suppression of the photocurrent J_{sc}, which is due to photo-generated holes tunnelling into the metal, does not occur.

The experimental measurements carried out on Schottky barrier and MIS diodes prepared on low resistivity CdTe were analysed using the theories and definitions discussed in this chapter. These results are presented in chapter seven.

CHAPTER 4

EXPERIMENTAL TECHNIQUES

4.1 SURFACE PREPARATION AND PRODUCTION OF OHMIC CONTACTS

The experimental results presented in this thesis were obtained for both n- and p-type cadmium telluride single crystals. These were grown at RSRE, Malvern, using a modification of the solvent evaporation technique reported by Lunn and Bettridge[1]. The slices of crystals (<111> orientation) were cut from the boules with thicknesses ranging from 0.5 mm to 1.5 mm. Some of the slices (1.0 - 3.0 cm^2 in area) contained a few grain boundaries especially near the edge of the crystal. These samples were mechanically polished to a finish of 0.25 μm using diamond paste and then chemically polished in a fresh solution of 1% bromine in methanol. Prior to the chemical etching, the samples were degreased by refluxing in methanol (BDH, Analar) or isopropyl alcohol (BDH,Analar). Immediately before evaporation of metal electrodes the samples were etched in 40% hydrofluoric acid (Analar) for one minute. This was found necessary to give reproducible Ohmic contacts.

In all cases the contacts were made by the evaporation of thick (≃ 200 Å) metal layers on to the samples in an Edwards pumping unit. The metals were evaporated from a molybdenum boat at a pressure of about 10^{-6} torr. The rate of evaporation was about 40 Å per minute.

Bi, Au or Au/Sb (≃ 3% Sb by wt) alloy produced noise free ohmic contacts to p-type samples and In/Sn (5∿ 6% Sn by wt) alloy to n-type samples. Care was taken to ensure that the evaporation of the In/Sn was carried out at the lowest pressure attainable (≃ 10^{-7} torr) to avoid any oxidation of the metal. When dealing with high resistivity materials, annealing at an elevated temperature (≃ 80° C) was often found necessary

to improve the ohmicity of contacts.

Study of the Surfaces

After each step of the sample preparation, the surfaces were studied with optical and scanning electron microscopes, and using the ESCA (Electron Spectroscopy for Chemical Analysis) technique. Optical micrographs of mechanically polished surfaces showed that this procedure alone did not produce well polished surfaces. Since CdTe crystals are soft, even careful mechanical polishing leaves scratches and damage on the surface. These blemishes can introduce surface states which produce a large number of discrete levels within the forbidden gap, and may prevent the production of ohmic electrical contacts. The etching procedure, in a suitable solution, can remove most of these scratches and produce clean surfaces.

Photographs of chemically polished surfaces (using Br_2/methanol) of various samples are shown in Fig.4.1. Large aggregates of a second-phase (precipitates) are clearly observed in Cl-doped materials. The precipitate in Fig.4.1(a) is approximately 100 microns in diameter. Precipitates of various size are also present and these are aligned in no particular crystallographic directions. Similar precipitates can also be observed in In-doped materials as shown in Fig.4.2 (b). However, these are comparatively small in size, the largest being about 40 microns in diameter. Such defects were not observed in any Cr-doped or undoped samples after Br_2/methanol polishing. These two cases are shown in Figures 4.1(c) and 4.1(d) respectively. As described in section 1.4, these second phases could well be $CdCl_2$ and In_2Te_3 in Cl-doped and In-doped materials respectively. The degree of precipitation depends on the enthalpy of formation (ΔH) of relevant compounds. Since ΔH of $CdCl_2$ is higher than that of In_2Te_3, the large clusters can be expected in Cl-doped CdTe.

Figure 4.2 shows the electron channelling patterns observed on these surfaces with a scanning electron microscope. These patterns are formed

FIGURE (4.1)

Photographs of chemically polished surfaces of CdTe doped with various elements

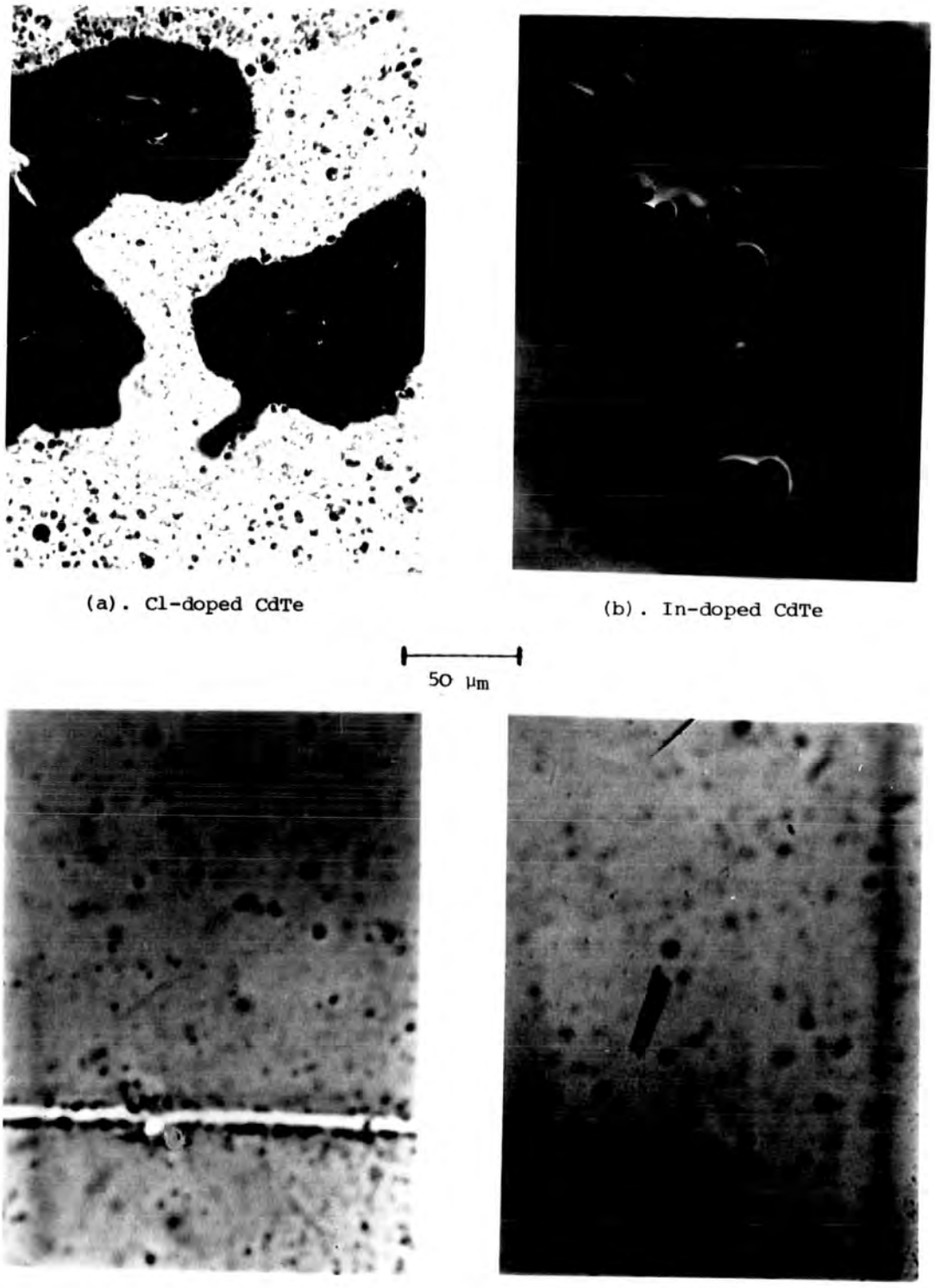

(a). Cl-doped CdTe

(b). In-doped CdTe

(c). Cr-doped CdTe

(d). Undoped CdTe

when a beam of electrons strike the surface of a single crystal specimen. At low magnification of the SEM, the Bragg reflection may occur at various sets of lattice planes normal to the specimen surface. This results in the formation of bands of contrast on micrographs which are called electron channelling patterns. These patterns completely disappear when treated in 40% hydrofluoric acid for about one minute. The crystalline property of the top layers (< 50 $\mathring{A}$)[2] of the sample therefore disappear when etched in HF acid. This was confirmed by re-etching the samples in 1% bromine in methanol and re-observing the electron channelling patterns.

The ESCA work on CdTe was carried out to study the chemical composition of surfaces obtained by various treatments. In this method the interaction of X-rays with a surface atom in the sample causes photo-ionization of the atom and ejection of an inner shell electron. The use of a known photon energy ($h\nu$) of excitation and energy analysis of the emitted electrons (E_{kin}) permits the determination of the binding energy (E_{bind}) of the electron from the relationship

$$E_{kin} = h\nu - E_{bind}.$$

The binding energy is characteristic of the emitting atom, and a surface analysis can be obtained from the electron energy spectrum.

This analysis revealed that etching CdTe in fresh 1% bromine-in methanol produces very clean surfaces. When these samples were left in air for a few days, the amount of O_2 and C were increased. This may well be due to the surface oxidation, adsorption of CO_2 and other contamination. Etching in 40% HF acid also provided fairly clean surfaces. These observations agree well with the surface studies reported by other researchers[3] in this field.

Figure (4.2)

Electron channelling pattern obtained from a single crystal of CdTe after etching in fresh bromine-methanol solution.

4.2 HALL EFFECT MEASUREMENTS

(a) Sample Preparation

Rectangular bar shaped specimens were cut from the crystal slices having length-to-width ratio (l/w) greater than 4[4]. The surfaces were treated as described in section 4.1 and ohmic contacts were prepared by vacuum evaporation of Au/Sb alloy.

The sample was then mounted on a piece of mica sheet, and electrical contacts to the crystal were made by fine copper wires. The wires were fixed to the evaporated contacts simply with (Acheson Electrodag 915) high conductivity air drying silver paste. The specimen was then fixed on the sample holder and connected to the electrical circuit shown in Fig. 4.3.

(b) Apparatus

The measuring circuit, designed for both D.C. and A.C. Hall effect measurements, is shown in Fig.4.3. The phase sensitive detection system was used for a.c. measurements and a stainless steel exchange gas cryostat was used to house the sample during all measurements. This cryostat consists of a large liquid nitrogen container surrounded by an outer jacket, and a long narrow cylindrical sample space. The sample is positioned near the bottom of this space between two polepieces of an electromagnet. The sample space could be evacuated or filled with helium gas during measurements. A 1.5 watt heater was fixed into the copper sample holder allowing temperatures up to 400 K to be obtained. A copper-constantan thermocouple fixed on to the sample holder was used to measure the temperature. The pressure in the outer jacket was maintained below 10^{-5} torr by an Edwards diffusion/rotary pumping unit.

The magnet used in this experiment possessed 5 cm diameter pole-pieces and produced a field of 0.17 Tesla across a 4.2 cm gap.

The five probe method was used for making measurements (Fig.4.3).

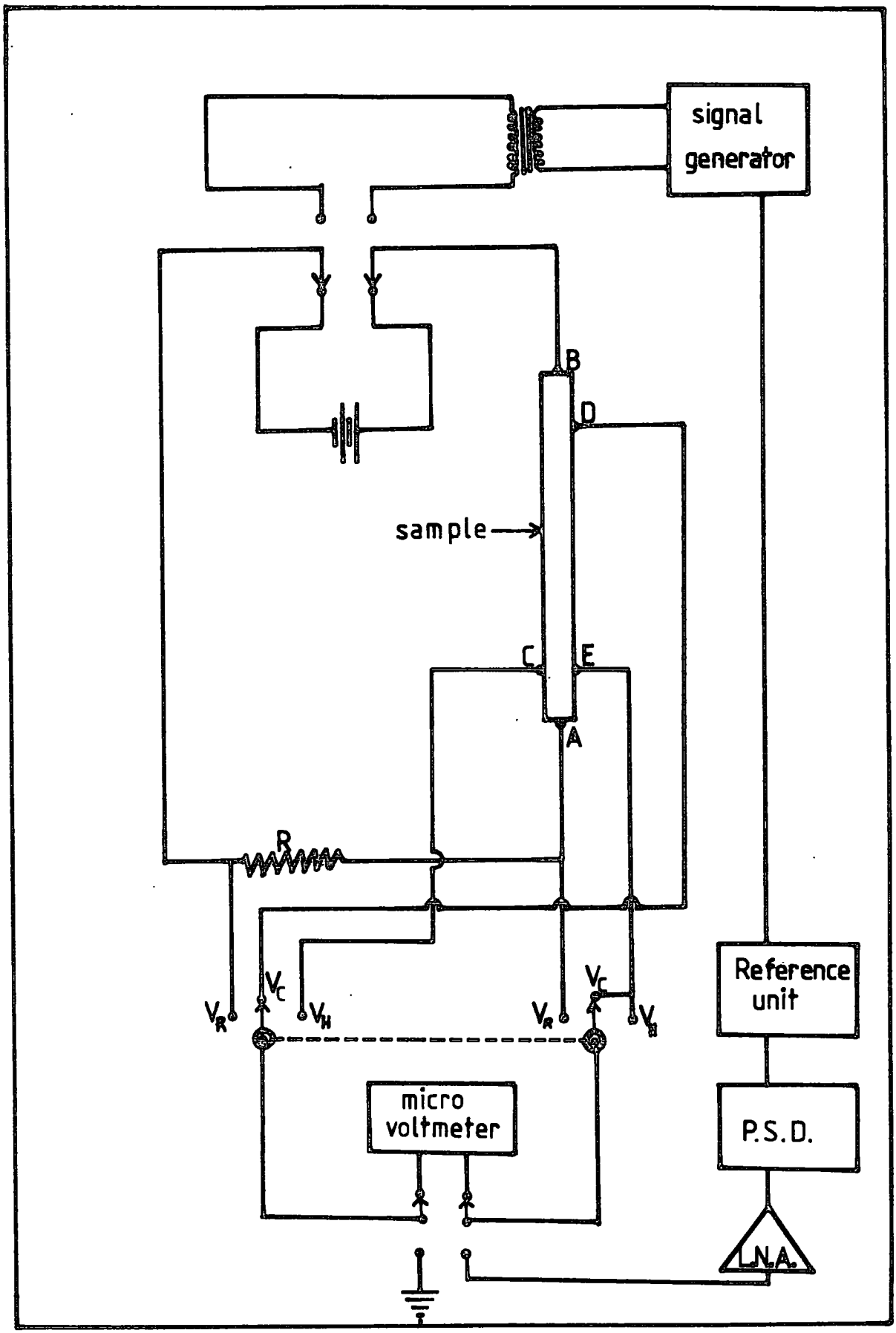

FIG. 4·3. ELECTRICAL CIRCUIT USED FOR BOTH D.C. AND A.C. HALL EFFECT MEASUREMENTS.

The electrical supply to the sample was a Keithley 240A high voltage supply. Bradley 188 and HP-3465B digital voltmeters were used to measure the various potential differences. The current normally used was 0.5 milliamperes and Hall voltages in the range 0.4 mv to 3.5 mv were encountered.

Equations 2.31 and 2.32 were used to calculate the Hall coefficient and conductivity. The material was assumed to be one-carrier type and hence equations 2.29 and 2.30 were used to obtain values for the carrier concentration, p , and the Hall mobility, μ_H. The scattering factor was assumed to be equal to unity. The D.C.Hall effect results obtained for Cr-doped and undoped CdTe samples are presented in Chapter 6. A.C.Hall effect measurements were unfortunately impracticable due to noise for these high resistivity (10^3-10^5 Ω.cm) materials.

4.3 D.C. CONDUCTIVITY MEASUREMENTS

The currents measured during the study of D.C. conductivity were in the range 10^{-13} - 10^{-3} Amperes. Fig.4.4 shows the block diagram of the simple electrical circuit used for these measurements. Co-axial leads, B.N.C. plugs and sockets were used for all external electrical couplings. The voltage (0-1000V) was supplied by a Keithley model 241 regulated high voltage supply which had an output resistance of less than 0.05 Ohm. The currents were measured by Keithley model 410A picoammeter. The input resistance of this instrument varied from 10^9 Ohms to a fraction of an Ohm, when measuring currents from 10^{-13} to 10^{-3} Amperes.

During these D.C. conductivity measurements, a definite procedure was followed to avoid any misleading current readings due to charge accumulation effects. After each current-voltage curve at a fixed temperature the sample was heated up to some definite maximum temperature in the dark with a small applied voltage. This procedure helps to release any excess charge in the crystal. The current corresponding to a low electric field value was measured and kept as a reference when taking the initial curve at room temperature. This value was checked for reproducibility

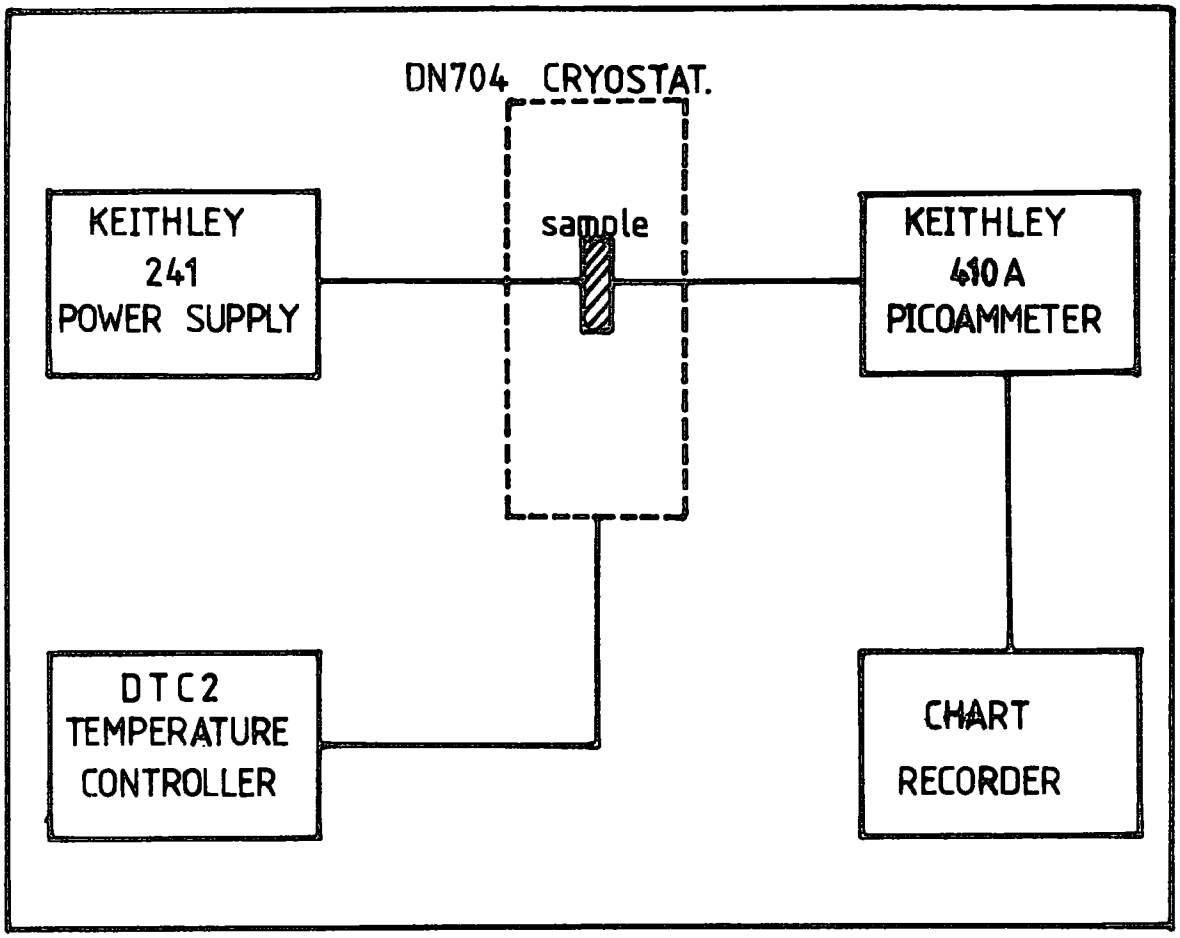

FIG. 4·4. BLOCK DIAGRAM OF THE SIMPLE ELECTRICAL CIRCUIT USED FOR D.C. CONDUCTIVITY MEASUREMENTS.

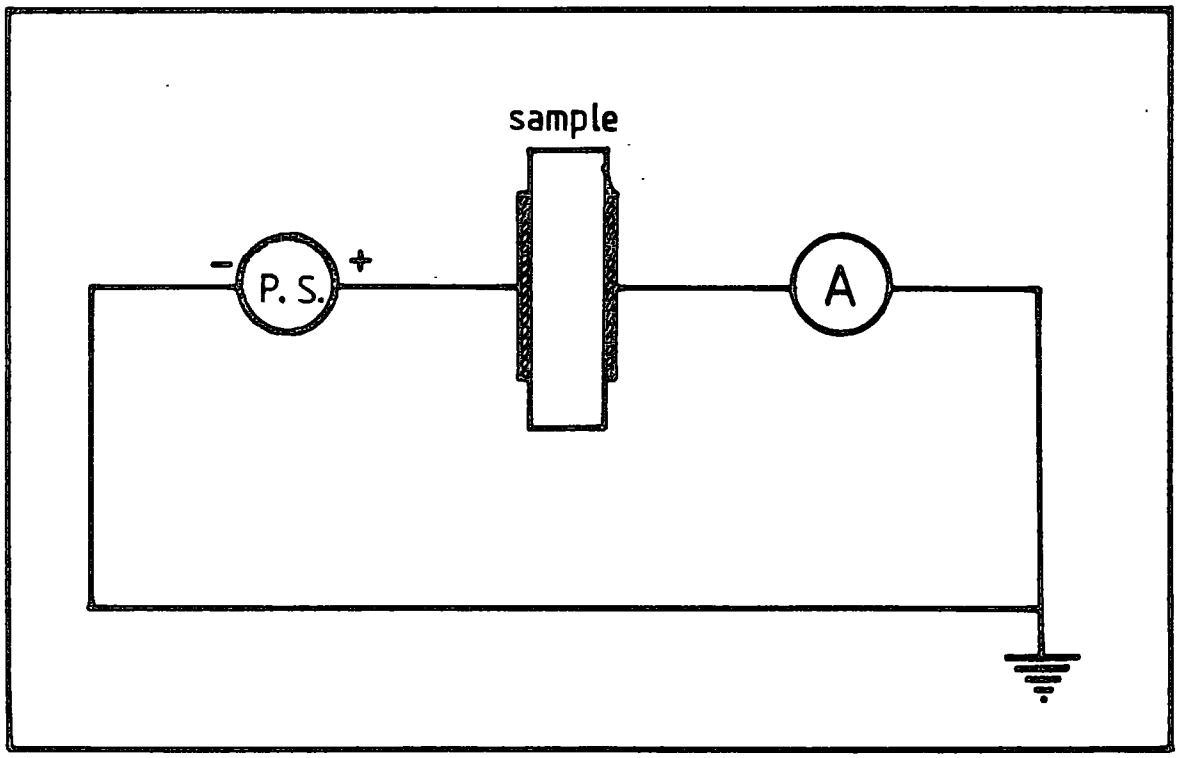

FIG. 4·5. SIMPLE ELECTRICAL CIRCUIT USED FOR D.C. CONDUCTIVITY MEASUREMENTS.

after each low temperature run and subsequent heating process. Two types of cryostat were used for these measurements and are described in the following section.

(a) DN704 Cryostat

The main parts of the commercial exchange gas cryostat (Oxford Instruments DN704) used for D.C. conductivity measurements is shown in Fig.4.6. The unit is designed around a 20mm clear internal diameter sample tube to which a heat exchanger is attached. The copper heat exchanger is cooled with liquid fed via a supply tube from the liquid nitrogen vessel. The gas exhausts from the heat exchange block and exits through an exhaust in the top plate as shown in the diagram.

In this cryostat the main vacuum does not have to be broken in order to change samples. The vessel is of welded stainless steel construction, and incorporates an activated charcoal sorb which cryopumps when cool. This ensures a good insulating vacuum without the need for continuous pumping. The sample changing is a very quick operation as it only necessitates removal and repositioning of a sample holder. The sample space can be evacuated and refilled with a suitable exchange gas to avoid condensation of water vapour on cooling.

As a standard unit, this cryostat is supplied with a platinum resistance thermometer and a 39 Ohm heater wired to the 10-pin electrical connector at the top plate. Variable temperatures are obtained by balancing the heat input to the heat exchange block against the cooling power available. Cooling power is regulated by opening or closing the gas exhaust valve. An Oxford Instruments digital temperature controller (DTC2) was used to measure the temperature of the system and to maintain this at some desired value. The measured temperature using this instrument was within an accuracy of $\pm$ 0.1 K.

(b) Helium Exchange Gas Cryostat

The salient features of the home-made helium gas cryostat are

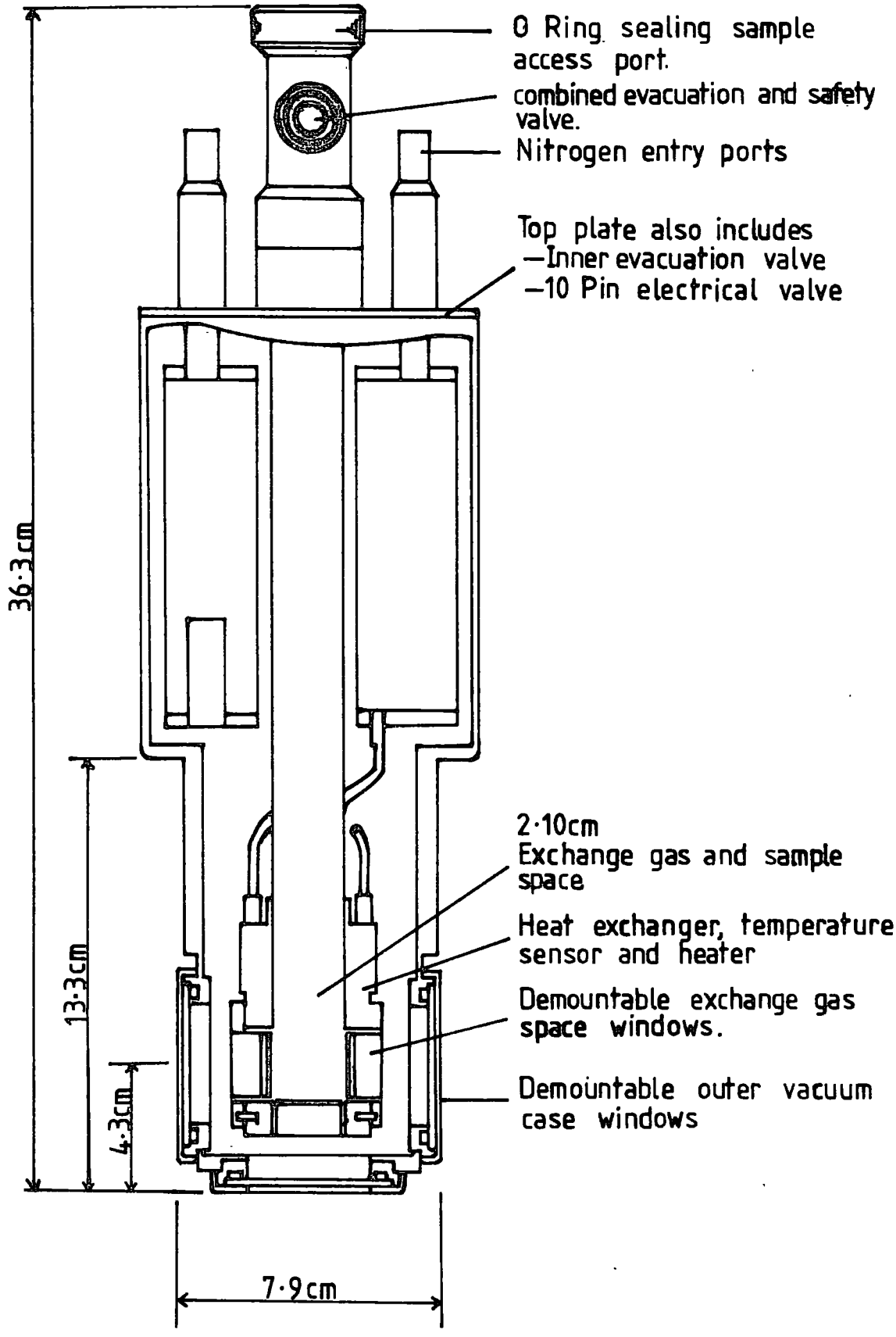

FIG 4·6. DN704 LN_2 CRYOSTAT

illustrated in Fig. 4.7. It consisted of a large stainless steel cylinder, mounted firmly on a supporting rack. The cryostat could be evacuated to a pressure of 10^{-3} torr using an Edwards ES 330 rotary pump. Helium gas was passed down a hollow metal tube to the bottom of the chamber, and allowed to permeate out slowly through a valve positioned at the top of the cryostat. The rate of flow could be adjusted accurately by a needle valve. The temperature of the sample was controlled by balancing the heat produced by a 150 Watt circular heater against the cooling power supplied by a jacket of liquid nitrogen surrounding the outside of the cryostat. The dewar containing liquid nitrogen was thermally insulated from outside and built into a wooden box for safety reasons and ease of handling. Cooling power was regulated by lifting or lowering this jacket around the cryostat. The power supplied to the heater was controlled by a Eurotherm temperature controller. The temperature of the sample was measured by means of a copper-constantan thermocouple placed near the sample, with an accuracy of about $\pm$ 1.0 K.

Samples were mounted on a PTFE disc and clamped in position on a PTFE table as shown in the diagram. Electrical contacts to the sample were made by means of fine wires taken from highly insulating lead-throughs in the wall of the cryostat and passed along the centre of two hollow supporting pillars. The cryostat was securely earthed and the above procedure ensured good screening and reduced the electrical noise. Most of the high temperature conductivity measurements were carried out in this cryostat, and the DN 704 cryostat was generally used for low temperature (below 200 K) conductivity measurements.

4.4 THERMALLY STIMULATED CURRENTS

(a) Apparatus

Thermally stimulated current measurements[5] were made using the DN 704 cryostat and DTC2 temperature controller described in section 4.3. Illumination was provided through one of the windows using a

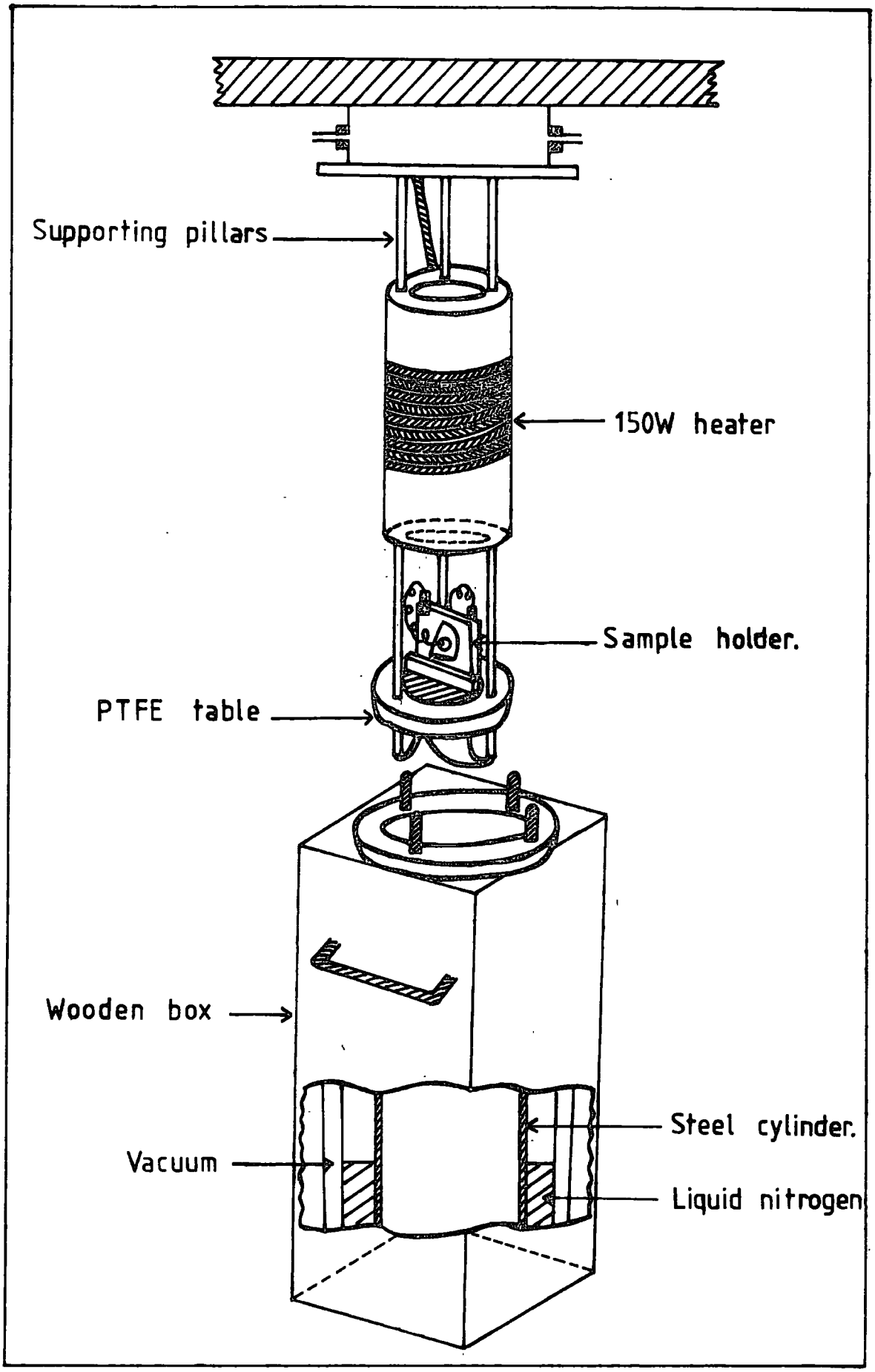

FIG. 4·7. Helium exchange gas cryostat used for D.C. conductivity measurements at high temperatures.

250 W silica-halogen lamp. This was filtered with a ≃ 2 cm path length of ≃ 10% by wt. copper sulphate solution to cut-off infra-red (below bandgap) radiation. With this arrangement the illumination intensity at the sample was approximately 100 $mW.cm^{-2}$. For measurements in the dark, a light-tight cap was placed over the window. The cryostat was heated at a constant rate using a voltage ramp generator to drive the temperature controller. The resultant thermally stimulated current was measured using a Keithley 410A picoammeter and displayed on a chart recorder. A constant voltage across the sample was applied by a Keithley model 240A high voltage power supply.

(b) Procedure

Measurements were carried out on very thin (340 μm) samples of high resitivity materials provided with two sandwich type Ohmic contacts. These semi-transparent contacts (≃ 100 Å) were made by evaporating Au, as described in the earlier part of this chapter. The sample investigated was mounted on the sample holder of DN704 cryostat using Oxford Instruments G.E. varnish and the electrical contacts were made using air drying silver paste. The cryostat was evacuated to a pressure of ≃ 10^{-4} torr and then filled with helium. This procedure provides a good thermal contact with the sample and avoids condensation of water vapour on the sample at low temperatures. In order that reproducible measurements could be obtained a strict heating and cooling cycle was followed. The sample was first heated in the dark to a temperature of 360 K with a small applied voltage and then cooled to liquid nitrogen temperature. When the lowest temperature, 77 K, was attained the sample was illuminated for 10 minutes in order to complete the trap filling. A fixed electric field of 10^{3} $V.cm^{-1}$. was then applied to the sample in the dark, and the T.S.C. was monitored while the sample was heated from liquid nitrogen temperature to about 300 K. It was found that the heating rate was not always constant throughout the run, but decreased with time due to an increasing temperature gradient

between sample and exchange gas. However, within the temperature region of a particular peak the deviation from linearity was small.

T.S.C. results obtained for high resistivity Cl-doped materials are presented and compared with previously reported results in Chapter 5.

4.5 MS AND MIS SOLAR CELLS

(a) Preparation of MS Barriers

Two different types of single crystals have been used to produce Schottky diodes in this series of experiments. The first was p-type material with a resistivity in the range 10^3-10^5 Ohm.cm (Cr-doped and undoped), and the second was n-type material having a resistivity in the range 0.01-1.00 Ohm.cm(undoped and In-doped). Schottky barriers were prepared by evaporation of Sn on to p-type and Au on to n-type samples. All surfaces were prepared initially by mechanical and chemical polishing as described in section 4.1. Some diodes were fabricated on samples transferred to the vacuum system immediately after this treatment. Other surfaces were either etched for 1 minute in 40% HF, or left in air for 2-3 days, prior to fabrication.

The electrical properties of Schottky barriers prepared on high resistivity material are presented in Chapter six. Barriers on low resistivity materials showed better electrical properties and they are presented and compared with those of MIS structures in Chapter seven.

(b) Preparation of MIS Barriers

Both undoped and In-doped low resistivity materials were used to prepare MIS devices. These single crystals (< 111> orientation) were n-type and their carrier concentrations were in the range (1.0-4.0) x 10^{17} cm^{-3}. The surfaces of the samples were prepared using the method described in section 4.1. No hydrofluoric acid treatment was used in this series of experiments. To compare the experimental results of MS and MIS solar cells, these were prepared side by side on the same CdTe surface using the following procedure : The Schottky contact

was first deposited by thermal evaporation of Au (20 nm thick) on to one half of the semiconductor surface and a common Ohmic back contact (In/Sn alloy) was evaporated on to the opposite side of the sample. Monolayer(s) of cadmium stearate or C_4 Anthracene were then deposited on to the sample using the Langmuir-Blodgett technique. The deposition conditions have been described elsewhere[7,8,9] in detail, and summarized in section 4.6. Monolayer thicknesses were 2.5nm and 1.2nm for $CdsI_2$ and C4 Anthracene respectively. The deposited film was stored in a desiccator under a low pressure of nitrogen for 2-3 days before an Au top electrode was deposited by vacuum evaporation at a rate of 2.0 nm. min^{-1}. The substrate was cooled to about -100° C during the process. The thickness of this top electrode was made identical to that of the Au Schottky contact by carefully monitoring the deposition using a crystal oscillator type film thickness monitor. Antireflection coatings were not used in this preliminary investigation.

(c) Measurements of Barrier Capacitance

The barrier capacitance of the MS and MIS diodes was determined as a function of applied voltage using a phase-sensitive detection technique. The frequency of the a.c. signal (≈ 25 mV) applied across the barrier was 20 kHz. Both cryostats described in section 4.3 were used for the measurements at different temperatures.

Figures 4.8 and 4.9 show the details of this measurement system and the equivalent circuit of appropriate circuit configuration. An a.c. voltage V_s is applied to the test capacitance C_x in series with a standard resistor R_m.

If I. $R_m << 1/G_x$ and

II. $R_m \omega^2 C_x^2 << G_x$

the voltage measured across R_m is ;

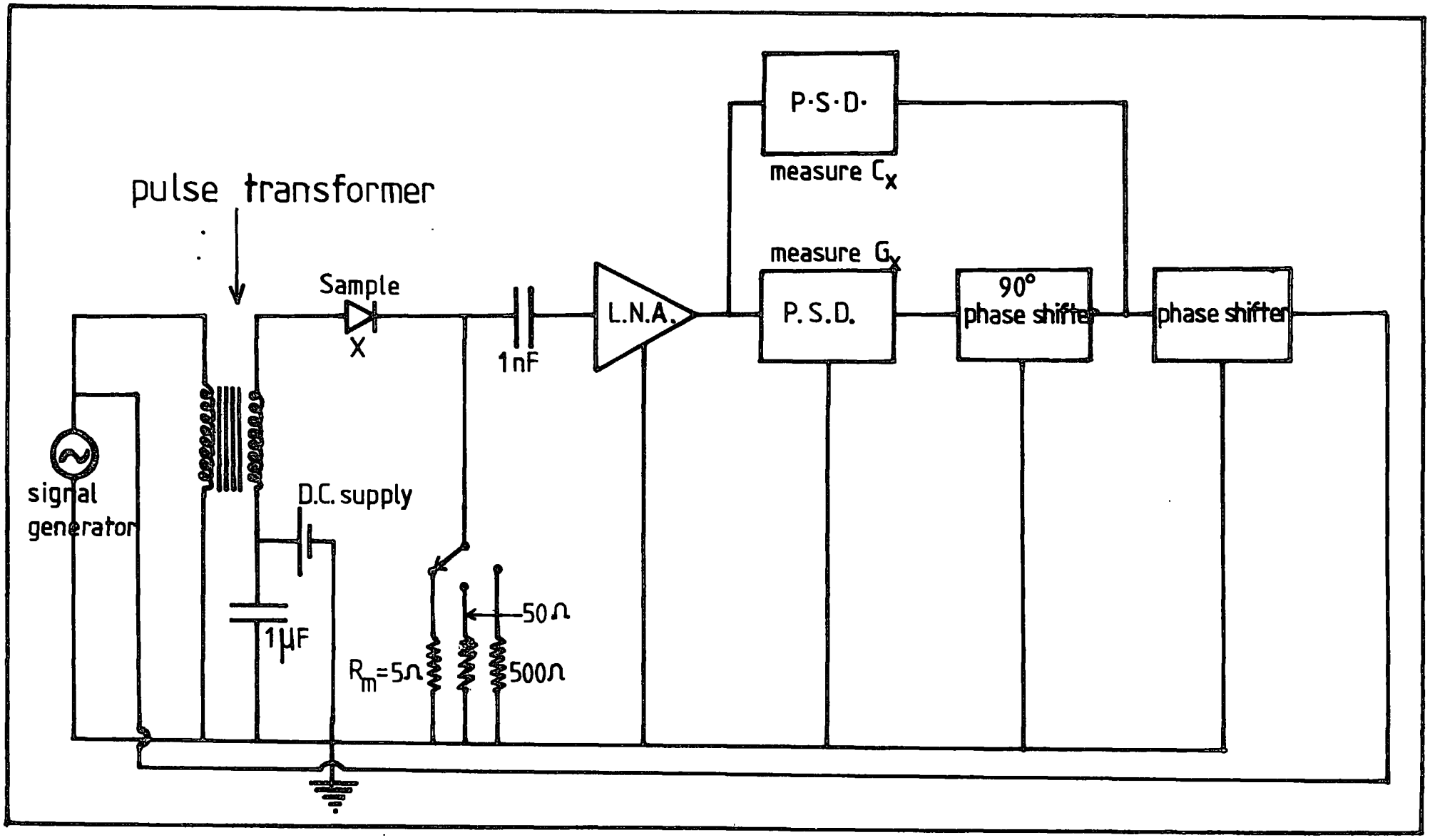

FIG. 4·8. PHASE SENSITIVE DETECTION TECHNIQUE.

Figure 4·9

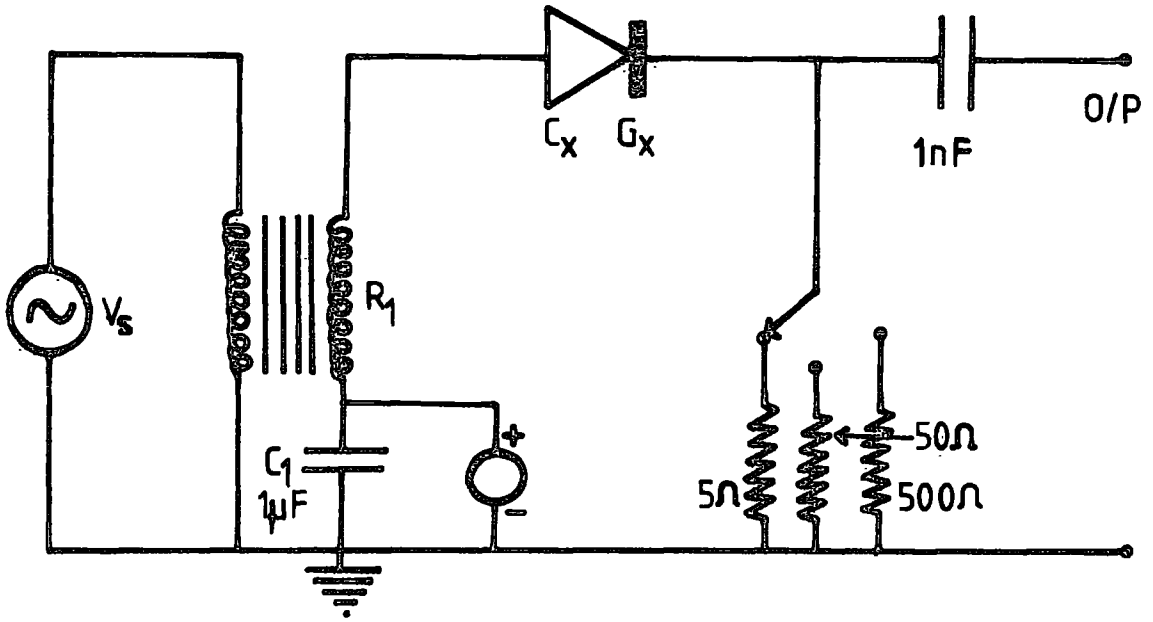

(A). THE SIMPLE CIRCUIT USED FOR MEASUREMENT OF METAL–SEMICONDUCTOR JUNCTION CAPACITANCE.

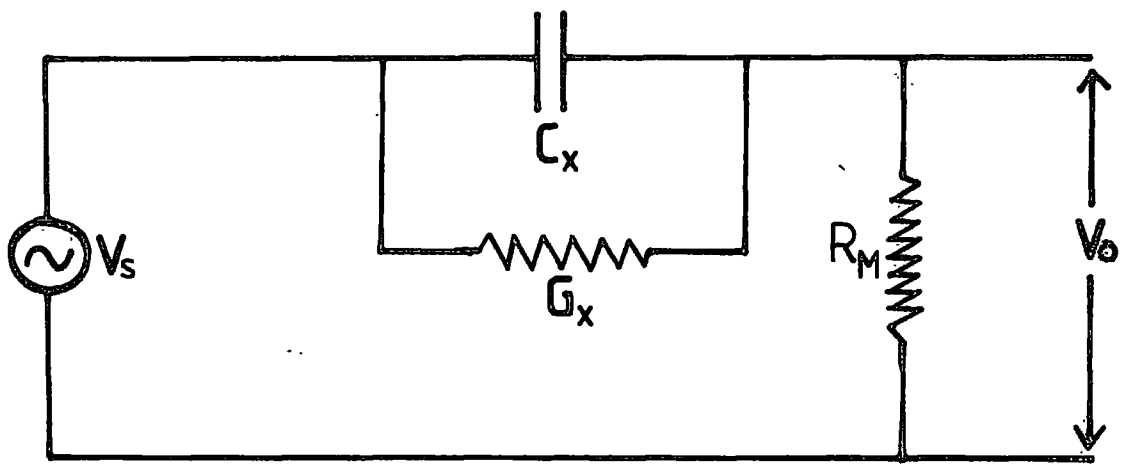

(B). THE EQUIVALENT CIRCUIT OF THE ARRANGEMENT USED FOR MEASUREMENT OF SCHOTTKY BARRIER CAPACITANCE.

$$V_o = V_s R_m (G_x + j\omega C_x) \quad (4.1)$$

which can be represented by two voltages ; one in phase with $V_s(V_s R_m G_x)$ and one in quadrature with $V_s(V_s R_m \omega C_x)$.

Both voltages can be measured simultaneously with a two channel phase-sensitive-detector (PSD) by simply measuring the in-phase and out-of phase components of voltage across R_m. In circuit arrangement the value of R_m was kept well below $1/G_x$ so that the entire d.c. volts appear across the device.

Before any measurements the set-up was calibrated using the following procedure : The output from the signal generator was adjusted to give as large an a.c. voltage as is allowable (< 100 mV to avoid non-linear effects) across the device under test. A suitable mica capacitor was connected across the test points, and the gain of the a.c. amplifier was then adjusted to give a reasonable output from the P.S.D. system. The phase shifter was adjusted so that no output was obtained from the conductance indicating P.S.D. The phasing could be rechecked by putting in the test points a non-reactive resistor when it should be observed that there was no output from the capacitance indicating P.S.D.

(d) Measurement of Solar Cell Parameters

The light source used was a 1.5 kW quartz halogen strip lamp with a parabolic reflector housing (Fig.4.10). The lamp was mounted in a levelled metal frame which contained a 2 cm deep tray of flowing water. Underneath the tray was a table of adjustable height on which the sample was mounted. The illumination at the surface of the sample was adjusted by altering the table height to give approximately AM1 characteristics. This illumination intensity was used for all of the experiments with this light source.

Measurements of the current-voltage characteristics in the dark were carried out using the simple circuit shown in Fig.4.5 with the device

FIG. 4·10. LIGHT SOURCE ARRANGEMENT USED TO MEASURE SOLAR CELL PARAMETERS.

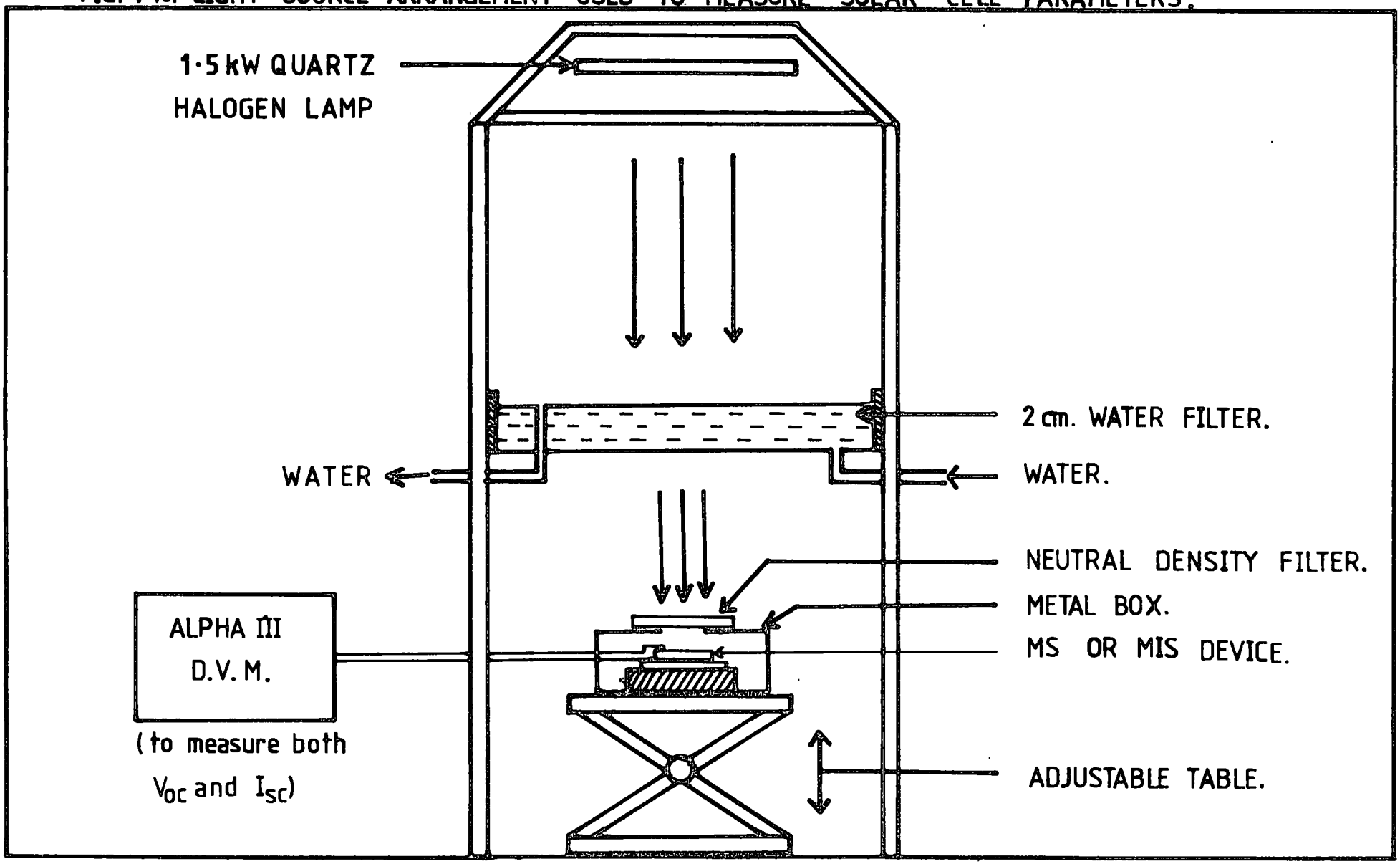

mounted in a cryostat or in a completely covered metal box. The same measurements under AM1 illumination were carried out under the lamp with a circular opening in the lid of the metal box. The intensity of light could be varied by placing neutral density filters on the lid to cover the opening. Both the open circuit voltage and short circuit current were measured by connecting an alpha III digital voltmeter directly to the device. This situation is clearly shown in the Fig. 4.10.

When making the electrical connections to the MIS devices, fine copper wires were used with a small amount of half dried silver paste. This procedure avoided the chance of dissolving the Langmuir film in the solvent used for silver paste.

4.6 LANGMUIR-BLODGETT FILMS

(a) Introduction

Langmuir-Blodgett films[10] are an interesting example of ordered organic systems. They can be assembled one monolayer at a time to form a planar 2-dimensional sheet of accurately controlled thickness. The preparation of such films was suggested by Langmuir (1920) and his ideas were extensively applied by Blodgett (1935). The technique consists of transferring monolayers of amphipathic molecules on to solid substrates by dipping and raising the latter through a compact monolayer floating on the surface of purified water. If the deposition conditions are carefully controlled, a single monolayer is transferred on to the substrate during each traversal of the water surface. The thickness of a Langmuir film is determined by the number of monolayers deposited and the molecular size of the material used. Various organic materials have been deposited using this technique,but most data have been obtained for fatty acids or their salts. These substances possess molecular structures which consist of a hydrophilic group (-COOH) at one end of a straight carbon chain and a hydrophobic methyl group ($-CH_3$) at the other end. Under normal deposition conditions the carbon chains are aligned normal to the substrate surface

with successive layers oriented in opposite directions. The molecular size (half the distance separating the carbonyl groups) is approximately 2.5 nm for stearic acid and ≈ 1.20 nm for C_4 anthracene[10]. Langmuir films formed from the cadmium salts of these materials provide good insulators with high breakdown fields[11].

(b) Thin Film Deposition

Cadmium stearate and C_4 anthracene films were used in MIS solar cells as an insulator, and deposited on to the CdTe surface using the Langmuir-Blodgett technique. A simplified diagram of the Langmuir trough is shown in Fig. (4.11).

The lower half of the CdTe substrates (i.e. the opposite end from that with the Schottky contact) was dipped into the surface of water obtained from a millipore purification system. This aqueous subphase contained 2.5×10^{-4} molar cadmium chloride (BDH, Analar) and its pH was adjusted by the addition of ammonia (BDH, Aristar) or hydrochloric acid (BDH, Analar). This value of pH was 5.6-5.8 for stearic acid and 4.4-4.6 in the case of C_4 anthracene. A micrometer syringe was used to spread a few drops of stearic acid (sigma grade 1) or C_4 anthracene (Synthesised in the Corporate Laboratory (ICI Ltd) by Dr. H Steven) dissolved in chloroform (BDH Aristar) on to the water surface. The surface area and hence the surface pressure of the monolayer could be varied using a motor-driven PTFE-coated glass fibre barrier. The surface pressure was measured with a Wilhelmy plate suspended from a sensitive microbalance. An electronic feedback system connected to the barrier motor was used to maintain a constant monolayer surface pressure of 2.5×10^{-2} N m^{-1} during the deposition process. In fact, both the surface area and the surface pressure were monitored continuously during the deposition process.

The CdTe substrates were raised and dipped through the compressed monolayer using a variable-speed motor attached to a micrometer. The

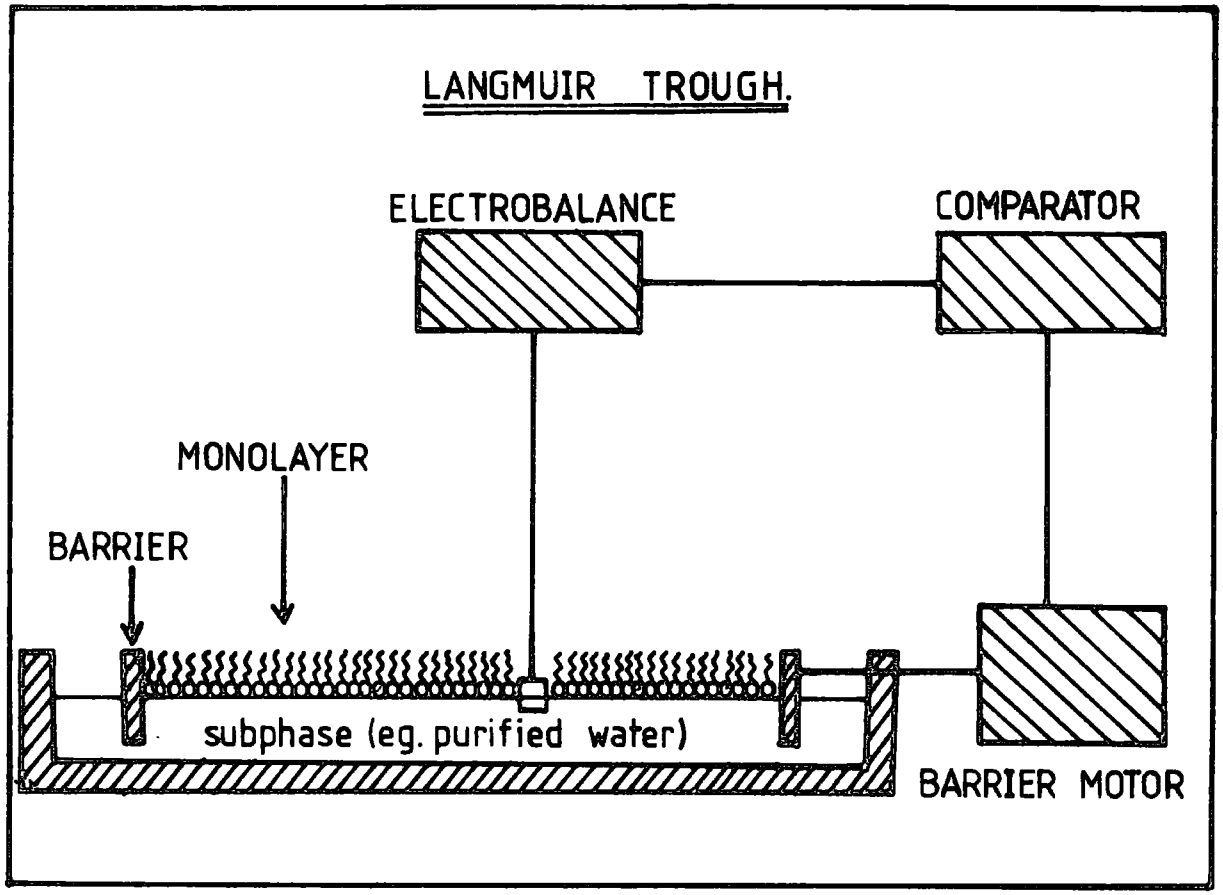

Fig. 4·11. Simplified diagram of the Langmuir trough.

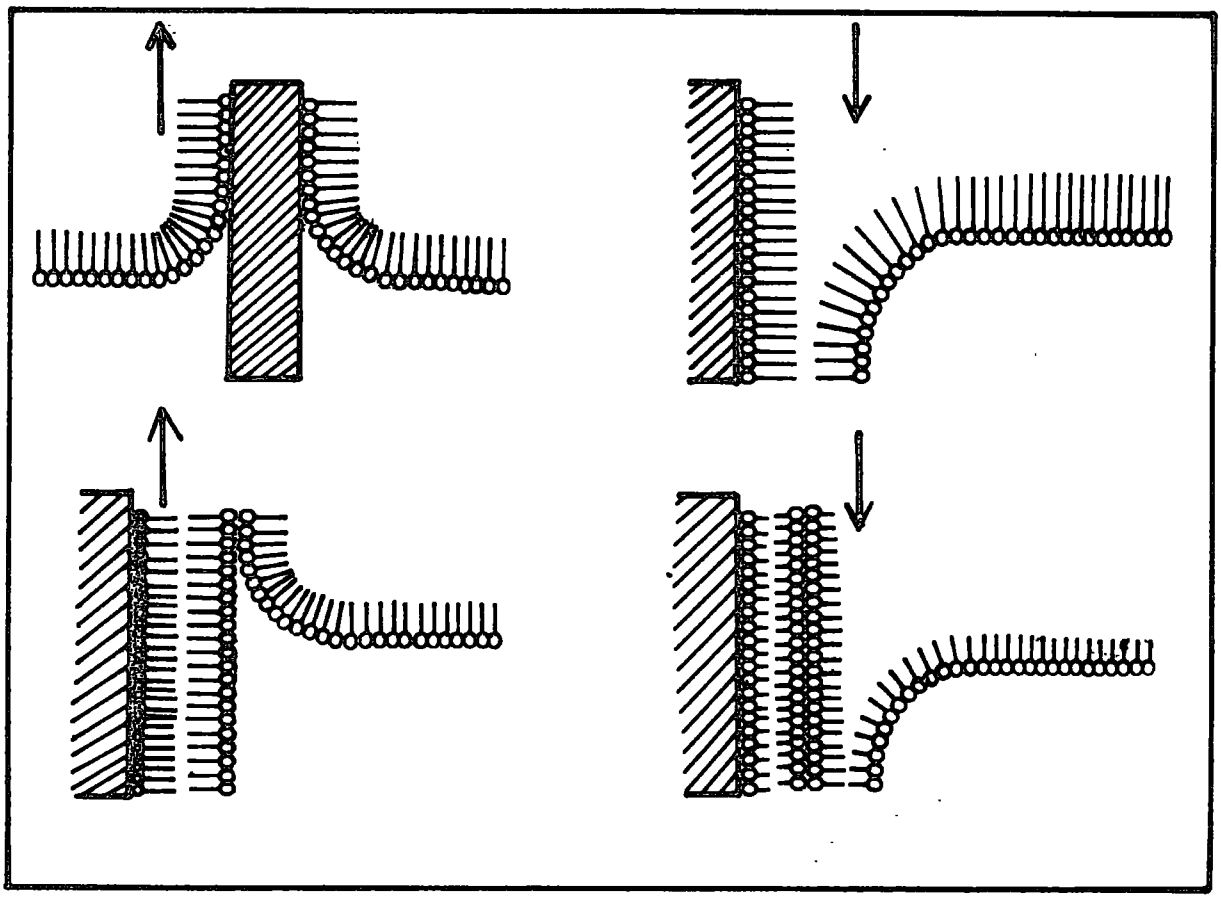

Fig 4·12. The deposition of monolayers on to solid surfaces.

first monolayer was transferred on to the substrate as it was raised through the interface (Fig. 4.12). A rate of about 2 mm.min^{-1} ensured that this first layer emerged completely dry from the subphase. Subsequent layers could then be transferred to the CdTe at dipping rates of about 1 cm.min^{-1}. The deposition of successive layers on to a substrate is shown schematically in Fig.4.12. The films were stored in a desiccator under a low pressure of nitrogen for at least 3 days before top electrodes (Au) were deposited by thermal evaporation.

CHAPTER 5

RESULTS: SEMI-INSULATING CdTe (Cl-DOPED)

5.1 INTRODUCTION

Because of its potential application in γ and X-ray detection systems (chapter 1), semi-insulating CdTe is attracting a great deal of interest. The performance of such devices based on CdTe is still, however, inferior to Ge and Si detectors due to the difficulty of controlling the crystal perfection in this material. The use of the latest developments in crystal growth techniques and the compensation of native defects by halogen doping[1] seem to be the most promising ways of improvement. A variety of experimental techniques has been used to identify the localized levels in CdTe. Some of the reported deep levels within the energy gap are shown in fig (1.3). Unfortunately there is still little agreement about the origin of these levels.

In this work a systematic investigation of the conductivity of a series of CdTe:Cl samples taken from one crystal boule is presented. The results are analysed and interpreted using theorems proposed by Roberts and Schmidlin[2-4]. A completely independent computer simulation is used to check and "fine-tune" the various parameters obtained by the above method. This produces the theoretical activation energy curves for a given semi-conducting system and facilitates the study of the effect of different parameters such as the position of the impurity levels, their concentrations and charge carrier mobilities. The computer program used for this purpose is given in Appendix 1.

The observation of the Meyer-Neldel rule for both different CdTe:Cl samples, and for one sample after different annealing conditions is also discussed in terms of a new model. Finally an investigation of

deep levels by TSC is presented and compared with the previously reported results.

5.2 D.C. CONDUCTIVITY MEASUREMENTS

(a) Space-Charge-Limited Currents

All conductivity measurements presented in this chapter were made using sandwich type geometries in a helium exchange gas cryostat. Sample preparation methods and the relevant experimental techniques are described in chapter 4. Bi, Au and Au/Sb made good Ohmic contacts to these high resistivity samples. Bi and Au, often required post-evaporation heat treatments, but Au/Sb made good Ohmic contacts as evaporated. The Ohmicity of the contacts could be checked by measuring the capacitance of the system and comparing this with the expected geometrical capacitance. The different samples used in this investigation are numbered as shown in table (5.1).

Typical I-V characteristics for these high resistivity samples are shown in fig (5.1). The curves display a low field Ohmic region followed by a square law region. One of these samples (No.2) shows a clear trap filled limit voltage of 370 V and this was used to calculate the trap density as described in chapter 2. Most of the high resistivity CdTe samples studied showed space charge limited conduction[5,6,7] due to their low density of thermally generated charge carriers.

(b) Activation Energy

Fig.(5.2) shows a typical plot of log I versus reciprocal temperature for both Ohmic and SCL currents. In the temperature range investigated, there is one activation energy (0.62 eV) for the SCL current, whereas the Ohmic current shows two distinct energies (0.62 eV, 0.80 eV) with a transition temperature of 256 K. All the other samples showed similar data, but the transition temperature varied from sample to sample. There was one exception, however, (sample No.2) which did not show a transition within our experimental temperature range (220 K-370 K).

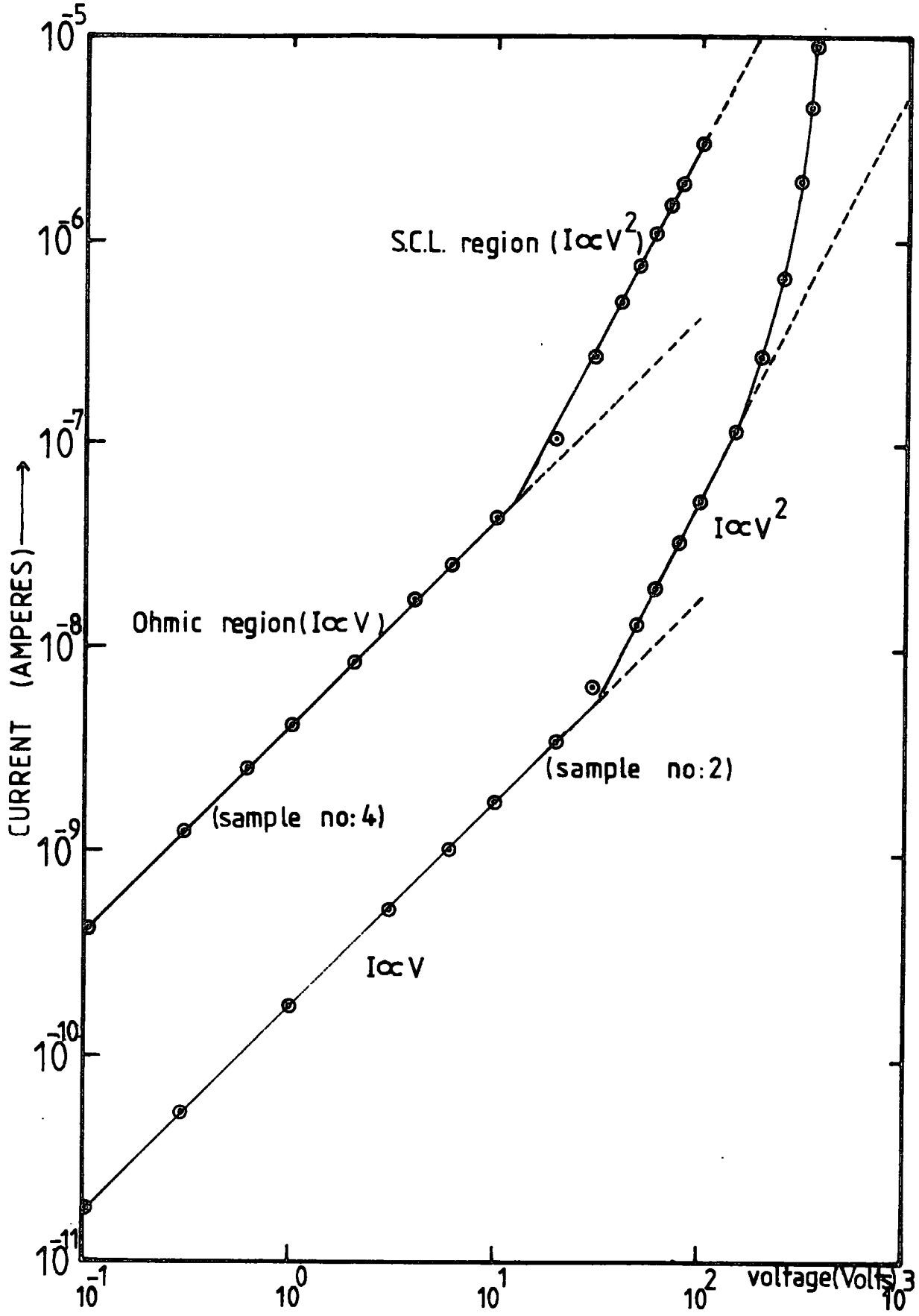

FIG. 5·1 CURRENT VOLTAGE CURVES AT ROOM TEMPERATURE FOR TWO Cl – DOPED CdTe SAMPLES.

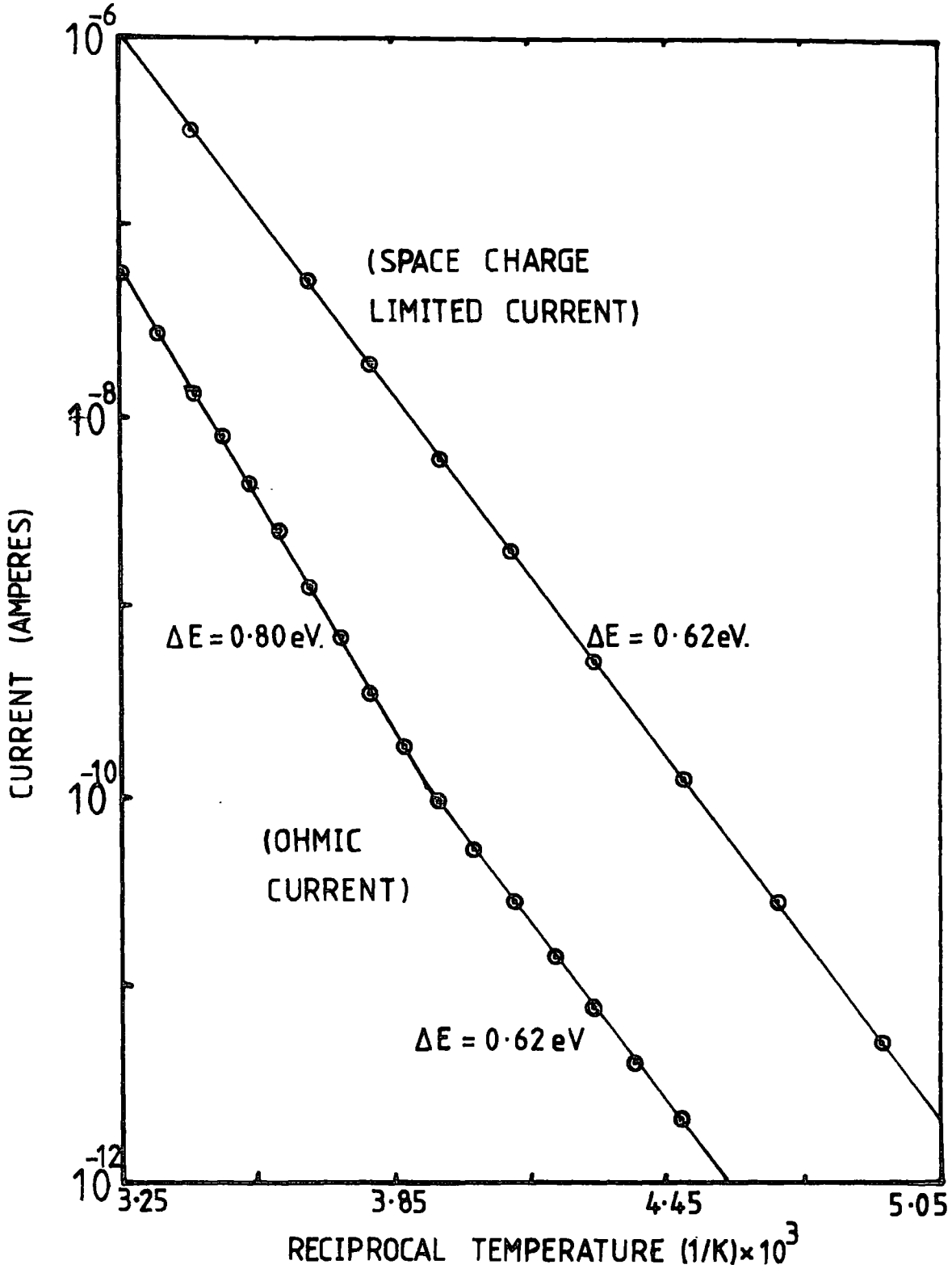

FIG. 5·2 CURRENT VERSUS RECIPROCAL TEMPERATURE IN THE OHMIC AND SCL REGIONS FOR A CdTe:Cl SAMPLE. (SAMPLE NO: 1.)

These different activation energies were interpreted using the theorem proposed by Roberts and Schmidlin[3]. Using the conductivity equations given in section 2.1.1(d) and the data from fig (5.2), it can be seen that the Ohmic conductivity in the sample is governed by two levels (E_m-E_v) = 0.62 eV and (E_q-E_v) = 0.98 eV. At temperatures below 256 K the conduction is extrinsic and the activation energy is simply 0.62 eV. Above 256 K the conduction becomes non-extrinsic with an activation energy of 0.62 + 0.5 (0.98 - 0.62) = 0.80 eV. The following section deals with the detailed analysis of data shown in fig (5.2).

(c) Detailed Analysis

For a complete interpretation of electrical conductivity data for these samples, the conductivity type must be known. Unfortunately, many of our samples were too resistive for simple Hall effect experiments. However, because Ohmic contacts could be made to the specimens using high work function metals (e.g. Au) and Schottky barriers were produced using low work function metal electrodes (e.g. In), it was concluded that the material was probably p-type. Since this agrees with other authors[8-10] results, the conductivity type was assumed to be p-type throughout this analysis.

In order to obtain information about the densities of the levels E_m and E_q and to explain the transition from extrinsic to non-extrinsic conduction, the following procedure was adopted.

(i) Using the values of the SCL and Ohmic currents for extrinsic conductivity, the value of the excess acceptor concentration, (N_a-N_d) was calculated via equations (2.4), (2.17) and (2.20). (These equations needed a slight modification for p-type conduction before the calculation).

(ii) A value for μ_p, the hole mobility, was assumed with the help of previously published data[1,8,10,11] and values for N_m and N_q were derived using the graphical approach described in section (2.1.2).

(iii) Finally an iterative routine on a computer was used to "fine-tune" the above values so as to obtain an exact fit with the experimental data. The required parameters such as bandgap, E_g, temperature coefficient of E_g, effective masses, dielectric constants and mobilities were taken from table (1.1). The temperature variation of levels E_m and E_q were taken as proportional to their distance from the valence band edge[12], i.e.

$$(E_v - E_m) = 0.62 - \left|\frac{0.62}{1.60}\right| \times \alpha T \quad \text{eV.}$$

and

$$(E_v - E_q) = 0.98 - \left|\frac{0.98}{1.60}\right| \times \alpha T \quad \text{eV.}$$

where α is the temperature coefficient of energy gap and T is the temperature (in Kelvin). The hole mobility, μ_p, was assumed to have a temperature dependence of the form :- $\mu_p(T) = \mu_p(0) \cdot T^{-1.5}$. No allowance was made for the spin degeneracy of levels E_m and E_q in the iteration. When the necessary parameters are fed in to the computer, the program assumes a Fermi energy at the middle of the forbidden gap for the first instance. With this value of Fermi energy the number of electrons (n) and holes (p) in transport bands are calculated using Fermi-Dirac statistics. If the charge neutrality is not fulfilled (i.e. if $n \neq p$), then the Fermi energy is adjusted so as to equalise n and p, and this iteration continues until $(n-p) \simeq 0$. When this is achieved the Fermi energy is fixed, the conductivity is calculated at different temperatures and activation energy curve is plotted together with the experimental results. The best computer fit (fig. 5.3) was obtained with the following set of parameters.

$$(E_v - E_m)_{OK} = 0.62 \text{ eV.} \qquad N_m = 1.0 \times 10^{12} \text{ cm}^{-3}.$$

$$(E_v - E_q)_{OK} = 0.98 \text{ eV.} \qquad N_q = 2.0 \times 10^{15} \text{ cm}^{-3}.$$

$$\mu_p(293 \text{ K}) = 169 \text{ cm}^2/\text{V.sec.} \quad (N_a - N_d) = 2.4 \times 10^{10} \text{ cm}^{-3}.$$

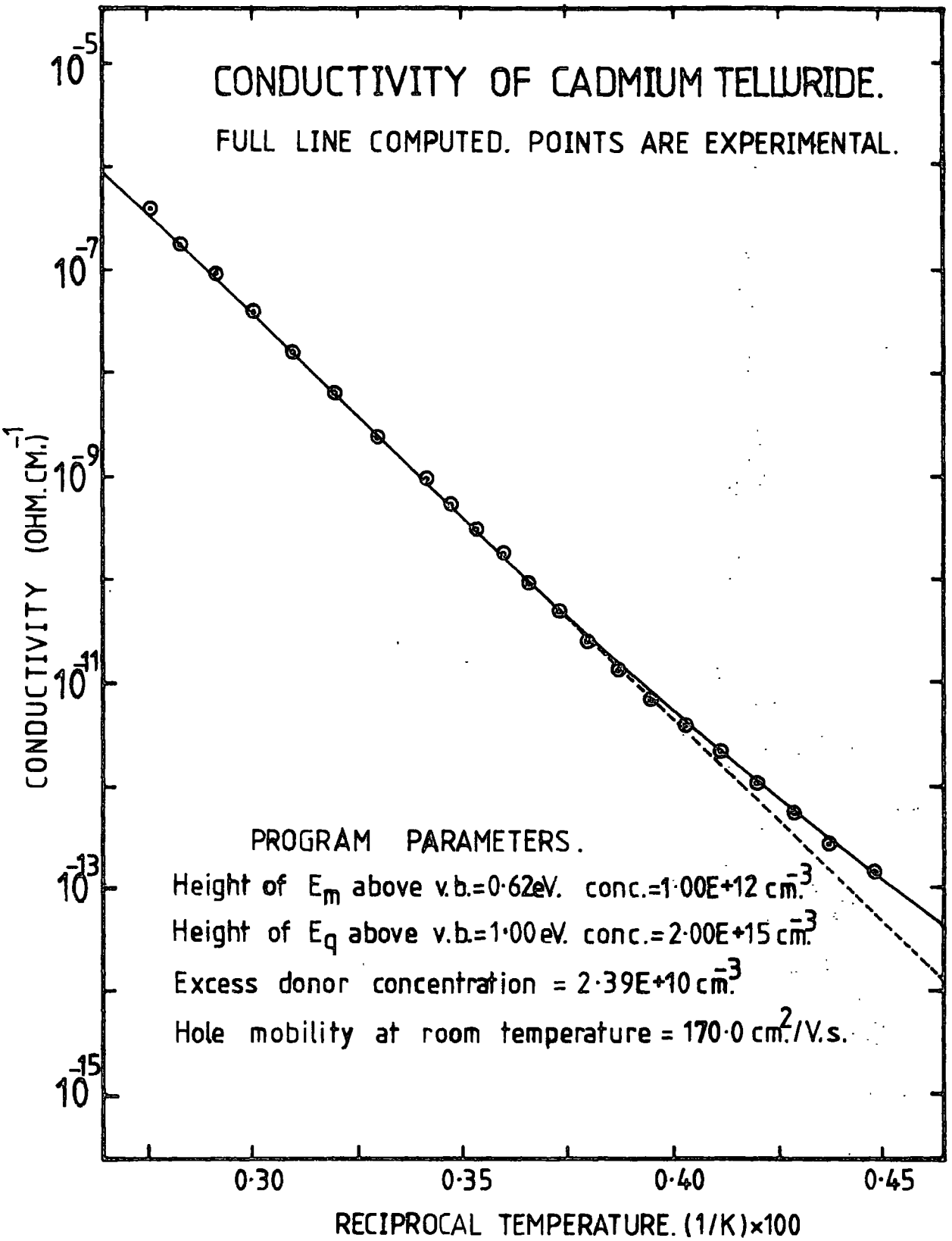

FIG. 5-3 COMPUTED ACTIVATION ENERGY CURVE WITH EXPERIMENTAL OBSERVATIONS FOR Cl-DOPED CdTe (SAMPLE. 1) SINGLE CRYSTAL.

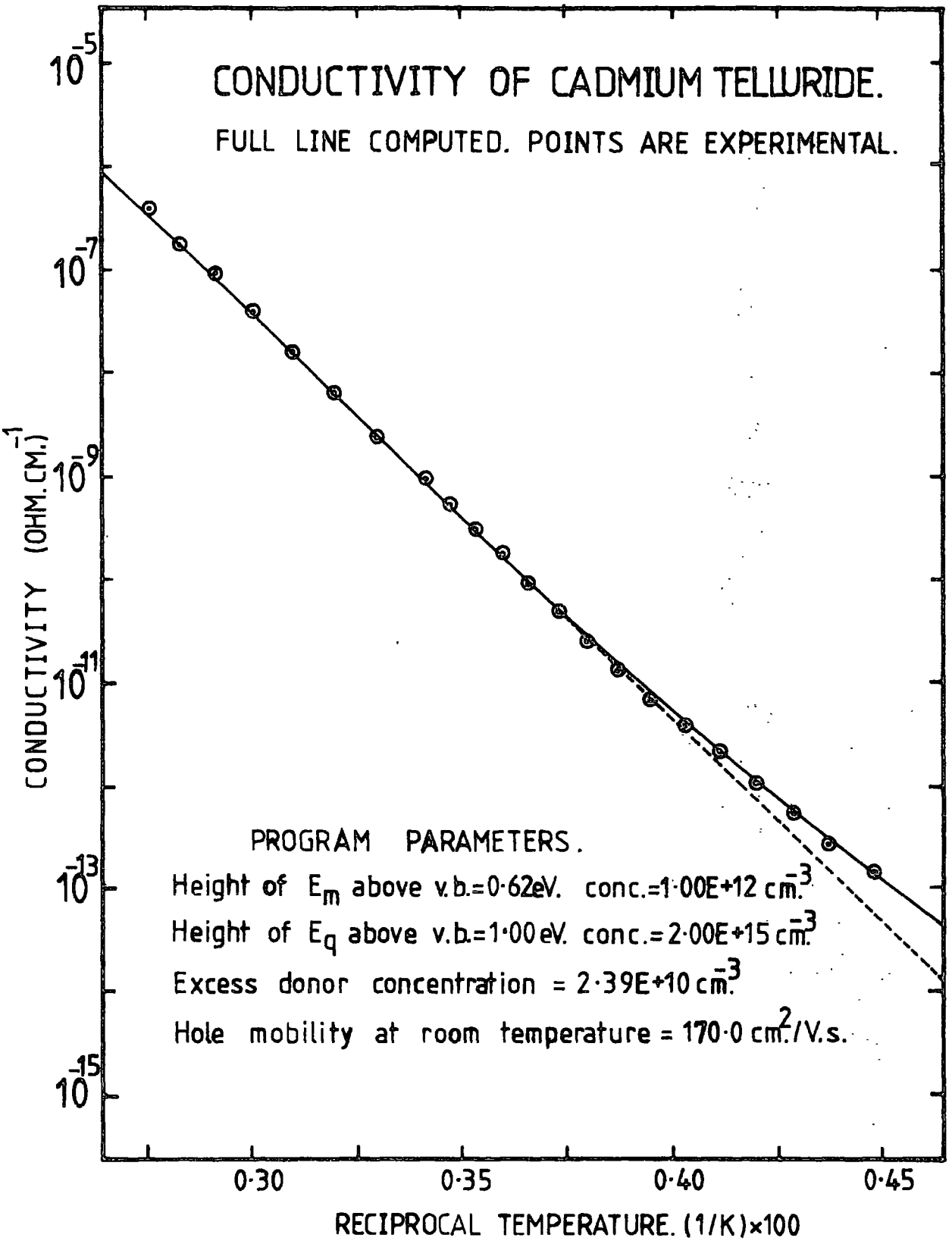

FIG. 5-3 COMPUTED ACTIVATION ENERGY CURVE WITH EXPERIMENTAL OBSERVATIONS FOR Cl-DOPED CdTe (SAMPLE. 1) SINGLE CRYSTAL.

The results are shown in fig (5.4) in a graphical form for both the extrinsic and non-extrinsic situations. Fig (5.4a) shows the situation at 220 K (extrinsic region). The dominant hole level is E_m and the Fermi level is positioned just above this level in the bandgap so that $(N_a - N_d) = p_m$. As the temperature increases the Fermi level must move to maintain this condition of charge neutrality. However, the population of electrons in E_q increases with temperature and carrier statistics will begin to become dominated by this level. At a certain temperature the concentration of electrons (n_q) in E_q will become equal to the concentration of holes (P_m) in E_m. The conductivity then becomes non-extrinsic with a resultant increase in the Ohmic activation energy of 0.5 $(E_m - E_q)$. The situation at 330 K, well above this transition temperature, is shown in fig (5.4 b).

Sample number 2 shows a clear trap filled limit voltage after a short space charge square law region (fig. 5.1). Making use of equation (2.8), the density of traps calculated to be 1.4×10^{12} cm^{-3}. This value is very similar to the concentration of E_m level obtained for other samples. Graphical analysis on this particular sample assuming the above value for N_m gives 4.4×10^{14} cm^{-3} for N_q. The experimentally observed data for 5 different samples are summarized in table (5.1).

Table 5.1

Summary of D.C. conductivity measurements of Cl-doped CdTe.

Sample Description	Sample No.	Activation energy ΔE_1	Activation energy $\Delta E_2 = E_m$	T (K) transition temp.	E_q (eV)	$(N_a - N_d)$ cm^{-3}	N_m cm^{-3}	N_q cm^{-3}	P (300 K) Ωcm
CTSE-177-2mm	1	0.80	0.62	256	0.98	2.4×10^{10}	1.0×10^{12}	2.0×10^{15}	2.8×10^{9}
" " -7mm(a)	2	0.84	0.75	-	0.93	-	1.4×10^{12}	4.4×10^{14}	1.3×10^{10}
" " -7mm(b)	3	0.92	0.83	351	1.01	-	-	-	6.0×10^{10}
" "-11mm	4	0.79	0.58	328	1.00	5.7×10^{10}	1.0×10^{12}	5.0×10^{15}	1.5×10^{9}
" "-60mm	5	0.66	0.32	333	1.00	-	-	-	3.0×10^{8}

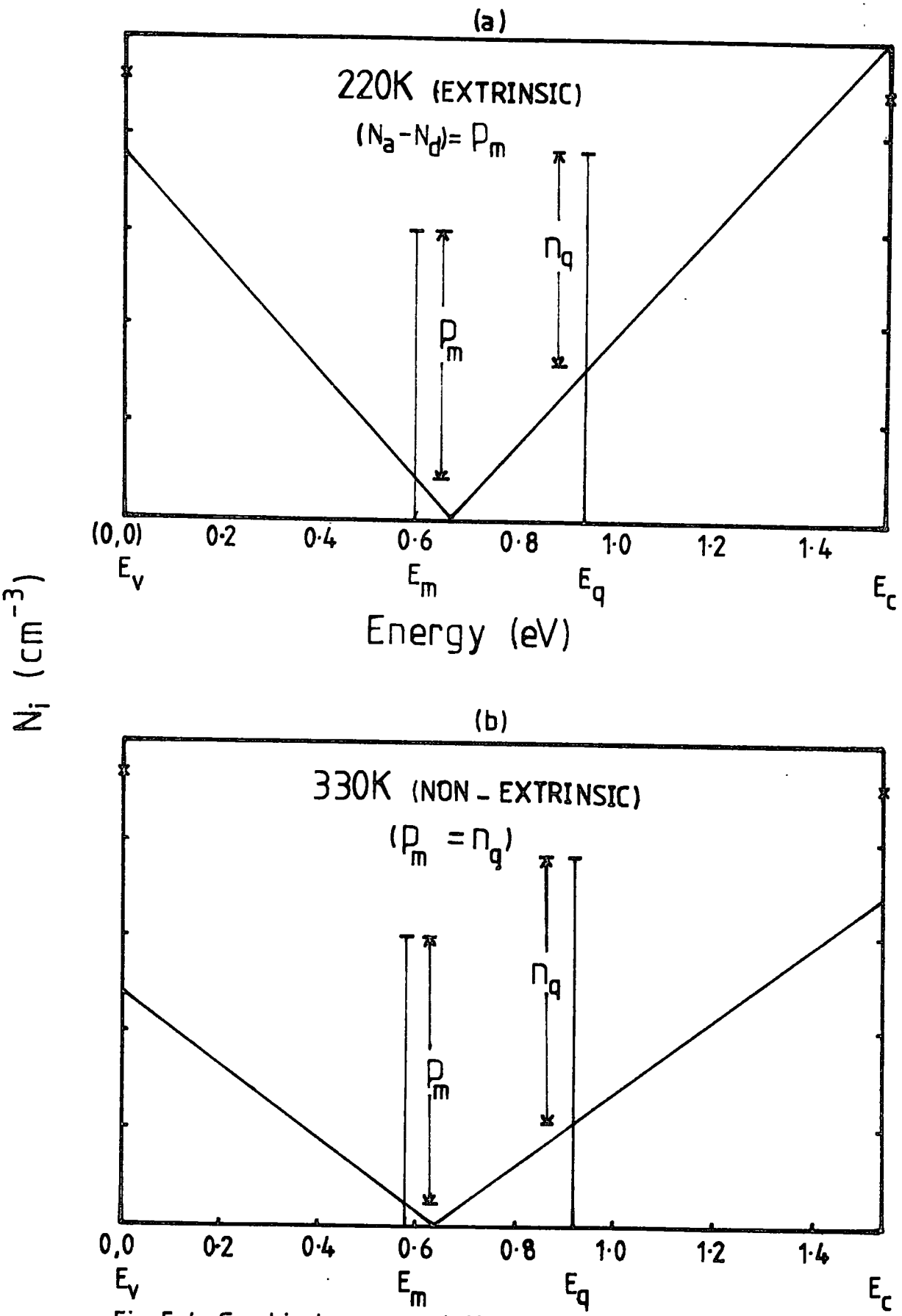

Fig. 5·4 Graphical representation of the state density as a function of energy for the CdTe:Cl sample whose conductivity characteristics are shown in fig.5·2.

(d) Sensitivity of Computer Fit

The different parameters obtained from the graphical method were all used in the computer simulation. In most cases an excellent agreement was immediately obtained but in some cases "fine-tuning" was necessary to give an exact fit. Fig(5.3) shows the theoretical curve alongside the experimental points for the above analysed sample.

To investigate the sensitivity of the computer fit the activation energy curves were produced with slight variations in the different parameters. Figures numbered (5.5) to (5.9) represent these situations, and the table (5.2) summarizes the main features of these curves. The behaviour of the curves are discussed according to the conductivity equations

$$P = \frac{(N_a - N_d)N_v}{N_m} \cdot \exp\left\{(E_v - E_m)/kT\right\} \qquad (A)$$

and

$$P = N_v\left(\frac{N_q}{N_m}\right)^{\frac{1}{2}} \cdot \exp\left[\left\{(E_v - E_m) + \frac{1}{2}(E_m - E_q)\right\}/kT\right] \qquad (B)$$

for extrinsic and non-extrinsic situations.

These theoretical curves clearly show the validity of the above two equations.

Figure 5.10 (full line) shows the computed Fermi level movement (sample number 1) over the temperature of the measurements. In the extrinsic conduction region the Fermi level moves away from the valence band as the temperature is increased to maintain the charge neutrality condition. At about 240 K (transition A) the direction of Fermi level shift with temperature changes as the conduction becomes non-extrinsic. At higher temperatures (dashed line) it is expected that the Fermi level would change direction again (transition B) as dominance is shifted from E_m to E_v and from E_q to E_c. The conductivity would then be intrinsic. For reasons given in section 5.2(f), these samples were not heated to the required temperature to observe this second transition.

Figure	Variable Parameter	Effect on the Conductivity Curve	
		Extrinsic Region	Non-extrinsic Region
(5.5)	(N_q)	Transition temperature changes.	Conductivity increases with increasing N_q according to equation (B).
(5.6)	(N_a-N_d)	Conductivity increases according to equation (A). The transition temperature also depends on this parameter.	Conductivity is affected by change in transition temperature.
(5.7)	(N_m)	Conductivity increases with decreasing N_m.	Conductivity increases with decreasing N_m, but the effect is small due to $\sqrt{N_m}$ dependence.
(5.8)	(μ_p)	Conductivity curves shift in parallel to each other as expected, in both regions with mobility.	
(5.9)	N_m and N_q but $N_m \cdot N_q$ = constant	Same effect in both regions and very similar to the variation with mobility.	

Table 5.2

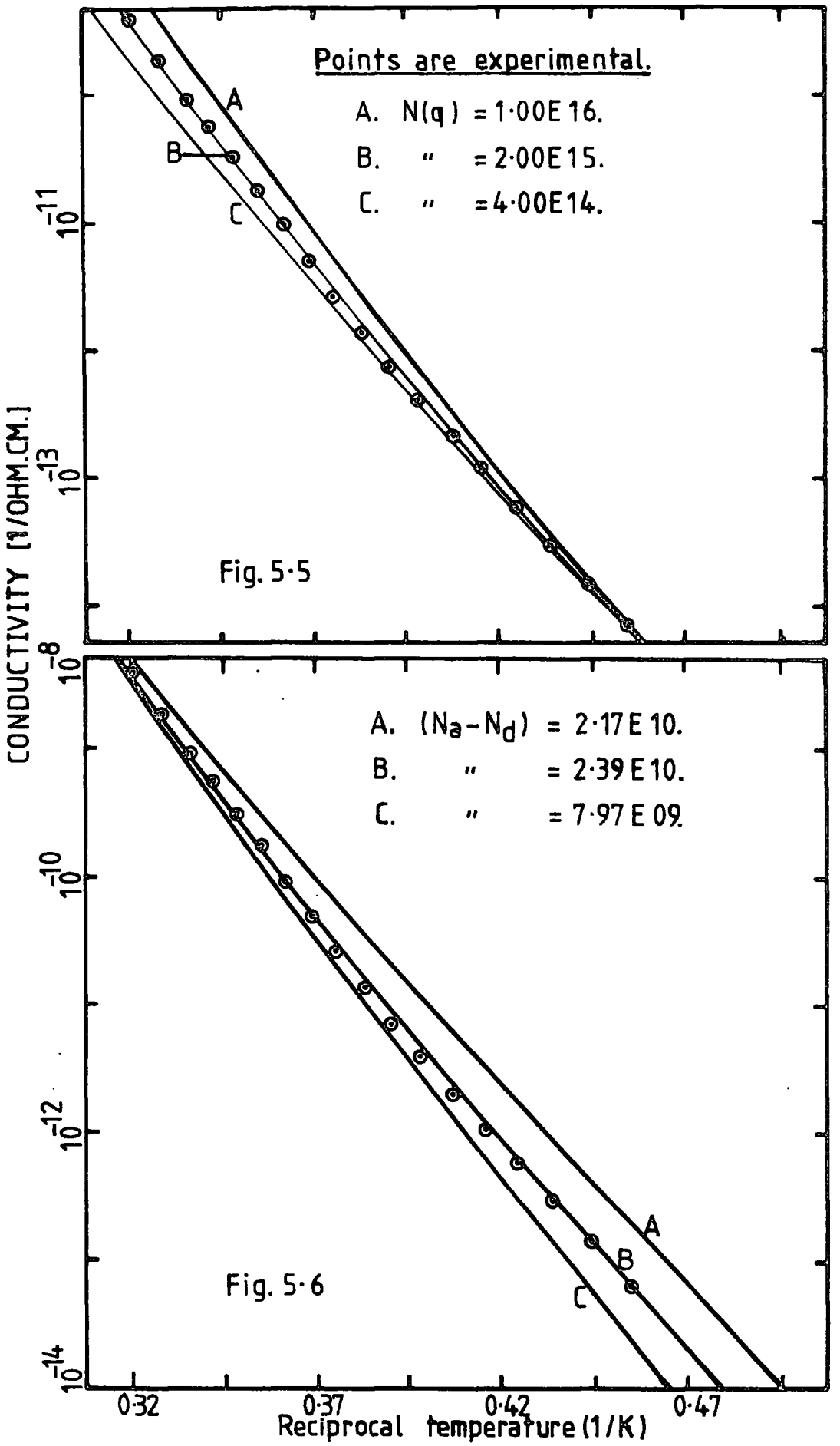

Effect of N(q) and (N -N) on the computed activation energy plot discussed in section

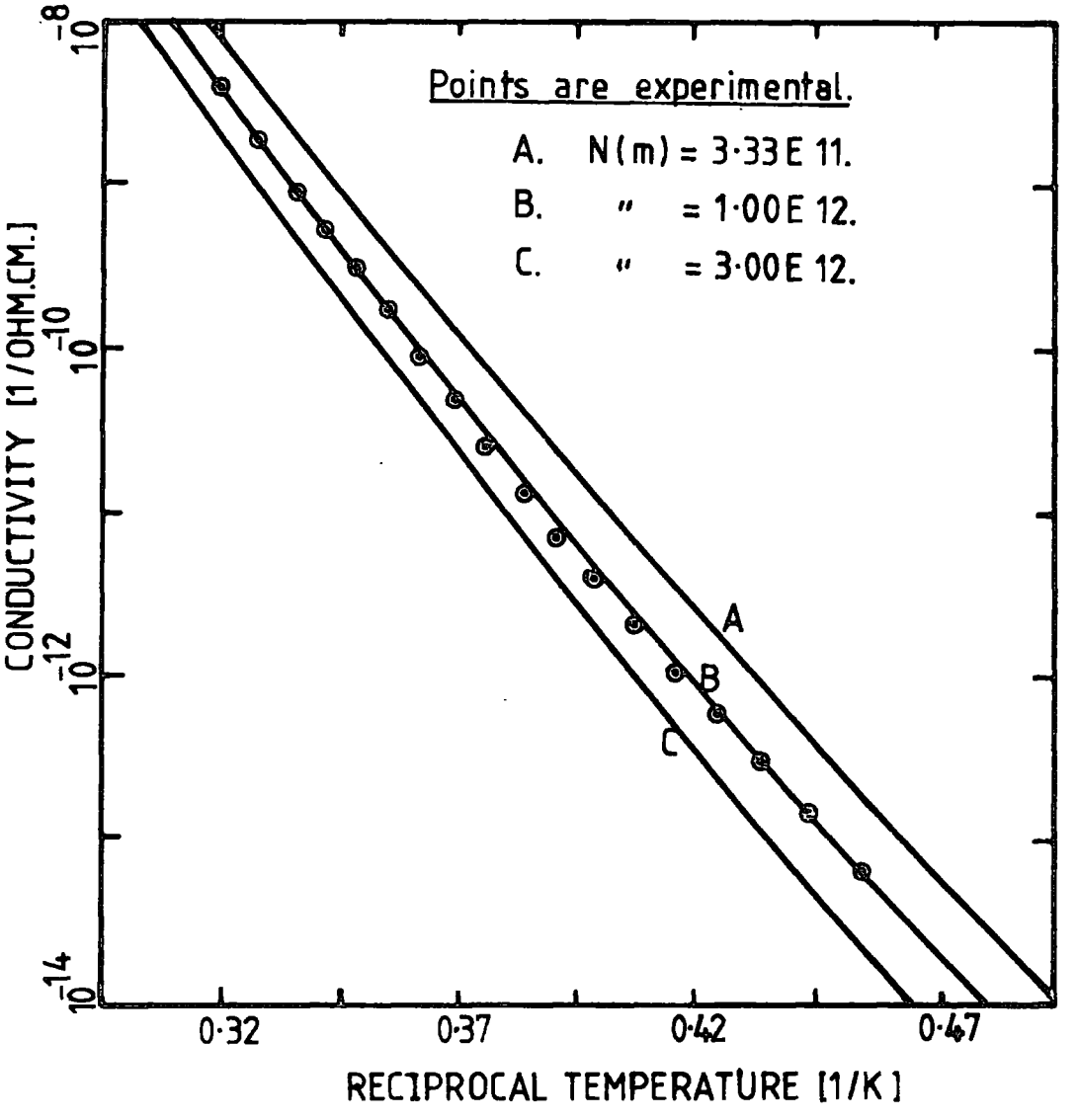

Fig. 5·7 Effect of N(m) on the computed activation energy plot discussed in section

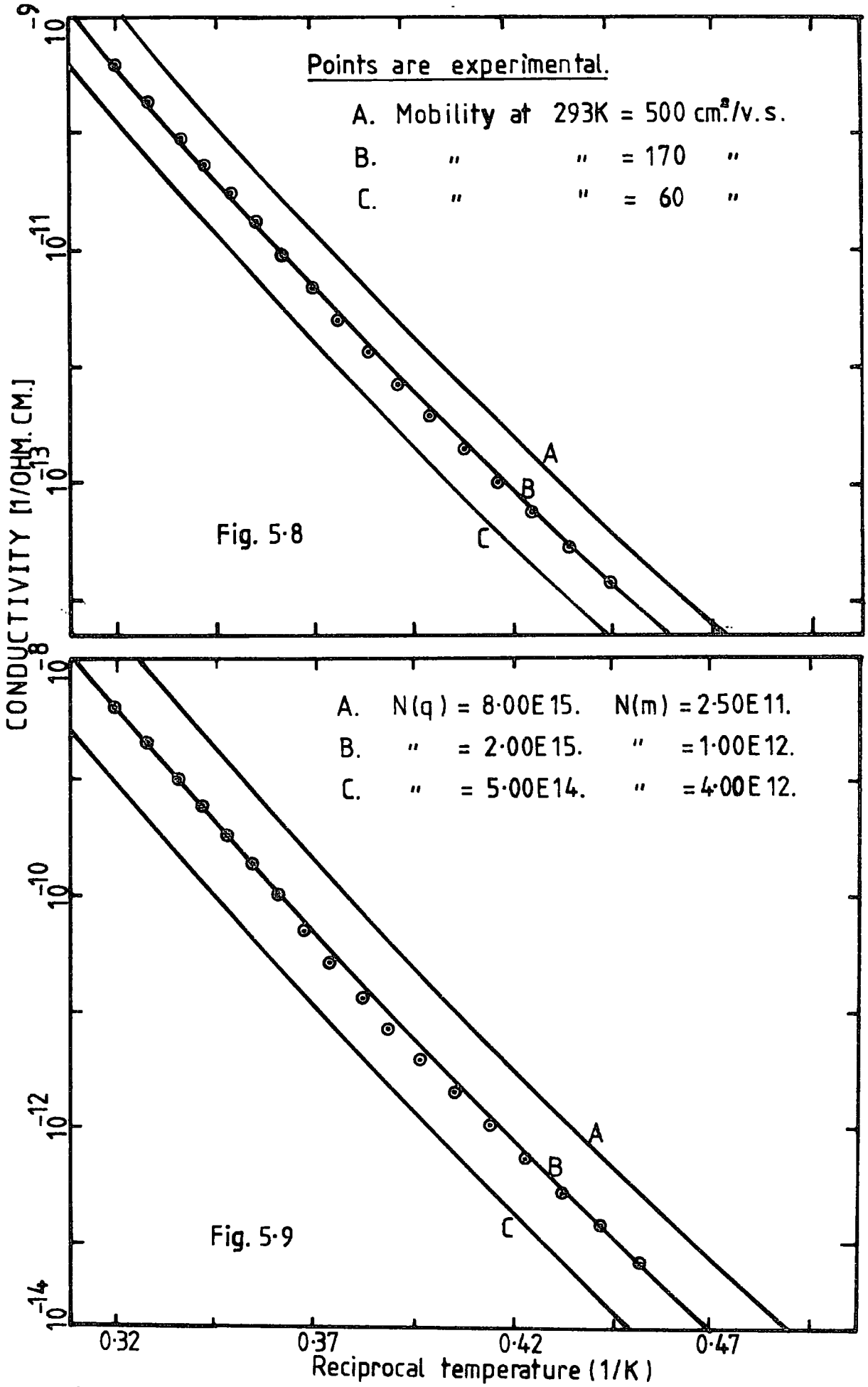

Effect of mobility and N(q) on the computed activation energy plot discussed in section

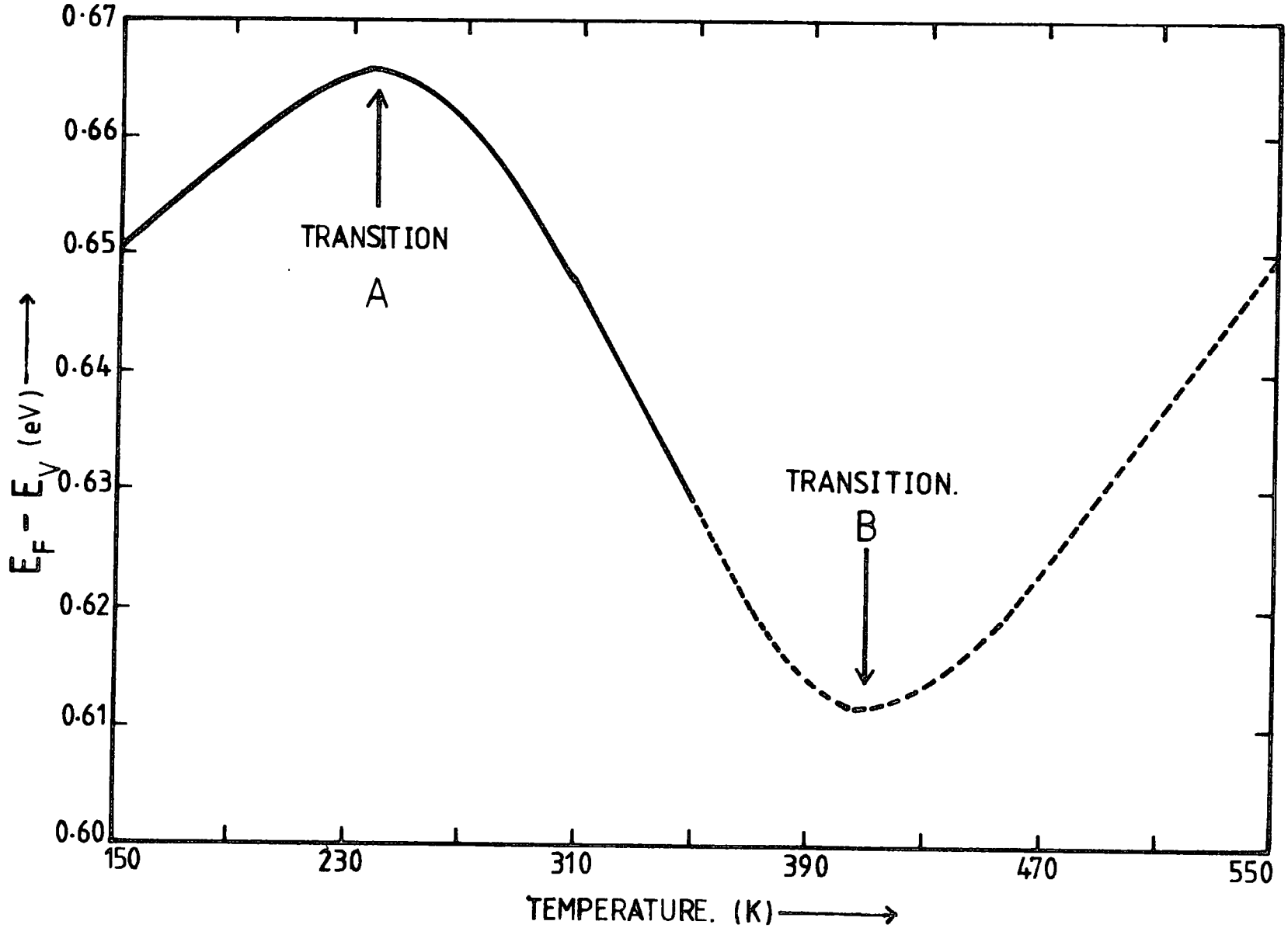

Fig.5·10 Computed Fermi level position (measured from the valence band edge) with tempe

(e) The Meyer-Neldel Rule

All of the CdTe:Cl samples investigated (except sample number 2) showed activation energies for Ohmic and SCL currents qualitatively similar to those in fig (5.2), i.e. in the temperature range 200-370 K, two activation energies were observed for Ohmic conduction and one such energy was observed for SCL conduction. However, the exact values of these activation energies and the transition temperature from extrinsic to non-extrinsic conduction varied from one sample to another. Following the same interpretation for each set of results, revealed that the deep E_q level remained in approximately the same position in the energy gap (1.00 eV above the valence band edge) for different samples whereas the position of the E_m level varied considerably (table 5.1).

Fig (5.11) shows the Ohmic activation energies in the extrinsic conduction region (i.e. simple ionization energies) for four samples sliced from different positions in the CdTe:Cl crystal boule. Thus the height of the level E_m from the valence band edge varies from 0.32 eV to 0.83 eV for different samples. In general the more resistive samples were cut near the seed end of the ingot. From these experiments it was difficult to determine whether there existed a continuous series of activation energies in different crystals or whether there was a finite number of discrete levels. As can be seen the conductivity versus reciprocal temperature curves meet at a focal point ($T = 478K, \sigma = 5.0 \times 10^{-4}$ $Ohm^{-1} m^{-1}$) when extrapolated to higher temperatures. A similar set of curves fig(5.12) was obtained when the Ohmic conductivity in the non-extrinsic region was plotted as a function of reciprocal temperature. In this case the curves when extended, passed through a focal point at $T = 806$ K, $\sigma = 16$ $Ohm^{-1} m^{-1}$.

The above experimental observations reveal that the semi-insulating CdTe:Cl samples exhibit the Meyer-Neldel rule in both extrinsic and non-extrinsic regions. An alternative way of demonstrating this rule, given by

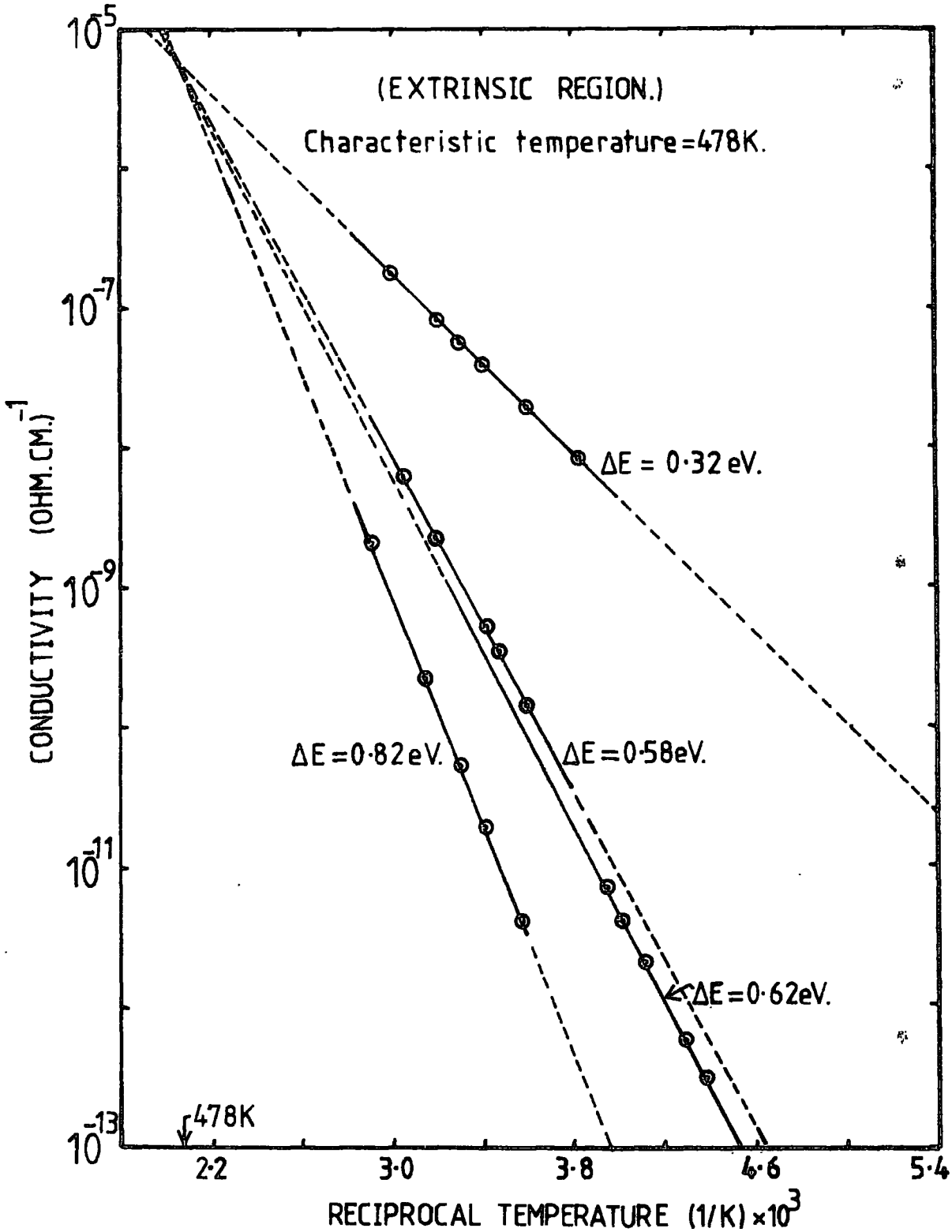

Fig. 5·11 Ohmic conductivity in the extrinsic region versus reciprocal temperature for four CdTe:Cl samples cut from the same crystal boule.

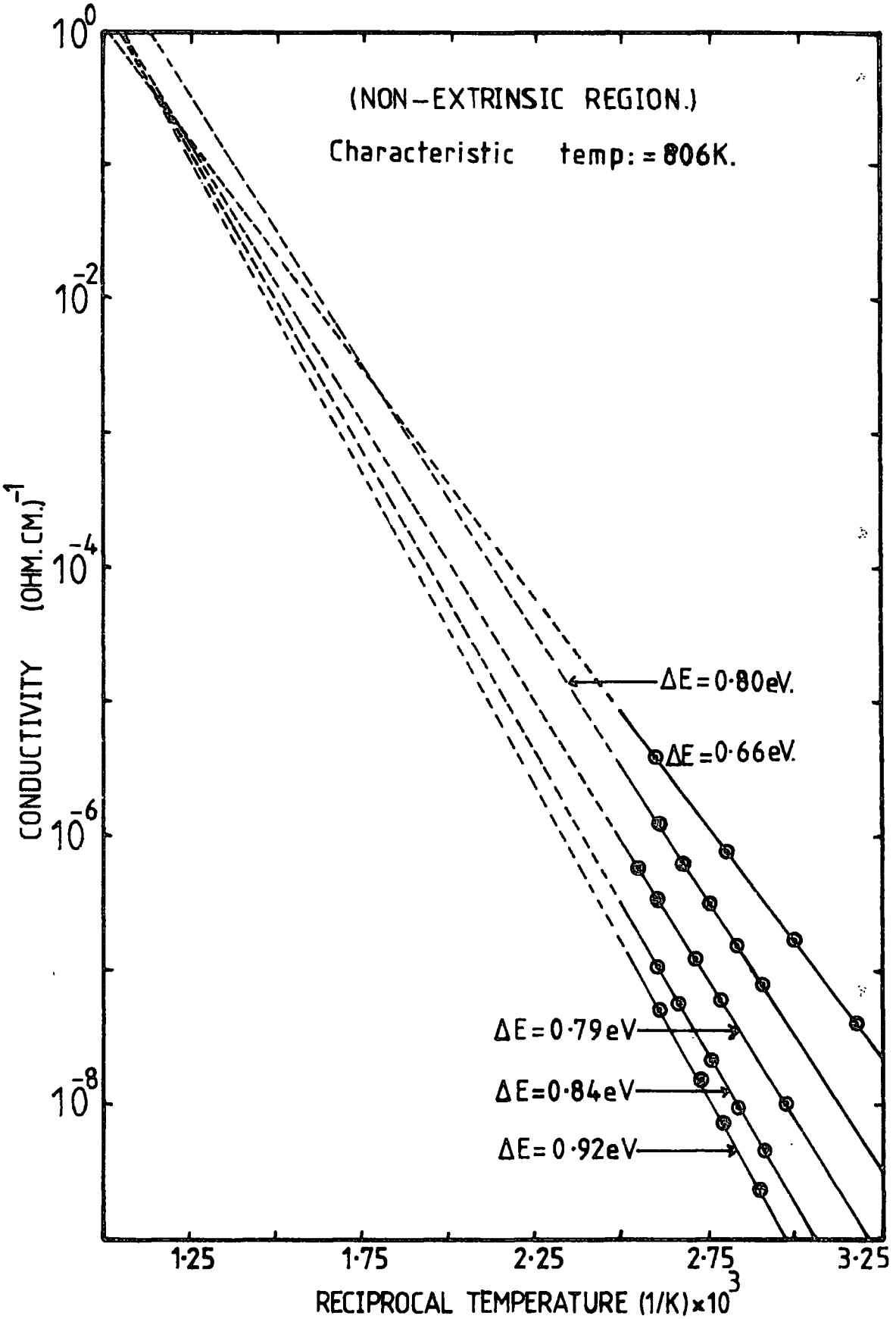

Fig. 5·12 Ohmic conductivity in the non-extrinsic region versus reciprocal temperature for five CdTe:Cl samples cut from the same crystal boule.

the relation (2.22), is shown in fig (5.13). The plots of activation energy against log σ_o for these different samples are good straight lines for both extrinsic and non-extrinsic conductions. The characteristic temperatures obtained from the slopes of these graphs are identical to those obtained from figures (5.11) and (5.12).

Since the activation energy is a function of sample position in the crystal boule and varied over a wide range, an attempt to observe activation energy changes for samples under different annealing conditions was made. This is discussed in the following section.

(f) Annealing Effects

If the CdTe:Cl crystal slices were heated to temperatures greater than 100° C in a vacuum ($\simeq 10^{-5}$ torr) irreversible changes in the electrical properties were observed. In particular, the conductivity curves displayed smaller activation energies as the annealing temperature was increased. If the activation energy data for one sample before and after various annealing treatments were plotted on the same graph a "fan" of curves, was obtained for both extrinsic and non-extrinsic conduction. One set of curves obtained for a sample with Bi contacts is shown in fig (5.14). This figure is redrawn in fig (5.15) to show the focal point more clearly for low temperature ($< 300^{\circ}$C) annealings. Note that the focal point obtained at $\simeq$ 483 K is lost for samples annealed at temperatures $> 300^{\circ}$ C (fig.5.14). A set of parallel curves is obtained in these cases. The alternative plot of demonstrating the Meyer-Neldel rule is also shown in fig (5.16) for these data. The characteristic temperature calculated from the slope of this straight line is 481 K. This value of characteristic temperature compares favourably with the value of 478 K obtained for different unannealed samples.

In order to check that we were not observing an annealing effect of the electrical contacts the following experiment was performed on a number of samples ; after heating the sample at a temperature of about 200° C the

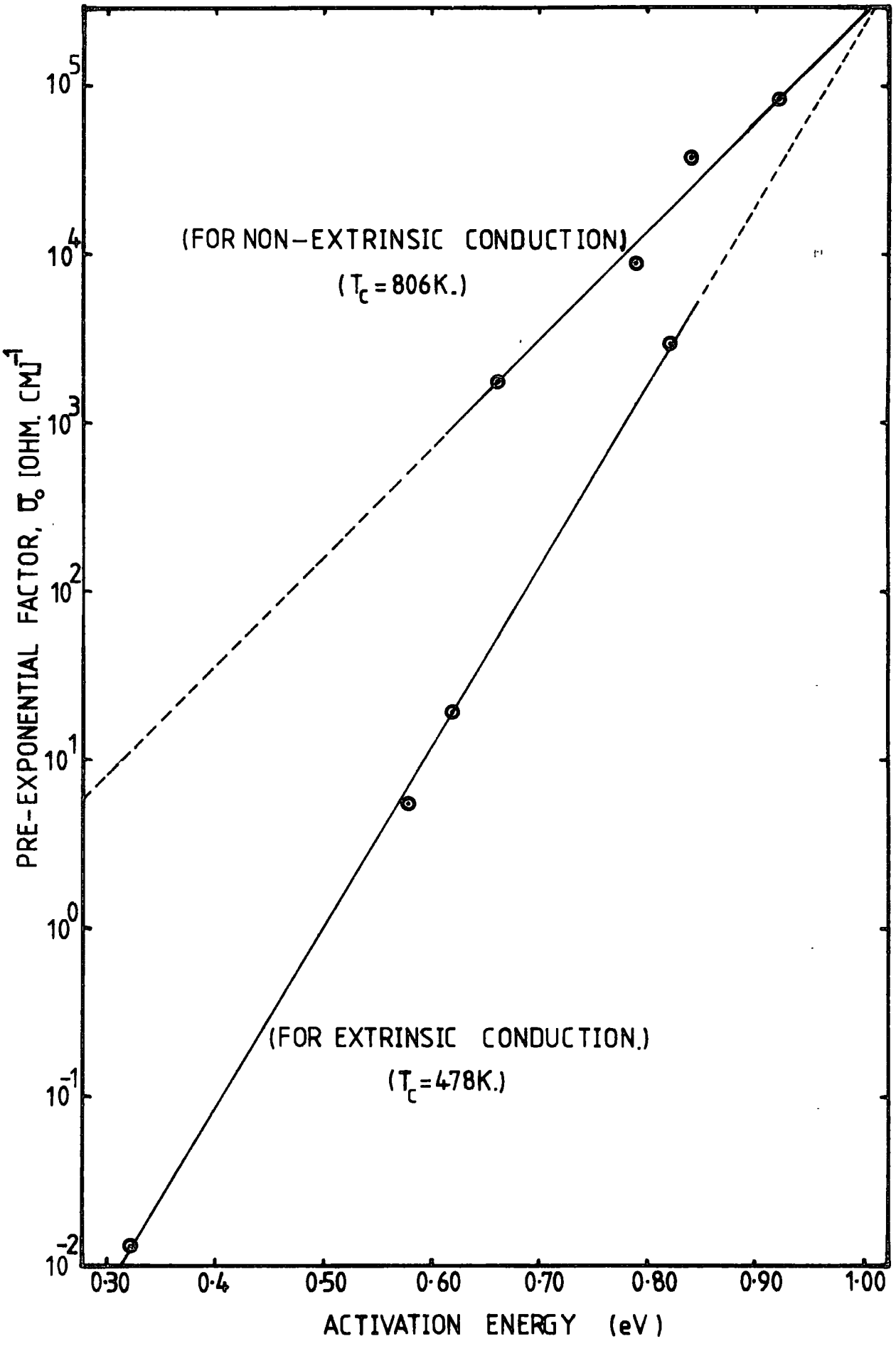

Fig. 5·13. Alternate plots of the data in figures 5·11 and 5·12 for Cl-doped CdTe.

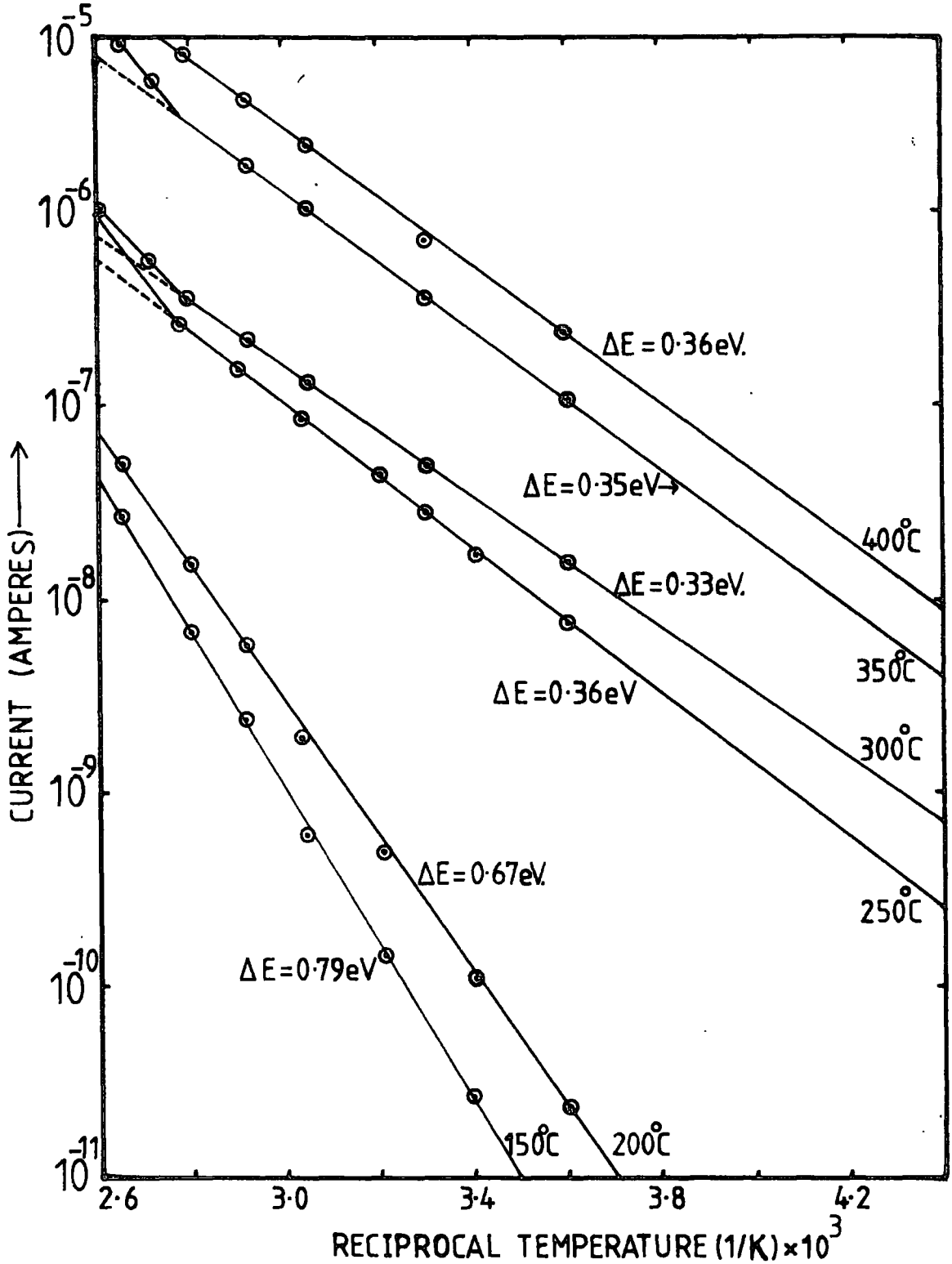

Fig. 5·14 Ohmic current versus reciprocal temperature for extrinsic conductivity of one CdTe:Cl sample after annealing in vacuum for 20 minutes at different temperatures (T_a).

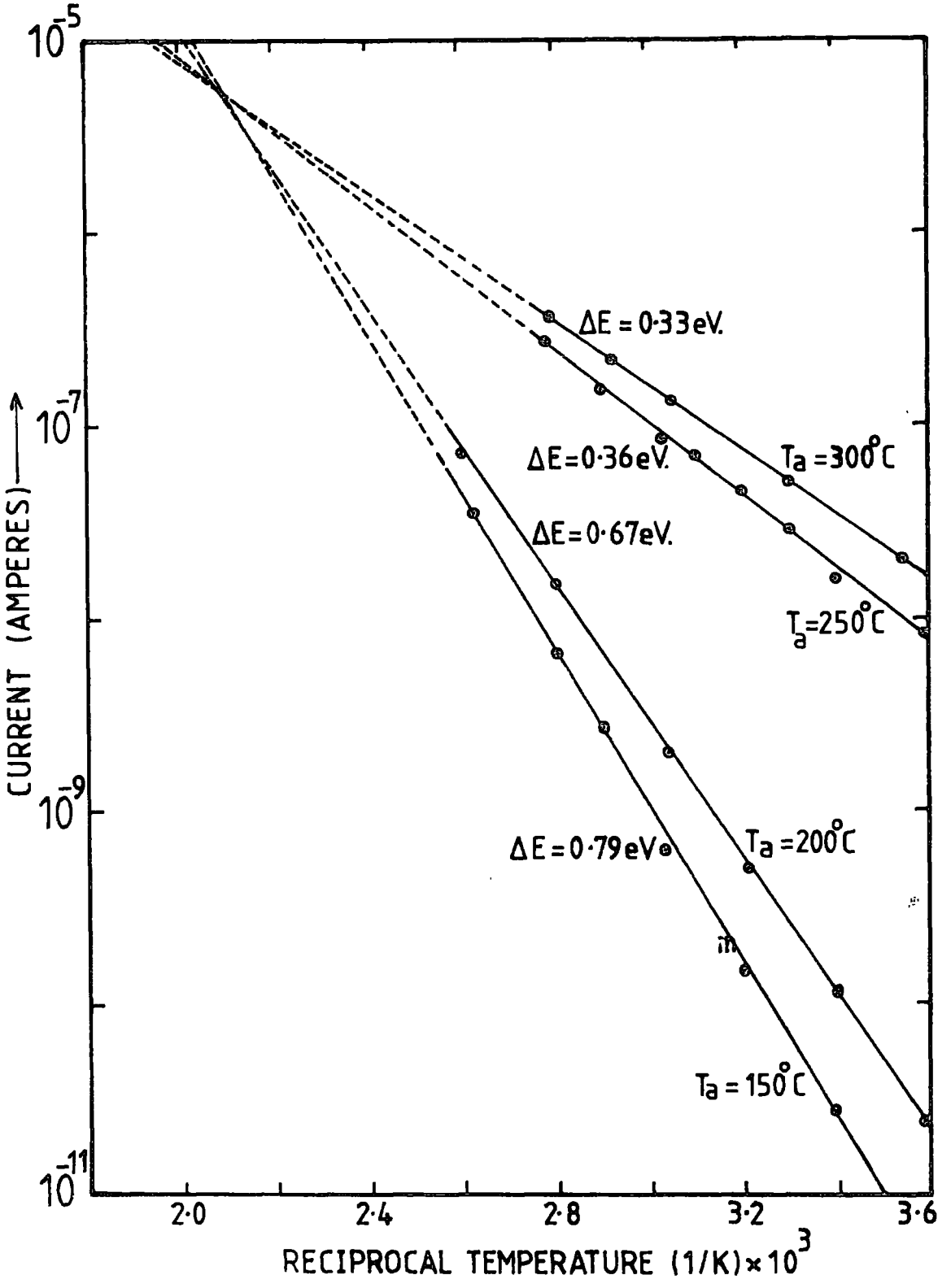

Fig. 5·15 Ohmic current versus reciprocal temperature for extrinsic conductivity of one CdTe:Cl sample after annealing in vacuum for 20 minutes at different temperatures(T_a).

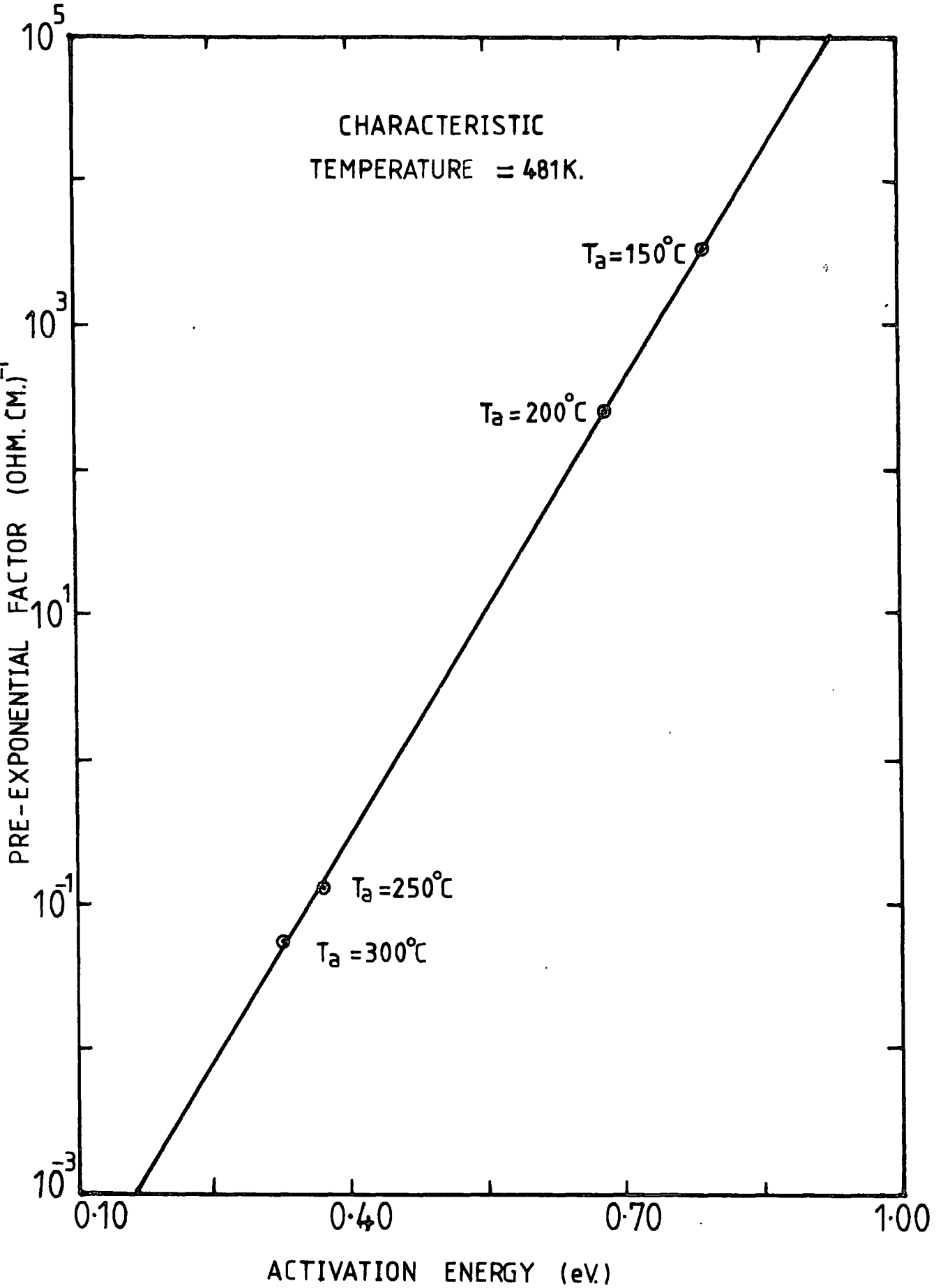

Fig. 5·16 Pre-exponential factor versus ohmic activation energy for extrinsic conductivity of one CdTe:Cl sample after annealing in vacuum for 20 minutes at different temperatures (T_a).

thermal activation energies for Ohmic conduction were obtained. The contacts were then etched away and new electrodes (Bi) deposited on to the crystal slice. Finally the Ohmic activation energies were re-measured. This experiment always produced identical results with the 'old' and the 'new' contacts inferring that the annealing treatment had affected the bulk of the CdTe:Cl crystal rather than the electrodes or the surface . To check both the reproducibility and the effect of electrode metal the above series of experiments were repeated with another sample provided with Au Ohmic contacts. These results showed the same effect and the characteristic temperature obtained for extrinsic conduction was about 470 K. The observed activation energies with different annealing conditions are summarized in table (5.3).

Table 5.3

Annealing effects on CdTe:Cl samples with Au electrodes

T (a) / A.E. (eV)	as grown	100° C	150°C	200°C	250°C	300°C	350°C
ΔE_1	0.92	0.92	0.91	0.72	0.47	-	-
ΔE_2	0.83	0.79	0.75	0.46	0.39	0.36	0.33
E_m	0.83	0.79	0.75	0.46	0.39	0.36	0.33
E_q	1.01	1.05	1.07	0.98	0.55	-	-

The conductivity curves produced a sharp focal point for low temperature (i.e. < 250°C) annealing. For heat treatments above a certain temperature (≃ 250°C), a constant extrinsic activation energy of ≃ 0.3 eV was obtained. If the annealing process was continued for about 3 hours the activation energy was reduced to about 0.15 eV. The conductivity data in these cases did not lie on the Meyer-Neldel plot (log σ_o vs ΔE), but the

pre-exponential factor continued to decrease with increasing annealing temperature.

Interpretation of the activation energy curves after annealing, using the theories of Roberts and Schmidlin[2,3] revealed, once again, that the energy position (E_m) of the dominant hole level was changed under different annealing conditions while the dominant electron level at E_q remained in the same position ($\simeq$ 1.00 eV) in the energy gap. In fact for annealing temperatures below $\simeq 250^{o}$ C the E_m level varied from about 0.83 eV to 0.33 eV above the valence band edge. This was approximately the same variation observed in different (unannealed) samples. It is also interesting to note that the E_q level remains constant (table 5.3) for low temperature annealing but varies above $\simeq 250^{o}$ C.

There is no well established theory to help understand and explain these experimentally observed results. Part of the model proposed by Roberts' (section 2.1.3) seems acceptable for these samples since the observed E_m level changes from sample to sample while the E_q level remains in approximately the same position in the energy gap. However, because the extrinsic and non-extrinsic conductivity versus reciprocal temperature curves have focal points at finite temperatures, and N_m seems to be constant (table 5.1) for different samples, equations (2.25) and (2.26) cannot provide a complete explanation for the occurrence of the Meyer-Neldel rule. In an attempt to explain these results, ideas based on multivalent defects have been used. This model is described in the following section.

(g) Multivalent Theory

Localized energy states can arise in the forbidden gap of a semiconductor due to several reasons. Complex defects can introduce difficulties in the interpretation of activation energy curves. In the following model multivalent impurities are considered and the resulting defect levels are used to explain the observation of the Meyer-Neldel effect in semi-insulating CdTe:Cl.

When an impurity or defect can contribute or accept more than one electron it can introduce a number of energy levels in the forbidden gap. For simplicity, only two states are considered in this theoretical discussion. A particular defect site can either be unoccupied ($E = 0$, non-degenerate), singly occupied ($E = T_o$, twofold degenerate), or doubly occupied ($E = 2T_o + U$, non-degenerate), where U represents the effective electrostatic attraction that exists when two electrons (one of each spin) are simultaneously present in the vicinity of the same defect. U is called the electronic correlation energy and is normally considered to be a positive quantity for crystalline materials. However, for electron states associated with dangling bonds in certain types of amorphous semiconductor, negative correlation energies have been proposed. For the majority of chalcogenide glasses, this quantity has been estimated to be of the order of 0.5 eV[13].

Our model considers a semiconductor with valence and conduction band edges at E_v and E_c, respectively, and with two localized states at energies T_o and $(T_o + U)$ in the energy gap. If N is the total number of electrons associated with N_o defects (the average number of electrons per defect, $n = \frac{N}{N_o}$), a complete analysis yields a quadratic equation similar in style to equation (2.14)[4], i.e. if $x = \exp(-E_f/kT)$

$$x^2(n-2)\,Q_p + x(n-1)\,Q_s + n = 0. \qquad (5.1)$$

where $Q_s = 2.\exp(-E_s/kT)$ and $Q_p = \exp(-E_p/kT)$ are the respective partition functions for the single electrons and pairs of electrons occupying the defect levels. The solution of the above equation gives the same relation[4]

$$E_f = T_o - kT\,\ell n \left\{ (1/n-1) + \left[(1/n-1)^2 + (2/n-1)\exp(U/kT) \right]^{\frac{1}{2}} \right\} \qquad (5.2)$$

as that first derived by Adler and Yoffa[14] using the grand canonical partition function. The Fermi energy may now be plotted as a function of n for both positive and negative correlation energies. Figures (5.17)

and (5.18) show the variation of E_f with n at two different temperatures for both cases with U = 0.50 eV. For negative correlation energies (fig.5.18), the Fermi level varies very little with the electron density or temperature ; i.e. E_f is pinned approximately midway (T_o-U/2) between the two energy levels of interest. This situation leads to non-extrinsic conduction as discussed in section (2.1.1d). Since CdTe is crystalline and hence U is positive, the following discussion concentrates mainly on the results shown in fig (5.17).

The results are quite different for a positive correlation energy. For example, the Fermi level lies at T_o for n <1 but moves to (T_o + U) for n >1. In the case of exactly one electron per defect, n = 1; the equation (5.2) reduces to

$$E_f = T_o + \frac{|U|}{2} \qquad (5.3)$$

and is independent of temperature. For n > 1, E_f slowly increases with increasing temperature, while for n < 1, E_f slowly decreases with increasing temperature. The behaviour of the Fermi level near n = 1 can be understood by obtaining approximate solutions to equation (5.2). In this region the equation reduces to

$$E_f = T_o - kT.\ \ell n\left(\frac{2\delta}{1-\delta}\right) \quad \text{for } n = (1-\delta) \qquad (5.4)$$

and

$$E_f = T_o + U - kT.\ \ell n\left(\frac{1-\delta}{2\delta}\right) \text{ for } n = (1+\delta) \qquad (5.5)$$

where δ represents a small positive quantity. It is, therefore, clear that from equations(5.4) and (5.5)

when $\delta = \frac{1}{3}$ or $n = 2/3$, $E_f = T_o$

and

when $\delta = \frac{1}{3}$ or $n = 4/3$, $E_f = T_o + U$

FIG. 5·17. [U=-0·50eV]

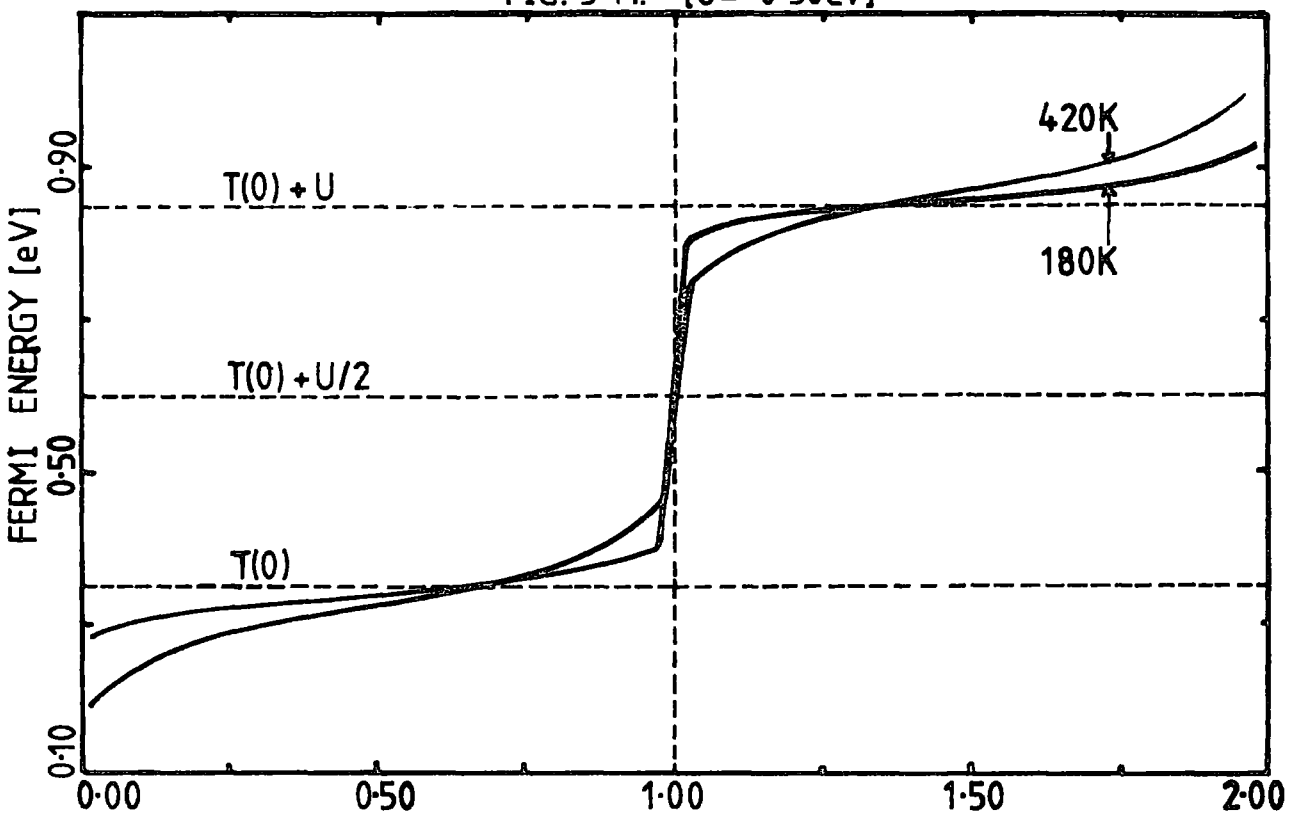

The average no. of electrons/defect.

FIG. 5·18. [U = - 0·50eV].

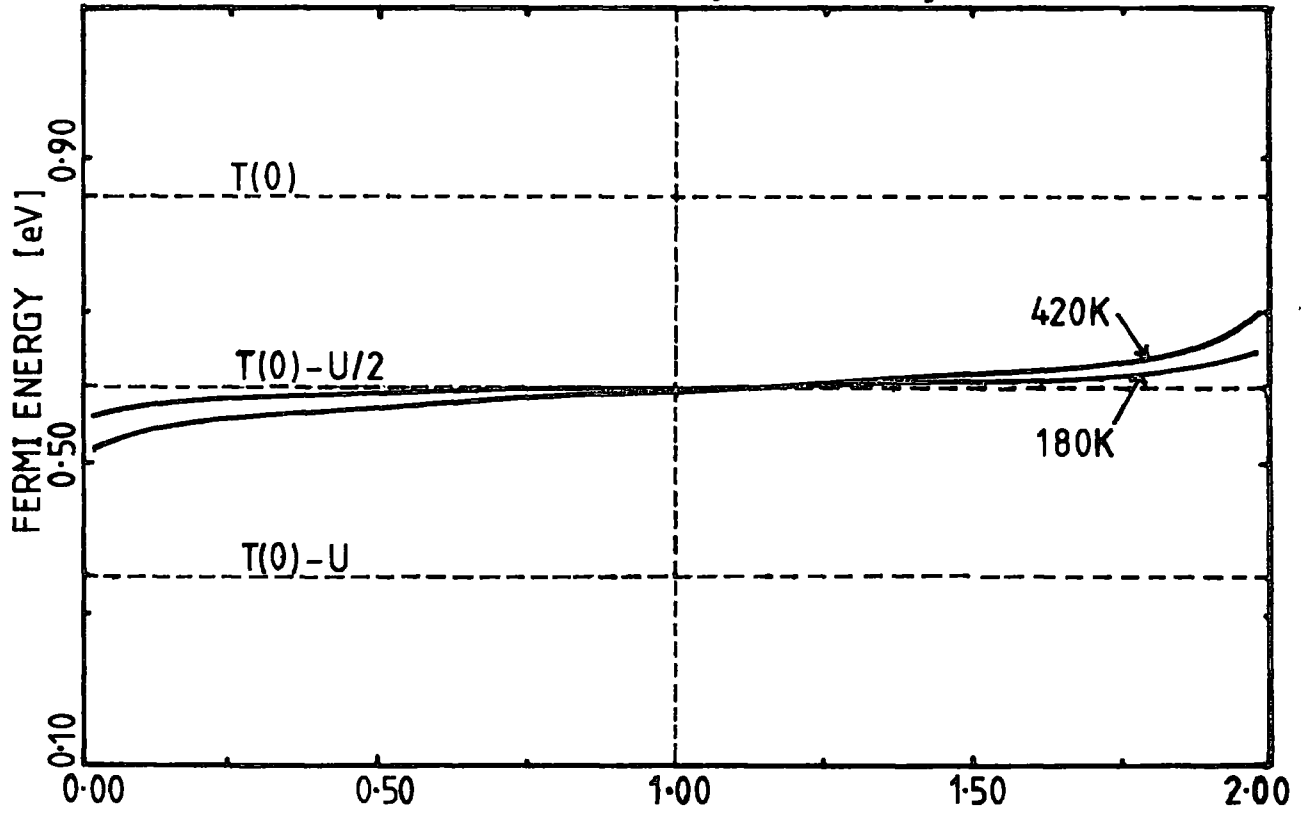

Fermi energy as a function of n, the average number of electrons per defect, at two different temperatures.

These two situations are shown by points A and B in fig (5.17). For positive correlation energies the Fermi level moves considerably with increasing temperature except for the particular values of n = 2/3, 1 and 4/3.

Since the Fermi level varies over a wide range (depending on the value of U) with the electron density, the activation energies can be different for various n values. If the value of n is not constant along a crystal boule or varies with annealing, a variation of ΔE can be expected. This possibility has been studied by computing the activation energy curves as a function of n. Two arbitrary values of T_o and U (0.35 eV and 0.50 eV) are assumed and other parameters such as bandgap, mobilities and effective masses have been taken from table (1.1). The temperature dependence of the mobilities and the bandgap are neglected in this computation ; their introduction would produce only slight variations, and would not significantly change the shape of the curves. Fig(5.19) shows the set of theoretical curves obtained with different n values in the region of $n \simeq 1$. By extrapolating certain curves to higher temperatures focal points can be obtained. These features are quite similar to the experimentally observed results (figures 5.11 and 5.14). The parallel lines observed when n takes values less than 1 are also experimentally determined features. Three different activation energies can be distinguished; these are 0.35 eV for $n < 1$, 0.60 eV for $n = 1$ and 0.85 eV for $n > 1$. In agreement with theory the activation energy corresponding to $n = 1$ is 0.60 eV = $(T_o + U/2)$, the average of the other two activation energies. Note that the similar behaviour can be observed for the ΔE values shown in fig (5.11). The same relation holds for the activation energy values reported by Arkadyeva et al[15] (0.61, 0.73 and 0.83 eV) and Höschl et al[16] (0.15, 0.50, 0.90 eV) for Cl-doped CdTe specimens. Both these groups found that the above values were the most commonly occurring activation energies for their particular CdTe crystals.

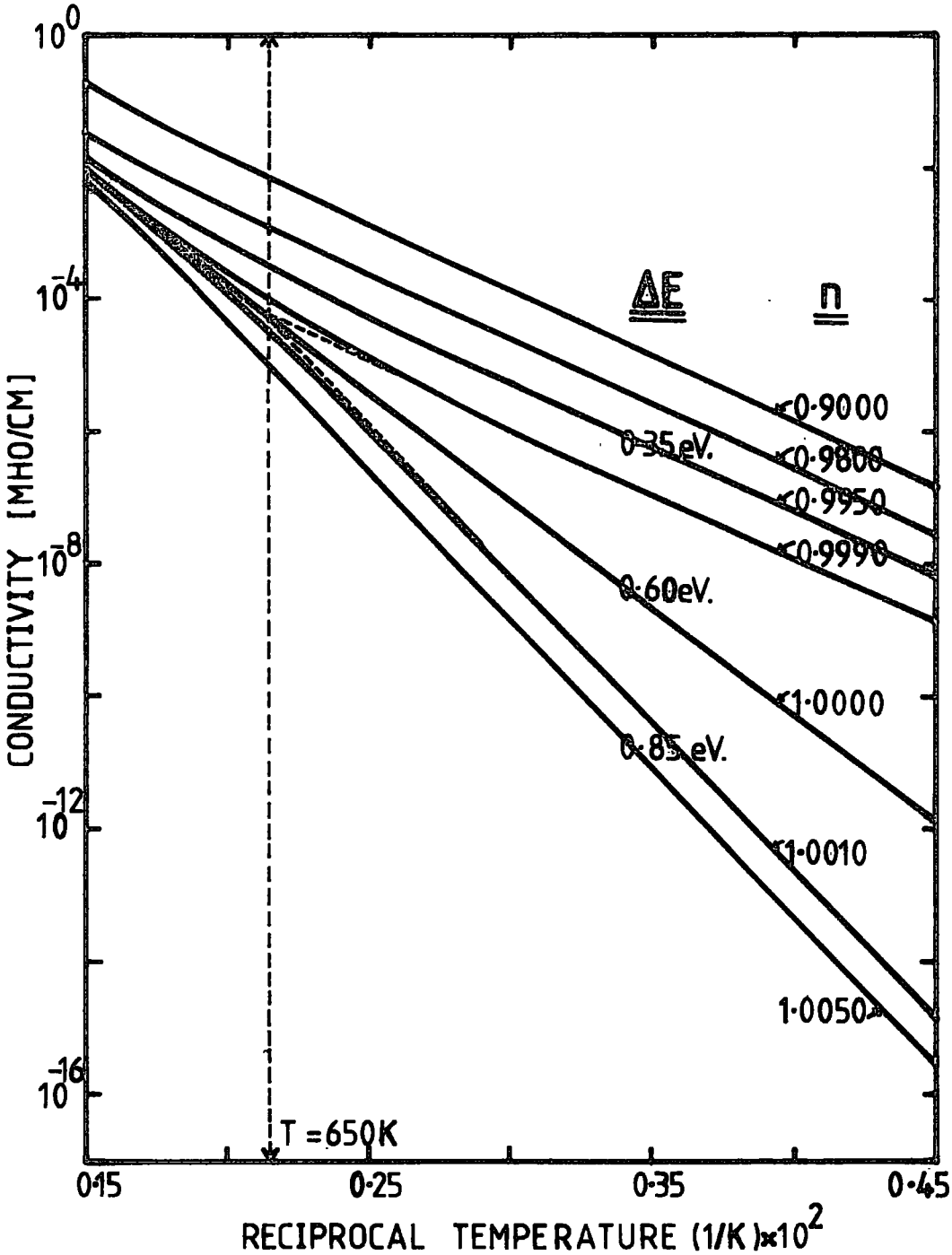

FIG. 5·19 THEORETICAL ACTIVATION ENERGY PLOTS AS A FUNCTION OF n, THE AVERAGE NUMBER OF ELECTRONS/DEFECT.

The value of T_c is a function of U and the relation between these two parameters can be derived using equations (5.4) and (5.5). At temperature T_c the Fermi level coincides for both cases and therefore

$$T_o - kT_c \cdot \ell n \left(\frac{2\delta}{1-\delta}\right) = T_o + U - kT_c \cdot \ell n \left(\frac{1-\delta}{2\delta}\right)$$

This gives the simple relation

$$U = 2kT_c \cdot \ell n \left(\frac{2\delta}{1-\delta}\right) \qquad (5.6)$$

and for very small values of δ

$$U \simeq 2kT_c \qquad (5.7)$$

According to this model the focal point temperature is a function of both U and δ. If δ is kept constant at a smaller value, T_c can be obtained by extrapolation of two curves taken from both sides of the line corresponding to n=1. One such focal point is shown in fig (5.19) for δ = 0.001. A set of characteristic temperatures have been obtained for the same δ value as a function of correlation energy. When T_c is then plotted against U, a good linear relationship is observed as expected from equation (5.7). This is shown in fig (5.20).

This model clearly shows the possibility of observing activation energies over a wide range for various specimens and for different annealing conditions. The value of n can vary for different specimens or, can change with the annealing temperatures. The defect levels responsible for this multivalent behaviour are, however, not exactly known. The possible origin of such defect levels in CdTe is discussed in section (5.4).

5.3 THERMALLY STIMULATED CURRENT MEASUREMENTS

The experimental TSC curve obtained for a very high resistivity sample (sample number 3) is shown in fig (5.21). Three peaks are clearly

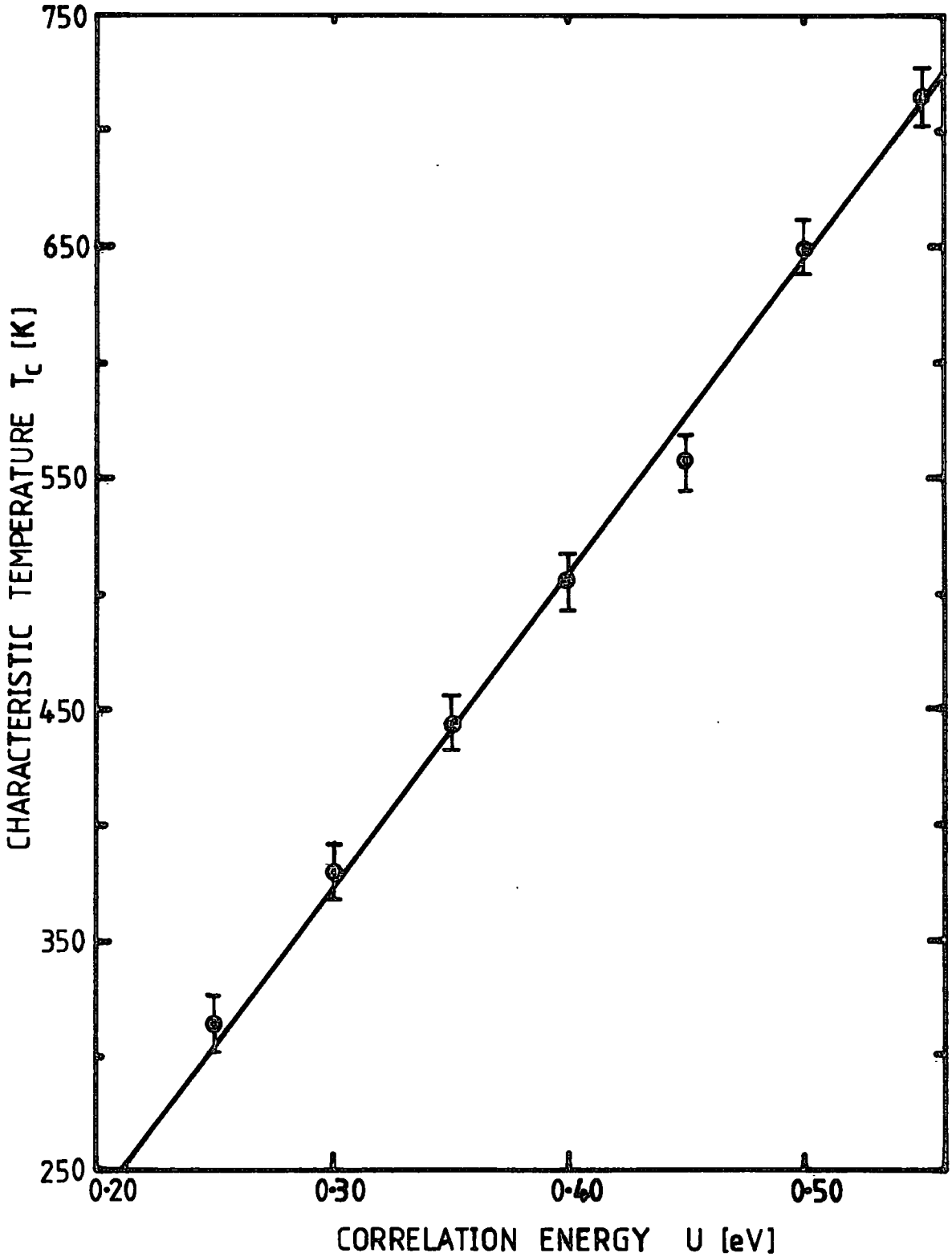

FIG. 5·20 Dependence of T_c on correlation energy, U, for $\delta = 0{\cdot}001$.

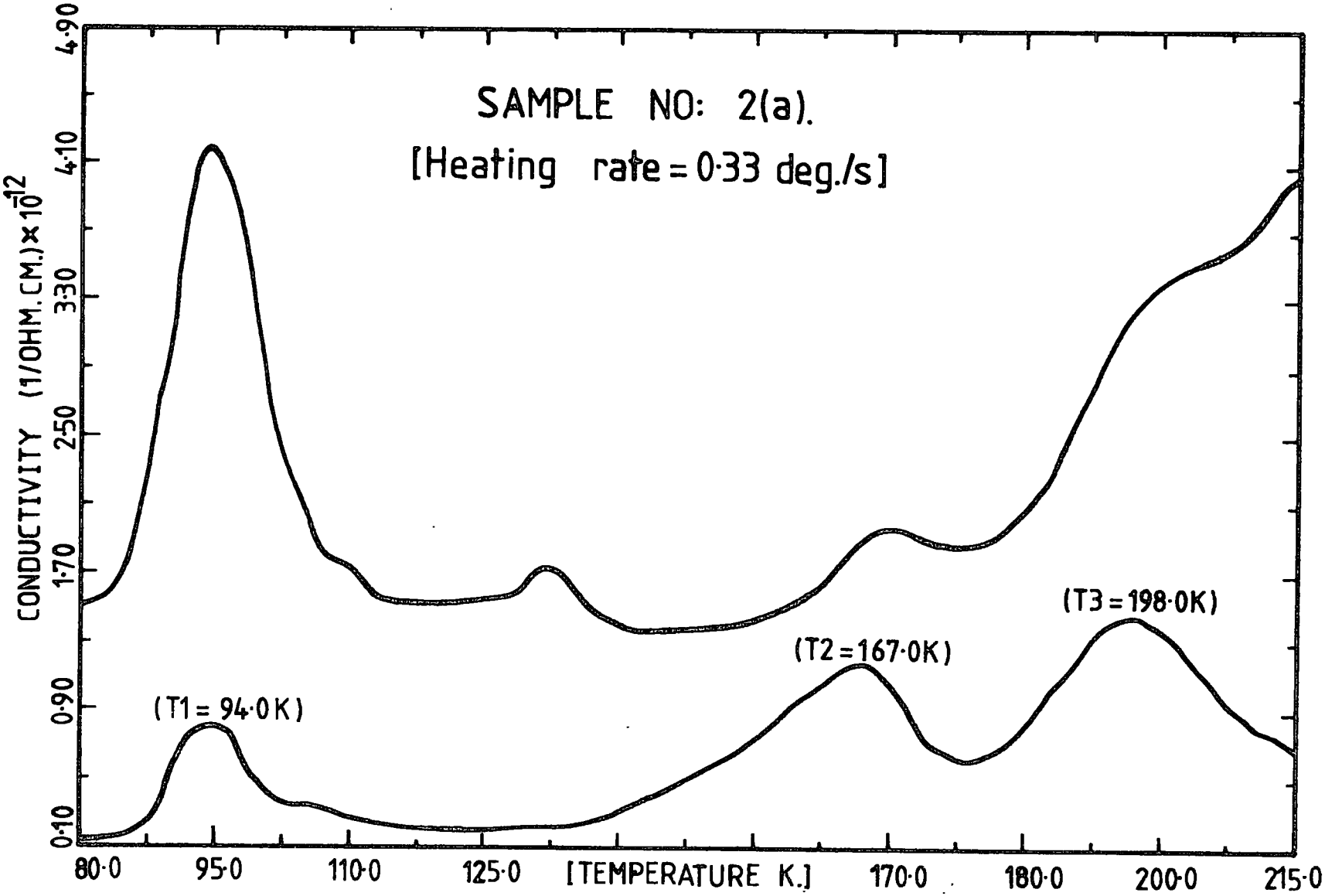

Fig. 5·21 TSC curves for a Chlorine doped CdTe crystal, before and after annealing at 150°C for 20 minutes.

resolved, located at 95, 165 and 198 K. In order to apply the analytical methods described in section (2.3), it is necessary to have isolated TSC peaks. The "thermal cleaning" of the TSC curves by interrupted heating was applied to separate these individual maxima. Fig (5.22) shows two such peaks separated by the above method. In fig (5.24), the thermally cleaned TSC peak at ≃ 198 K is shown for three different heating rates. These peaks were analysed by the five different methods described in section (2.3.2), and the results are summarized in table (5.4). The results obtained by applying Garlick-Gibson[17] and Hoogenstraaten[18] methods to the two main peaks are shown in figure (5.23) and (5.25) respectively. Unfortunately all these analyses are impracticable for the peak at ≃95 K since it occurs at the very beginning of the TSC spectrum.

Table 5.4

Summary of TSC measurements

(a) Peak at ≃198 K.

β deg/s.	Randall & Wilkins	G & G.	Chen 4.	Hoogenstraaten	Bube.
0.14	0.41 (eV)	0.32 (eV)	0.31 (eV)		0.52 (eV)
0.20	0.42	0.40	0.36	0.37 (eV)	0.53
0.27	0.42	0.36	0.34		0.53
0.33	0.43	0.36	0.40		0.53
Average	0.42	0.36±0.04	0.35±0.05	0.37	0.53

(b) Peak at ≃ 165 K.

β deg/s.	Randall & Wilkins	G & G	Chen 4.	Hoogenstraaten	Bube.
0.14	0.34	0.21	0.26		0.43
0.20	0.35	-	0.26		0.44
0.27	0.36	-	0.23	-	0.45
0.33	0.36	0.24	0.27		0.45

(c) Peak at ≃ 95 K.

0.20	0.20	-	0.15	-	-

Observation of the table 5.4(a) shows that the only exception is the quasi Fermi level (Bube's) method[19], which assumes a strong retrapping and which, in almost all cases, gives results in strong disagreement with the other methods. Chen's method[20] is in very good agreement with Garlick-Gibson's and Hoogenstraaten's methods. If the conductivity peaks can be isolated easily,this method should be clearly preferable for the analysis of TSC results for CdTe. Randall and Wilkins method[21] was the first used to analyse the TSC results and was found to be very convenient to check the trap depths immediately after the experiments. The level at E_v + (0.36 ± 0.05) agrees well with the previously reported TSC results by many authors. This particular centre is present in Cl-doped[22-25] In-doped[24], and Zn-doped[25] CdTe samples. In the literature, this level is generally assigned to the singly-ionized Cd vacancy[27].

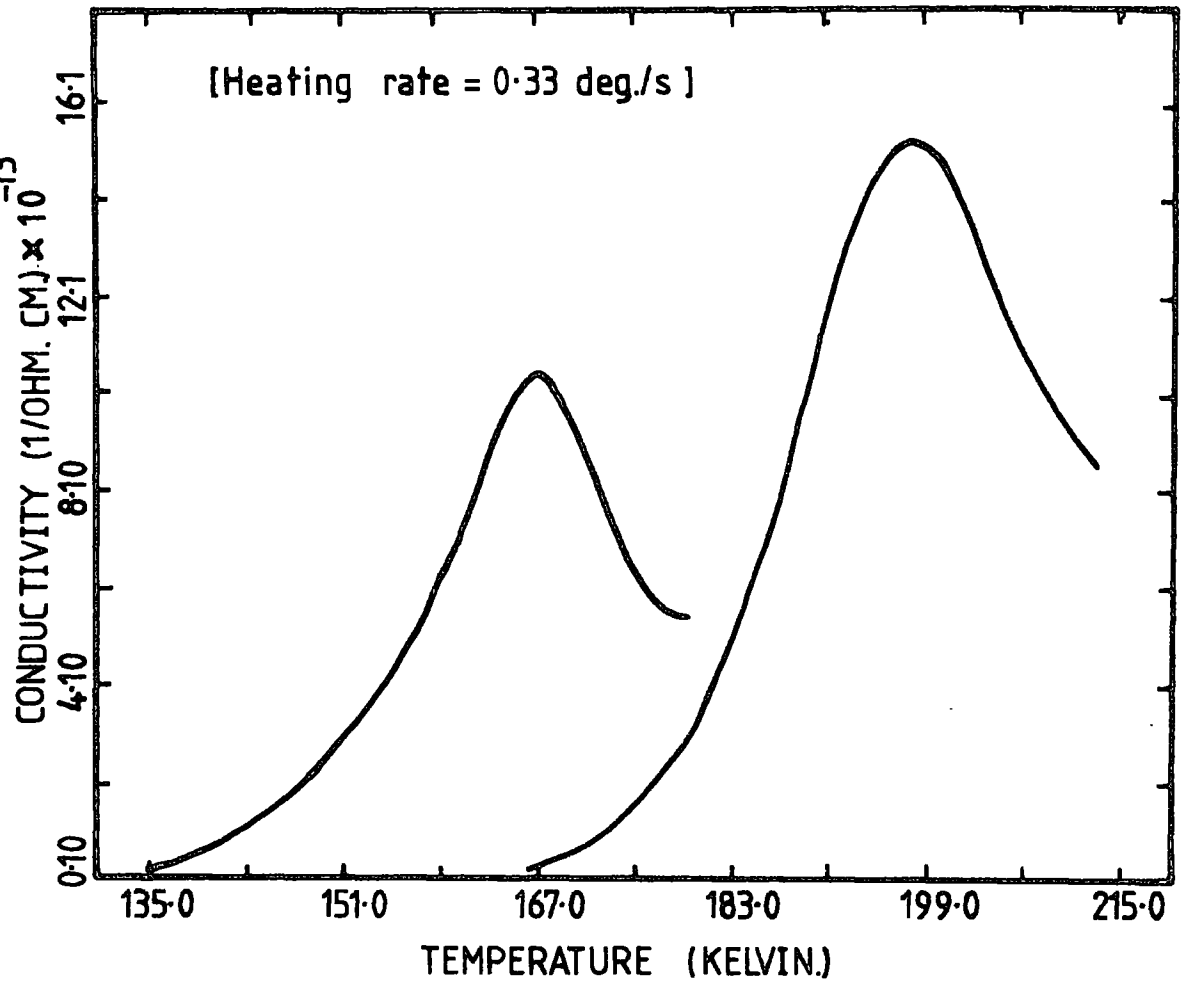

Fig. 5·22 Two main peaks after thermal cleaning process.

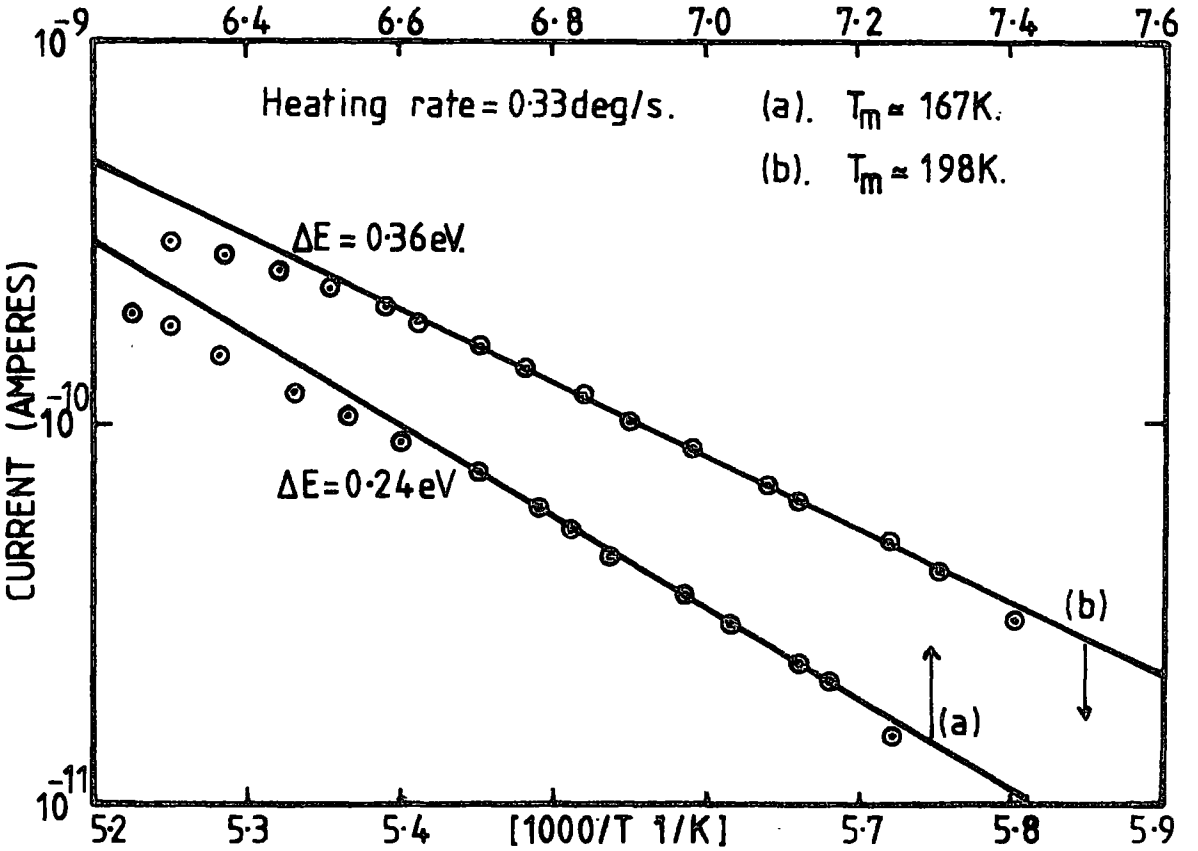

Fig.5·23 Analysis with the G & G method of the rising side of the peaks at 167K and 198K.

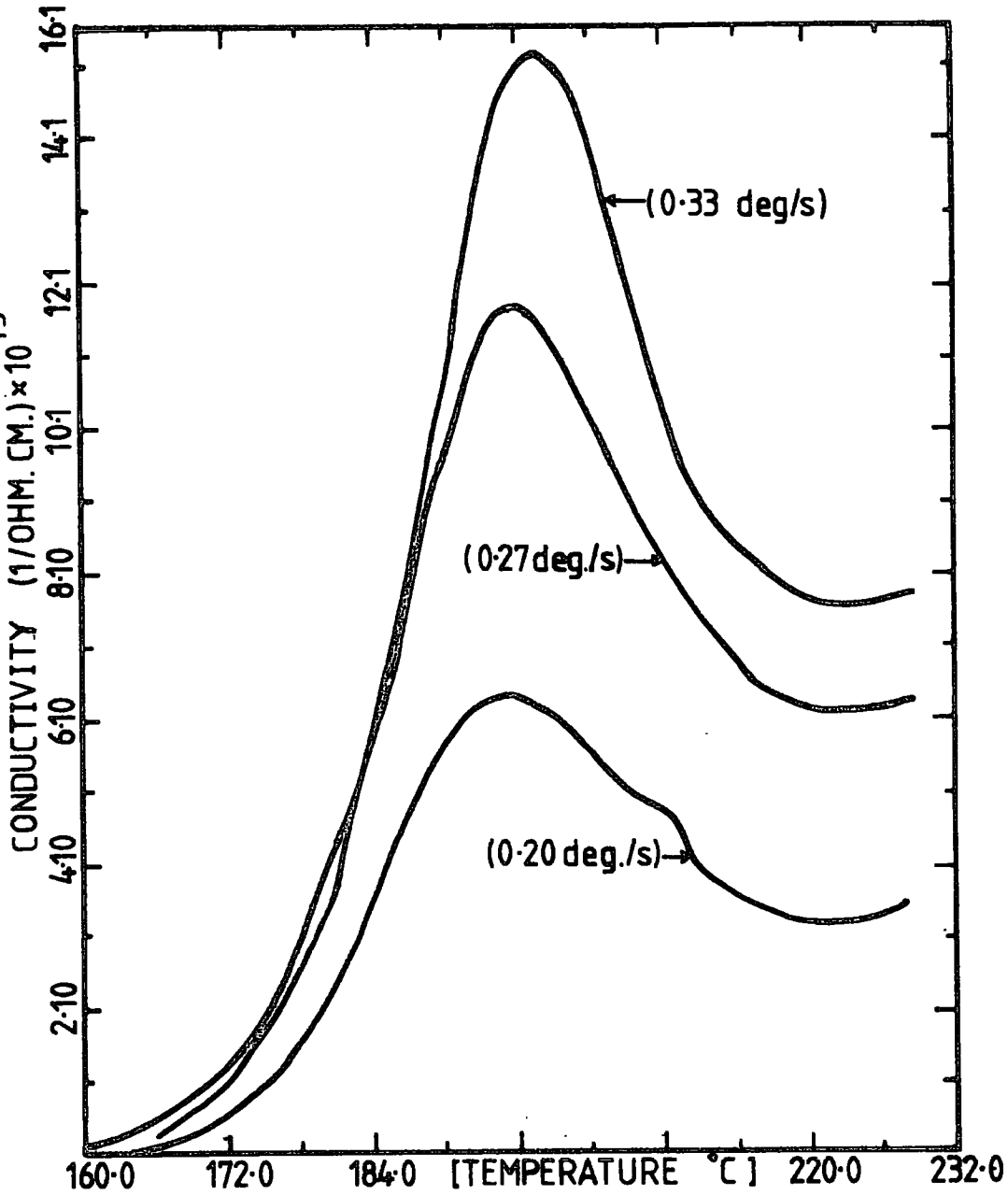

Fig. 5·24 TSC peak at ≈ 198K, measured at 3 different heating rates.

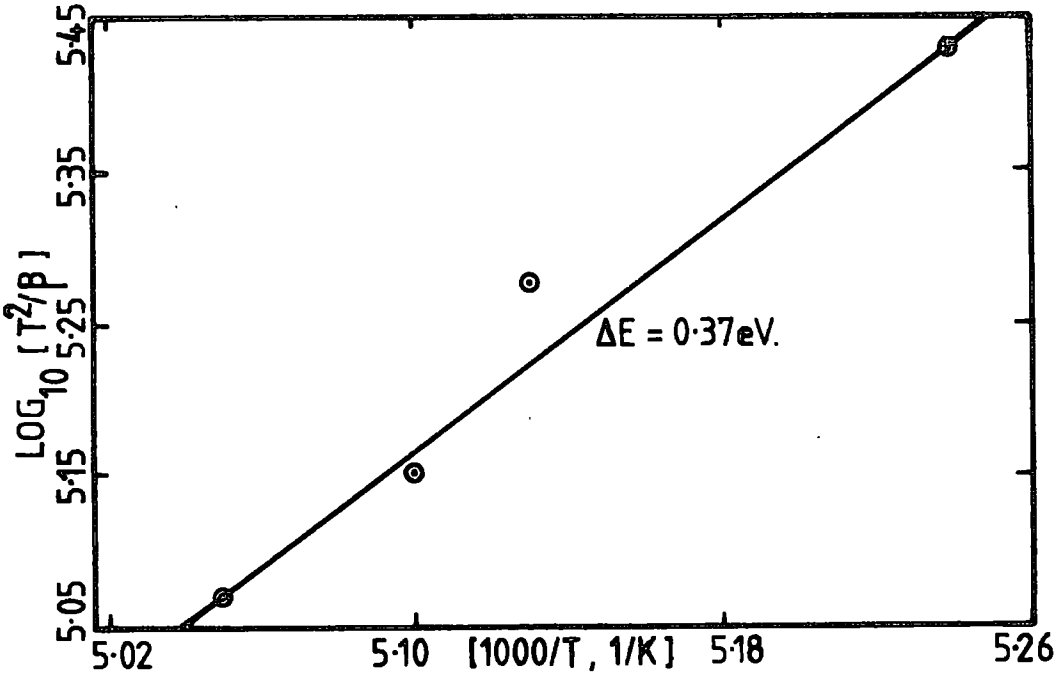

Fig. 5·25 Analysis with the Hoogenstraaten method for the peak at 198K.

The analysis of the TSC peak at 165 K does not lead to any definite conclusions about the trap depth due to the scattered values obtained from different methods. This peak, however, has been observed for Cl-doped CdTe by other authors[24,25,27] and analysed to give an energy value of 0.35 eV.

The peak at 95 K is a very common and dominant one for CdTe samples. Chen's analysis method produced an energy value of 0.15 eV for the trap depth. Martin et al[22] have observed all the above peaks for their Cl-doped p-type CdTe samples and obtained a value of 0.18 eV for the peak at ≈ 98 K. This peak has also been observed by Stuck et al[24] for both Cl-doped and In-doped samples. These authors analysis gives an activation energy of 0.19 eV.

Fig (5.17) shows the effect of annealing on the TSC curve for this material. The resultant TSC curve increases with annealing temperature. The height of the peak at ≈ 95 K increases considerably and another peak appears around 130 K. Martin et al[22] have observed a clear peak at 130 K for their Cl-doped samples and yield an energy level at 0.25 eV. The resultant dark current also increases as a result of annealing the sample in a vacuum. The increase in TSC curve may possibly be due to either an increase in trap concentration or lifetime of the charge carriers.

The levels observed from the TSC method may well be the same as the E_m levels calculated from d.c. conductivity measurements. The deep E_q level, however, cannot be observed in these specimens due to increase in dark currents at high temperatures. The nature of the traps (electron or hole traps) cannot be determined from these measurements alone.

5.4 ORIGIN OF DEEP LEVELS

Single crystals of CdTe grown from tellurium rich solution will be deficient in cadmium. Cd vacancies behave as acceptors in CdTe, and can substantially influence the electrical properties of the single crystals. These native defects can be in neutral, singly or double ionized states. Doping with chlorine, which creates shallow donor levels in CdTe, compensates these acceptors and produces high resistivity single crystals. Various authors[29,30] report the formation of complexes in CdTe when doped with chlorine. Then the native defects or their complexes with chlorine in different charge states are possibly responsible for the electrical conduction in these crystals.

From the experimental data presented in this chapter, it is difficult to accurately assign the energy levels observed to specific defects in the CdTe. However, some tentative conclusions may be drawn. We note that the E_q(deep acceptor) level is observed in approximately the same position in the bandgap (1.00 eV above the valence band edge at OK) in all the samples. This level agrees well with the electron trap reported by Ottaviani (1.00 eV) and Zoul (0.97 eV) by different experimental techniques (Fig.1.3). One possible interpretation would be to assign this level to a double ionized cadmium vacancy, which is the most frequently reported deep acceptor-type defect in CdTe:Cl[1,28].

The 0.15 eV activation energy, observed after annealing the crystals above 300^{o} C for longer periods, has also been reported by many authors and assigned to singly ionized cadmium vacancy[1,7].

The explanation of the variable E_m(deep donor) level is more difficult. It would seem likely that this is associated with the chlorine because this variable level is not observed in undoped CdTe crystals grown under similar conditions (Pande and Roberts, 1978)[6]. Current models for compensation in CdTe:Cl favour the presence of a complex defect in which chlorine is involved[29,30]. The energy level of such complexes will, of

course, depend on the degree of association of the constituent defects. Höschl et al (1977)[27] have shown that a cadmium vacancy/chlorine complex can give rise to a series of discrete energy levels within the bandgap of CdTe. If the complexes of native defects and chlorine give rise to a multiplicity of levels associated with electronic states of different valency, then the multivalent theory discussed in section (g) may possibly account for the observation of Meyer-Neldel rule in the Cl-doped CdTe.

5.5 SUMMARY

The results of an activation energy analysis for both Ohmic and SCL current in high resistivity CdTe:Cl crystals show that the conductivity is controlled by two levels in the bandgap. A deep level, 1.00 eV above the valence band edge, is found in all of these samples and may possibly be attributed to the doubly ionized Cd vacancy reported by other workers. The depth of the second level controlling the conductivity of our samples is found to depend where the specimen is cut from the crystal boule and the temperature of any annealing treatment.

Fig (5.26) summarizes all values obtained for E_m, during this series of experiment together with TSC results and an up-to-date review of previous work. Each line corresponds to one observation of E_m from activation energy or TSC measurements. This easily variable energy level, E_m, may be associated with the chlorine impurity, although other investigations are necessary to confirm this.

The conductivity of these samples is found to obey the Meyer-Neldel rule. This is clearly observed for samples taken from different positions along the crystal boule and for one sample under different annealing conditions. The multivalent theory proposed in this work produces conductivity characteristics that are similar to those observed experimentally. This may, therefore, explain the occurrence of Meyer-Neldel rule. The origin of multivalent centres could well be the complexes of Cd vacancies

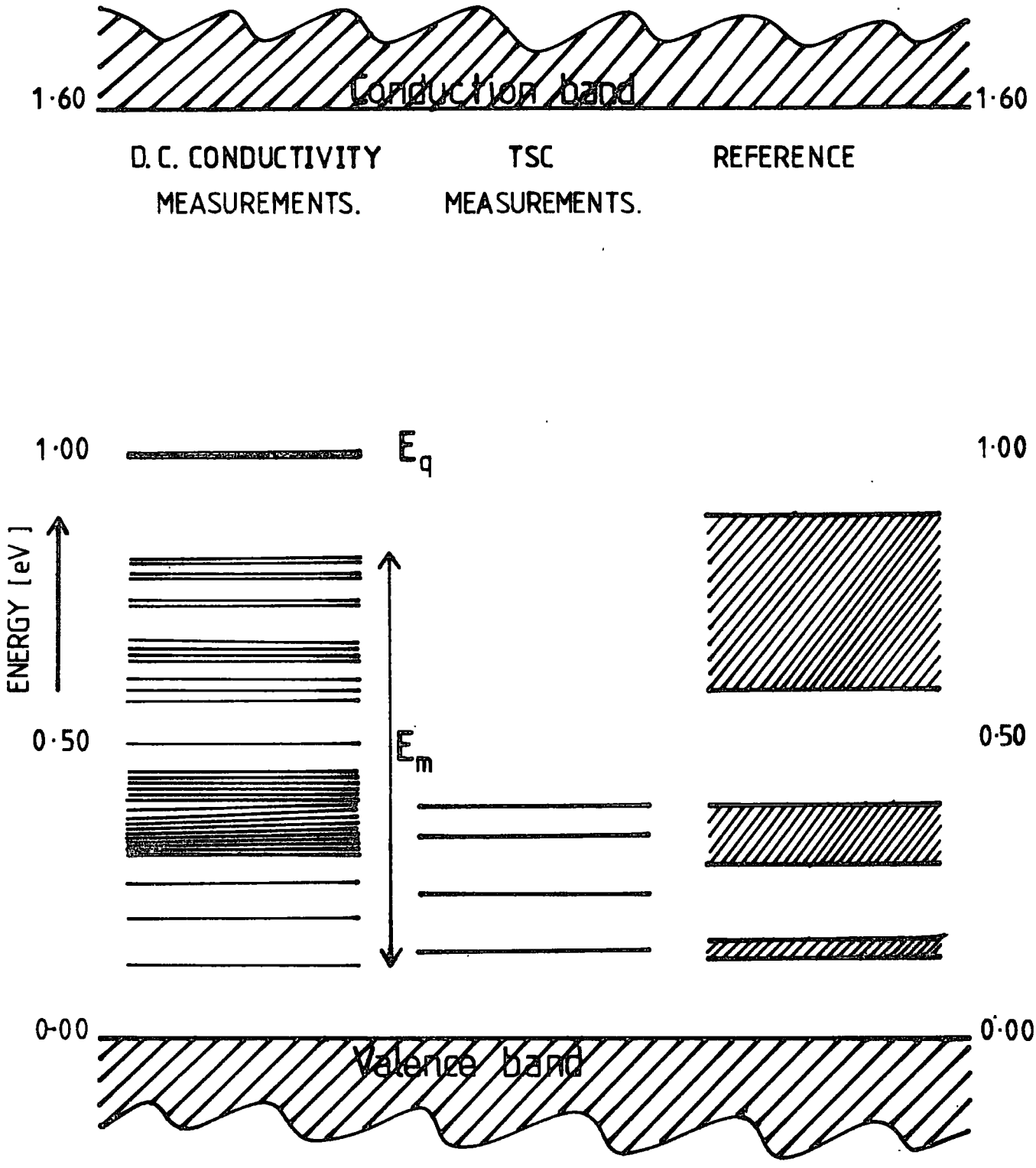

FIGURE 5·26.

LOCALIZED ENERGY LEVELS IN THE BAND GAP OF SEMI-INSULATING CdTe.

with chlorine. A possible explanation for the different activation energy curves observed in these samples would then be that n, the average number of electrons/defect , is a function of position in the crystal boule and of subsequent heat treatment.

The TSC technique appears to be quite useful for the study of high resistivity CdTe, since it not only yields a spectrum of deep levels, but also an estimation of deep energy level positions. These measurements show the existence of energy levels at 0.37 eV, 0.35 eV and 0.15 eV in these Cl-doped samples. The nature of these levels, however, cannot be determined from these measurements alone. The annealing creates an extra level at ≃ 0.25 eV and increases the relative magnitude of the current peak at 95 K. This corresponds to a well-known level in CdTe (≃ 0.15 eV) and is often ascribed to singly ionized Cd vacancies.

The above experimental evidence shows that Cl-doped CdTe has very unstable electrical characteristics. Clearly this material is, at present, unsuitable for use in any commercial devices. Further work is therefore necessary to understand, in more detail, the nature of the defects in this material in order that crystals with reproducible, stable properties can be grown.

CHAPTER 6

RESULTS:- SEMI-INSULATING CdTe (Cr-DOPED)

6.1 INTRODUCTION

In this chapter, the electrical properties of Cr-doped cadmium telluride single crystals are presented. Measurements of thermal activation energies for both Ohmic and SCL conduction have been used primarily to characterise the material. Since these crystals show a complicated behaviour in the SCL region at low temperatures,a complete analysis has been carried out in a similar way to Cl-doped CdTe samples. Supplementary Hall effect and Schottky barrier data have also been obtained. The Hall effect measurements on these crystals show very similar properties to those of CdTe samples doped with Au, Cu and Ag reported by D. Nobel[1]. The Schottky barriers prepared on chemically etched surfaces show reproducible characteristics and these results confirm some of the parameters obtained from d.c. conductivity measurements. Experimental results obtained on undoped specimens are also given in each section and compared with those of Cr-doped material.

6.2 D.C. CONDUCTIVITY

In order to study the positions and concentrations of deep impurity levels, both Ohmic and SCL conductivity measurements have been performed on this material. Such experiments were carried out on specimens with sandwich type Ohmic contacts. These were prepared by vacuum evaporation of Au or Au/Sb on to the chemically etched surfaces. The helium exchange gas cryostat was used for most of the measurements, but the DN704 LN_2 cryostat described in chapter 4 was used at very low temperatures.

(a) SCL Currents

Fig (6.1) shows a set of current-voltage curves at several different temperatures for one of the measured Cr-doped CdTe samples. Before each of

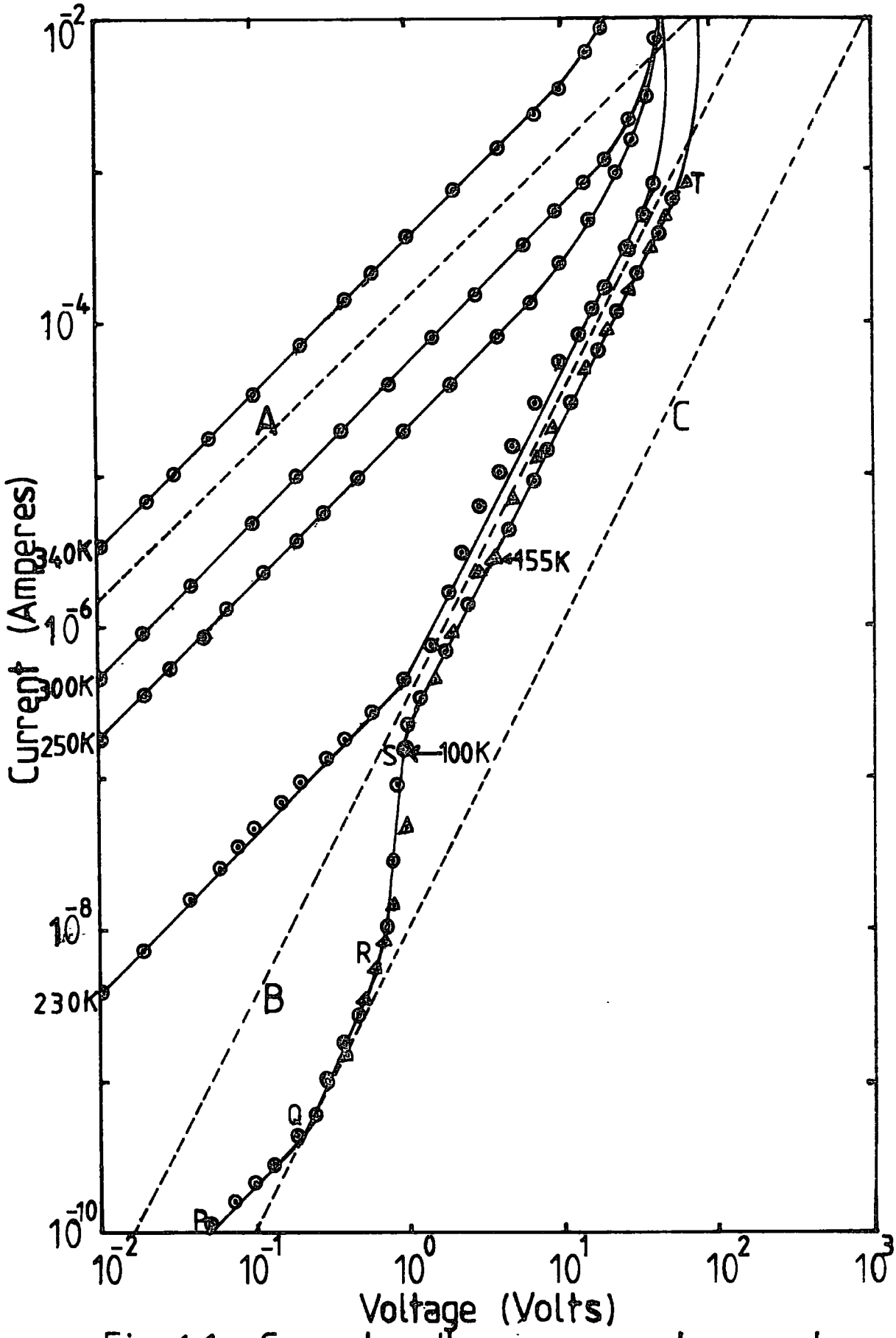

Fig. 6.1 Current-voltage curves at several different temperatures for single crystals of Cr-doped CdTe.

these current-voltage measurements were taken, the samples were heated in the dark to about 350 K with a small applied voltage and cooled down to the required temperature in order to remove any trapped charge carriers.

In the high temperature region long linear (Ohmic) branches followed by a section of steep current rise with voltage are observed. At low temperatures (230 K), the Ohmic region becomes shorter and a square law region becomes apparent. As temperature decreases further, the I-V curves (PQRST) show a very complicated behaviour. These curves display a short linear (PQ) Ohmic region followed by a low field square law branch (QR), which extends over nearly two decades. A rapid rise (RS) is then followed by another good square law region (ST). The main features of these low temperature I-V curves are the long square law branches, which extend over about four decades of current. In this region the current is almost independent of the temperature.

The current-voltage characteristics obtained for other samples of this material show the same linear (Ohmic) behaviour at high temperatures. In the low temperature region (230 K-100 K) however, these characteristics are complicated again and vary considerably for different samples. One of the specimens (sample No:2 in table 6.1) showed a $I\alpha V^3$ relation over six orders of magnitude of current. An $I \alpha V^{\frac{1}{2}}$ behaviour after the low field Ohmic regions were also observed for some specimens.

In order to understand these complicated current-voltage curves, the thickness dependence of currents were measured in both linear and square law regions. All the measurements were obtained at a constant temperature of 300 K. Experimentally observed results for one of these samples (No:1) are shown in Fig (6.2). The Ohmic and SCL currents at constant applied voltages (0.01V and 1.0V respectively) are proportional to L^{-1} and $L^{-(4\sim5)}$ for this particular sample.

To analyse the above current-voltage characteristics, three different theoretical curves (A,B and C) have also been plotted in Fig (6.1).

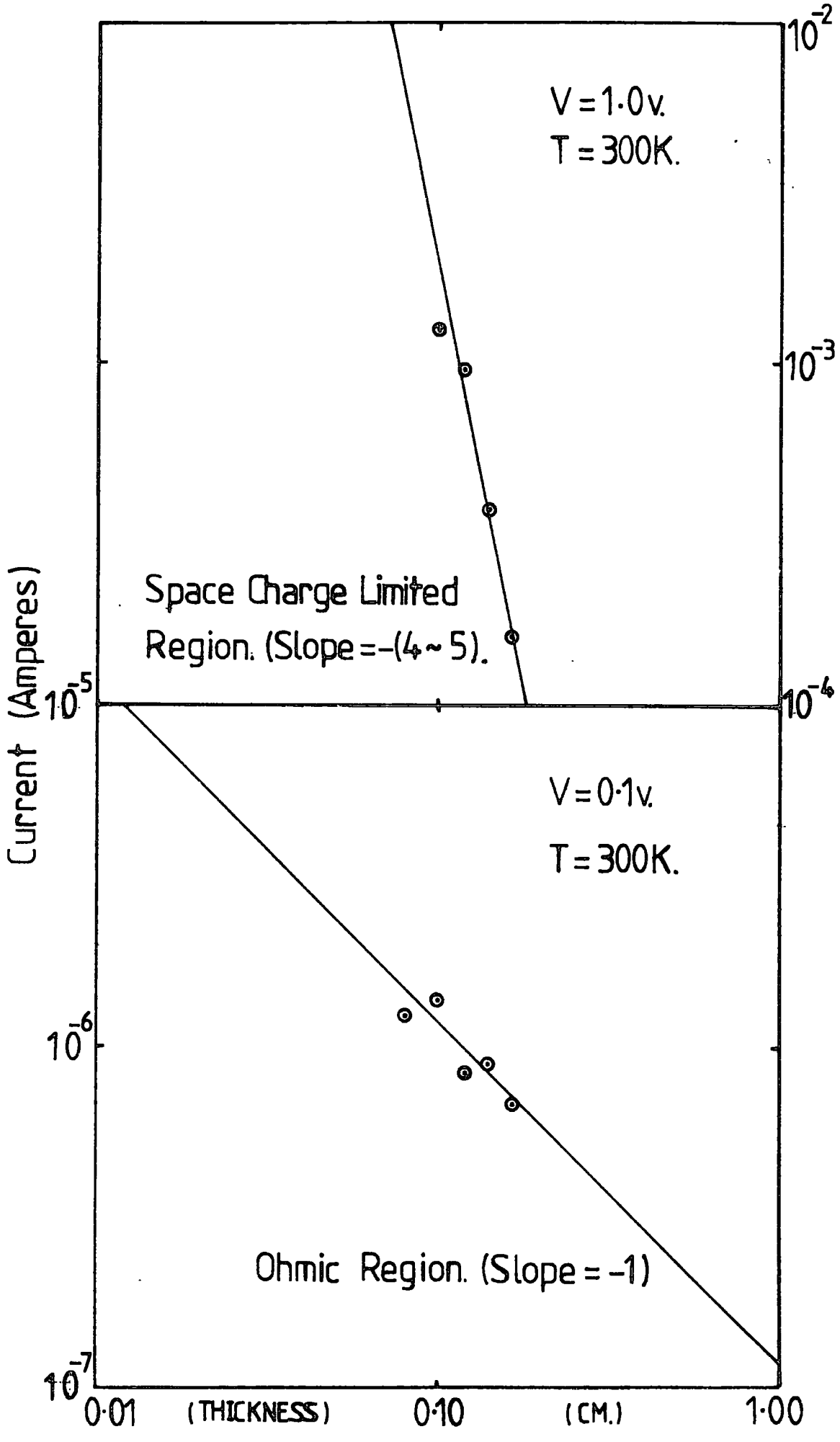

FIG. 6·2 OHMIC AND S.C.L. CURRENTS AS A FUNCTION OF THICKNESS.

The dashed line A shows the theoretical I-V curve calculated for the Ohmic conduction at room temperature. The values of carrier concentration and the hole mobility were taken from the Hall effect measurements (section 6.3). These data show that this material is p-type at high temperatures and low fields. It can be seen that the theoretical curve A agrees well with the measured curves. The thickness dependence measurements also confirm that the currents at low fields are Ohmic ($I\alpha L^{-1}$) and are determined by the bulk resistance of the material. The steep rise in current at higher voltages is possibly due to Joule heating or trap filling by injection of charge carriers.

Two other theoretical lines B and C plotted in Fig (6.1) show the maximum possible one-carrier SCL currents with two different mobilities, 750 cm^2/V. sec (Curve B) and 25 cm^2/V. sec (Curve C). These were computed from the relation (2.4),

$$I = \frac{9A\varepsilon\varepsilon_o\mu\theta V^2}{8L^3}$$

with $\theta = 1$ for the trap free situation. Since $\theta << 1$ for normal one carrier SCL currents due to trapping effects, the I-V curves should lie below the line C. The square law region (QR) of the I-V curve at 100 K, coincides with this line and therefore the injected holes may be responsible for this conduction. All the other currents lie above the line C and the long square law branch (ST) agrees well with the curve B. These currents therefore produce a value of 750 cm^2/V.sec for the mobility of charge carriers in this region. Since this value is too high for the hole mobility in CdTe, it can be concluded that the conduction at low temperatures might be due to injected electrons. The temperature independence of the currents shows that the electron mobility at low temperatures remains approximately constant. The rapid rise in current (RS) at $\simeq$ 1.0V by a factor of about 30 may be due to the difference in electron and hole mobilities. If the steep rise at the high current end shows a trap filling, the density of traps can be evaluated from

equation (2.8). These voltages yield an unusually low trap density ($\simeq 2.0 \times 10^{11}$ cm^{-3}), and hence the thermal breakdown rather than trap filling is probably responsible for the rapid increase in current.

The thickness dependence measurements in the SCL region, reveal that the currents through these specimens do not vary with the inverse cube of the thickness according to equation (2.4). Even though these measurements do not provide very accurate results, the $L^{-(4\sim5)}$ dependence suggests that the SCL currents in this material is due to two-carrier injection rather than one-carrier injection. The observation of $I\alpha V^3$ over six orders of magnitude for a similar sample indicates again that the electrical conduction at low temperatures is probably due to double injection according to the theoretical relation given by equation (2.6). Preliminary drift mobility measurements carried out on these samples (in York University) also indicate that the conduction in this material is due to both electron and holes. However, detailed experimental evidence is needed to draw any definite conclusions on space charge limited currents in this material.

(b) Activation energy analysis

The d.c. conductivity measurements were made on these specimens in the temperature range 100-340 K. Fig (6.3) shows a typical plot of log I versus reciprocal temperature obtained for both Ohmic and SCL currents. The activation energy obtained for Ohmic conduction is $\simeq$ 0.26 eV at high temperatures and 0.41 eV at low temperatures. The SCL current activation energy at high temperature region is 0.34 eV. An unusual transition occurs at low temperature region and produces a value of 0.14 eV for the activation energy. Because of the uncertainty of the conduction process in this region, the absolute values of SCL currents (apart from ΔE value) were not used in the following analysis. Because the activation energies of the Ohmic and SCL currents are different, the material may be regarded as a non-extrinsic semiconductor[2] whose Fermi level is controlled by two dominant levels situated at 0.34 eV($E_m - E_V$) and 0.53 eV($E_q - E_m$) from the valence band edge.

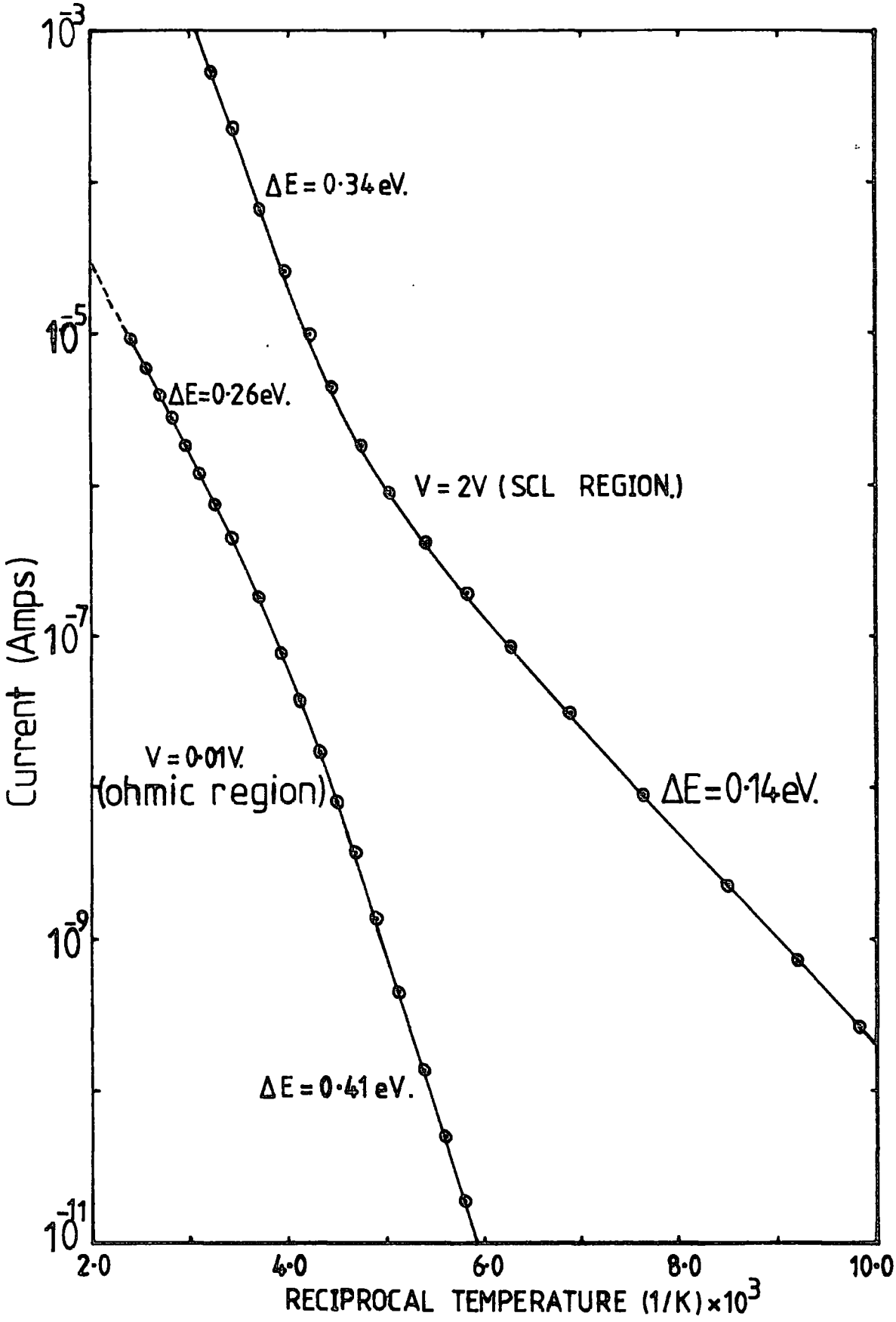

Fig. 6·3 Variation of current with temperature in ohmic and SCL regions for Cr-doped CdTe.

The concentrations of these dominant levels were obtained by the inverse graphical method introduced by Schmidlin and Roberts (1974)[3]. The hole mobility used in this analysis was taken from the Hall effect measurements. A complete analysis was carried out on the Ohmic activation energy curve and the final results are shown in Fig (6.4). The procedure of the complete analysis is outlined below :

1. The "V" shape is constructed whose sides have slopes $\pm$ 0.434/kT at 383 K. Its location on the ordinate was determined by calculating the hole concentration in the valence band at this temperature using a hole mobility of 25.0 cm^2/V.sec.

2. Since the high temperature Ohmic activation energy (0.26 eV) is equal to $(E_q - E_v)/2 = 0.26$ eV, the non-extrinsic conduction in this region is controlled by two levels E_q and E_v. By equating the two extensions above "V"of the two levels, the concentration, N_q, is determined.

3. At low temperatures, however, the activation energy is 0.41 eV, and the non-extrinsic conduction is controlled by the levels E_m and E_q. Since N_q is known, the concentration of E_m level, N_m, is determined using the non-extrinsic condition $(p)_m = (n)_q$ at a lower temperature of 285 K. The important parameters obtained for this material from the d.c. conductivity measurements are

$(\mu_p)_{300\ K}$ = 25.0 cm^2/V.sec(From Hall effect measurements)

$(E_m - E_v)$ = 0.34 eV. $N_m = 6.31 \times 10^{13}\ cm^{-3}$.

$(E_q - E_v)$ = 0.52 eV. $N_q = 1.58 \times 10^{16}\ cm^{-3}$.

The apex of the "V" lies at approximately 0.36 eV which is therefore the height of the Fermi level above the valence band.

To check these results obtained from the above analysis, the computer simulation described in section (5.1) was used. The computer

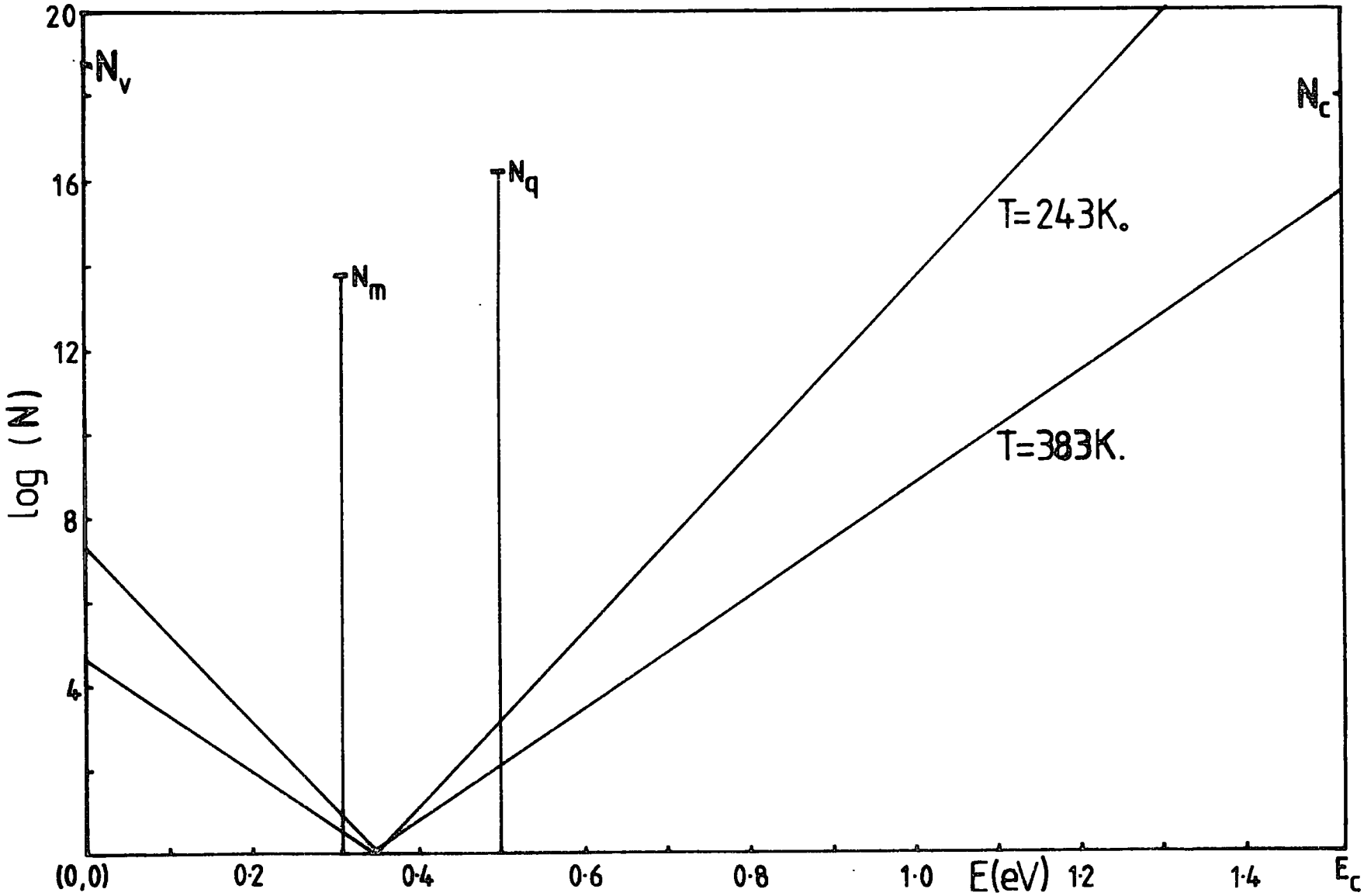

FIG. 6.4 GRAPHICAL ANALYSIS OF THE POPULATION OF STATES OF [illegible] DOPED [illegible]

fit obtained for this particular sample is shown in Fig.(6.5), and the excellent agreement between the computed curve and the experimental data shows the accuracy of the above analysis. The various parameters obtained for different samples are summarized in table (6.1) for comparison.

Table 6.1

Summary of D.C. conductivity measurements of Cr-doped CdTe.

Sample Description	Sample No.	E_m (eV)	E_q (eV)	N_m (cm^{-3})	N_q (cm^{-3})	ρ (Ω cm)
CTSE-201-15mm	1	0.33	0.53	6.30×10^{12}	2.50×10^{16}	6.7×10^{4}
CTSE-201-16mm	2	0.34	0.48	2.51×10^{14}	3.16×10^{15}	4.5×10^{4}
CTSE-201-30mm	3	0.33	0.53	6.31×10^{13}	1.58×10^{16}	2.7×10^{3}
CTSE-191-NO:3	4	0.34	0.50	5.00×10^{13}	8.00×10^{15}	1.0×10^{5}
CTA 72	5	0.35	0.51	-	-	5.0×10^{5}

The same measurements and analysis were performed on some semi-insulating undoped CdTe specimens. These also showed p-type conduction , and similar analysis produced the following parameters.

$(\mu_p)_{300\ K}$ = 30.0 $cm^2/V.sec$ (From Hall effect measurements).

$(E_m - E_v)$ = 0.31 eV. $N_m = 1.25 \times 10^{14}\ cm^{-3}$.

$(E_q - E_v)$ = 0.56 eV. $N_q = 4.00 \times 10^{16}\ cm^{-3}$.

Although the resistivity of undoped CdTe can vary over a very wide range, the semi-insulating specimens studied in this work showed very similar behaviour to Cr-doped material. Therefore, the Hall effect and Schottky barrier measurements were also carried out on both materials for further comparison.

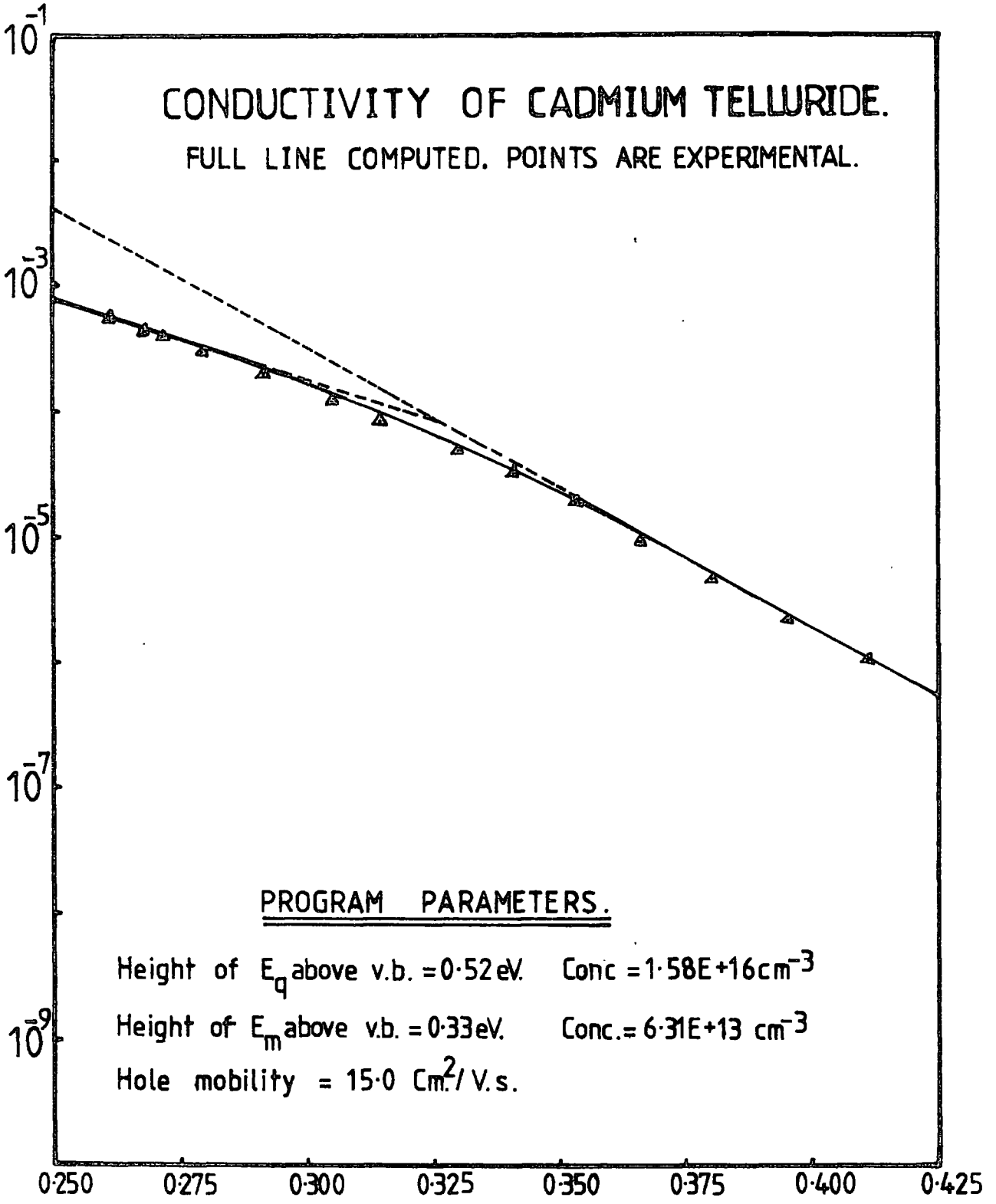

Fig. 6·5 Computed activation energy curve with experimental observations for Cr-doped CdTe (sample 3) single crystals.

6.3 HALL EFFECT MEASUREMENTS

The d.c.Hall effect measurements were performed on both Cr-doped and undoped materials using the experimental technique described in Chapter 4. Standard bar-shaped specimens were used and results are presented in fig.(6.6). This shows the Hall mobility as a function of reciprocal temperature. The a.c. Hall effect measurements were not successful due to noise, with these high resistivity specimens.

Cr-doped material shows p-type conductivity with a Hall mobility of about 25.0 $cm^2/V.sec$. The resistivity lies in the range 10^3-10^5 Ω cm. at room temperature. For temperatures below about 250 K, the measurements become impracticable due to the unreliability of the voltmeter reading. The experiments were carried out only at high temperatures with these semi-insulating specimens. Undoped specimens used in this experiment also show p-type conductivity with Hall mobility of about 50 $cm^2/V.sec$. The resistivity lies in the same range as Cr-doped material at room temperature. The various parameters obtained for these two different materials are shown in table (6.2).

Table 6.2

Summary of Hall effect measurements

Sample	Type of Material	(μ) $cm^2/V.sec$ 300 K	(p) cm^{-3} 300 K
Cr-doped CdTe	P	25.0	7.8×10^{13}
Undoped CdTe	P	50.0	8.4×10^{13}

In fig.(6.6) the Hall mobilities for these high-resistivity CdTe samples are shown as a function of reciprocal temperature. The temperature range in which mobility values are determined is too small in this case to discuss any scattering mechanisms in these materials. Similar results have been obtained for p-type, high resistivity CdTe by various authors[4,5,6,1].

FIGURE 6·6

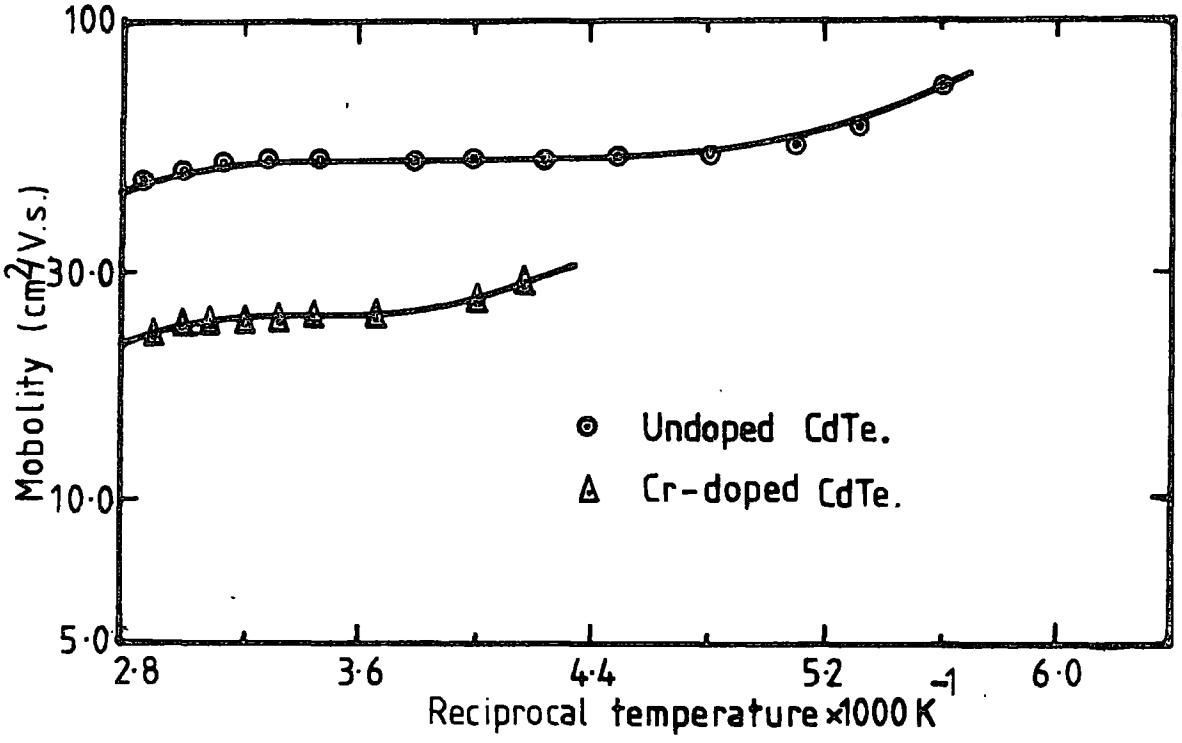

Mobility as a function of reciprocal temperature for free holes in semi-insulating CdTe single crystals.

The value of Hall mobility is quite low (30-60 cm^2/V.sec) at room temperature and the temperature dependence of mobility is weak. Ottaviani et al[7,8] have performed, with time-of-flight technique, an extensive investigation of the transport properties of holes in high-resistivity CdTe in a very wide temperature range. Their experimentally observed hole mobility ($\simeq$ 45.0 cm^2/V.sec at 300 K) decreased slightly on lowering either temperature or the electric field. These features are not in agreement with either optical ($\mu \alpha T^{-3/2}$) or ionized impurity ($\mu \alpha T^{3/2}$) scattering mechanisms, and have been interpreted on the basis of the electrical field effect on trapping and retrapping phenomena (Poole-Frenkel effect) which cause a reduction of the mobility. They also have observed a trapping level at 0.14 eV, and have concluded that such traps cause the reduction of the mobility.

6.4 SCHOTTKY BARRIERS

D.C. conductivity and Hall effect measurements show that the Cr-doped material has similar properties to the undoped material used in this work. Both materials show p-type conduction at low fields, and resistivities at room temperature in the range 10^3-10^5 Ω cm. Schottky barrier measurements were performed on both materials in order to determine the excess acceptor concentrations. The barriers were fabricated by evaporation of Sn on to chemically etched CdTe surfaces and Ohmic contacts were obtained by evaporation of Au/Sb alloy.

The current-voltage characteristics in the dark at room temperature are presented in fig.(6.7). To obtain the forward current-voltage curve, the bias voltage was applied positively to the Au Ohmic contact since the material used here is p-type. These devices show a rectification factor of about 500 when 0.5V is applied. The forward I-V characteristics show a saturation towards higher voltages due to the effect of the large bulk resistance. The ideality factor as determined from the slope of the forward characteristics, corrected to allow for a bulk series resistance of 6.5 k Ω,

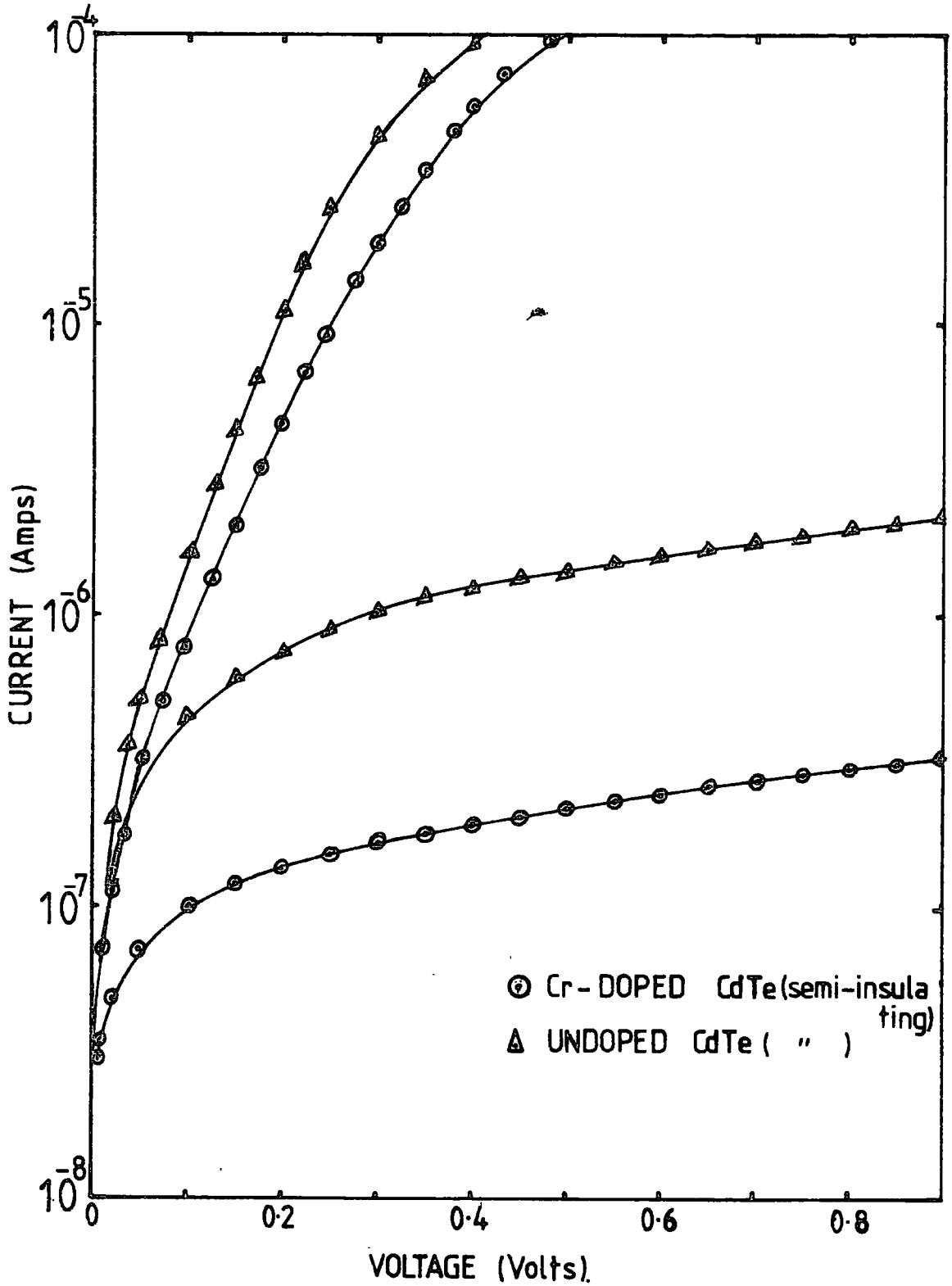

FIG. 6·7 CURRENT - VOLTAGE CHARACTERISTICS OF Sn/P-TYPE CdTe SCHOTTKY DIODES AT ROOM TEMPERATURE.

is about 1.73. This modified forward characteristics for Sn/CdTe:Cr diode is shown in fig (6.8). The reverse I-V characteristics do not completely saturate but slightly increases with voltage in the region where saturation might ideally be expected. This current however varied from diode to diode and is a function of diode fabrication. The average saturation current density of these Sn/p-type CdTe barriers was measured to be about 2.0×10^{-4} A.cm^{-2}.

The differential capacitance of the diodes was determined as a function of applied voltage at a frequency of 20 kHz. The $1/C^2$ versus V plots are shown in fig (6.9) for the above two diodes. These are linear up to about 1.5V in accordance with the theoretical relation (3.16). From the slope of the linear characteristics and assuming a relative permittivity of 11.0, the excess acceptor concentration, (N_a-N_d), was calculated to be 1.65×10^{16} cm^{-3}, for Cr-doped material. The diffusion voltage, V_d, was obtained from the intercept on the voltage axis and the barrier height was calculated from the relation (3.46). The value of $V_n \simeq \Delta E$ (0.33 eV) was taken from the activation energy measurements and the barrier height, ϕ_b, was calculated to be 0.98 eV, at room temperature. The other two small terms were neglected for this calculation. Table (6.3) summarizes the various parameters obtained for diodes prepared on these two materials.

Table 6.3

Summary of Schottky Barrier measurements

Diode	n	V_d(eV)	$V_n=\Delta E$(eV)	$(\phi_b)_{293K}$ eV	(N_a-N_d) cm^{-3}
Sn/Cr-doped CdTe	1.73	0.65	0.33	0.98	1.6×10^{16}
Sn/undoped CdTe	1.80	0.58	0.31	0.89	2.0×10^{16}

Fig (6.10) shows the reverse I-V characteristics of the Sn/CdTe:Cr diode at several different temperatures. The straight line (a) in fig (6.11)

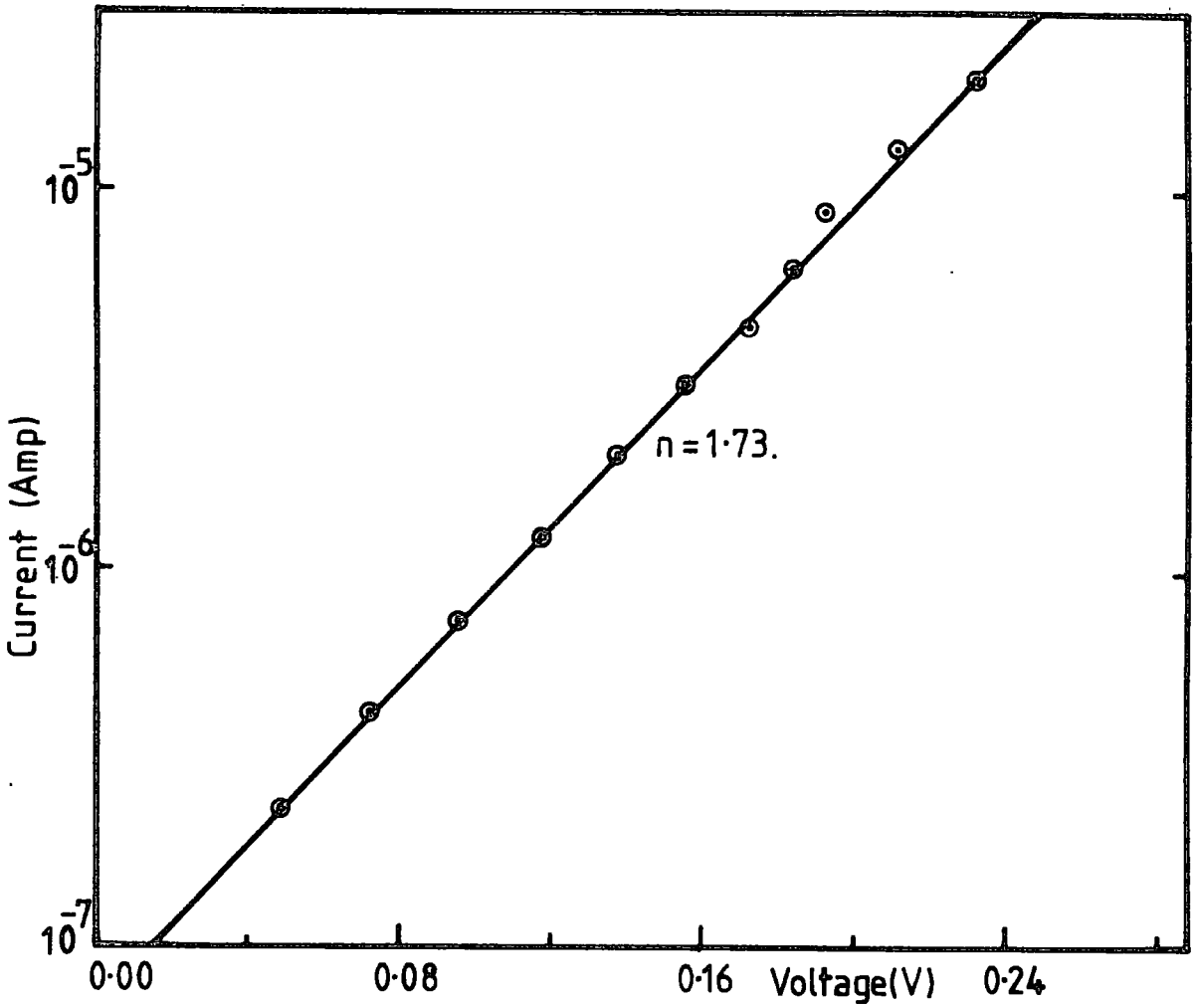

Fig.6·8 Forward I-V characteristics of Sn/CdTe:Cr diode at 293K, corrected to allow for a bulk series resistance (6·5kΩ).

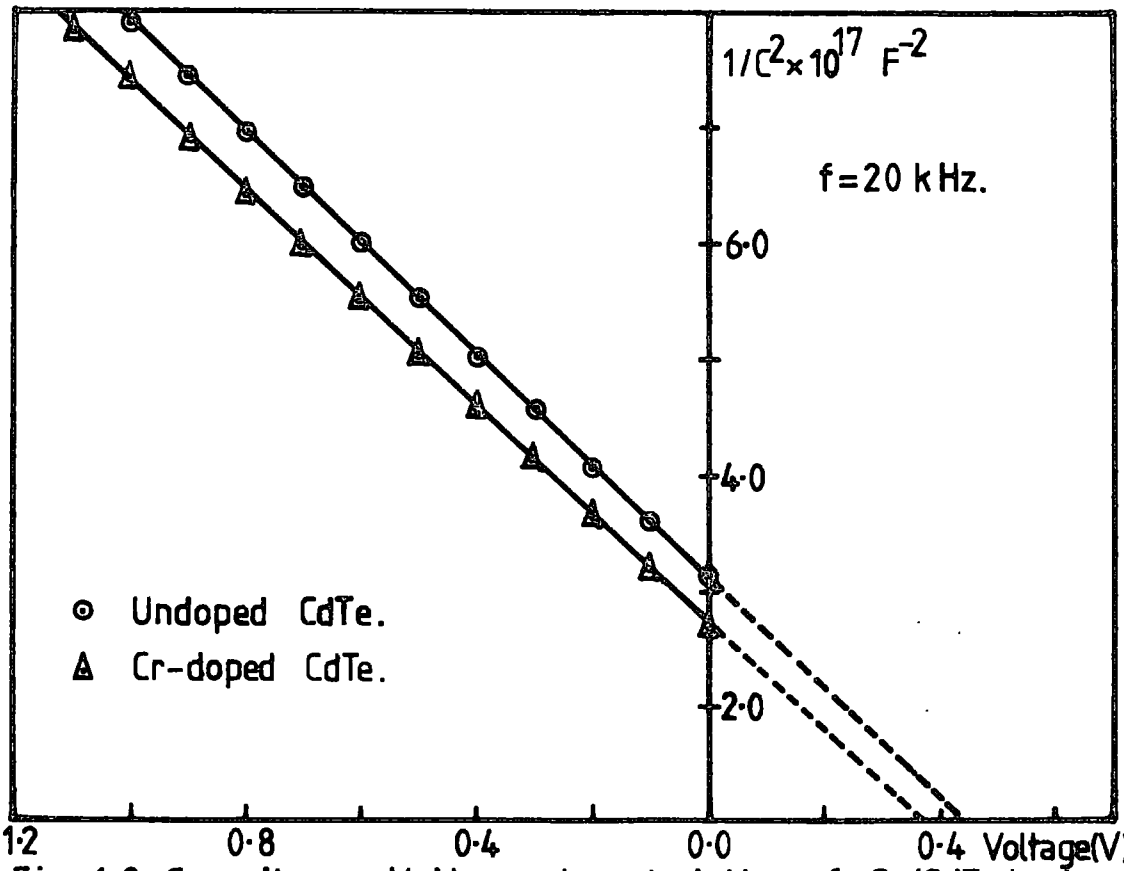

Fig. 6·9 Capacitance-Voltage characteristics of Sn/CdTe (p-type) Schottky diodes at 293K.

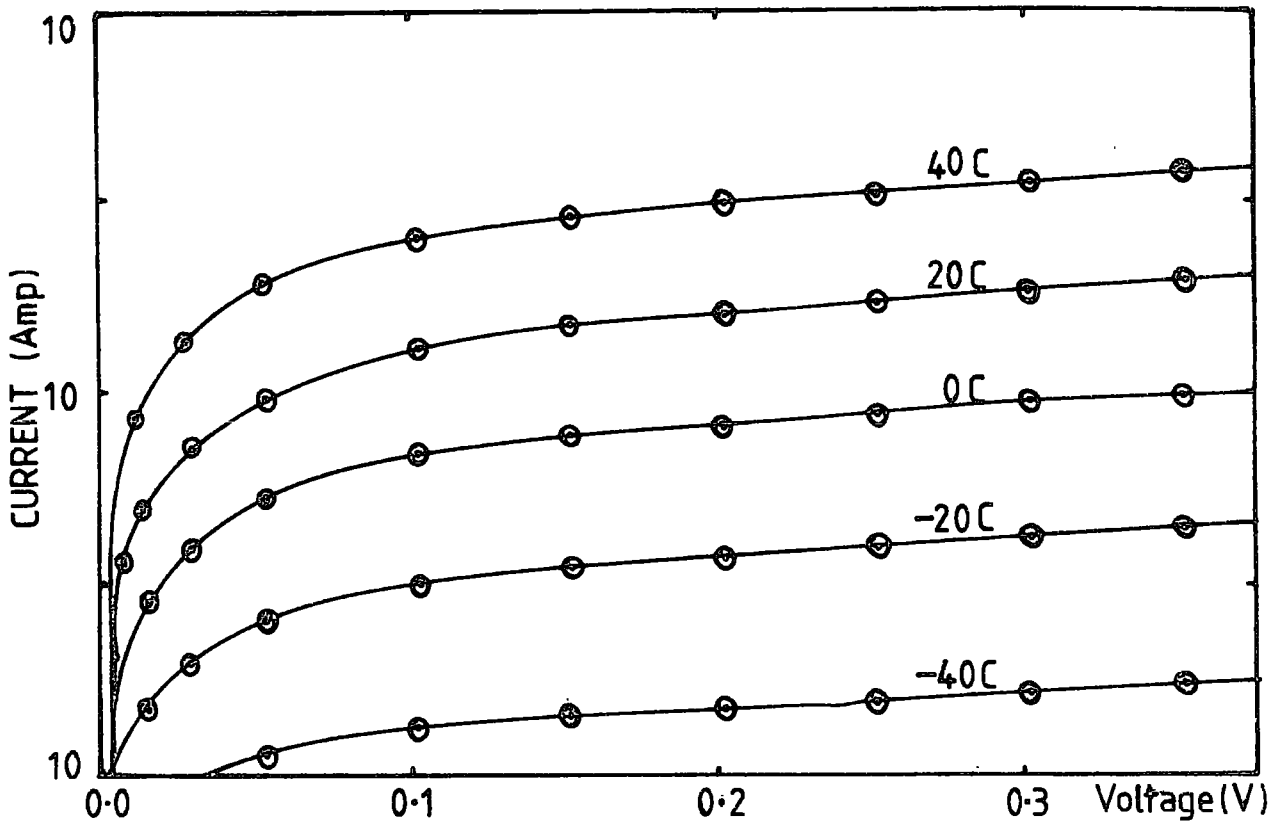

Fig. 6·10 Reverse I-V characteristics of a Sn/(p-type)CdTe:Cr Schottky diode at different temperatures.

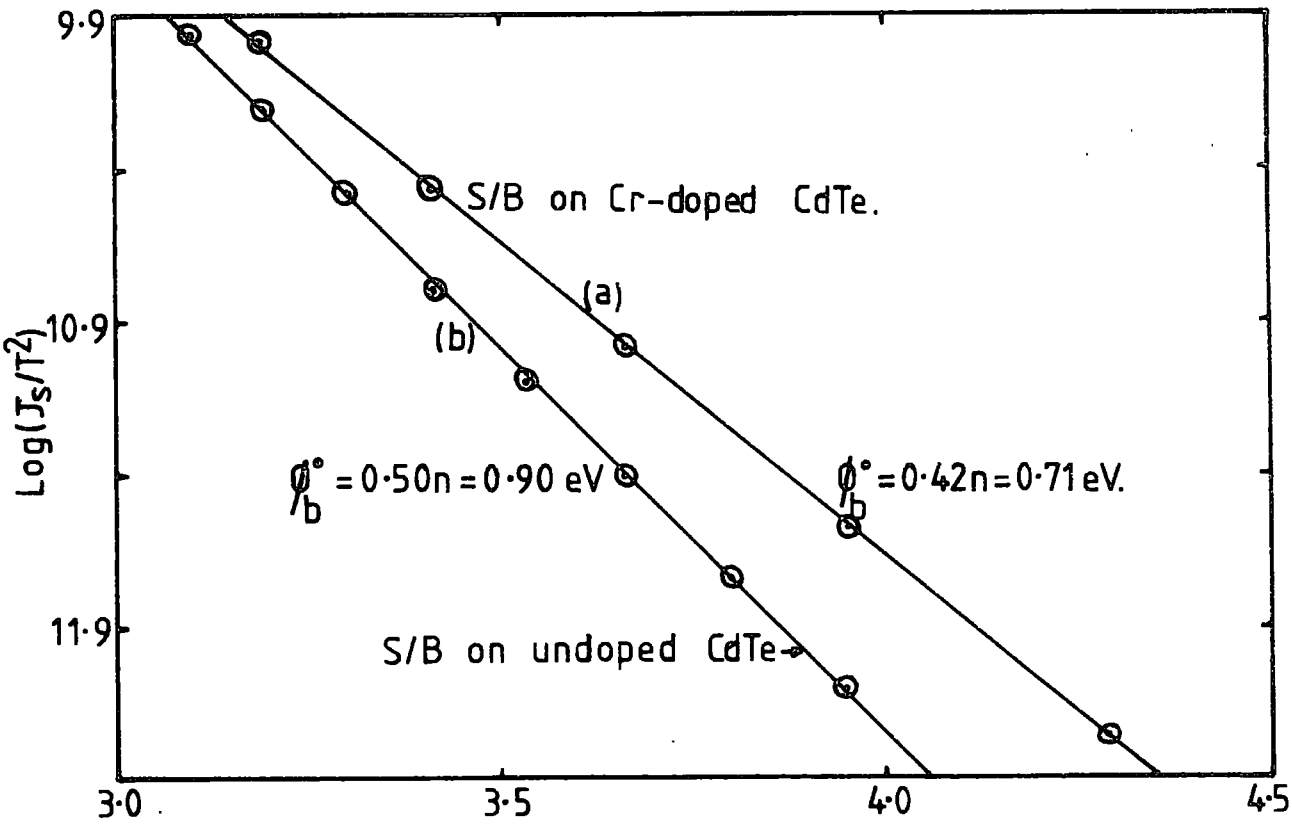

Fig. 6·11 Dependence of reverse saturation current on temperature for Schottky diodes prepared on Cr-doped and undoped CdTe.

shows the I_s/T^2 (I_s taken at 0.1V) against 1/T plot for this particular diode. The value of ϕ_b^o was found to be about 0.71 eV with n = 1.73. The activation energy plot (b) is also shown for the diode prepared on undoped material, and this yields a value of 0.90 eV for ϕ_b^o. Although these plots are straight lines as expected, the values of ϕ_b^o are less than room temperature barrier heights obtained from C-V measurements. One reason for this discrepancy is the assumption made in the calculation of ϕ_b^o (i.e. constant n for all temperature). The ideality factor, n, for Schottky barriers on CdTe is not constant, but a function of temperature. This is discussed in the next chapter.

The above measurements reveal that the evaporation of Sn on the chemically etched surfaces of these materials produce reasonably good Schottky diodes. The forward currents are limited by the bulk resistance of these high resistivity materials, but should improve with low series resistances. This has been achieved with low resistivity CdTe and the results are presented in the following chapter. The slight increase of reverse current with voltage can most probably be attributed to a combination of image force lowering of the barrier, carrier generation within the depletion region and the effect of tunnelling. The variation of reverse characteristics for different diodes can well be due to a surface contamination left by chemicals during the fabrication procedure.

The data obtained from C-V measurements are in good agreement with the results obtained from Hall effect and D.C. conductivity measurements. Some of these results are given in fig (6.12). This shows the band diagram of a Schottky diode deposited on p-type semiconductor (Cr-doped CdTe) with two impurity levels. The energy E_q represents the deep acceptor level in the forbidden gap. The position of these energy levels are shown with the experimental values obtained from D.C. conductivity measurements. The diffusion voltage, V_d, is as determined from the C-V

FIGURE 6·12

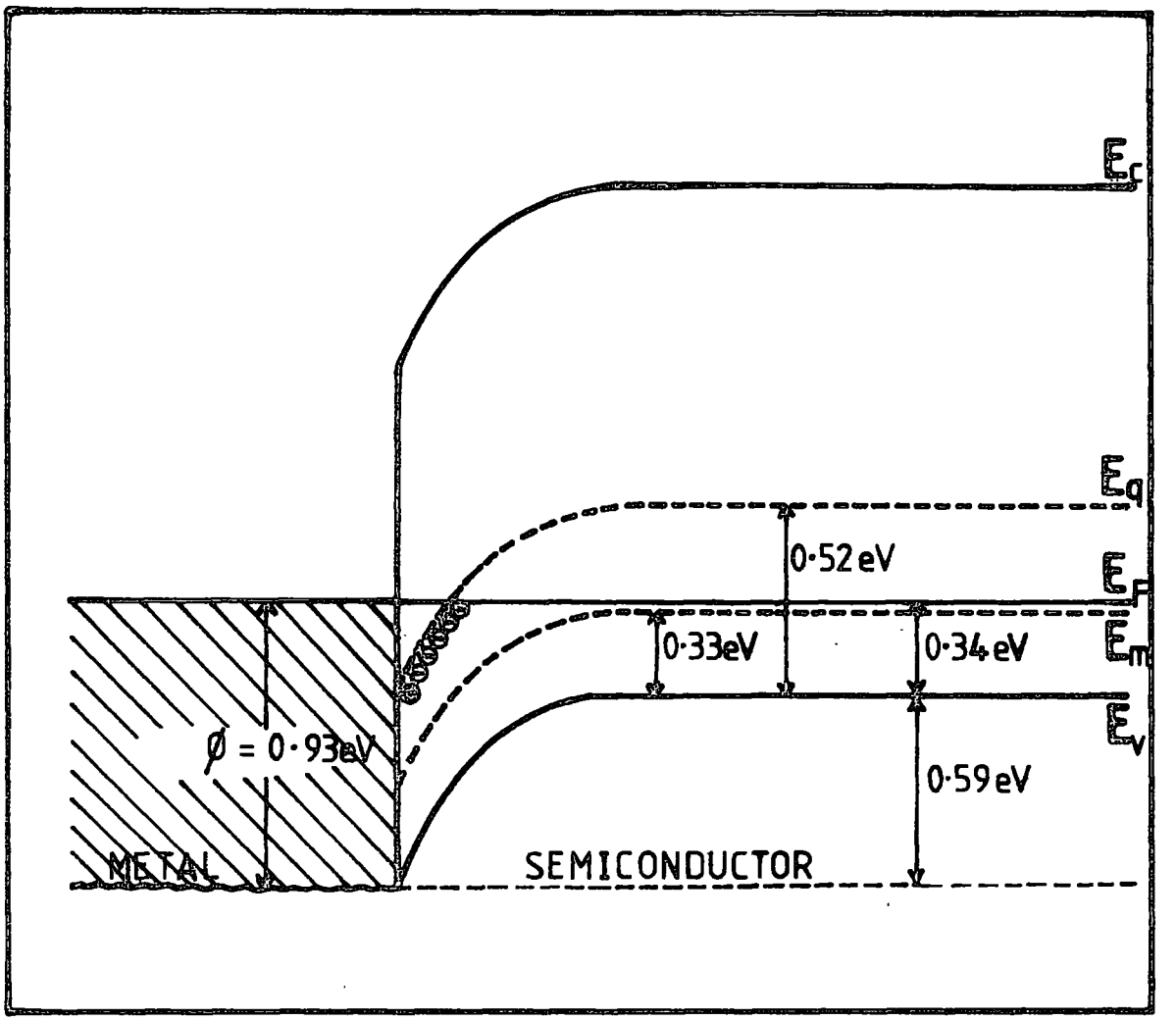

BAND DIAGRAM OF A SCHOTTKY DIODE DEPOSITED ON P-TYPE SEMICONDUCTOR WITH TWO IMPURITY LEVELS.

measurements. In the depletion region the level E_q is below the Fermi-level due to band bending and acts as a shallow acceptor level. Since the level E_q is completely ionized in this region, the value obtained for (N_a-N_d) from C-V measurements should be equal to N_q, the concentration of level E_q. The experimentally observed values for Cr-doped material are $N_q = 1.58 \times 10^{16}$ cm^{-3} and $(N_a-N_d) = 1.65 \times 10^{16}$ cm^{-3}, from two different methods. These two values agree well with the theoretical prediction.

6.5 SUMMARY

The D.C. conductivity data for semi-insulating Cr-doped CdTe single crystals show that this material is non-extrinsic. p-type Ohmic conduction at high temperatures and low fields is controlled by two dominant levels in the forbidden gap. These two levels 0.33 eV and 0.52 eV above the valence band, have concentrations of $(6.3 \pm 0.6) \times 10^{13}$ cm^{-3} and $(1.6 \pm 0.3) \times 10^{16}$ cm^{-3}. respectively. The current-voltage characteristics show that the conduction in this material at low temperatures is possibly due to injected electrons. Well-defined square law regions produce a mobility value of 750 cm^2/V.sec, a reasonable value for electrons in CdTe.

Hall effect measurements show that the material is p-type at high temperatures with Hall mobility $\simeq$ 25.0 cm^2/V.sec. at room temperature. These results are very similar to those of CdTe doped with Au, Cu and Ag. All these materials show p-type conduction with an activation energy of $(0.32 \pm 0.03$ eV). The electrical properties obtained for this material are also similar to those of semi-insulating undoped specimens used in this work.

The data obtained from the Schottky barrier measurements also confirm the above results and Cr-doped material possess similar electrical properties to the undoped specimens studied in this series of experiments.

CHAPTER 7

RESULTS: MS AND MIS BARRIERS ON LOW RESISTIVE CdTe

7.1 INTRODUCTION

In this chapter, the results obtained for barriers fabricated on low resistive CdTe samples are presented. Both undoped and In-doped materials used in this series of experiments were n-type with carrier concentrations in the range $(1.0 \sim 3.0) \times 10^{17}$ cm^{-3}. Sample thicknesses were typically about 1 mm. Schottky barrier devices were fabircated by evaporation of Au on to chemically etched CdTe surfaces as described in Chapter 4. Ohmic contacts were obtained by evaporation of In/Sn alloy. The electrical properties of these Schottky diodes in the dark are presented and discussed in section 2.

The Schottky diodes were tested as solar cells under AM1 conditions, and the results obtained are given in section 3. The short circuit currents of the devices were improved by optimising the barrier electrode thickness and the open circuit voltages by introducing an insulating layer between the metal electrode and the semiconductor. Cadmium stearate and C4 anthracene Langmuir films were used as the insulators in these MIS devices. Important parameters of the MIS devices were measured and compared with those of the MS solar cells. The variation of these parameters as a function of illumination and some preliminary cell degradation measurements are also presented.

7.2 SCHOTTKY BARRIERS

Although Schottky diodes have been prepared using a variety of surface treatments as described in section (4.5), the results described in this chapter are limited to those devices prepared immediately after etching in 1% bromine in methanol solution. This treatment was found to produce the best diode characteristics.

Fig (7.1) shows the dark current-voltage characteristics at room

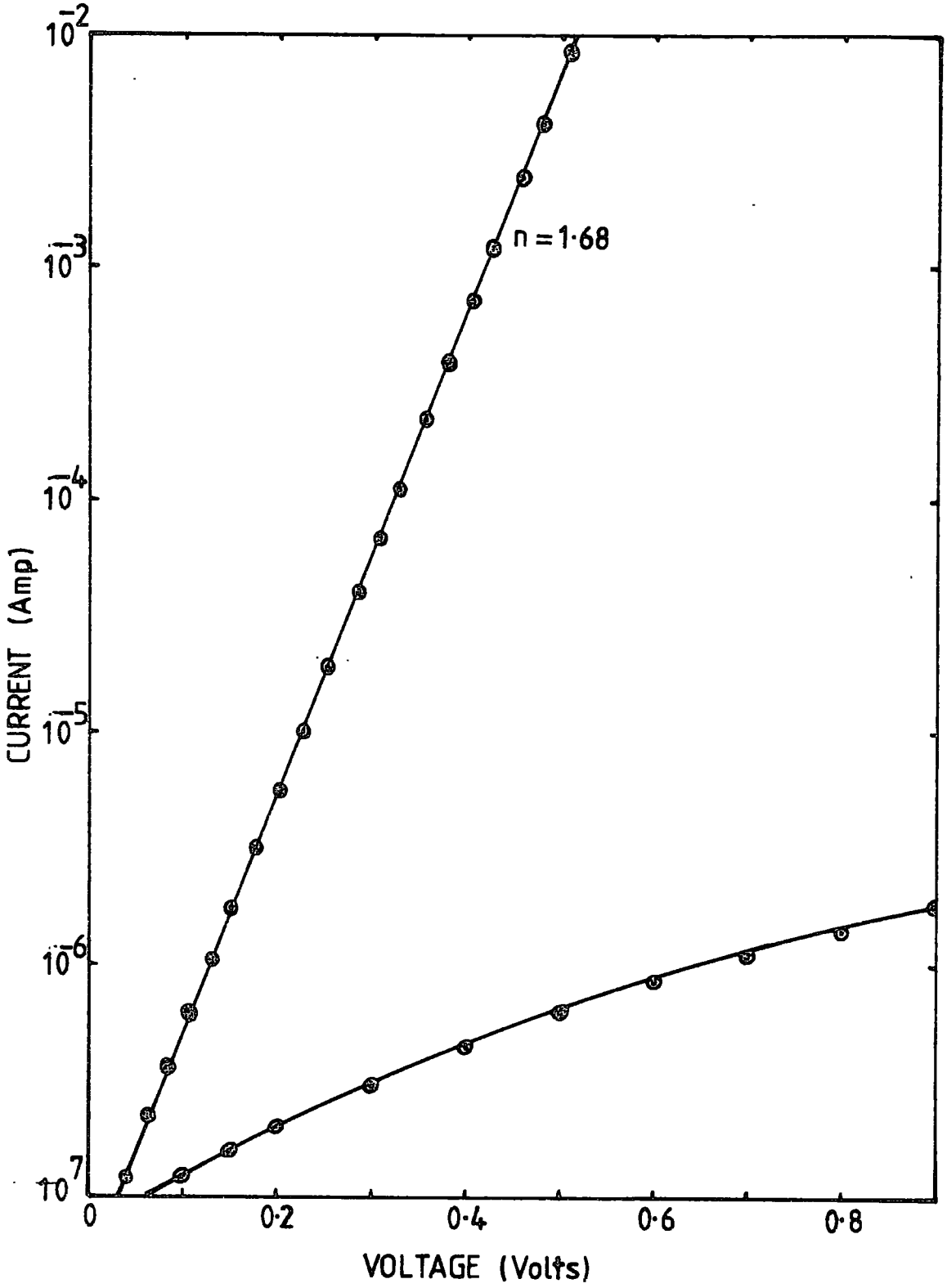

Fig. 7·1 Current-Voltage characteristics in the dark at 293K, for a Au/CdTe Schottky barrier.

temperature for a Schottky diode prepared on an undoped CdTe sample. This device shows a rectification factor of about 5×10^4 when 0.5 V is applied. The forward bias current has a log(I) versus V linear region over approximately 5 orders of magnitude of current. The ideality factor, n, calculated from the slope of this straight line is 1.68 for this particular device. The value of saturation current, I_s, which is obtained by extrapolating the forward I-V plot to zero bias, was used to estimate the barrier height $(\phi_b)_{I-V}$, using equation 3.43. This value was about 0.90 eV at room temperature for this diode.

The shapes of the current-voltage characteristics in reverse bias are very similar to those prepared on p-type materials. The magnitude of the reverse current, however, varies considerably from device to device. The current does not saturate completely, but increases slightly with applied voltage. This can be due to one or more of the reasons described in section (3.1.3).

Capacitance-voltage measurements in reverse bias, at 20 kHz,have been made on this device(Fig 7.7). The $1/C^2$ versus V plot is extremely linear up to ≃ 2 V. This indicates a uniform doping (N_d-N_a) in the material which is obtained from the slope of the straight line plot as $2.0 \times 10^{17} cm^{-3}$. From the intercept on the voltage axis, the diffusion voltage V_d is obtained as 0.83 eV which gives a barrier height of 0.91 eV.

In one series of experiments the surface barriers were prepared on the same specimen with the same surface treatment. Even though the fabrication procedure was identical for all the devices, the electrical properties were found to vary from device to device. For example, the ideality factor of these diodes varied over a range from 1.01 to 1.90. Most of the devices prepared on chemically etched surfaces showed non-ideal behaviour with the higher values of n (n> 1.2). However, as a result of repeated etching in fresh bromine in methanol, well polished surfaces were obtained and diodes

with low ideality factors (n< 1.2) were produced. A current-voltage curve for a one such diode is shown by the curve (a) in fig (7.10). The experimentally observed parameters for this device are given in table (7.1) together with those of a device with a much higher ideality factor.

Table 7.1

Various parameters of two different S/barriers prepared on undoped CdTe.

Diode	n	$(\phi_b)_{I-V}$ (eV)	$(\phi_b)_{C-V}$ (eV)	(N_d-N_a) cm^{-3}
non-ideal	1.68	0.71	0.90	2.0×10^{17}
near-ideal	1.01	0.71	0.70	2.3×10^{17}

In the case of the diode with the low n factor, the excellent agreement of barrier heights obtained from two different techniques suggest that this device is nearly "ideal". For non-ideal devices, this agreement cannot be observed.

The variation of the n factor might be due to modification of majority-carrier transport over the barrier in the presence of (a) surface states (b) an oxide layer or (c) other surface contamination. The etching procedure using freshly prepared bromine in methanol may either reduce the concentration of surface states or remove surface contamination and, therefore, produce diodes with low n values. It was found that the bromine in methanol solution, even a few hours old, causes an increase in the value of n. This was confirmed by etching away a near-ideal diode by old bromine in methanol and producing a new diode with a higher n value. If the same procedure was followed with fresh bromine methanol a near-ideal diode was obtained again. Therefore, to obtain these near-ideal diodes, two procedures must be followed. The samples should be well polished (chemically

rather than mechanically) and the 1% bromine in methanol etch should be freshly prepared.

The Schottky diodes were also prepared on an In-doped CdTe specimen using the same procedure. Fig (7.2) shows the I-V characteristics of one such diode. This particular device shows a rectification factor of $\simeq 5.0 \times 10^5$ when 0.5 V is applied. The forward current has a log(I) versus V, linear region over six orders of magnitude of current and the ideality factor calculated from the slope is $\simeq 1.17$. The barrier heights obtained from two different methods are $(\phi_b)_{I-V} = 0.77$ eV and $(\phi_b)_{C-V} = 0.82$ eV; slightly different due to the deviation from ideal behaviour. The C-V measurement yields a value of 1.3×10^{17} cm^{-3} for the free carrier concentration.

The diodes on In-doped CdTe often possessed fairly low ideality factors. In general these devices showed better diode characteristics than those prepared on undoped material. This improvement could either be due to good quality of the crystal or the different value of carrier concentration. The properties of these diodes, however, also depends on the surface preparation. As an example, curve (a) in fig (7.13) shows the I-V characteristics of another diode fabricated later on the same CdTe substrate as used for the device shown in fig (7.2). The saturation current of this device has increased by a factor of about 30. The value of n has also increased.

The near-ideal diodes with $n \simeq 1.01$ (only observed on undoped CdTe), can be explained quantitatively by thermionic-emission theory. To understand the transport mechanisms involved in non-ideal diodes, the electrical properties were studied at different temperatures.

A typical set of the forward current-voltage characteristics for the non-ideal Schottky diode at different temperatures is shown in fig(7.3). The logarithm of the current is a linear function of the applied bias at

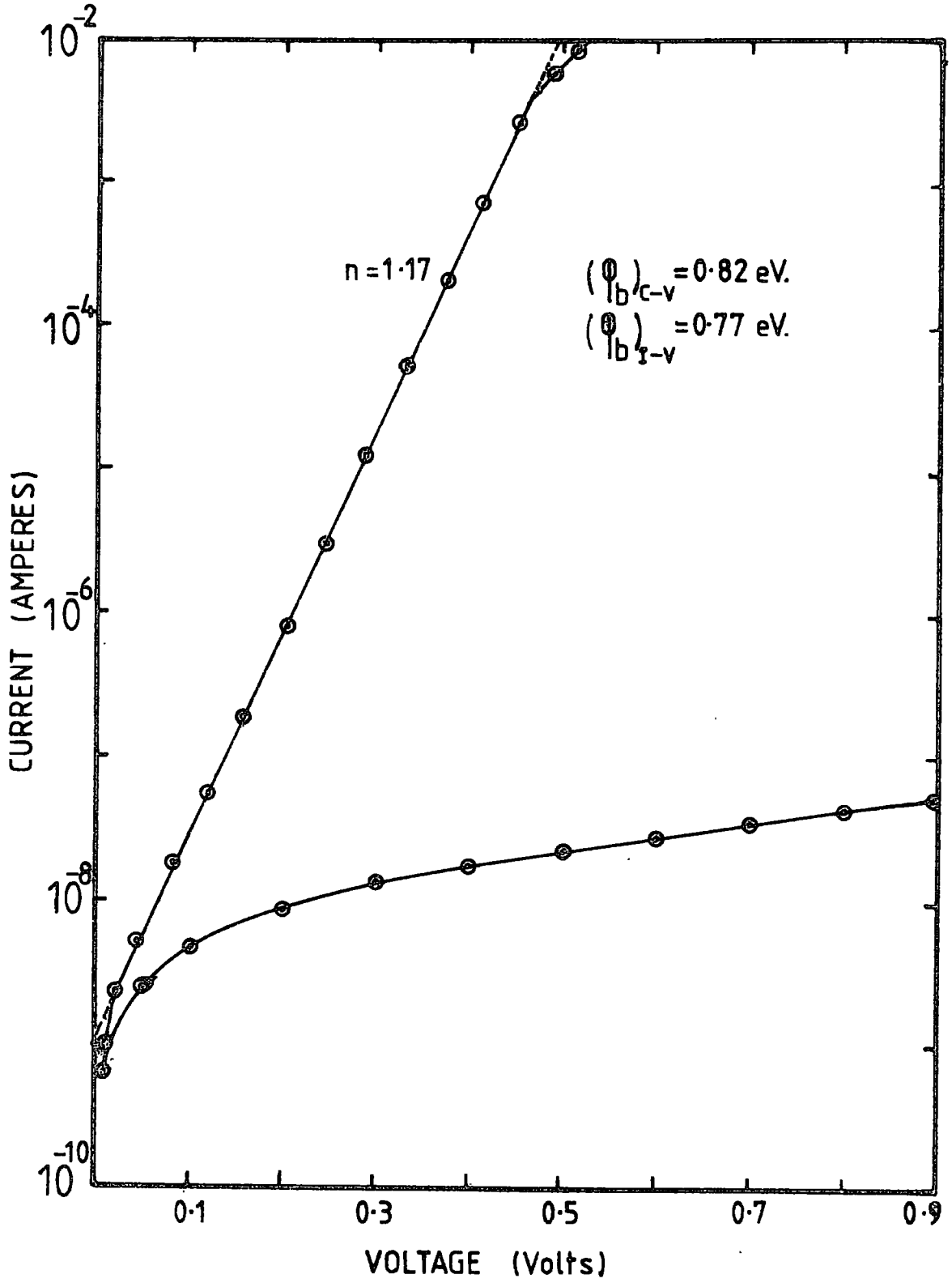

FIG. 7·2 FORWARD AND REVERSE CURRENT – VOLTAGE CHARACTERISTICS OF Au-(n-type)CdTe:In SCHOTTKY BARRIER.

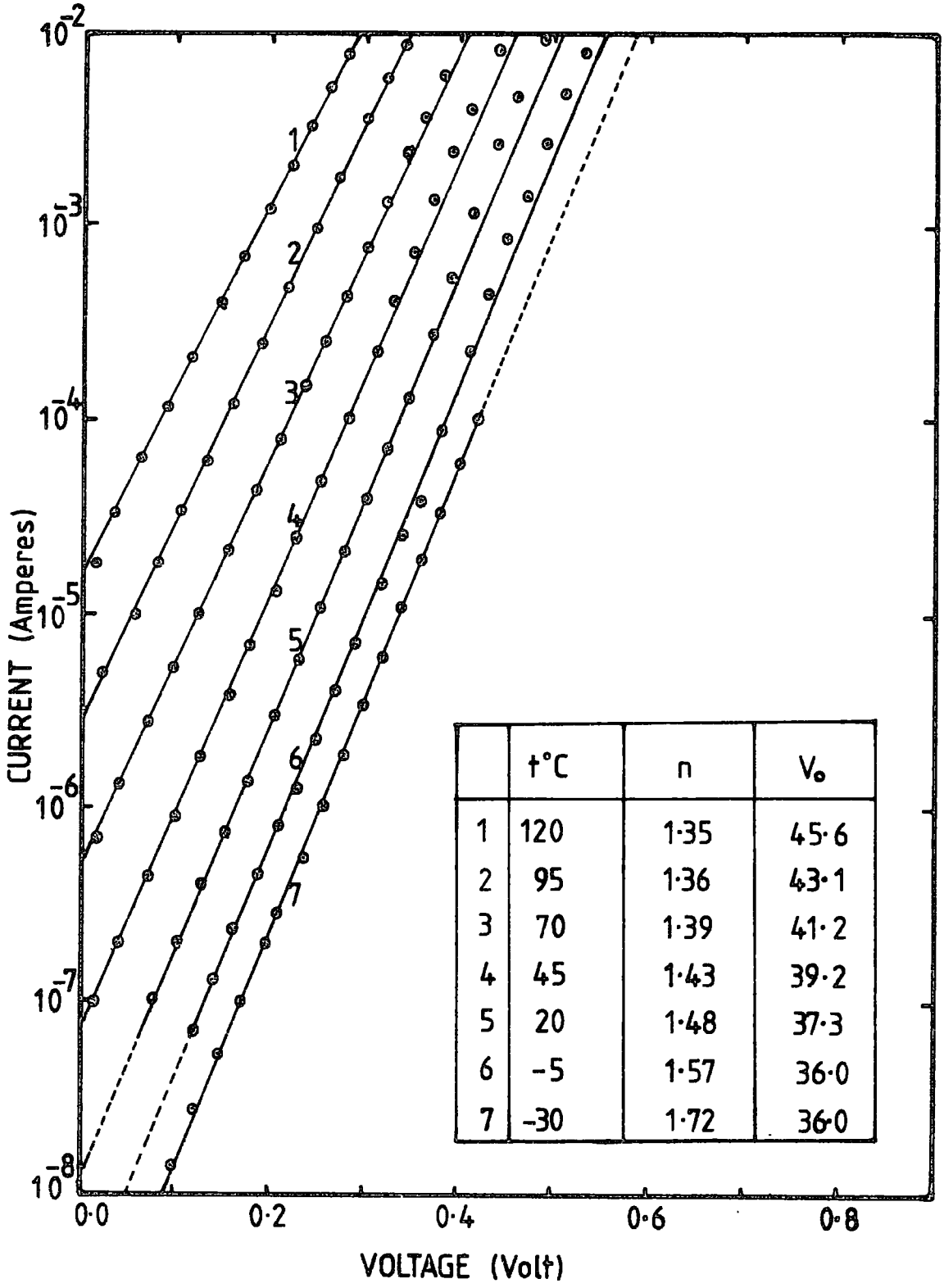

	t°C	n	V_o
1	120	1·35	45·6
2	95	1·36	43·1
3	70	1·39	41·2
4	45	1·43	39·2
5	20	1·48	37·3
6	-5	1·57	36·0
7	-30	1·72	36·0

FIG. 7·3 FORWARD I-V CHARACTERISTICS OF Au/CdTe SCHOTTKY DIODE AT SEVERAL TEMPERATURES.

all temperatures, but it deviates slightly from a linear dependence in the high bias region. Some of the devices show a saturation (fig 7.2) due to the effect of series resistance introduced in the bulk of the material and the Ohmic contact. Some diodes, however, show an increase in forward current (fig 7.3) in the high bias region. This is more prominent at low temperatures and is probably caused by thermionic-field emission. Since these diodes did not have guard rings, high electric fields are present at the edges of the diodes causing some thermionic-field-emission to occur.

From the current-voltage plots at various temperatures the values of V_o, the gradients of log (I) versus V (section 3.1.4), were determined. The temperature range studied here was -30° C to $+ 130^{\circ}$ C. Fig (7.4) shows the V_o versus $\frac{kT}{q}$ data for two such diodes as described in section (3.1.4). Curve (A) was obtained from the I-V plots shown in fig (7.3) and curve (B) represents data for a similar diode. In comparing these data with those in fig (3.4), it is observed that the data could be fitted with a straight line labelled as 3 in figure (3.4). The excess temperatures calculated from the intercepts of the two graphs were 136 K and 90 K. The variation of ideality factors with temperature for both diodes are shown in fig (7.5). V_o data at low temperatures deviate from the straight line, and lie between the two curves labelled as 3 and 4 in fig.(3.4). The similarity of the experimental curves, A and B in fig (7.4) with curve 4 in fig (3.4) shows that there is a possible contribution from thermionic-field emission to the forward current at low temperatures.

Similar experimental results have been reported by Saxena (1969) [1] on two commercially available diodes (HP-2900 and FH-1100) and on four different Schottky barriers on silicon. All diodes without guard rings showed the low temperature deviation. Diodes with guard-rings showed no deviation at low temperatures and a line drawn parallel to the unity slope

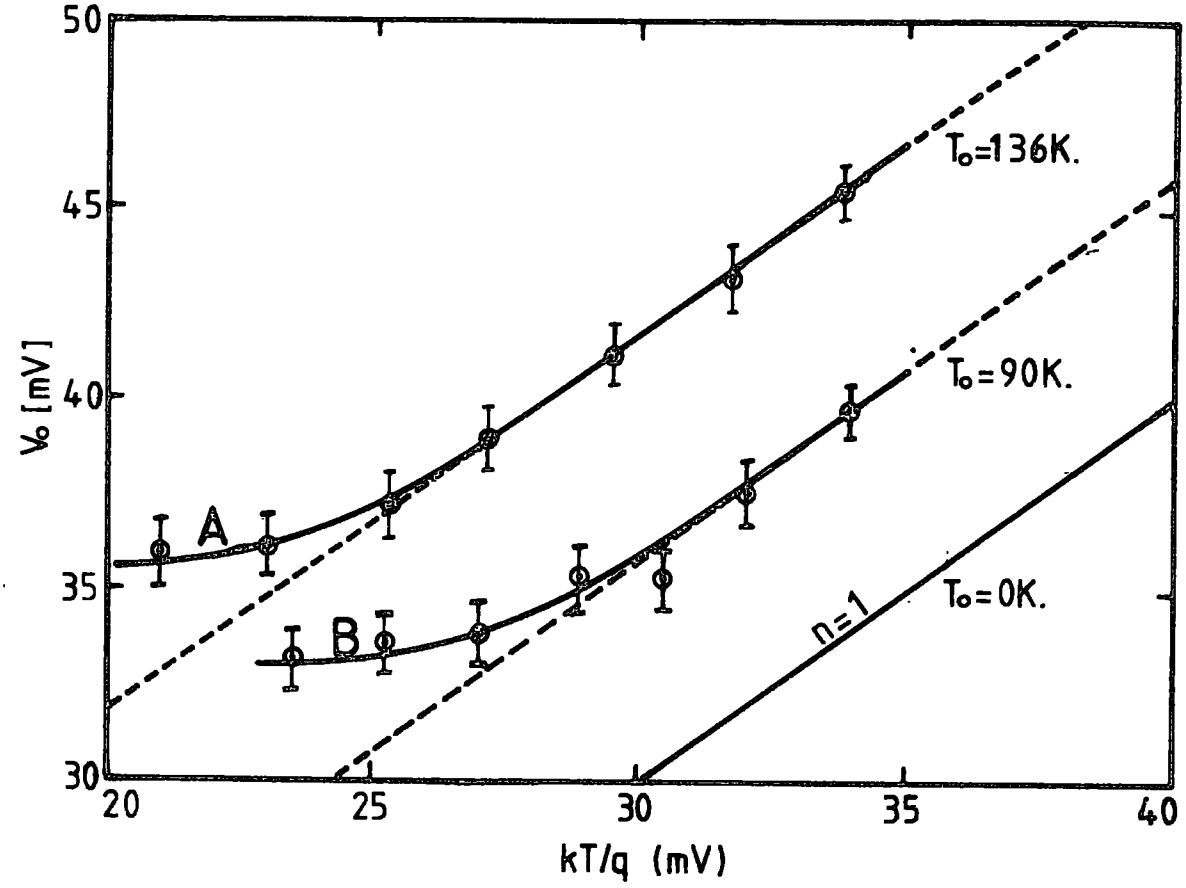

FIG.7·4 PLOT OF V_o VERSUS [kT/q] FOR TWO Au-CdTe S/B DIODES.

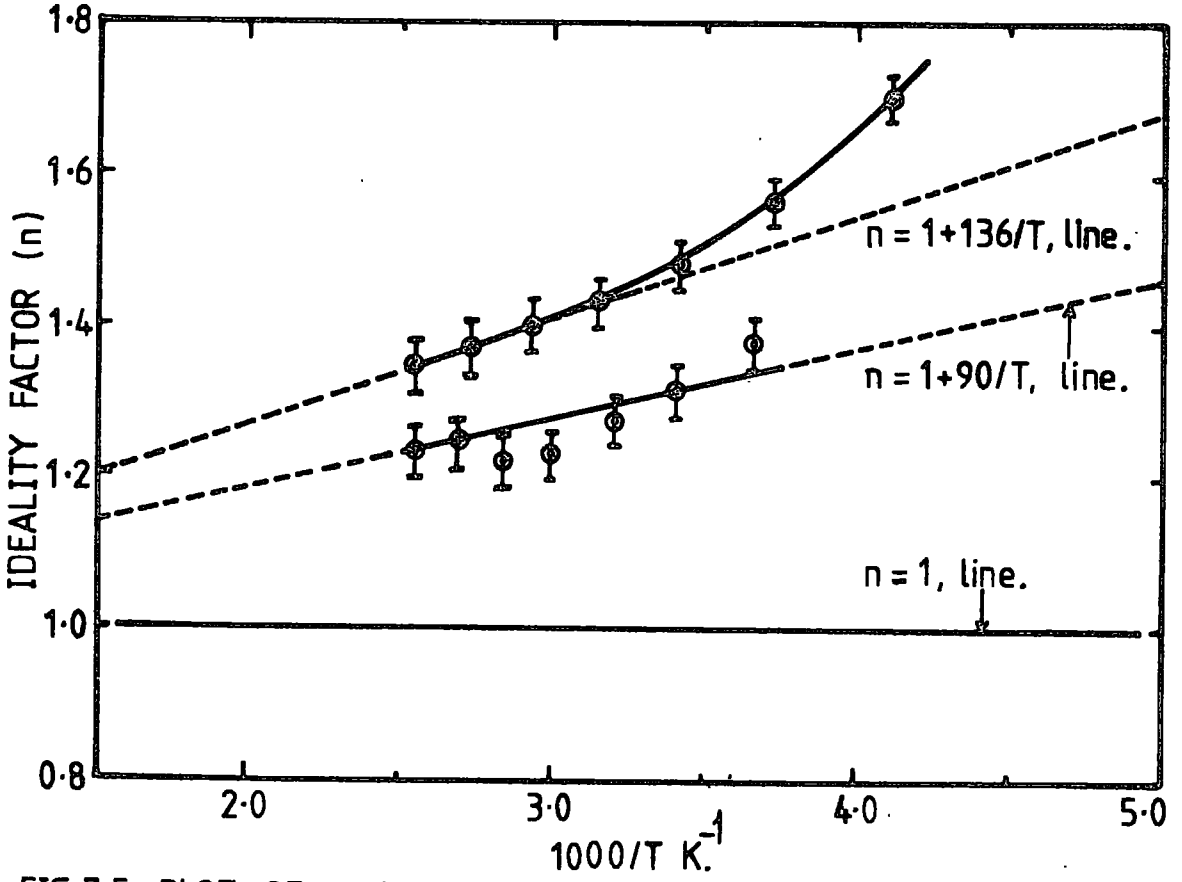

FIG.7·5 PLOT OF n VERSUS 1000/T FOR THE SAME DIODES.

line fitted the data nicely. These data show that if the high electric fields from the edge of the Schottky barrier diodes are eliminated by using a guard ring or a mesa structure, the I-V behaviour of the Schottky barrier is described quite well by equation (3.36) with parameter T_o.

As discussed in Chapter 3, the variation of saturation current with temperature can be used to evaluate the barrier height of these Schottky diodes. If the ideal Schottky theory were to hold, then curves of I_s/T^2 versus 1/T would be straight lines whose slope is related to ϕ_{bo}, the barrier height at absolute zero. However, if the ideal Schottky theory does not hold, and if an equation of the type (3.36) containing an excess temperature in the exponent holds, then I_s/T^2 versus $1/(T+ T_o)$ plots will yield straight lines.

A set of saturation currents for different temperatures were obtained from the intercepts of log(I) versus V plots shown in fig (7.3). The two plots of I_s/T^2 versus 1/T and $1/(T + T_o)$ are shown in fig (7.6), for comparison. It is clear that the data plotted versus 1/T cannot be fitted with a straight line. The activation energy obtained from the high temperature region is 0.70 eV, which is less than the barrier height at room temperature. If the same data are plotted versus $1/(T + T_o)$, it is found that they can be fitted into a better straight line. This shows that the saturation characteristics of these diodes are described well by

$$I_s = A^*T^2 \cdot e^{-\phi_{bo}/k(T + T_o)}$$

The temperature independent part of the barrier height, ϕ_{bo}, calculated from the slope of the straight line is $\simeq$ 1.30 eV for this particular diode. This experimental evidence confirms again that the current-voltage characteristics of these diodes are described reasonably well by the equation (3.36).

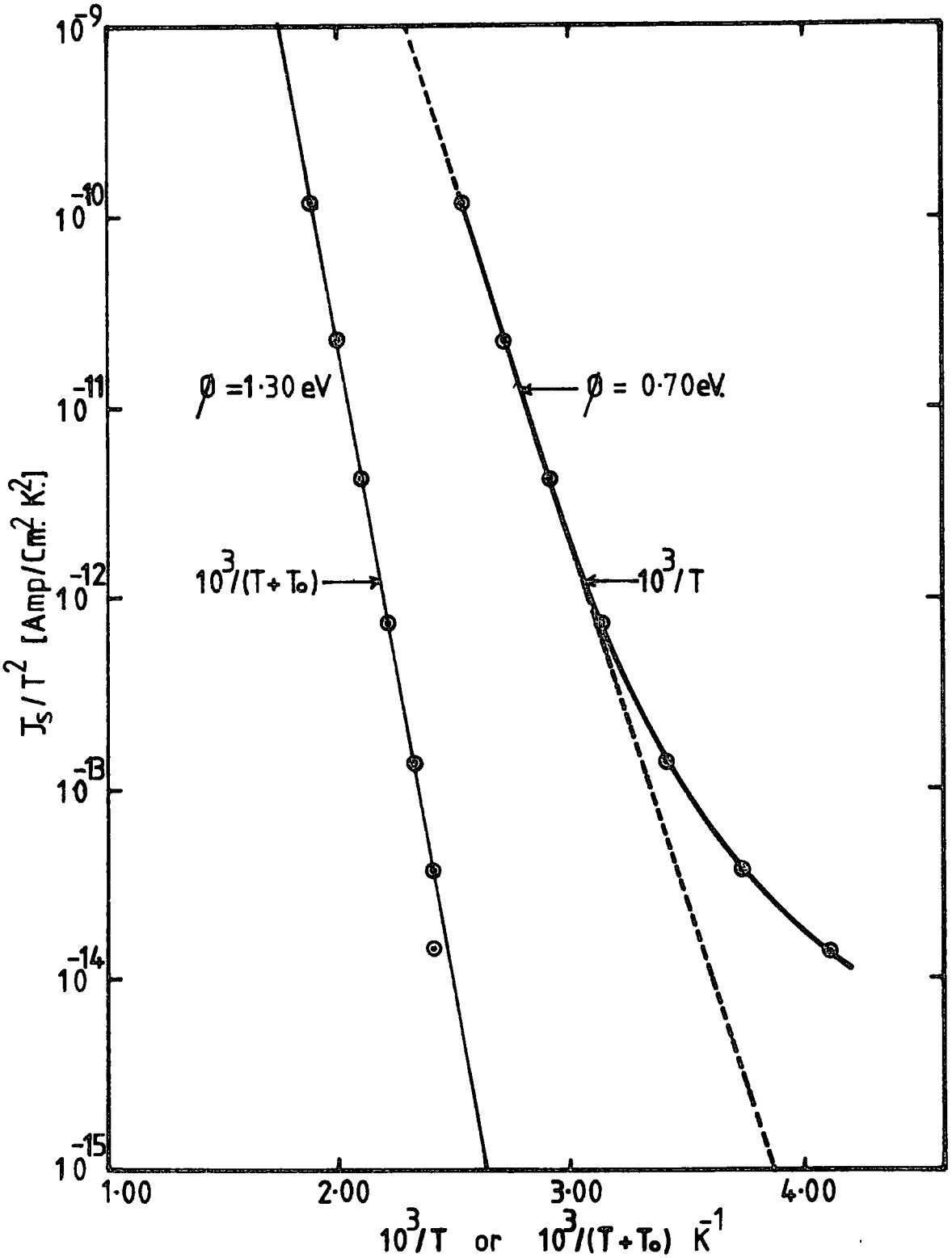

Fig. 7·6 Plot of J_s/T Vs $1000/(T+T_o)$ and Vs $1000/T$ for Au/CdTe Schottky barriers.

The variation of the barrier height with temperature has been studied using the capacitance-volage method described in section (3.1.5). The plots of $1/C^2$ against reverse voltage for the same diode at different temperatures are shown in fig (7.7). The experimentally determined values of V_d which are displayed in fig (7.8) show clearly that the barrier height decreases with increasing T. The temperature coefficient of the barrier height, $(\partial\phi_b/\partial T) \simeq (\partial V_d/\partial T)$, is calculated to be about -5.5×10^{-4} eV/K. The reported value of the variation of the optical bandgap of CdTe is -3.0×10^{-4} eV/K[2], hence $(\partial\phi_b/\partial T)$ is the same order of magnitude. Assuming the temperature dependence of the barrier height given by equation (3.44),

$$\phi_b = \phi_{bo} - \alpha T,$$

the value of ϕ_b at room temperature was calculated to be about 1.13 eV, using the value of ϕ_{bo} = 1.30 eV.

Several authors[3,4,5] have reported similar Schottky barrier work on CdTe. The results reported by Takebe et al[3] show that the diodes prepared on vacuum cleaved surfaces are close to the ideal situation (n ≈1.01), but those prepared on air cleaved and chemically etched surfaces possessed non-ideal behaviour with n ≈1.08 and 1.20 respectively. This clearly shows that the defects introduced by surface oxidation or by surface contamination during chemical etching can yield non-ideal Schottky barriers. The near-ideal diodes obtained in this work possess similar electrical properties to those prepared on vacuum cleaved surfaces. Schottky barrier results with various barrier metals reported by Ponpon et al[6] indicate the strong influence of surface states on the barrier heights. They have shown that the relation between the barrier height (ϕ_b) and the metal work function (ϕ_m) deviates from the simple Schottky theory, which gives the relation $\phi_b = \phi_m - 4.28$, for cadmium telluride[6]. Levine has explained

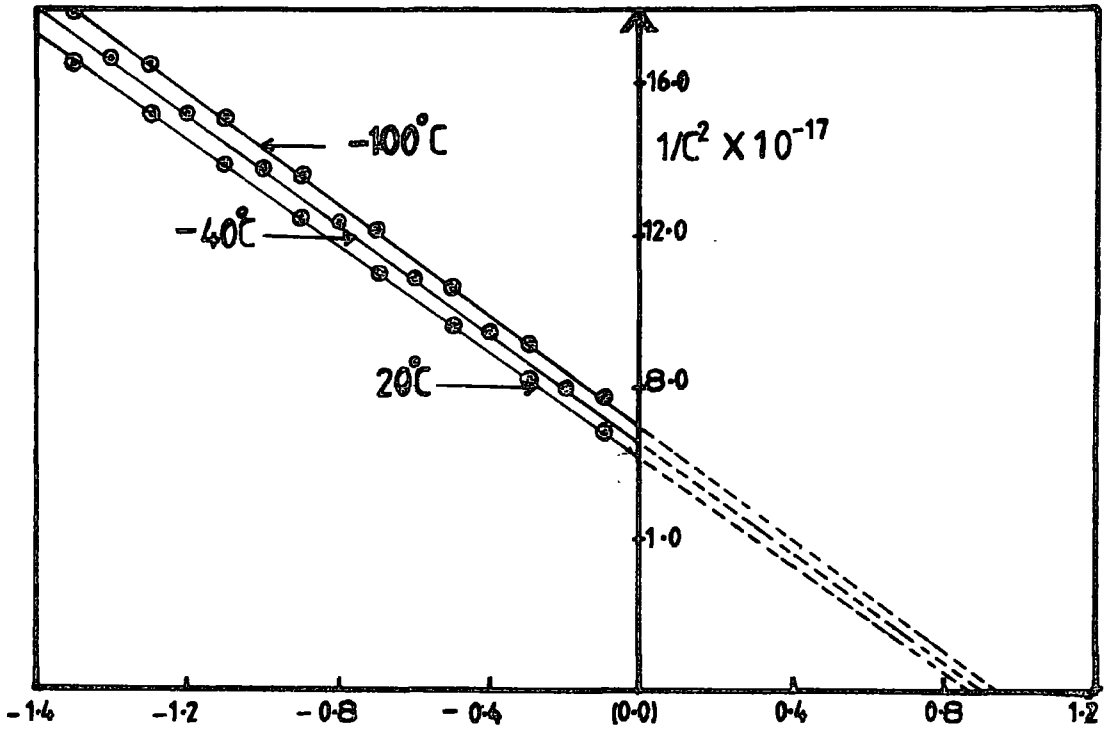

FIG. 7·7 CAPACITANCE – VOLTAGE CHARACTERISTICS OF AU/CdTe SCHOTTKY DIODES AT THREE DIFFERENT TEMPERATURES.

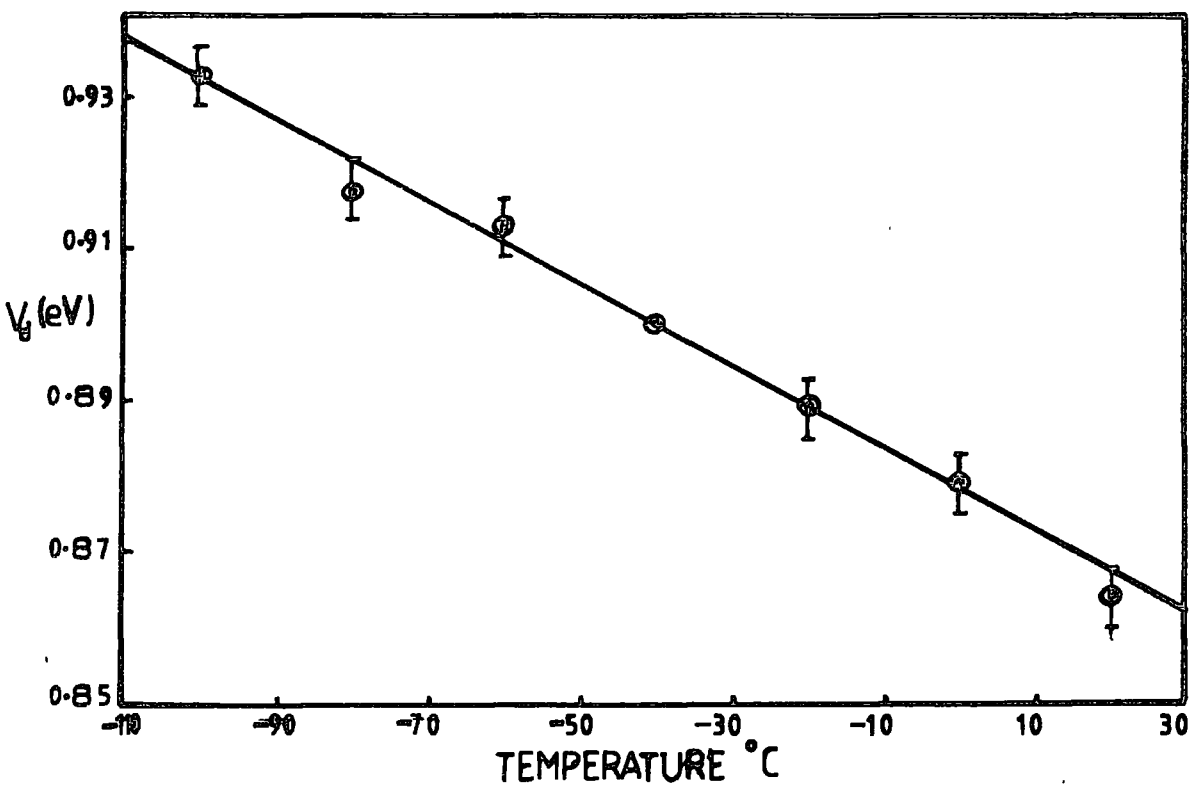

FIG. 7·8 TEMPERATURE DEPENDANCE OF THE DIFFUSION VOLTAGE DETERMINED USING THE CAPACITANCE TECHNIQUE.

Schottky barrier anomalies in terms of an effective exponential energy density of interface states. This author has also explained the appearance of T_o, an important empirical constant in the current-voltage relationship. The physical significance of the T_o anomalies in Schottky-barriers are discussed in detail by Crowell[8].

7.3 MS AND MIS SOLAR CELLS

Cadmium telluride possesses most of the necessary properties required for a good photovoltaic solar cell material. This has been discussed in Chapter 1. Since this material also shows both n- and p-type conduction, it may easily be incorporated into any efficient collector junction. Such collector structures could be p-n junctions, heterojunctions, metal-semiconductor barriers or MIS structures. Different techniques have been used to prepare p-n junction and heterojunction solar cells with CdTe by various authors[9,11]. The conversion efficiencies of these structures vary considerably and the reported maximum value is about 10.5%[11,12].

Although many papers deal with metal-CdTe structures, very few of such structures have been tested as solar cells. Au/CdTe Schottky barrier solar cells have been studied by two authors[13,14] and the reported conversion efficiencies were around 1.5% under AMO conditions. No reports of MIS studies on CdTe have been found in the literature. This is probably due to the lack of a suitable insulator for this material. However, recent reports[15,16] on MIS structures with CdTe have demonstrated the successful deposition of novel Langmuir films on to CdTe surfaces. These insulating films were therefore used to fabricate MIS structures. Both MS and MIS diodes were studied in view of their potential application in solar cells. The following sections describe and compare the solar cell parameters obtained for these two different kinds of devices.

(a) MS Solar Cells

The Schottky barrier diodes described in the earlier section of this chapter, were tested as solar cells under AM1 conditions. The open-

circuit-voltage of the devices varied over a range from 150 mV-400 mV. This value was very sensitive to the surface preparation. The short circuit current also varied from device to device, depending on the barrier electrode thickness. The best performance was obtained for the Schottky diode, whose dark I-V characteristics are shown in fig (7.2). The current-voltage characteristics in the dark and under illumination are presented in fig (7.9) for this particular diode with a barrier electrode thickness of $\simeq$ 100 Å. The OCV, SCC density and fill factor of this cell were 380 mV, 11.5 mA/cm^2 and 0.68 respectively. The conversion efficiency of this cell was calculated to be about 3.0%.

(b) MIS Solar Cells

The main disadvantage of the Schottky barrier solar cells is their low value of open-circuit-voltage. To improve this value, MIS structures were fabricated using $CdSt_2$ and C4 anthracene Langmuir films as described in chapter 4. Both MS and MIS devices were prepared on the same surface with the same barrier electrode thickness. This procedure provided similar surface effects and equal light transmission through the electrodes for both devices. A direct comparison of MS and MIS structures could therefore be made.

The forward and reverse current-voltage characteristics for three different types of CdTe solar cells, measured in the dark at room temperature, are shown in fig (7.10). The curves (a), (b) and (c) show the I-V curves of the Schottky barrier, and MIS structures with one ($\simeq$ 25 Å) and three ($\simeq$ 75 Å) layers of $CdSt_2$ Langmuir films respectively. The current through the MIS devices seem to follow an exponential relationship of the form given by equation (3.49),

$$J = A^*T^2 . \exp(-\chi^{\frac{1}{2}}.d) . \exp(-q\phi_b/kT) \left[\exp(qV/nkT) - 1 \right]$$

The dark current, due to majority carriers, in the MIS devices has been reduced due to the mean barrier height ($\chi^{\frac{1}{2}}.d$) introduced by the

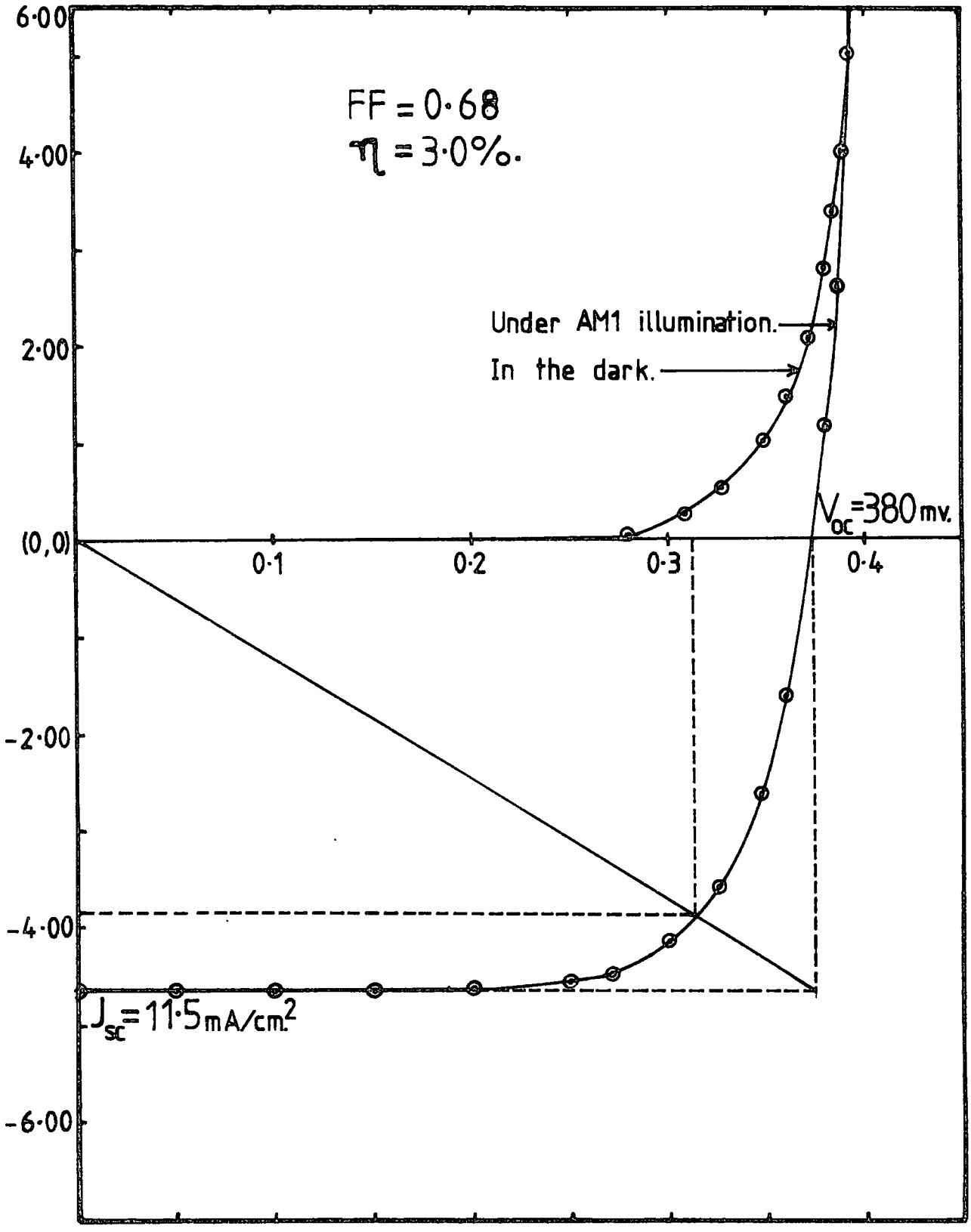

FIG. 7·9 CURRENT-VOLTAGE CHARACTERISTICS OF A S/B SOLAR CELL PREPARED ON IN-DOPED CdTe (n-type).

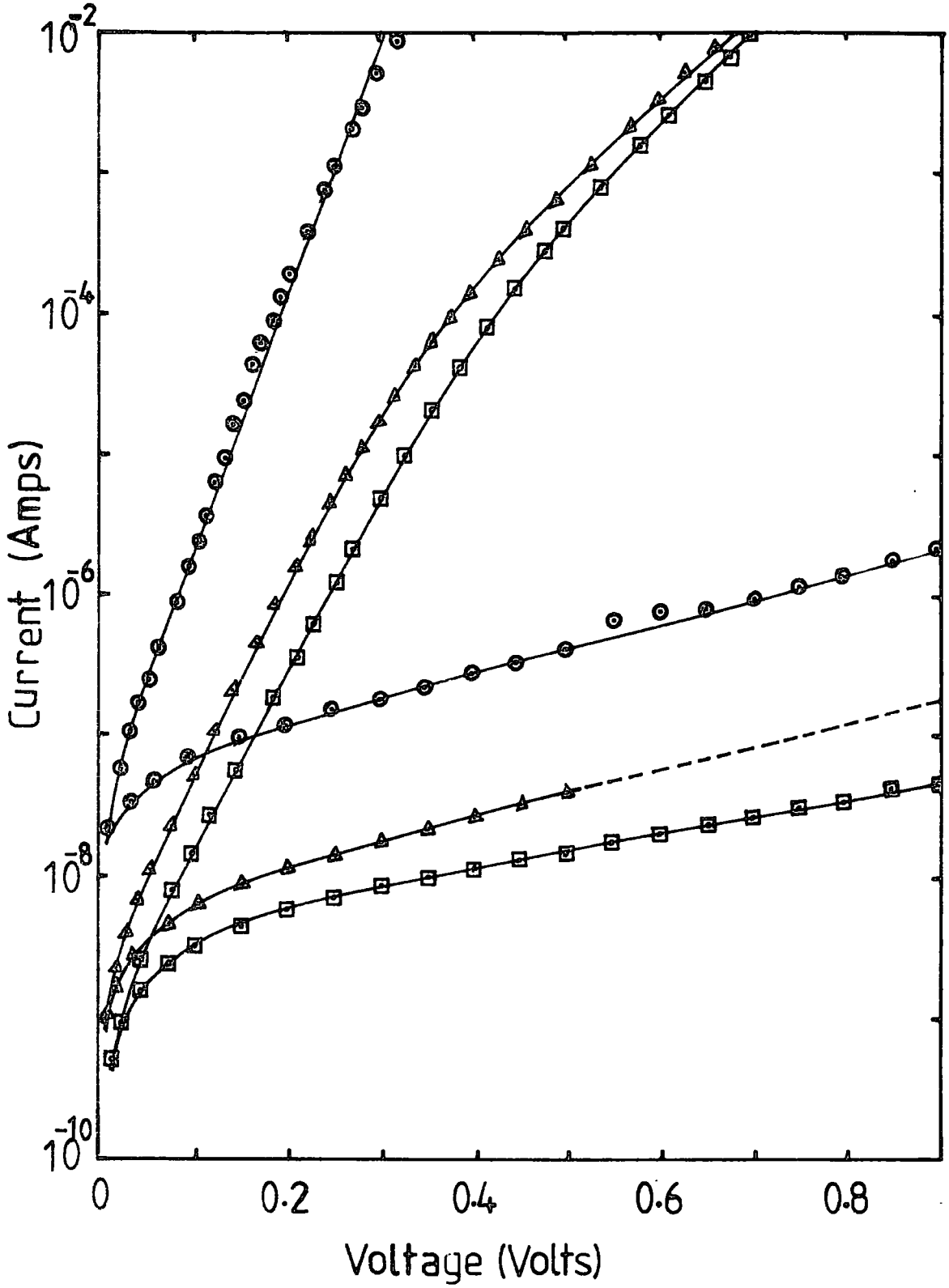

Fig. 7·10 Forward and reverse current-voltage characteristics for three different CdTe solar cells measured in the dark at room temperature.

⊙ Au/CdTe Schottky-barrier solar cell.

△ m.i.s. solar cell with 1 monolayer of cadmium stearate.

⊡ m.i.s. solar cell with 3 monolayers of cadmium stearate.

insulating layer. A finite series resistance is noticed in the MIS devices at higher current levels which is caused by the insulating layer. Saturation currents in MIS devices are about one order of magnitude lower than that in the MS diode. The ideality factor, n, also increases with the insulating film thickness according to the theoretical relation given by equation (3.50).

The reverse bias capacitance-voltage measurements are presented in fig (7.11) for these three devices. The $1/C^2$ versus V plots are linear, and the barrier heights were obtained from the intercepts of these straight lines on the voltage axis. Experimentally determined parameters for the above 3 different devices are summarized in table (7.2). These values show the increase of the barrier heights with the thickness of the insulating layer. The plots in fig (7.11) show also the decrease of capacitance of whole structure with the introduction of insulating film. Although the plots are linear for MIS structures the slope increases with the film thickness. In these MIS structures a part of the applied voltage is dropped across the insulating layer and hence these plots cannot be used to calculate the doping concentration of the semiconductor. The state of surface charges can be different from that of a Schottky barrier in the presence of an insulating layer. Various authors[17,18,19] have discussed in detail the effects of surface states and interfacial layers on the capacitance-voltage relationship in Schottky barriers.

Fig (7.12) shows the photovoltaic characteristics under AM1 conditions for the same devices. By the use of a Langmuir film at the interface the OCV is increased by ≈50% for the device with one layer and 65% for the device with 3 layers. The latter,however, has a very low value of short-circuit current due to high resistance introduced by the thick insulating layer. The most attractive feature of the device with one Langmuir film is that the increase of OCV is achieved without degrading the SCC. This indicates that the one layer of $CdSt_2$ (≈ 25 Å) is definitely of tunnellable thickness. The value of the fill-factor decreases slightly for

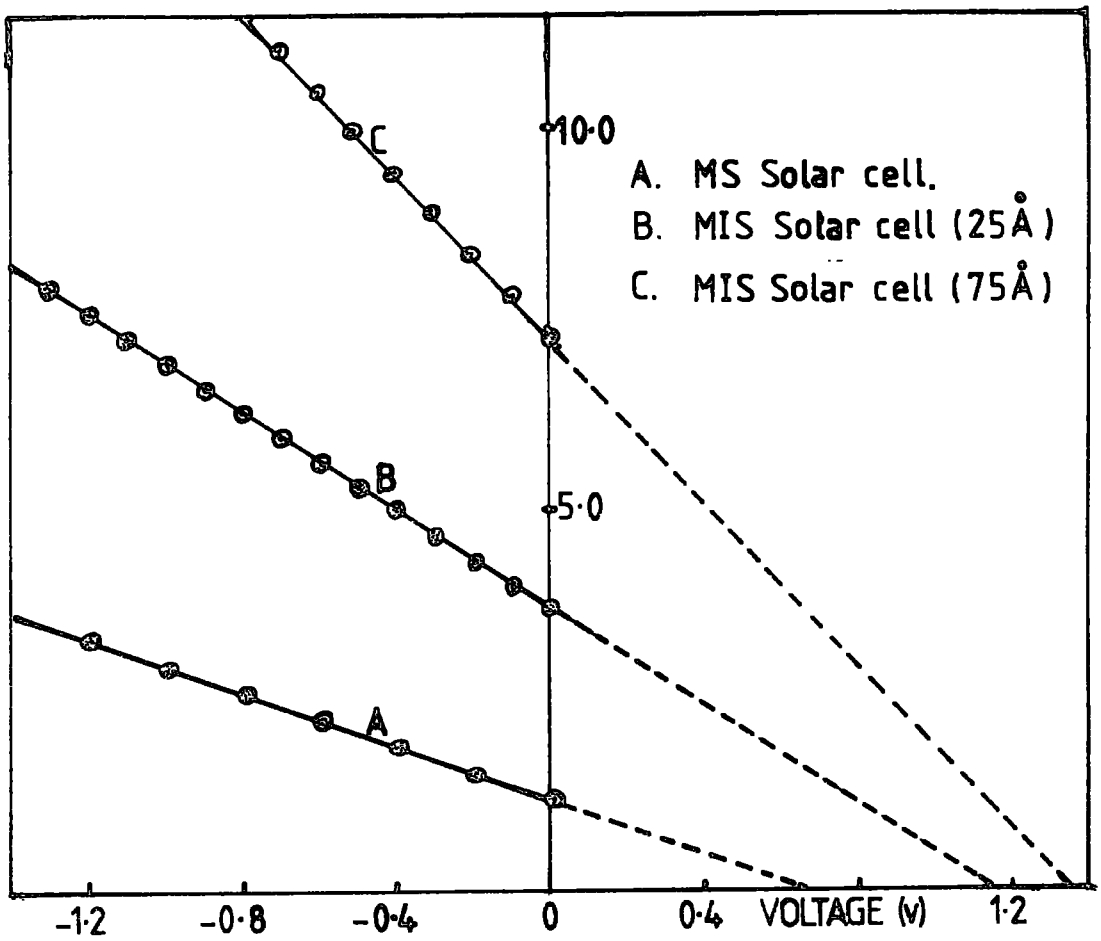

Fig.7·11.1/C^2 vs V plots for 3 different kinds of devices.

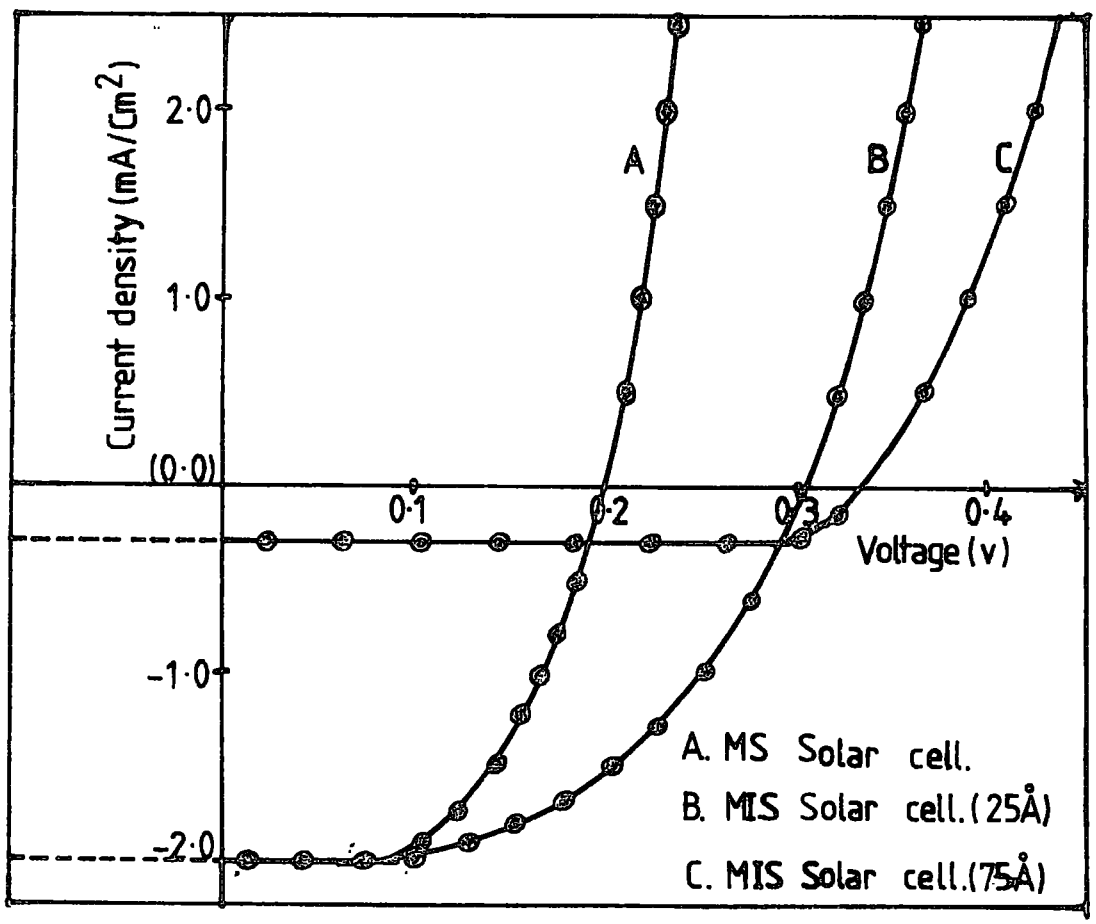

Fig. 7·12. I-V Characteristics under AM1 illumination.

the MIS devices with Langmuir films. The solar cell parameters obtained from the photovoltaic characteristics of fig (7.12) are also summarized in table (7.2). This compares the data for MS and MIS devices with different thickness of insulator.

Table 7.2

Electrical properties of CdTe/Langmuir film MIS solar cells

No. of Lang.films	n	$(\phi_b)_{I-V}$ eV.	$(\phi_b)_{C-V}$,eV	V_{oc}(mV)	J_{sc}(mA/cm^2)	FF	η%
0	1.01	0.71	0.70	200	2.0	0.6	0.24
1	1.22	-	1.13	305	2.0	0.5	0.30
3	1.33	-	1.37	330	0.3	-	-

By incorporating one monolayer of a $CdSt_2$ Langmuir film at the interface between the metal and the semiconductor, an overall improvement of the conversion efficiency by about 25% is obtained. The table (7.2) shows that the absolute values of η for these cells are very low. This can be attributed to the very low transmission of radiation through the thick (200 Å) barrier electrodes used in these devices. The transmission of light through the front barrier metal can be increased by reducing the film thickness at the expense of increasing the series resistance of the cell. To investigate this possibility a series of MS solar cells were fabricated with different barrier electrode thicknesses. The observed results are given in table (7.3).

Table 7.3

Variation of SCC with barrier electrode thickness

Sample thickness (μ_m)	Electrode thickness (Å)	n	V_{oc} (mV)	J_{sc} (mA/cm^2)
1200	200	1.01	225	2.0
900	80	1.71	330	4.8
400	50	1.52	310	7.6
350	40	1.72	330	4.0

It can be seen that the SCC increases with decreasing electrode thickness down to a thickness of 50 Å, after which J_{sc} decreases. The reduction of sample thickness also reduces the series resistance of the cell and hence the improvement in SCC. However, at very low barrier electrode thicknesses (40 Å), the sheet resistance becomes more important and the resultant J_{sc} decreases. A series resistance of even 5 Ω can substantially reduce the fill factor[20] and hence lower the conversion efficiency.

To improve the solar cell parameters discussed above, MIS structures were prepared on In-doped CdTe specimens with one layer of $CdSt_2$ and a Au-barrier electrode thickness of 80 Å. The results obtained are presented in figures (7.13) and (7.14). The important parameters obtained from these characteristics are summarized in table (7.4).

Table 7.4

Electrical properties of solar cells prepared on In-doped CdTe

No.of Lang.films	n	$(\phi_b)_{I-V}$ .eV	$(\phi_b)_{C-V}$ .eV	J_{sc} (mA/cm^2)	V_{oc} (mV)	FF	η%
0	1.55	0.71	0.77	12.0	325	0.61	2.38
1	1.73	-	1.20	11.5	550	0.50	3.16

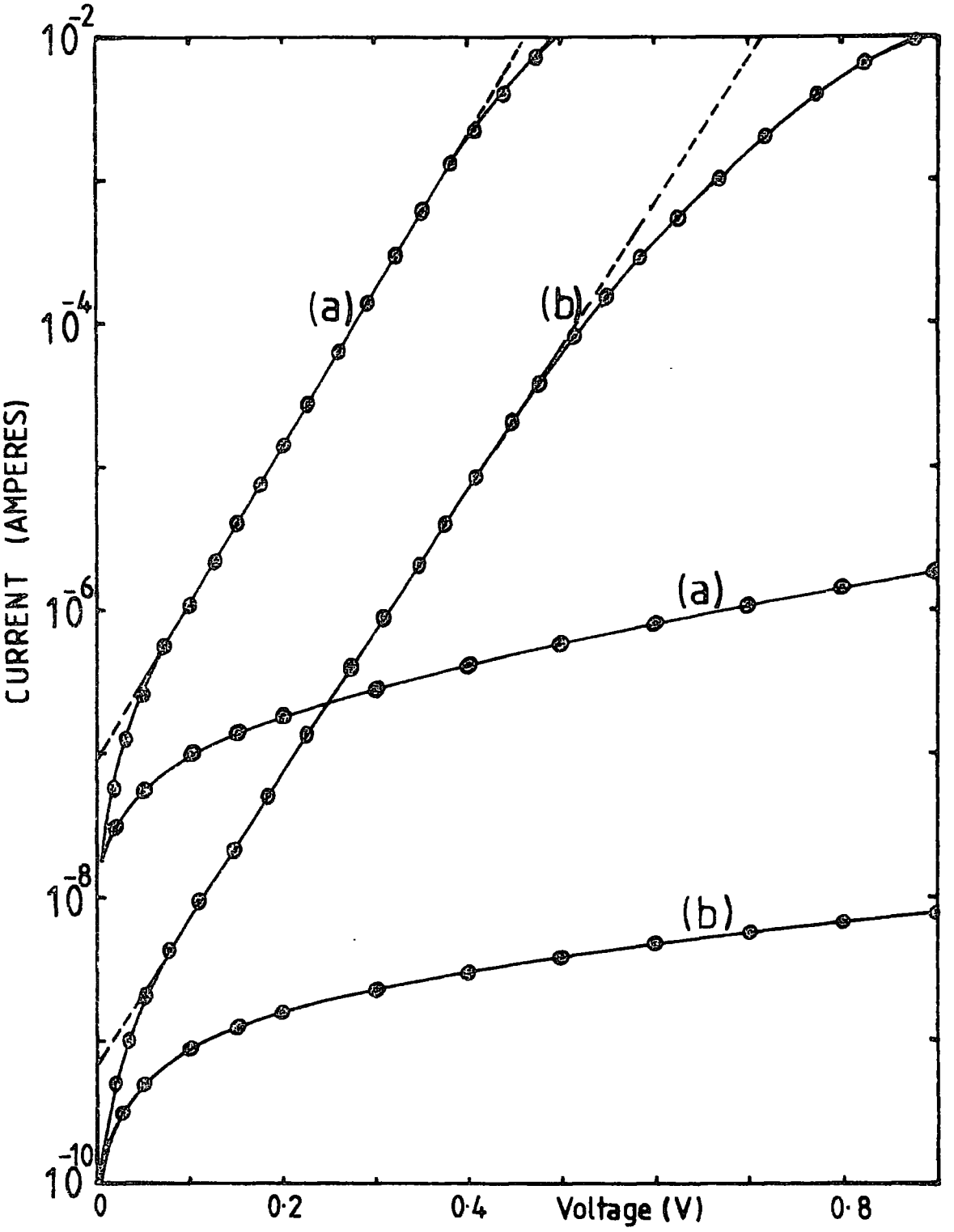

FIG. 7·13. CURRENT - VOLTAGE CHARACTERISTICS FOR TWO DIFFERENT CdTe SOLAR CELLS MEASURED IN THE DARK AT ROOM TEMPERATURE.

(a). Au/CdTe (In-doped) S/B solar cell.

(b). MIS solar cell with one monolayer of $Cdst_2$.

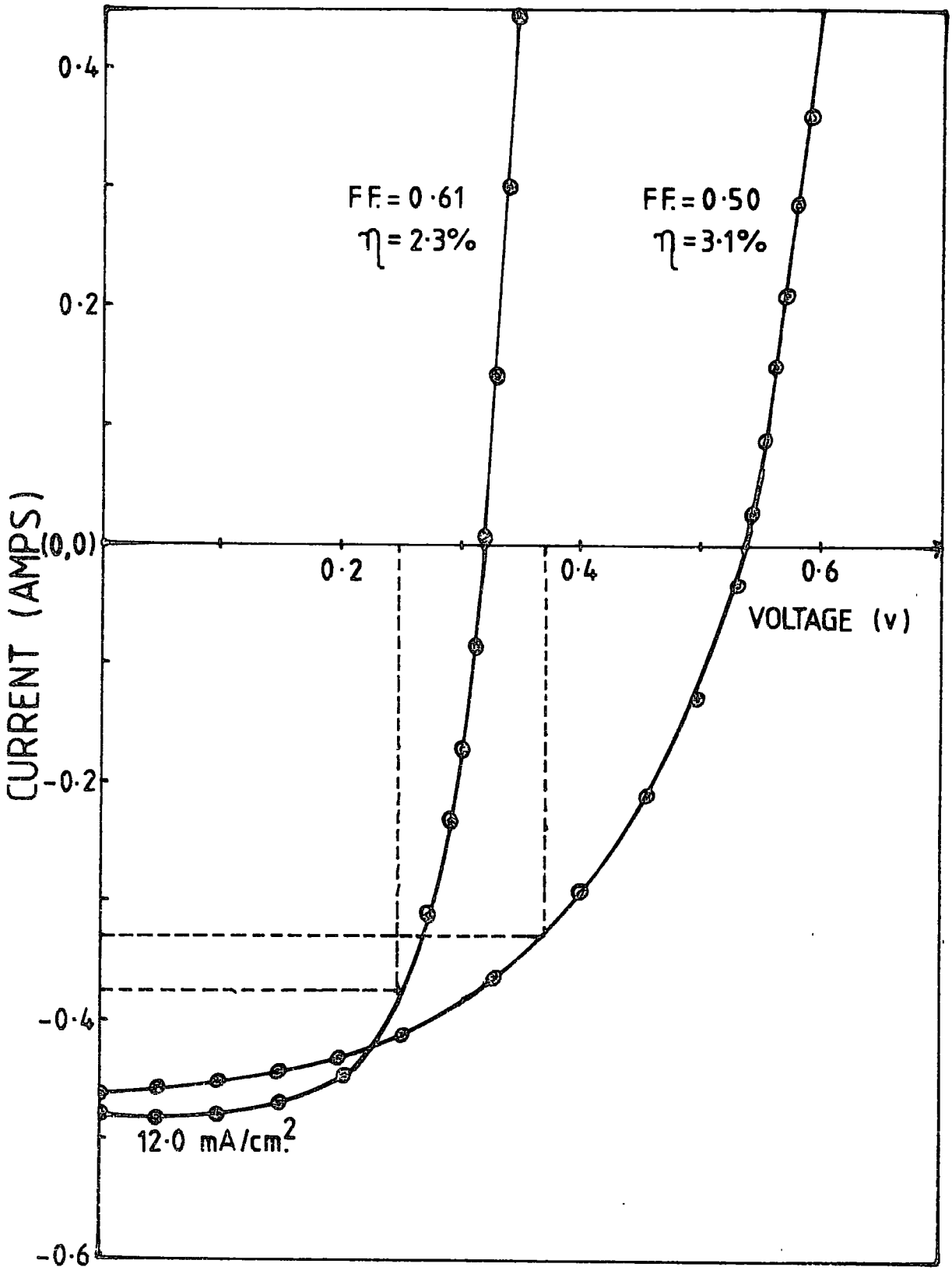

Fig. 7·14 I-V characteristics under AM1 illumination for MS and MIS solar cells prepared on In-doped CdTe.

Even though there is a considerable reduction in dark current, there is no suppression in the photogenerated current (due to holes) in the cells incorporating an insulating layer of thickness ≈ 25 Å. The poor photo-voltage response observed with Schottky barrier solar cells has been considerably improved by incorporating these thin layers at the interface. The enhancement in OCV is observed according to the relation given by equation (3.56),

$$V_{oc} \simeq n\left[\phi_b + \frac{kT}{q}\cdot\chi^{\frac{1}{2}}\cdot d + \frac{kT}{q}\cdot \ell n\left(\frac{J_L}{A^*T^2}\right)\right]$$

The improvement in V_{oc} appears to occur for two reasons ; the increase in the ideality factor, n , and the additional barrier height $\chi^{\frac{1}{2}}d$ provided by the insulating layer of thickness d. The increase of V_{oc} with the insulating film thickness was clearly observed (table 7.2) in this series of experiments. Note that it is not necessary to have a "near-ideal" diode (n< 1.2) to obtain the improvement in solar cell characteristics with the Langmuir films.

(c) Optimization of the insulating film thickness

In the previous sections the discussions were confined to MIS structures prepared with $CdSt_2$ Langmuir films. It was found that the one layer (25 Å) of $CdSt_2$ improves the OCV of the device without suppression of the SCC. The following measurements were carried out in order to investigate the optimum value of insulator thickness.

Langmuir films based on C4 anthracene provide thinner (≈ 12 Å) insulating films due to the shorter carbon chain. The deposition conditions and electrical properties of these films are reported in recent publications[21,26]. To compare the improvement in cell parameters, a Schottky barrier and an MIS structure incorporating C4 anthracene films were prepared side by side on the same surface following the method described

in section (4.5). Only two devices (MS and MIS) were prepared each time, since the specimens used were very small. The OCV and the SCC of the two devices were measured under same conditions and this procedure was repeated for MIS structures with different insulator thicknesses. The ratio of the OCV and SCC for MIS and MS diodes were then plotted against the insulating layer thickness. The results obtained from measurements carried out on both undoped and In-doped specimens are shown in fig (7.15). These data clearly show the increase in OCV with the insulator thickness, and the decrease in SCC for thicknesses greater than ≃ 30 Å. Therefore, a peaked dependence of cell efficiency with insulator thickness exists, and the optimum value for these structures is about 30 Å. This value is larger than the optimum thickness (≃ 20 Å) reported for Si/SiO_2, MIS structures[22-24].

(d) Cell parameters as a function of illumination

All current-voltage characteristics under illumination described in this chapter have been measured using a high illumination level of approximately 100 mW. cm^{-2}. However, for terrestrial use as photovoltaic energy converters, it is unlikely that cells would be used under constant illumination only. Obviously, the intensity of illumination would vary considerably and would be lower than AM1 for most devices being used as solar cells. For these reasons it is clearly necessary to investigate how the cell parameters depend on the intensity of illumination.

The OCV and SCC as functions of intensity of illumination were investigated over five orders of magnitude from about 100 $mW.cm^{-2}$ down to 1 μ $W.cm^{-2}$. The lamp described in section 4.5(d) was used for this purpose. Each cell to be investigated was placed in a light tight container and the different illuminations were obtained by placing various combinations of neutral density filters between the device and the source. Both the OCV and SCC were monitored using an HP-3465B digital voltmeter connected directly to the device.

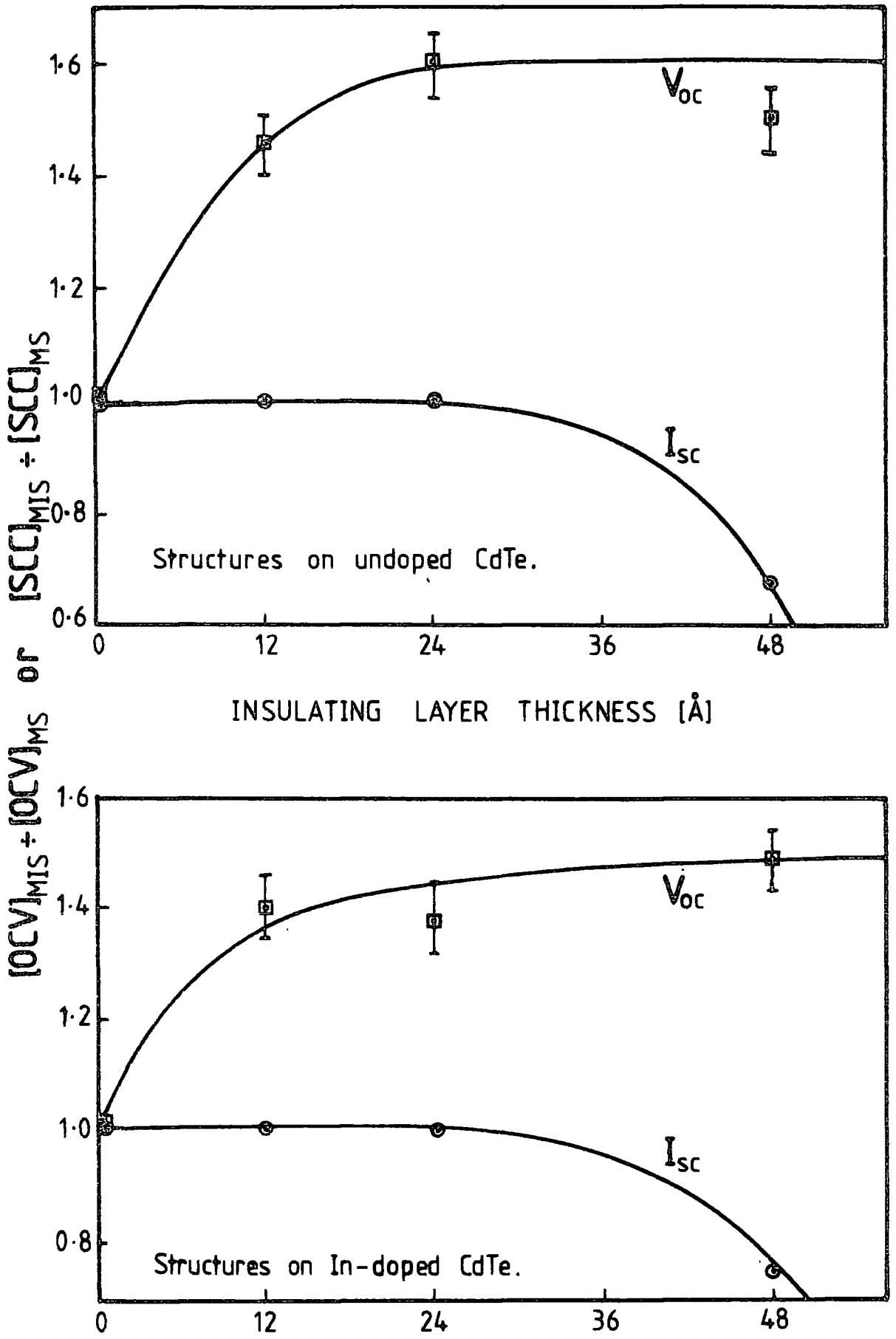

FIG. 7·15. Dependence of OCV and SCC on insulating layer thickness(under AM1 conditions).

The curves of OCV as a function of intensity for three different types of device are shown in fig (7.16). Both MS and MIS devices show the saturation at high light intensities. The SCC is a linear function of intensity above 1 $mW.cm^{-2}$ (fig. 7.17). At lower intensities the response is relatively insensitive to light intensity.

The OCV and SCC at a constant illumination for a MS solar cell are related by equation (3.52),

$$V_{oc} = n\left[\phi_b + \frac{kT}{q} \cdot \ell n \frac{I_{sc}}{AA^* T^2}\right]$$

which can be re-written as

$$\underline{V_{oc}} = \left(\frac{2.303\ nkT}{q}\right) \cdot \underline{\log_{10} I_{sc}} + \left[n\phi_b + \frac{2.303\ nkT}{q} \cdot \log_{10}\left(\frac{1}{AA^* T^2}\right)\right]$$

To evaluate the ideality factor, n, under illumination, the OCV is plotted against the $\log_{10}.I_{sc}$ at different light intensities. The experimentally observed results for the same devices are shown in fig (7.18). For comparison, the ideality factors in the dark and under illumination are also tabulated in the same figure. For all the devices investigated, the ideality factor under illumination is lower than that in the dark. To confirm this low value of n under illumination, the current-voltage characteristics of diode (a) were measured under AM1 illumination. The ideality factor determined from this measurement is also shown in fig (7.18).

(e) Spectral response of the solar cells

The spectral response of the OCV for both MS and MIS diodes prepared on the In-doped sample is given in fig (7.19). The points plotted refer to the steady-state values of the OCV reached after several

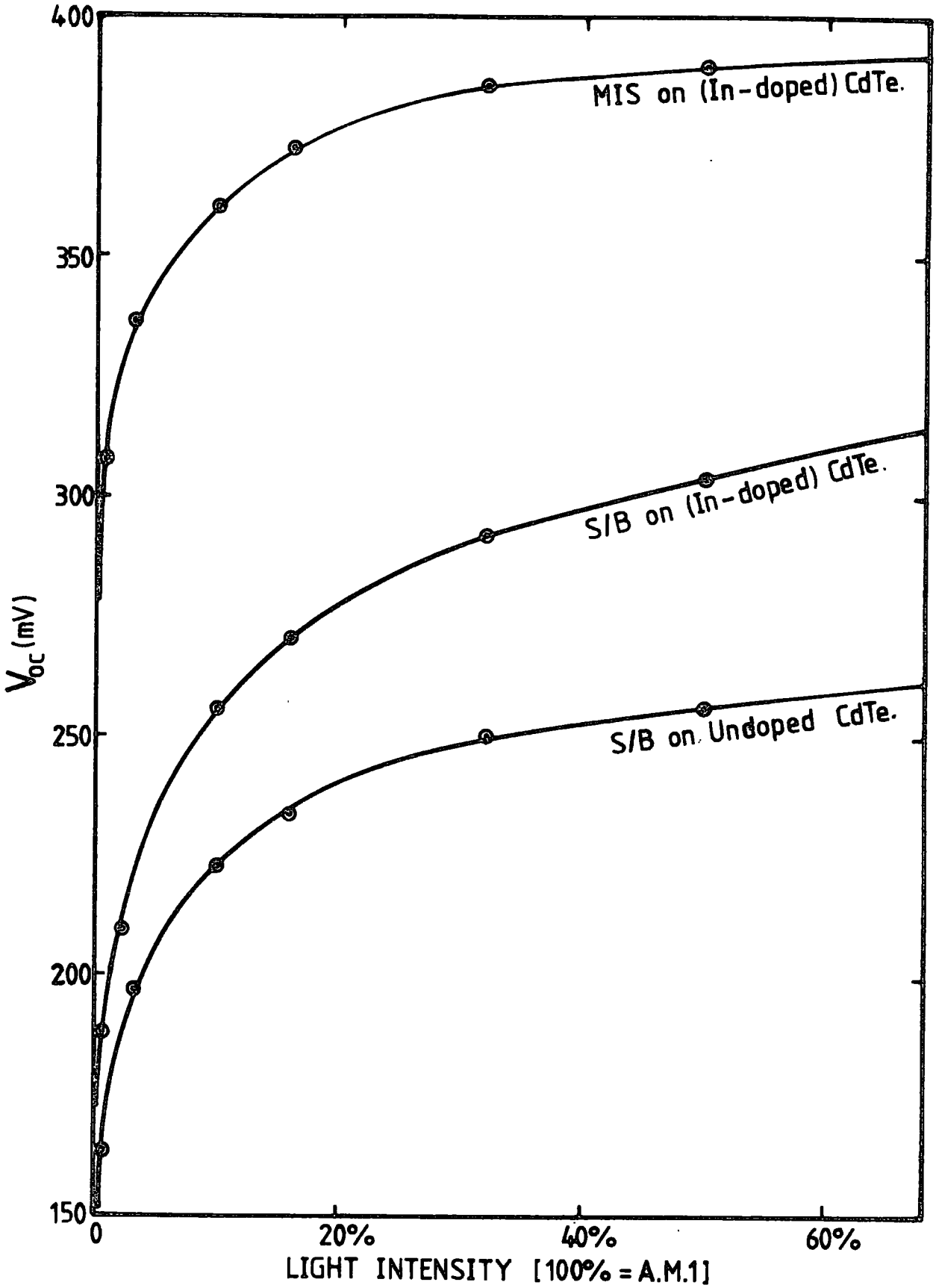

Fig. 7·16 Dependence of O·C·V· on illumination intensity for three different devices prepared on n-type CdTe single crystals.

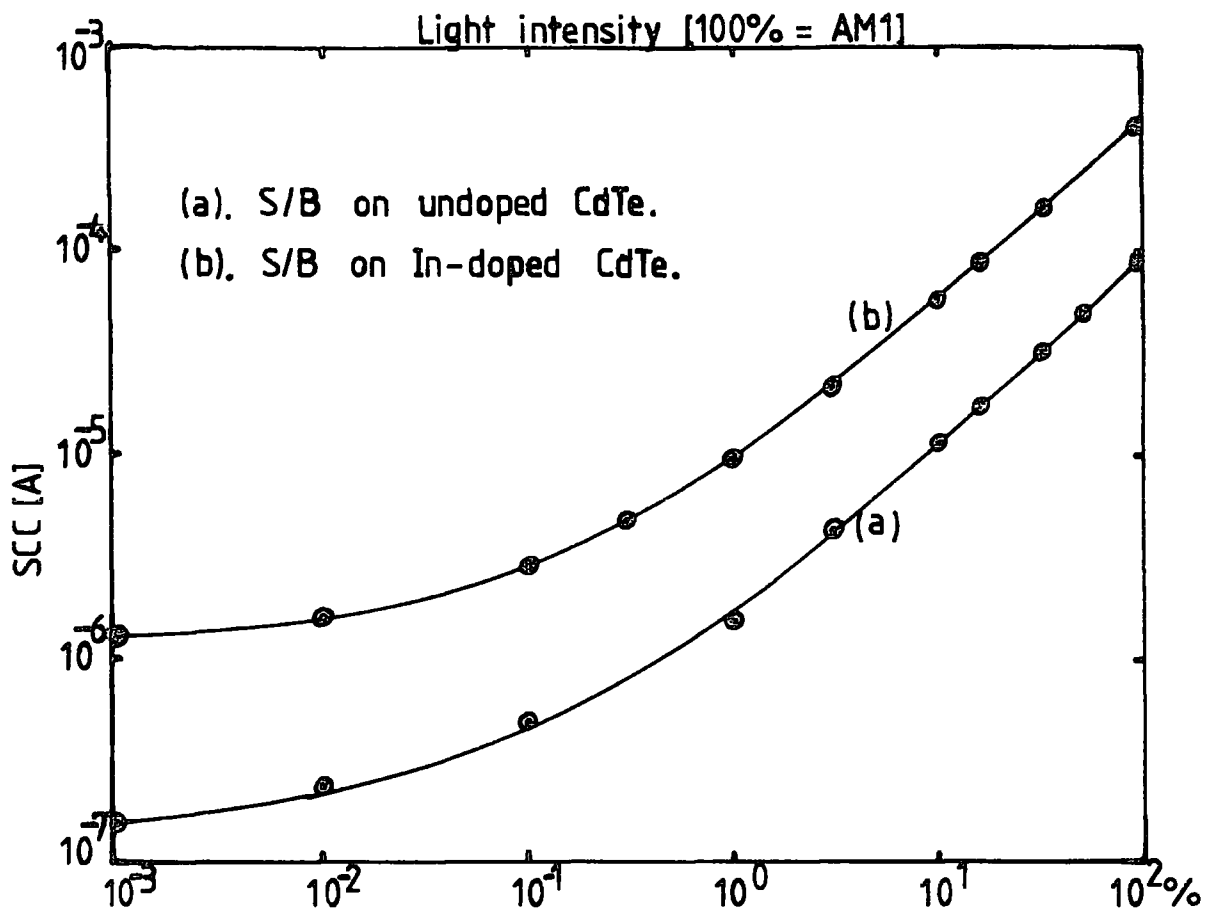

FIG. 7·17. Dependence of S·C·C· on illumination intentensity for Schottky barriers formed on CdTe surfaces.

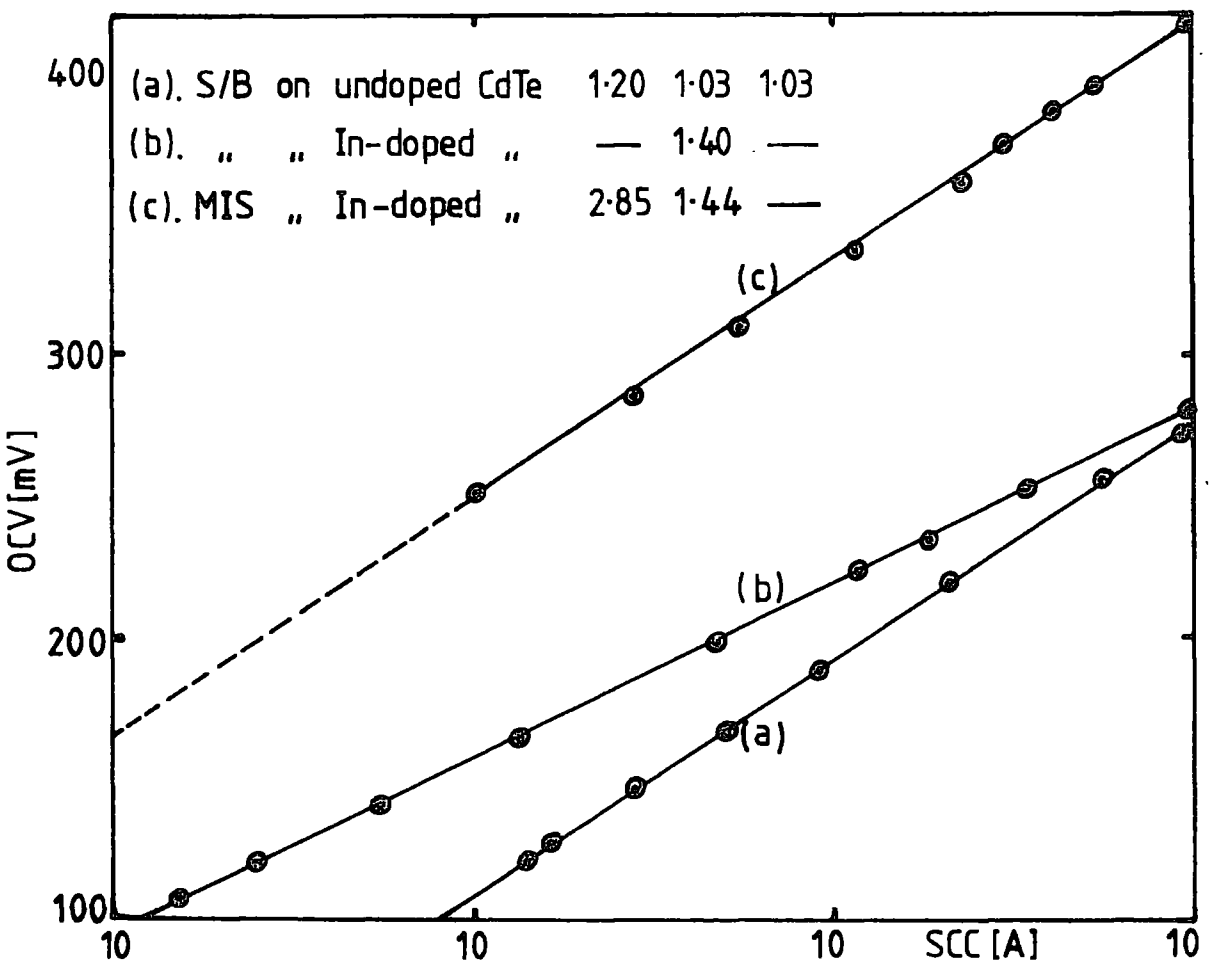

Fig. 7·18 Plots of OCV vs SCC for three different photo-voltaic devices. Exp. pts. correspond to diff. intensities of illumination.

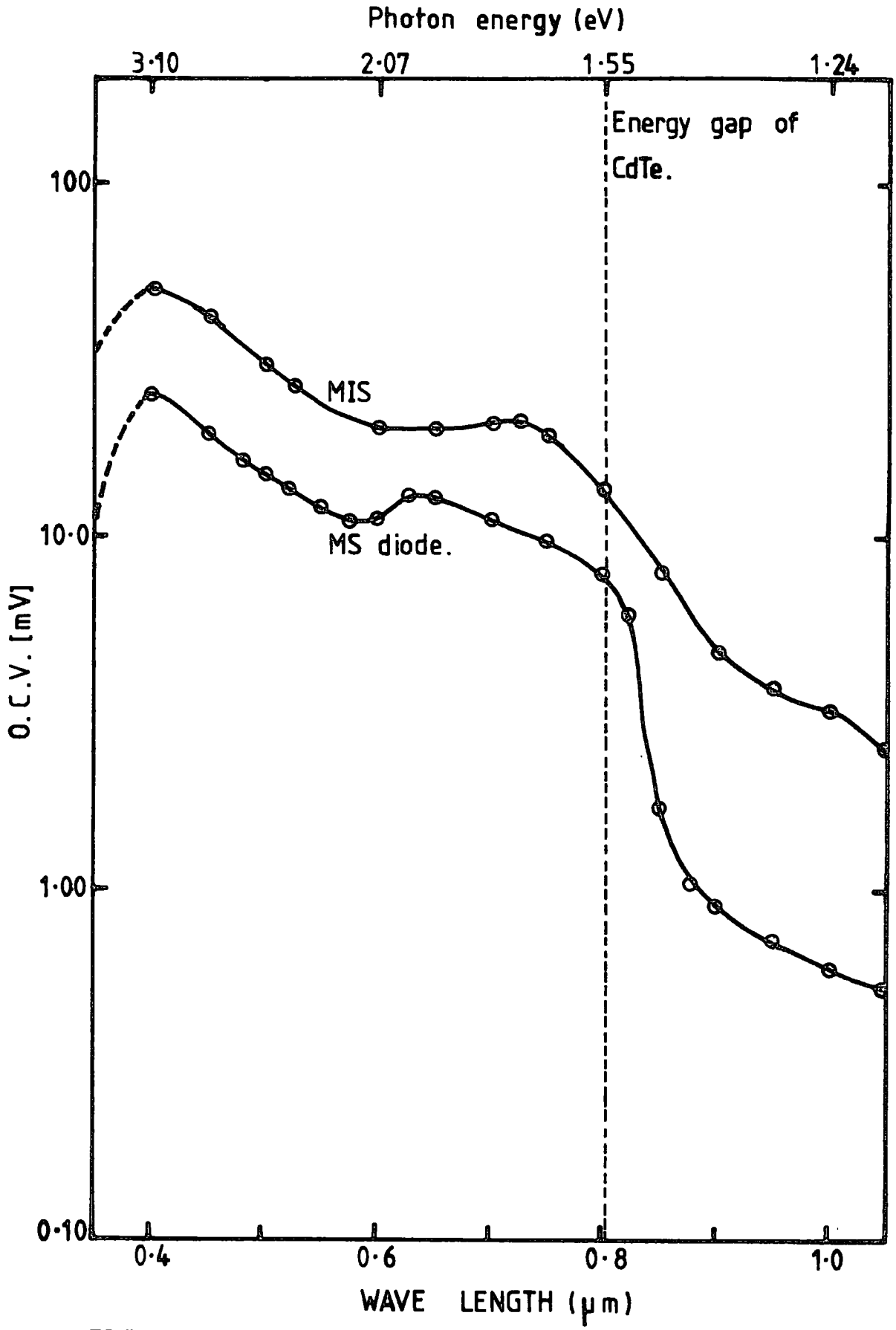

FIG. 7·19 Spectral response of MS and MIS solar cells prepared on In-doped CdTe.

tens of seconds of illumination. Both cells have a wide sensitivity in the wavelength region between 0.4 and 1.0 μm. The response begins at ≃ 0.8 μm (bandgap energy) and reaches a peak at around 0.4 μm.

At high photon energies ($E > E_g$) the spectral response of both the MS and MIS structure is better than that reported for CdTe p-n junctions[25]. The barrier near the surface has greatly improved the response at high energies (section 3.3(a)). The MIS device provides an additional improvement of the long wavelength edge of this curve.

(f) Cell degradation

All the results discussed in earlier sections were obtained within a few days after fabrication of devices. To investigate the ageing effects of these devices, the electrical properties were measured as a function of time. The devices were left in air and the measurements were repeated at regular intervals.

Fig (7.20) shows results obtained for a Schottky barrier prepared on an undoped CdTe sample. This particular diode possessed an ideality factor close to unity (1.01), when measured within a few days after preparation. However, the forward current decreased by nearly two orders of magnitude and the ideality factor increased up to 1.21 after 3 months. After further storage the forward current remained constant with n ≃ 1.21, and the reverse current continued to drop gradually. The capacitance of the same barrier also decreased with time and C-V measurements clearly showed an increase in barrier height from 0.70 eV to 0.79 eV. The OCV of the cell also increased from 180 mV to 270 mV, while the SCC slightly decreased over a 3 month period.

The above observations could be due to an insulating layer introduced by oxidation of the metal-semiconductor interface. Since the Au electrode used is very thin (80 Å), the diffusion of oxygen is quite possible when left in air. As a result the device becomes an MIS structure

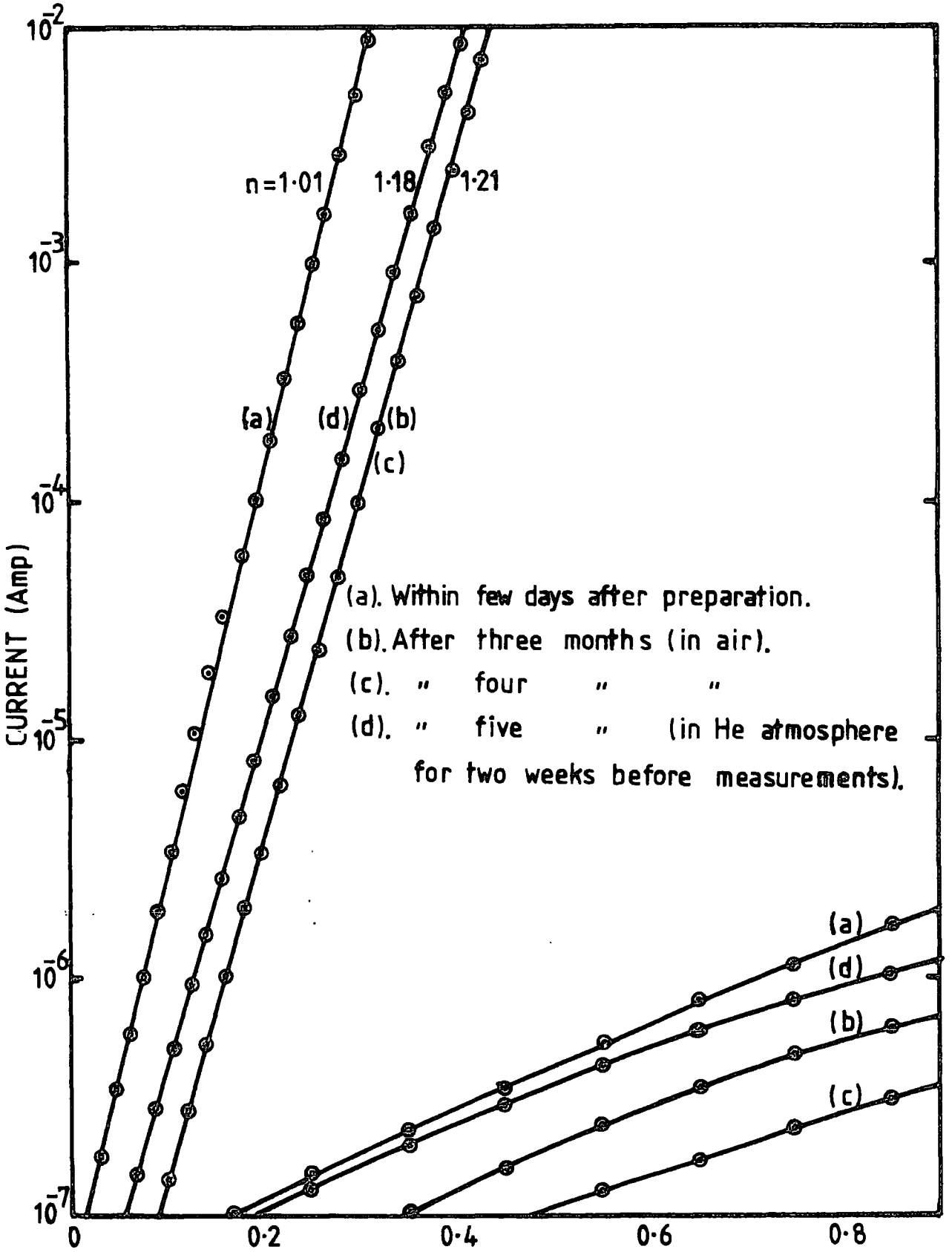

FIG. 7·20. AGEING EFFECT OF SCHOTTKY DIODES PREPARED ON UNDOPED CdTe.

and all the above observations can be explained. Since the ideality factor, n, and the barrier height, ϕ_b, is higher than those of a Schottky barrier, the new OCV should be higher according to the equation (3.52). When the degraded diode was left in a helium atmosphere for 2 weeks, the forward current increased slightly and the reverse current regained the original value. This is also shown in fig (7.19).

The degradation properties of cadmium stearate Langmuir film MIS structures were also evaluated in the same manner. The forward and reverse currents were reduced as a function of time when left in air for a few months. The OCV of one of these devices reduced from 560 mV to 400 mV within two months. When the same device was left in a desiccator under low nitrogen pressure for two weeks the forward current increased slightly and the reverse current exceeded the original value by about a factor of 6. Clearly degradation with time is extremely important in these devices. More detailed measurements of both MS and MIS structures are therefore required in order to ascertain the exact degradation mechanisms.

7.4 SUMMARY

Summarizing the results presented in this chapter, it can be concluded that the Schottky barriers prepared on low resistive n-type CdTe possess good diode characteristics with rectification factors of about 1×10^5. Most of the devices show ideality factors between 1.20 and 1.90 in the dark, the value being very sensitive to the surface preparation. Barrier heights obtained from different methods (I-V and C-V) do not agree exactly but show values in the range 0.75-0.90 eV. The current-voltage characteristics of these devices may be described well by the equation

$$J = A^*T^2 \cdot \exp\left\{-\phi_{bo}/k(T + T_o)\right\} \cdot \left[\exp\left\{qV/k(T + T_o)\right\} - 1\right]$$

The appearance of an excess temperature, T_o, may be due to the

presence of surface states, an interfacial layer or a combination of the two.

The devices prepared on well polished CdTe surfaces using freshly prepared 1% bromine in methanol, possess near ideal characteristics with $n \simeq 1.01$. Barrier heights from I-V and C-V measurements show an excellent agreement and a value of 0.70 eV was obtained for these Schottky barriers. The current-voltage characteristics may then be described using the well known Schottky equation

$$J = A^* T^2 . \exp\left(- \phi_b/kT\right) \left[\exp (qV/nkT) - 1\right]$$

These characteristics are similar to those reported for Au electrodes deposited on to vacuum cleaved CdTe surfaces[3]. In fact, the ESCA technique confirmed that the particular surface preparation technique used produces a relatively clean CdTe surface.

The carrier concentration of the materials used in this series of experiments varied from $(1.30 - 2.30) \times 10^{17}$ cm^{-3}. Schottky barriers based on In-doped material (1.3×10^{17} cm^{-3}) showed better characteristics and produced a maximum photoconversion of 3% under AM1 conditions. The optimum barrier electrode thickness was found to be 60 Å. The solar cell parameters are also highly sensitive to the preparation method and the OCV varied from 150 mV to 400 mV. The SCC depends on the barrier electrode thickness and is about 10 $mA.cm^{-2}$ for a 60 Å thick electrode. The Schottky diodes show a slow degradation with time when left in air. The values of ideality factor and the barrier height increase to a certain value and then remain approximately constant. As a result the OCV is increased and SCC is decreased slightly. If this degradation is due to oxidation at the interface, a suitable anti-reflection coating will encapsulate the structure and reduce the diffusion rate of oxygen, while also helping to improve the conversion efficiency of the device by increasing the short-circuit-current.

It is demonstrated in the present study that the presence of an insulating layer has modified the majority-carrier (electrons) transport and the current through the interfaces follows an exponential relationship of the form given by equation (3.49). The device ideality factor, n, also increases with increasing insulator film thickness, according to the theoretical prediction given by equation (3.50).

The experimental results presented in this chapter show conclusively that the introduction of Langmuir film of thickness $\simeq 25$ Å at the interface, increases the open-circuit-voltage by about 65% , without degrading the short-circuit-current. Even though there is a slight decrease in the fill factor, the overall efficiency is increased by $\simeq$ 35%.

CHAPTER 8

CONCLUSIONS AND SUGGESTIONS FOR FUTURE WORK

8.1 CONCLUSIONS

One aim of the research reported in this thesis was to investigate semi-insulating CdTe:Cl grown for use in solid state nuclear detectors and as a possible substrate material for other devices (i.e. FET's, IR detectors, etc). The activation energy measurements reveal that the conductivity of the material is controlled by two levels in the forbidden energy gap. A deep level, 1.00 eV above the valence band edge is found in all the samples studied and may possibly be attributed to the doubly ionized cadmium vacancy reported by other workers. The depth of the second level controlling the conductivity of these samples is found to depend on where the specimen is cut from the crystal boule and the temperature of annealing treatment. This energy level may be associated with the complexes of chlorine with native defects.

The conductivity of Cl-doped CdTe is found to obey the Meyer-Neldel rule. In an attempt to explain this effect, a new model incorporating multivalent centres has been put forward. Theoretical conductivity characteristics obtained from this model produced similar features to those obtained experimentally. This, therefore, shows the possibility of the existence of multivalent centres in this material.

The thermally stimulated current measurements confirm the positions of some of the observed impurity levels in CdTe: Cl and also agree well with previously reported TSC results. While this is a good method for comparing one sample with another, it is difficult to obtain precise information about the impurity levels in the material.

It is evident that the electrical properties of this material are

very sensitive to low temperature (< 250^{o} C) annealing and the activation energies can vary over a wide range. Because of this instability, the performance of devices prepared on CdTe:Cl substrates is likely to be adversely affected. In particular, γ-ray detectors made from this material will probably have a short lifetime due to the effects of radiation damage. Without further improvement, CdTe:Cl is, therefore, unlikely to form the basis for reliable devices.

In the course of this work the electrical properties of single crystals of semi-insulating CdTe:Cr have also been investigated. At high temperatures and low fields the material shows p-type conduction and is controlled by two impurity levels, 0.33 eV and 0.52 eV, above the valence band edge. The low temperature and high field conduction in this material is rather complicated. Injected electrons may be responsible for this behaviour and further experimental evidence is needed before any definite conclusions can be drawn. The electrical properties of CdTe:Cr seem to be very similar to those of undoped semi-insulating CdTe also studied in this thesis. The impurity levels may, therefore, be associated with the same defect levels observed in undoped material.

The other aim of this work was to study MS and MIS photovoltaic structures on CdTe. Single crystals with electron concentrations $\simeq 1.0 \times 10^{17}$ cm^{-3} were found to be satisfactory for the production of good Schottky diodes. Most of the barriers produced by evaporation of Au on etched surfaces of n-CdTe single crystals possess a rectification factor of $\simeq 5 \times 10^{4}$, at $\simeq$ 0.5 V. The behaviour of capacitance with reverse voltage is as expected. The barrier heights and the ideality factors of these rectifying structures are very sensitive to the surface preparation. This non-ideal behaviour could be due either to the strong influence of surface states or possibly an interfacial layer between the metal and semiconductor. The n value for a given diode increases with decreasing temperature and the

electrical properties can be explained by equation (3.36).
The diodes prepared on well chemically polished surfaces using fresh bromine in methanol, showed nearly ideal Schottky barrier behaviour. The forward current transport in these devices can be explained quantitatively by pure thermionic emission. The barrier height was determined for these structures to be 0.70 eV using different experimental techniques.

The performance of Schottky barrier diodes as solar cells has also been studied. The open-circuit-voltage measured under AM1 condtions was in the range 150 mV to 400 mV. Short-circuit-currents around 12 mA/cm^2 were obtained with a barrier electrode thickness of 60 Å. The fill factor varied slightly for different devices and the highest conversion efficiency measured for these MS solar cells was 3.0%.

The open-circuit-voltage of the Schottky barrier solar cells was considerably enhanced by the use of a thin layer (≈ 25 Å) of cadmium stearate or C4 anthracene Langmuir film in the structure. A maximum increase in OCV by about 65% was attained without any reduction in the SCC. The fill factor of the MIS devices decreased slightly, but the overall conversion efficiency increased by ≈ 35%. It is expected that higher short circuit currents and, therefore, higher conversion efficiencies should be obtained by the use of a suitable anti-reflection coating on the MIS structures.

8.2 SUGGESTIONS FOR FUTURE WORK

The results described in this thesis indicate several interesting areas for future work. One would be a further investigation of the mechanism involved in the annealing process of highly resistive Cl-doped CdTe specimens. A proper understanding might enable this process to be reversed and perhaps more stable semi-insulating material could then be obtained.

Several additional techniques would be useful in order to understand the current transport mechanism involved in the Cr-doped single

crystals at low temperatures. Drift mobility measurements would be especially helpful in measuring the mobilities and identifying the charge carriers.

The solar cell work presented in this thesis reveals that the incorporation of Langmuir films in Schottky barriers prepared on single crystal CdTe enhances the cell parameters. It is, therefore, interesting to study the MIS solar cells on good quality CdTe thin films and other potential photovoltaic materials, such as amorphous Si. The efficiency of cadmium mercury telluride IR-detectors could also be improved by exploiting a similar MIS structure. Since the Langmuir film materials used in this work possess low melting points ($\simeq 80^{o}C$), it is unlikely that these would form the basis of practical devices such as solar cells. Similar work using organic compounds like phthalocyanine (melting point $\simeq 450^{o}C$) and polymers with high melting points is, therefore, invaluable in order to surmount this problem.

Ageing effects of solar cells are very important, and only preliminary studies have been carried out during this work. A more systematic look at on cell degradation studies is, therefore, necessary for both MS and MIS solar cells. It might also be worthwhile studying the effect of heat treatments on MS structures.

REFERENCES

CHAPTER 1

1. F.V.Wald, Rev.de Phys.Appl., No:12 (1977) pp 277-290.
2. M. Fabre, Ann.Chim.Phys., 14 (1888) p 110.
3. C.A.Tibbals, J.Am.Chem.Soc., 31 (1909) p 902.
4. R.Frerichs and R.Warminsky, Naturwissenschaften, 33 (1946) p 251.
5. F.A.Kröger and D. De Nobel, J.Electron, 1 (1955) p 190.
6. B.I.Boltaks, P.P. Konorov and O.A.Matveev, Z. Tekh.Fiz., 25 (1955) p 2329.
7. D. De Nobel, Philips Res.Repts., 14 (1959) pp 361-399 and 430-492.
8. K. Zanio, "Semiconductors and Semimetals", Vol.13, "Cadmium Telluride". Academic Press (1978).
9. J.B.Mullin and B.W.Straughan, Rev.Phys.Appl., T.12, No.2 (1977) pp 105-115.
10. B.Schaut, J. Gallet, A.Brunet-Jailly and B. Pelliciari., Rev.Phys.Appl., T.12(1977) pp 147-150.
11. T. Taguchi, J. Shirafuji and Y. Invishi., Rev. Phys. Appl., T.12 (1977) pp 117-122.
12. F.V.Wald and R.O.Bell., Rev. Phys.Appl., T.12(1977) pp 203-204.
13. B. Lunn and V. Bettridge., Rev.Phys.Appl., No.12 (1977) pp 151-154.
14. W. G. Pfann., J.Metals, N.Y.4., (1952) pp 747-753.
15. N.V.Agrinskaya and O.A.Matveev., Sov.Phys.Semicond., Vol.10, No.1 (1976) pp 96-98.
16. A.N.Mariano and E.P. Warekois., Science 142(1963) p 682.
17. R.O.Bell, F.V. Wald, C. Canali, F. Nava and G. Ottaviani., IEEE. Trans.Nucl.Sic., NS-21 (1974) pp 331-341.
18. M.G.Williams, R.D.Tomlinson and M.J.Hampshire, Solid State Commun., 7 (1969) p 1831.

19. T.F.Smith and G.K.White., J.Phys. C., 8 (1975) p 2031.

20. A.J.Strauss., Rev.Phys.Appl., T12, No.2 (1977) pp 167-184.

21. D.T.F. Marple, Phys.Rev., 150 (1966) p 728.

22. D.G.Thomas., J. Appl. Phys., 32 (Supp)(1961),p 2298

23. B. Segall ., Phys.Rev., 150 (1966) p 734.

24. M.V.Alekseenko, E.N.Arkadeva, V.S.Kisilenko, L.V.Maslova, O.A.Matveev, S.V.Prokof'ev, S.M.Ryvkin and A.Kh. Khusainov., Fiz. Tekh. Poluprov., 8 (1974) p 550 (Sov.Phys.-Semicond.8 (1974) p 351).

25. J. Gu, T. Kitahara, K. Kawakami and T. Sakaguchi., J.Appl.Phys., 46 (1975)p.1184.

26. R. Triboulet and Y. Marfaing., J. Electrochem. Soc., 120 (1973) p 1260.

27. A. Zoul and E. Klier., Czech. J.Phys. B., 27 (1977) pp 789-796.

28. A. M. Mancini, C. Manfredotti, C. de Blosi, G. Micocci and A. Tepore, Rev. Phys. Appl., T.12 (1977) pp 255-261.

29. P. Höschl, P. Polívka, V. Prosser, A. Sakalas., Czech. J.Phys., B 25 (1975) pp 585-596.

30. Ngo-Tich-Phuoc, G.M. Martin, C. Belin and E. Fabre., Rev.Phys.Appl., T.12 (1977) pp 195-198.

31. G.M.Martin, E. Fogarassy and E. Fabre., J. Appl. Phys., Vol.47, No. 1 (1976) pp 264-266.

32. R. Stuck, J.C.Muller and P. Siffert., Rev.Phys. Appl., T.12 (1977) pp 185-188.

33. P. Höschl, P. Moravec, A. Martinaitis and A. Sakalas., Phys. Stat. Sol. (a), 48 (1978) K 43.

34. P. Höschl, P. Polivka, V. Prosser and M. Vanecek., Rev.Phys.Appl., T.12 (1977) pp 229-233.

35. G. Ottaviani, C. Canali, C. Jacoboni, A. Alberigi Quaranta and K. Zanio, J.Appl. Phys., Vol.44, No: 1 (1973) p 360.

36. M. Caillot., Rev.Phys. Appl., T.12 (1977) p 241.

37. G. Ottaviani, Rev.Phys. Appl., T.12 (1977) pp 249 - 254.

38. Y. Marfaing, J. Lascaray and R. Triboulet., Institute of Physics Conf. Ser. No.22, pp 201-209.

39. E.J.Danielewicz and P.D. Coleman., Appl. Opt., 13 (1974) p 1164.

40. S. Perkowitz and R.H. Thorland., Phys. Rev., B9 (1974) p 545.

41. D.T.F. Marple., Phys.Rev., Vol.150, No.2 (1966) pp 728-734.

42. J. Camassel, D. Auvergne, H. Mathieu, R. Triboulet and Y. Marfaing, Solid Stat. Com., Vol.13 (1973) pp 63-68.

43. Y.F. Tsay, S.S. Mitra and J.F. Vetelino., J.Phys. Chem.Solids, 34(1973) p 2167.

44. A. Cornet, P. Siffert, A. Coche and R. Triboulet., Appl.Phys, Lett., 17 (1970) p 432.

45. E. N.Arkadyeva and O.A. Matveev., Rev.Phys.Appl., T.12, No.2(1977) pp 239-240.

46. N.V.Agrinskaya and O.A.Matveev., Sov.Phys. Semicond., 12 (2) (1977) pp 187-190.

47. K. Yamaguchi, M. Matsumoto, N. Nakayam, S. Ikegami., Japan. J. Appl. Phys., 15 (1976) pp 1575 - 1576.

48. K. Yamaguchi, N. Nakayama, M. Matsumoto, S. Ikagami., Japan. J. Appl. Phys., 16 (1977) pp 1203 - 1211.

49. D. A. Cusano., Solid State Electron., 6 (1963) pp 217-232.

50. D. A. Cusano, Rev. Phys. Appl., 1 (1966) pp 195-200.

51. R.O.Bell, H.B. Serreze, F.V. Wald., Proc. 11th Photovoltaic Spec.Conf. (IEEE.N.Y, (1975)), pp 497-502.

52. J.P.Ponpon, P.Siffert., Rev.Phys., Appl., 12 (1977) pp 427-430.

53. R.H.Williams and H.R.Johnson., Solid Stat.,Com., Vol.16, (1975) pp 873-875.

54. H.R.Johnson, R.H.Williams and C.H.B. Mee., J.Phys.D: Appl.Phys., Vol.8 (1975) pp 1530-1541.

55. M.Rodot., Rev. Appl., No. 12 (1977) pp. 411-416.

REFERENCES

CHAPTER 2

1. E.H.Rhoderick, "Metal-Semiconductor Contacts", Oxford University Press (1978).
2. J.S.Blakemore, "Solid State Physics",second edition (1974).
3. M.A.Lampert, "Current Injection in Solids", Academic Press (N.Y. and London). 1970.
4. N.F.Mott and R.W.Gurney, Electronic Processes in Ionic Crystals, Oxford University Press, Oxford, (1940), p 156.
5. M.A.Lampert, RCA Review., Vol.XX, No.4 (1959) pp 682-701.
6. M.A. Lampert, Proc.of the IRE (August 1962) pp 1781-1798.
7. M.A.Lampert, Phys.Rev., 103 (1956) p 1648.
8. G.G.Roberts and F.W.Schmidlin., Phys.Rev., Vol.180, No.3 (1969) pp 785-794.
9. F.W.Schmidlin and G.G.Roberts, Phys.Rev. B., Vol.9, No :4 (1974) pp 1578-1590.
10. G.G.Roberts, N.Apsley and R.W.Munn., Phys.Reports Vol.60, No.2 (1980) pp 59-150.
11. R. Dewsberry, J.Phys. D: Appl.Phys., Vol.9 (1976) pp 265-272.
12. F.L.Welchman and R.Kuzel., Can.J.Phys.Vol.48 (1970) pp 63-69.
13. K.O.Lee, Phys. Stat. Sol.(a)., 47, K47 (1978) pp K47-K49.
14. G.G.Roberts and D.G.Thomas, J.Phys. C: Solid State Physics, Vol.7 (1974) pp 2312 - 2316.
15. G.R. Johnston and L.E.Lyons., Phys. Stat. Sol., 37 (1970) pp K43-K45.
16. W.Meyer and H.Neldel., Z.Tech. Phys., Vol.18 (1937) pp 588-593.
17. B. Rosenberg, B.B. Bhowmik, H.C. Harder and E.Postaw., J.Chem. Phys., Vol. 49, No.9 (1968) pp 4108-4114.
18. G.G.Roberts, J.Phys. C: Solid St.Phys., Vol.4 (1971) pp 3167-3176.

19. G.G.Roberts, "Transfer & Storage of Energy by Molecules - Chapter 3", John Wiley (1974) pp 153-222.

20. E.H.Putley, "The Hall Effect and Related Phenomena", (1960).

21. S.M.Sze., "Physics of Semiconductor Devices" Wiley International.

22. F.Urbach, Winer Ber.II (a), 139 (1930) p 363.

23. J.T.Randall and M.H.F.Wilkins, Proc.Roy.Soc.A., 184 (1945) p 366.

24. P. Kivits and H.J.L.Hagebeuk, Journal of Luminescence, Vol.15, No.1 (1977) pp 1-27.

25. K.H.Nicholas and J.Woods., Brit. J. Appl. Phys., Vol.15 (1964) pp 783-795.

26. R.H.Bube, "Electronic Properties of Crystalline Solids".

REFERENCES

CHAPTER 3

1. S.M.Sze, "Physics of Semiconductor Devices",Wiley International Edition (1969), Chapter 8.
2. E.H.Rhoderick, "Metal-Semiconductor Contacts", Oxford University Press (1978).
3. F.A.Padovani and R.Stratton, Solid-State Electron, 9 (1966) p 695.
4. F.A. Padovani and G.G.Sumner, J.Appl.Phys., 36 (1965) p 3744.
5. F.A.Padovani, "Semiconductors and Semimetals" (Ed. Willardson Beer), (1971) 6A, Chap.2, Academic Press, New York.
6. Y.A.Goldberg, E.A. Posse, B.V. Tsarenkov., Soviet. Phys.Semicond., 9 (1975) p 337.
7. C.R. Crowell and V.L.Rideout, Solid-State Electron., 12 (1969) p 89.
8. A.N.Saxena., Surface Science., 13 (1969) pp 151-171.
9. J.D.Levine, J.Appl.Phys., 42 (1971) pp 3991-3999.
10. E.H.Rhoderick,, J.Appl.Phys., 46 (1975) p 2809.
11. C.R.Crowell, Solid-State Electron., 20 (1977) p 171.
12. P.V. Gray., Phys.Rev., Vol.140 (1965) p.A179.
13. A.Waxman et al., Solid-State Electron., Vol.10 (1967) p 865.
14. W.E.Dahlke and S.M.Sze., Solid-State Electron., Vol.10, (1967) pp 865-873.
15. L.B.Freeman and W.E.Dahlke,, Solid-St.Electron., 13 (1970) p 1483.
16. H.C.Card and E.H.Rhoderick., J.Phys. D : Appl.Phys., 4(1971) pp 1589-1601.
17. R.A. Clarke and J.Shewchun., Solid-St.Electron., 14 (1971) p 957.
18. S. Kar and W.Dahlke., Solid-State Electron., 15 (1972) p 221.
19. The Open University, "Solar cell", The Open University Press (1973).

20. H.J.Hovel., "Semiconductors and Semimetals - Volume 11 - Solar Cell", Academic Press (N.Y., S.F, London) 1975.

21. R.J.Stirn and Y.C.M.Yeh., Appl.Phys., Lett., 27 (1975) p 95 ; Proc.IEEE 11th Photovoltaic Specialists Conf., IEEE, New York (1975) p 437.

22. J. Schewchun, M.A.Green and F.D.King., Solid-St. Electron., 17 (1974) p 563.

23. E.J.Charlson and J.C.Lien., J.Appl.Phys., 46 (1975) p 3982.

24. D.R. Lillington and W.G.Townsend, Appl.Phys. Lett., 28 (1976) p 97.

REFERENCES

CHAPTER 4

1. B. Lunn and V. Bettridge., Rev.Phys. Appl., 12 (1977) pp 151-154.
2. P. J.Grundy and G.A. Jones, "Electron Microscopy in the Study of Materials", Edward Arnold Ltd (1976).
3. M.H. Patterson and R.H. Williams, J.Phys. D: Appl.Phys., Vol.11 (1978).
4. E.H.Putley, "The Hall effect and related phenomena" (1960).
5. R.H.Bube., "Electron properties of crystalline solids", Chapter 10.
6. S.M.Sze., "Physics of semiconductor devices", Wiley International Edition.
7. G.G.Roberts, K.P.Pande and W.A.Barlow, "Solid state and electron devices", Vol.2, No.6 (1978) pp 169-175.
8. G.G.Roberts, P.S. Vincett and W.A.Barlow, J.Phys. C: Solid St. Phys. Vol.11 (1978) pp 2077-2085.
9. M. C.Petty and G.G.Roberts, Inst.Phys. Conf. Ser. No. 50, Chapter 3, pp 186-192.
10. G.L.Gaines, "Insoluble monolayers at liquid-gas interfaces" (London: Wiley).

REFERENCES

CHAPTER 5

1. P. Höschl, P. Polívka, V. Prosser, A. Sakalas., Czech. J.Phys.,B., 25 (1975) pp 585-596.
2. G.G.Roberts and F.W.Schmidlin, Phys.Rev., Vol.180, No.3 (1969) pp 785-794.
3. F. W.Schmidlin and G.G.Roberts, Phys.Rev. Vol.9, No.4 (1974) pp 1578-1590.
4. G.G.Roberts, N. Apsley and R.W.Munn., Phys.Letters (Review section), Vol.60, NO.2 (1980) pp 59-150.
5. C. Canali, M.A.Nicolet and J.W.Meyer., Solid Stat.Electronics, Vol.18 (1975) pp 871-874.
6. K.P.Pande and G.G.Roberts., IEEE Trans.Nucl.Sci., NS-24 (1977) pp 2017-2020.
7. A. Zoul, E.Klier., Czech. J.Phys., B 27 (1977) pp 789-796.
8. R.O.Bell.,F.V. Wald, C. Canali, F. Nava, and G. Ottaviani., IEEE Trans. Nucl.Sci., NS-21 (1974) pp 331-341.
9. N.V. Agrinskaya and O.A. Matveev., Sov.Phys. Semicond., Vol.10, No.1 (1976) pp 96-98.
10. E.N.Arkadyeva and O.A.Matveev., Rev.de Phys.Appl., T12, No.2 (1977) pp 239-240.
11. N.V.Agrinskaya and O.A.Matveev., Sov.Phys. Semicond., 12 (2) (1977) pp 187-190.
12. J. Camassel, D. Auvergne, H.Mathieu, R. Triboulet and Y. Marfaing, Solid Stat. Commun., 13 (1973) pp 63-68.
13. N.F.Mott, E.A.Davis and R.A.Street, Philos. Mag. 32 (1975) pp 961-967.
14. D. Adler and E.J.Yoffa., Phys.Rev.Lett., Vol.36 (1976) p 1197.

15. E.N.Arkadyeva and O.A.Matveev., Rev.Phys. Appl., T 12, No.2 (1977) pp 239-240.

16. P. Höschl, P. Poliŭka, V. Prosser, A. Sakalas., Czech. J.Physics, B. 25(1975) pp 585-596.

17. G.F.J. Garlick and A.F.Gibson., Proc.Phys.Soc., 60 (1948) p 574.

18. W. Hoogenstraaten., Philips Res.Rept., 13 (1958) p 515.

19. R.H.Bube., J.Chem. Phys., 23 (1955) p 18.

20. R. Chen., J.Appl.Phys., 40 (1969) p 570.

21. J.T. Randall and M.H.G. Wilkins., Proc.Roy.Soc., A 184 (1945) p 366.

22. G.M.Martin, E. Fogarassy and E. Fabre., J.Appl.Phys., Vol.47, No. 1 (1976) pp 264-266.

23. Ngo-Tich-Phuoc, G.M. Martin, C. Belin and E. Fabre., Rev.de Phys. Appl., 12 (1977) pp 195-198.

24. R. Stuck, J.C. Muller and P. Siffert., Rev. de Phys. Appl., 12 (1977) pp 185-188.

25. A.M.Mancini and C. Manfredotti., Rev. de Phys. Appl., 12 (1977) pp 255-261.

26. Shigaru Fuyuki, Nobuo Hyakutake and Sohachiro Hayakawa., Japanese J. Appl.Phys., Vol.17, No.5 (1978) pp 851-855.

27. P. Höschl, P. Poliŭka, V. Prosser, M. Vaněcek., Rev. de Phys. Appl., 12 (1977) pp 229-233.

28. F. A. Kröger., Rev.Phys. Appl., T 12,No2 (1977) pp 205-210.

29. Y. Marfaing., Rev.Phys. Appl., 12 (1977) pp 211-217.

30. R. Legros, Y. Marfaing and R. Triboulet., J.Phys. Chem. Solids, 39 (1978) pp 179-184.

31. P. Siffert, B. Rabin, H. Y. Tabatabai and R. Stuck., Nuclear instruments and methods 150 (1978) pp. 31-37.

REFERENCES

CHAPTER 6

1. D. de Nobel., Philips Res. Repts., 14 (1959) pp 361-399 and 430-492.

2. G.G.Roberts and F.W.Schmidlin., Phys. Rev., Vol.180, No.3 (1969) pp 785-794.

3. F.W.Schmidlin and G.G.Roberts., Phys.Rev., Vol.9, No.4 (1974) pp 1578-1590.

4. E.N.Arkadyeva and O.A.Matveev., Rev.de Phys. Appl., T.12, No.2 (1977) pp 239-240.

5. P. Höschl, P. Moravec, A. Martinaitis and A. Sakalas., Phys.Stat. Sol. (a), 48, K43 (1978) pp K43-K46.

6. P. Höschl, P. Polívka, V. Prosser, A. Sakalas., Czech. J.Phys. B., 25 (1975) pp 585-596.

7. G. Ottaviani, C. Canali, C. Jacoboni, A. AlberigiQuaranta and K. Zanio., J.Appl.Phys., Vol.44, No.1 (1973) pp 360-371.

8. G. Ottaviani, Rev. de Phys. Appl., T.12, No.2 (1977) pp 249-254.

REFERENCES

CHAPTER 7

1. A.N.Saxena., Surface Science., Vol.13 (1969) pp 151-171.
2. J. Camassel, D. Auvergne, H. Mathieu, R. Triboulet and Y. Marfaing, Sol.Stat. Com., Vol.13 (1973) pp 63-68.
3. T. Takebe, J. Saraie and T. Tanaka., Phys. Stat. Sol.(a)., 47 (1978) pp 123-130.
4. J. Touskova and R. Kuzel., Phys. Stat. Sol (a), 36 (1976) pp 747-755.
5. J. Touskova and R. Kuzel., Phys. Stat. Sol (a)., 40 (1977) pp 309-314.
6. J. P. Ponpon and P. Siffert., Rev. de Phys. Appl., T 12, No: 2 (1977) pp 427-430.
7. J.D. Levine., J. Appl.Phys., 42 (1971) pp 3991-3999.
8. C. R. Crowell., Solid State Electronics., Vol.20 (1977) pp 171-175.
9. D.A. Cusano., Rev. de Phys. Appl., 1 (1966) pp 195-201.
10. J. Bernard., R. Lancon, C. Paparoditis, M. Rodot., Rev. de Phys. Appl., 1 (1966) pp 211-218.
11. K. Yamaguchi, H. Matsumoto, N. Nakayama, S. Ikegami., Japan. J. Appl.Phys., 15 (1976) pp 1575-1576.
12. K. Yamaguchi, N. Nakayama, H. Matsumoto, S. Ikegami., Japan. J. Appl. Phys., 16 (1977) pp 1203-1211.
13. J. Lebron, Proc. 8th Photovoltaic Spec. Conf: (IEEE,New York) (1970) pp 33-39.
14. R.O. Bell, H.B. Serreze and F.V. Wald., Proc.11th Photovoltaic Spec.Conf. (IEEE, New York)(1975), pp 497-502.
15. M.C.Petty and G.G.Roberts, Elec.Lett. 15(1979) pp 335-336.
16. M.C.Petty and G.G.Roberts., Inst.Phys.Conf.Ser.No.50: (1980) pp 186-192.

17. A.M.Goodman., J.Appl.Phys., Vol.34, No.2 (1963) pp 329-338.

18. C.R.Crowell and G.I. Roberts., J.Appl.Phys. Vol.40, No.9 (1969) pp 3726-3730.

19. C. Lawther and J.Woods., Phys.Stat.Sol.(a) 46 (1978) p 245.

20. S.M.Sze., "Physics of semiconductor devices", Wiley International Edition.

21. G.G.Roberts, M. McGinnity, W.A.Barlow and P.S. Vincett., Solid State Com., Vol.32 (1979) pp 683-686.

22. D.L.Pulfrey., Solid State Electronics., Vol.20 (1977) pp 455-457.

23. R.B.Godfrey and M.A. Green., Monitor-Proceedings of the IREE Aust., (1978) pp 87-91.

24. D.L.Pulfrey., IEEE Trans.Elec. devices., Vol.ED-25, No.11 (1978) pp 1303-1317.

25. D.A. Cusano., Solid-State Electronics., Vol.6 (1963) pp 217-232.

26. G.G.Roberts., T.M. McGinnity, W.A.Barlow and P.S. Vincett., Thin Solid Films., Vol.68 (1980) pp 223-232.

APPENDIX I

COMPUTER PROGRAM USED FOR SIMULATION OF CONDUCTIVITY OF CADMIUM TELLURIDE

```
      FDIR(A,B,T)=1./(1.+EXP((A-B)/(8.63E-05*T)))
      DIMENSION RT(100),OHM(100),ARR(1000),EXTEMP(200),EXCOND(200)
     1,RTEMP(200),CURR(200)
C
C           READ IN MATERIAL CONSTANTS
C
      READ(5,100)EC,CMASS,VMASS,ALPHA,EMOB,HMOBO
  100 FORMAT(F4.2,6X,F4.2,6X,F4.2,6X,E8.2,2X,F6.1,4X,E10.4)
      WRITE(6,1000)
 1000 FORMAT(1H1,/////41X,'SIMULATION OF CONDUCTIVITY OF CADMIUM TELLURI
     1DE')
      WRITE(6,2000)EC,ALPHA,CMASS,VMASS,EMOB,HMOBO
 2000 FORMAT(///10X,'BAND GAP AT OK =',F4.2,'EV',//10X,'TEMPERATURE DEPE
     1NDENCE OF BAND GAP =',E8.2,'EV K-1',//10X,'EFFECTIVE MASS OF CONDU
     2CTION BAND =',F4.2,//10X,'EFFECTIVE MASS OF VALENCE BAND =',F4.2,/
     3/10X,'ELECTRON MOBILITY =',F7.1,'CM2 V-1 S-1',//10X,'HOLE MOBILITY
     4AT OK. =',E10.4,'CM2 V-1 S-1')
C
C           READ IN PROGRAM PARAMETERS
C
      READ(5,200)EM1,CM1,EM2,CM2,EQ1,CQ1,EQ2,CQ2,EXTRIN
  200 FORMAT(4(F4.2,2X,E8.2,2X),E9.2)
      WRITE(6,3000)
 3000 FORMAT(/////50X,'FIXED INPUT DATA')
      WRITE(6,4000)EM1,CM1,EM2,CM2,EQ1,CQ1,EQ2,CQ2,EXTRIN
 4000 FORMAT(///10X,'DEPTH OF EM1 LEVEL BELOW CONDUCTION BAND AT OK=',F
     14.2,'EV',16X,'CONCENTRATION =',E8.2,'CM-3',//10X,'DEPTH OF EM2 LEV
     2EL BELOW CONDUCTION BAND AT OK=',F4.2,'EV',16X,'CONCENTRATION =',
     3E8.2,'CM-3',//10X,'HEIGHT OF EQ1 LEVEL ABOVE VALENCE BAND AT OK='
     4,F4.2,'EV',18X,'CONCENTRATION=',E8.2,'CM-3',//10X,'HEIGHT OF EQ2
     5LEVEL ABOVE VALENCE BAND AT OK=',F4.2,'EV',18X,'CONCENTRATION=',
     6E8.2,'Cv-3',//10X,'EXCESS DONOR CONCENTRATION =',E8.2,'CM-3')
```

```
      READ(5,300) IT,IFT,INCT
  300 FORMAT(I3,2X,I3,2X,I2)
      WRITE(6,500)
 5000 FORMAT(///10X,'TEMP',5X,'1/TEMP',5X,'ENERGY GAP',5X,'EF ABOVE VB',
     15X,'ELECTRONS IN CB',5X,'HOLES IN VB',5X,'CONDUCTIVITY',/12X,'K',8
     2X,'K-1',10X,'EV',12X,'EV',16X,'CM-3',14X,'CM-3',11X,'(OHM-CM)-1'
C
C           READ IN SAMPLE DATA
C
      READ(5,400) NDATA,NSAMP,AREA,VOLTS,THICK
  400 FORMAT(I3,2X,I3,2X,F4.2,2X,F4.1,2X,E8.2)
      READ(5,500) (EXTEMP (I), CURR (I), I=1,NDATA)
  500 FORMAT (F5.1,2X,E8.3)
      DO 6 I=1,NDATA
      RTEMP (I)=1.0/EXTEMP (I)
      EXCOND(I)= (CURR(I)*THICK)/ (VOLTS*AREA)
     6CONTINUE
      ECO=EC
      EM1O=EM1
      EM2O=EM2
      EQ1O=EQ1
      EQ2O=EQ2
      ARR(1)=1.0
      EF=EC/2.0
C
C           SET UP TEMPERATURE COMPUTATIONAL LOOP
C
      DO 1  J=IT,IFT,INCT
      M=2
      Y=1.0
      L=(J-IT) /INCT+1
      N=(IFT-IT)/INCT+1
      T=J
C
C           ADJUST ENERGY GAPS FOR TEMPERATURE EFFECTS
C
      EC=ECO+ALPHA*T
      EM1=EM1O +ALPHA* (EM1O/ECO)*T
      EM2=EM2O+ALPHA*  (EM2O/ECO)*T
```

```
      EQ1=EQ1O+ALPHA* (EQ1O/ECO)*T
      EQ2=EQ2O+ALPHA* (EQ2O/ECO)*T
      HMOB=HMOBO/(T**1.5)
      CSTATE=4.82E+15* (CMASS*T)**1.5
      VSTATE=4.82E+15* (VMASS*T)**1.5
     5M=M+1
C
C           COMPUTE TOTAL NO.ELECTRONS-TOTAL NO. OF HOLES
C
      CNEX=CSTATE*FDIR(EC,EF,T)+CM1*FDIR(EC-EM1,EF,T)+CM2*FDIR(EC-EM2,EF
     1,T)-VSTATE*FDIR(EF,O.,T)-CQ1*FDIR(EF,EQ1,T)-CQ2*FDIR(EF,EQ2,T) .
C
C           COMPUTE DIFFERENTIAL
C
      DIF=(CSTATE*EXP((EF-EC)/(8.63E-O5*T))+
     1CM1*EXP((EC-EM1-EF)/(8.63E-O5*T))*(FDIR(EC-EM1,EF,T))**2+
     2CM2*EXP((EC-EM2-EF)/(8.63E-O5*T))*(FDIR(EC-EM2,EF,T))**2+
     3VSTATE*EXP((-EF)/(8.63E-O5*T))+
     4CQ1*EXP((EF-EQ1)/(8.63E-O5*T))*(FDIR(EF,EQ1,T)**2+
     5CQ2*EXP((EF-EQ2)/(8.63E-O5*T))*(FDIR(EF,EQ2,T))**2
     6)/(8.63E-O5*T)
      ARR(M)=CNEX-EXTRIN
      IF(DIF.EQ.O.) GO TO 2
C
C           IS EF OK?
C
      IF(ABS((CNEX-EXTRIN)/DIF).LE.1.OE-4) GO TO 3
      IF(ARR(M)*ARR(M-1).LT.O.O) Y=-Y/2.O
C
C           NEXT VALUE OF EF
C
      EF=EF+O.2*Y
C
C           STOP ITERATION IF EF EXCEEDS LIMITS
C
      IF(EF.GE.EC.OR.EF.LE.O.)  GO TO 1
      GO TO 5
    2 EF=EF+O.O1
      GO TO 5
```

```
C
C           COMPUTE CONDUCTIVITY
C
      3 ELECT=CSTATE*FDIR(EC,EF,T)
        HOLES=VSTATE*FDIR(EF,0.,T)
        COND=(ELECT*EMOB+HOLES*HMOB)*1.6E-19
        RT(N-L+1)=1./T
        OHM(N-L+1)=COND
C
C           PRINT OUT RESULTS
C
        WRITE(6,6000)J,RT(N-L+1),EC,EF,ELECT,HOLES,COND
   6000 FORMAT(/11X,I3,5X,E9.3,5X,F5.3,8X,F5.3,12X,E8.2,12X,E8.2,12X,E8.2
      1 CONTINUE
        XMIN=2.5E-03
        XF=2.5E-04
        YMIN=-14.0
        YF=1.0
C
C           GRAPH PLOTTING ROUTINE
C
        CALL PLTOPS(XMIN,XF,YMIN,YF,1.0,1.0)
        CALL PAXIS(1.0,1.0,'1/TEMP (K-1)',-12,10.0,0.0,XMIN,
       1XF,1.0)
        CALL PAXIS (1.0,10.0,' ',0,-10.0,0.0,XMIN,XF,1.0)
        CALL PLGAXS(1.0,1.0,'CONDUCTIVITY (OHM-CM)-1',23,9.0,90.0,
       1YMIN,YF)
        CALL PLGAXS(11.0,1.0,' ',0,-9.0,90.0,YMIN,YF)
        CALL PSYMB(3.0,9.5,-0.2,'CONDUCTIVITY OF CADMIUM TELLURIDE',
       10.0,33)
        CALL PSYMB(3.0,9.0,-0.1,'FULL LINE COMPUTED,POINTS ARE EXPERIMENT
       1AL',0.0,43)
        CALL PNUMBR(7.0,9.0,0.1,NSAMP,0.0,'''HOLE MOBILITY.='',I3*')
        CALL PSYMB(2.5,3.5,-0.1,'PROGRAM PARAMETERS',0.0,18)
        CALL PNUMBR(1.5,3.0,0.1,EM10,0.0,'''DEPTH OF EM1 BELOW CB='',WF1.
       12,''EV''*')
        CALL PNUMBR(4.5,3.0,0.1,CM1,0.0,'''CONC.='',WE1.2,''CM-3''*')
        CALL PNUMBR(1.5,2.6,0.1,EM20,0.0,'''DEPTH OF EM2 BELOW CB ='',WF1.
       12,''EV''*')
```

```
154          CALL PNUMBR(4.5,2.6,0.1,CM2,0.0,'''CONC.='',WE1.2,''CM-3''*')
155          CALL PNUMBR(1.5,2.2,0.1,EQ10,0.0,'''HEIGHT OF EQ1 ABOVE VB='',WF1
156         1.2,''EV''*')
157          CALL PNUMBR(4.5,2.2,0.1,CQ1,0.0,'''CONC.='',WE1.2,''CM-3''*')
158          CALL PNUMBR(1.5,1.8,0.1,EQ20,0.0,'''HEIGHT OF EQ2 ABOVE VB='',WF1
159         1.2,''EV''*')
160          CALL PNUMBR(4.5,1.8,0.1,CQ2,0.0,'''CONC.='',WE1.2,''CM-3''*')
161          CALL PNUMBR(1.5,1.4,0.1,EXTRIN,0.0,'''EXCESS DONOR CONCENTRATION=
162         1'',WE1.2,''CM-3''*')
163          CALL PRSTER(1.0,1.0,10.0,9.0)
164          CALL PONRST
165          CALL PLTLOG(1)
166          CALL PLINE(RT(1),OHM(1),N,1,0,0,1.0)
167          CALL PLINE(RTEMP(1),EXCOND(1),NDATA,1,-1,2,1.0)
168          CALL PLTEND
169          STOP
170          END
```